Aus dem Physiologischen Institut, Lehrstuhl: Physiologische Genomik
im Biomedizinischen Zentrum (BMC)
der Ludwig-Maximilians-Universität München
Vorstand: Prof. Dr. Magdalena Götz

The role of *Additional sex combs-like* genes in human pluripotent stem cell differentiation and congenital disorders

Dissertation

zum Erwerb des Doktorgrades der Naturwissenschaften
an der Medizinischen Fakultät der
Ludwig-Maximilians-Universität zu München

vorgelegt von

Friederike Matheus
aus Berlin

2018

Gedruckt mit Genehmigung der Medizinischen Fakultät der Universität München

Betreuerin: Prof. Dr. Magdalena Götz

Zweitgutachter: Prof. Dr. Gunnar Schotta

Dekan: Prof. Dr. med. dent. Reinhard Hickel

Tag der mündlichen Prüfung: 22.08.2018

This work is dedicated to children that are diagnosed with rare diseases,
and to their caring families and friends.

Table of contents

Zusammenfassung

Chromatinstrukturen modulieren und stabilisieren die transkriptionellen Veränderungen, die die umfassenden zellulären Veränderungen während der Embryonalentwicklung steuern. Mutationen in Chromatin-modifizierenden Proteinen können daher fötale Fehlentwicklungen zur Folge haben. Die Familie der Additional sex combs-like (ASXL1/ASXL2/ASXL3)-Proteine ist eine Gruppe von transkriptionellen Regulatoren, die verschiedene Chromatinmodifikatoren und Transkriptionsfaktoren an Zielgenen zusammenbringen. ASXL Proteine rekrutieren beispielsweise den Polycomb repressive complex 2 (PRC2), welcher die repressive Lysin 27-Trimethylierung an Histon 3 (H3K27me3) katalysiert; andererseits bewirken ASXL Proteine in Kooperation mit BRCA1-associated protein-1 (BAP1) die De-Ubiquitinierung von Lysin 119 an Histon 2A (H2AK119). Mutationen im humanen *ASXL1*-Gen sind mit Bohring-Opitz-Syndrom (BOS) assoziiert, ein schwerer Geburtsfehler, der unter anderem mit neuronalen Defiziten und kraniofaziellen Anomalien einher geht. Ein Teil dieser Symptome deutet auf eine Entwicklungsstörung der Neuralleistenzellen (NLZ) hin, eine multipotente, migratorische Vorläuferpopulation. Die Rolle der ASXL Proteine in der humanen Embryonalentwicklung und der Pathogenese der verbundenen Geburtsdefekte ist bis jetzt ungeklärt.
Um zu untersuchen, welche molekularen Mechanismen zur Entstehung von BOS beitragen, habe ich humane BOS-Modelle entwickelt, basierend auf induziert pluripotenten Stammzellen, die aus BOS-Patientenzellen generiert wurden (BOS-iPSZ), sowie genetisch modifizierten humanen embryonalen Stammzellen, die BOS-relevante Mutationen im *ASXL1*-Gen tragen (*ASXL1*$^{PSC/PSC}$). Ich konnte zeigen, dass diese BOS-Modelle verkürzte Versionen des ASXL1-Proteins exprimieren, was den pluripotenten Status der undifferenzierten Zellen nicht drastisch beeinflusste. Ich fand jedoch in Differenzierungsexperimenten *in vitro*, dass die Präsenz des verkürzten ASXL1-Proteins die Auswanderung von NLZ aus Neuroepithelstrukturen verminderte, was ich in Transplantationsexperimenten in Hühnerembryonen bestätigte. Der Effekt der mutanten Proteinform war dominant und störte auch die Migration von hühnereigenen embryonalen NLZ *in vivo*. Das regulatorische Netzwerk an Genen, das die Entwicklung von NLZ steuert, wurde in *ASXL1*$^{PSC/PSC}$ -Neuroepithelstrukturen unzureichend aktiviert. Dabei schien die drastische Verminderung des *ZIC1*-Genes eine entscheidende Rolle zu spielen, da die Überaktivierung von *ZIC1* in *ASXL1*$^{PSC/PSC}$ Neuroepithelstrukturen den NLZ-Entwicklungsdefekt rückgängig machen konnte. Die negative Regulierung von für die Neural-/NLZ-Entwicklung wichtigen Faktoren wurde begleitet von einer lokal verstärkten Markierung dieser Gene mit H3K27me3-Modifizierungen, während auf globaler Ebene sowohl H3K27me3- als auch H2AK119-Level reduziert waren. Ich konnte zudem die Expression von *asxl1* und *asxl2* in Zebrafisch-Embryonen bestätigen und habe eine *asxl1*-Zebrafischmutante entwickelt.
Zusammenfassend stellt meine Arbeit die erste Studie zur Expression und Funktion von Proteinen der ASXL-Familie während der Differenzierung von humanen Stammzellen dar. Ich konnte einen neuen, dominanten Mechanismus aufzeigen, demzufolge BOS-assoziierte Mutationen zur Expression von verkürzten ASXL1-Proteinformen führen. Diese hemmen die Entwicklung zu neuroektodermalen Vorläufern und NLZ, was die kraniofaziellen und kognitiven Defizite von BOS erklären kann. Ich habe eine entscheidende Rolle für *ZIC1* in der Entwicklung der humanen NLZ *in vitro* identifiziert, und stelle die Hypothese auf, dass mutante Proteinformen von ASXL1 zur aberranten Rekrutierung des PRC2 und damit zu der von mir beobachteten Herunterregulierung von wichtigen Faktoren für die neurale und NLZ-Entwicklung führen könnten. Meine Ergebnisse zur globalen Verminderung der H2AK119Ub/H3K27me3-Level bestätigen die bereits beschriebene Überaktivierung von BAP1 durch mutante ASXL1-Formen in Tumorzellen, und erweitern sie um den Kontext der humanen Stammzelldifferenzierung. Die Ergebnisse der von mir angewandten Modelle ordnen BOS, und potenziell weitere ASXL-assoziierte Syndrome, als Defekte der neuralen und NLZ-Entwicklung ein, und können zukünftige Studien und Therapien in diesen und verwandten Syndromen unterstützen.

Abstract

During embryonic development, chromatin landscapes play a central role in orchestrating the transcriptional networks that steer cellular identities. *De novo* mutations in proteins that modify chromatin can severely compromise developmental gene networks, leading to defects in the formation of fetal organs. The Additional sex combs-like (ASXL1/ASXL2/ASXL3) proteins are a family of highly conserved transcriptional regulators that act as epigenetic scaffolds, assembling chromatin modifiers and transcription factors at genomic targets. Via recruitment of the Polycomb repressive complex 2 (PRC2), ASXL proteins promote Histone 3 Lysine 27 trimethylation (H3K27me3) and repression of target genes, while their cooperation with BRCA1-associated protein-1 (BAP1) effects Histone 2A Lysine 119 (H2AK119) de-ubiquitination. *De novo* truncating mutations in *ASXL1* are linked to the severe birth defect Bohring-Opitz Syndrome (BOS), which is characterized by intellectual disabilities, craniofacial dysmorphisms and musculoskeletal defects, among other symptoms. A subset of BOS features suggests perturbation of the neural crest (NC), a multipotent, migratory embryonic cell population. To date, the functions of *ASXL* genes in human embryonic development and the pathogenesis of related birth defects remain elusive.

To decipher the developmental and molecular mechanisms underlying BOS, I generated a panel of human pluripotent stem cell lines, including BOS patient-derived induced pluripotent stem cells (BOS-iPSC) and genetically engineered human embryonic stem cell lines bearing BOS-associated mutations (*ASXL1*$^{PSC/PSC}$ hESC). I could show that BOS mutations lead to expression of truncated ASXL1 proteins (aa 1-900), which did not affect the overall pluripotent state of undifferentiated cells. However during NC differentiation *in vitro*, expression of mutant ASXL1 impaired the emigration of NC cells from neuroepithelial structures, which was confirmed upon xenotransplantation into developing chicken embryos. This was a dominant effect, as overexpression of truncated ASXL1 variants in chicken NC progenitors *in vivo* perturbed their emigration. I demonstrated that the characteristic gene regulatory network controlling NC development was negatively regulated in *ASXL1*$^{PSC/PSC}$ neuroepithelial cultures, including a panel of neuroectoderm determinants and of *ASXL1* and *ASXL3*. Drastically impaired induction of the neural plate border specifier *ZIC1* was central to the NC developmental defect, as the re-establishment of *ZIC1* expression in mutant NC cultures rescued the emigration phenotype. Negative regulation of neural/NC specifiers and *ASXL1/ASXL3* in *ASXL1*$^{PSC/PSC}$ NC progenitor cultures was associated with target-specific local increase of H3K27me3, while global levels of H3K27me3 and H2AK119Ub were reduced. I furthermore confirmed expression of *asxl1* and *asxl2* in zebrafish embryos and developed a CRISPR-based model for truncated asxl1 function in this model.

In summary, my study for the first time examined expression and functions of ASXL paralogs during commitment of human developmental progenitors. I discovered a novel dominant mechanism of BOS-associated mutations in *ASXL1,* leading to expression of truncated variants that perturb neuroectoderm and NC progenitor development, which could explain the craniofacial and possibly the cognitive symptoms of BOS. I furthermore demonstrated a crucial role of *ZIC1* during human NC differentiation, and showed that its induction is perturbed in the BOS model. My study provides initial results indicating that truncated ASXL1 aberrantly recruits or retains PRC2 at negatively regulated neural/NC specifiers; on the other side, global reduction in H2AK119Ub/H3K27me3 in BOS NC models is in line with studies on the overactivation of BAP1 by truncated ASXL1 in somatic cells, and implies this scenario in differentiation and development. Taken together, this study should stand as a paradigmatic case for pathological development arising from *ASXL* mutations, and furthermore suggests that BOS joins a group of neuronal and NC-related disorders arising from chromatin-based transcriptional misregulations. The established models should thus be an important foundation for future research on therapeutic intervention in related disorders.

1. Introduction

1.1 Developmental modeling systems

Our development from a small group of uncommitted pluripotent cells in the pre-implantation embryo is a fascinating biological process. While sharing identical genomes, embryonic cells phenotypically diversify, a process named differentiation, through mechanisms that modulate the expression of the genome[2]. This results in the emergence of germ layer progenitors that further become committed to precursors of fetal tissues. Advancements in molecular biology have demonstrated that intricate molecular networks control these differentiation processes to ensure lineage fidelity and stability. However, understanding the details of these regulatory circuits is still in its infancy, and while the investigation of developmental mechanisms in animal models provides the crucial framework to comprehend embryogenesis, they can only partially explain human development because of evolutionary divergence in regulation [3-6].
This is why the derivations of human pluripotent stem cells – of human embryonic stem cells (hESCs) initially, and of induced pluripotent stem cells (hiPSCs) later – are considered breakthroughs in the study of human embryonic regulation[7,8]. Indeed, by the collective investment of efforts, it has been clarified that differentiation of human pluripotent stem cells *in vitro* mimics embryonic processes as shown by the transition from pluripotency to fetal and tissue progenitors and further to specialized tissues[9,10]. Accordingly, human pluripotent stem cells are fundamentally important for elucidating pathogenic mechanisms of congenital disorders that arise from perturbations in embryonic regulation. The latter paradigm has been exemplified extensively[11,12], and is the cornerstone of my PhD thesis. Finally, the potency of human pluripotent stem cells represents an additional breakthrough in medicine as they could serve as unlimited source for generating transplantable differentiated cells for the treatment of numerous diseases and injuries[13,14].

1.1.1 Human pluripotent stem cells

Pluripotent human embryonic stem cells (hESCs) are derived from the inner cell mass of the blastocyst, representing a cell population that *in vivo* gives rise to all fetal organs[7] (**Fig. 1**). Although pluripotent cells are transient in the early embryo, application of specific pathway modulators promotes their indefinite renewal as stem cells *in vitro*, while maintaining their potential to differentiate[15]. This knowledge, and characterization of the gene regulatory network governing pluripotency in mouse ESCs, has led to the derivation of mouse and human iPSCs by the process of reprogramming, which relies on the so called four Yamanaka factors *Oct4, Sox2, Klf4* and *c-Myc*[8] (**Fig. 1**). The reprogramming process has since been refined and improved in many studies, including the transient ectopic expression of factors via transfection of reprogramming factors as modified mRNA[16], episomal plasmids[17] or proteins[18]. These delivery methods in conjunction to optimized protocols and reagents produce hiPSC lines that display the capacities of hESC, including self-renewal and differentiation into progenitors of all germ layers[19].
The possibility of generating hiPSCs on a personalized basis opens up the possibility to produce autologous tissues and organs for cell replacement therapies[14]. Moreover, and as discussed herein, patient derived hiPSCs could serve as a platform to model genetic

and environmental diseases[11,12], in particular those with congenital presentation according to the logic that differentiation *in vitro* mimics embryonic and fetal development[10].

1.1.2 Genetic engineering of human pluripotent stem cells

Genome-editing techniques that allow for targeted modification of single nucleotides or larger genomic regions have opened up new avenues for disease research using human pluripotent stem cells[20]. The most recent development exploits the prokaryotic defense mechanism CRISPR/Cas (Clustered Regularly Interspaced Short Palindromic Repeats/CRISPR-Associated)[21]. In an adaptation of this system to cultured pluripotent stem cells, Caspase 9 (Cas9) nucleases can be recruited to specific genomic sites via short guide RNAs (gRNAs) for introducing point mutations, deleting genomic regions or for integrating reporter genes[22]. Further improvement of the method has led to high editing efficiencies and low off-target effects in diverse applications[23].
These techniques become highly relevant for disease modeling using human pluripotent stem cells, primarily for the introduction of disease-relevant mutations into human pluripotent stem cell lines for direct comparison to the parental lines as isogenic controls, and by correcting mutations in patient derived iPSCs as a basis for comparison. These steps are performed when the cells are in the undifferentiated state, so that any desired differentiated progeny type can be generated and studied directly in comparison to the isogenic control cells (**Fig. 1**). It has been further shown that this modality can be used for tailoring individualized treatments and identifying drug candidates in screening settings[24,25].

1.1.3 Differentiation of human pluripotent stem cells

During embryogenesis, signaling pathways as a means of cell-to-cell communication guide the patterning of the embryo, the establishment of cell type diversity, and the formation of tissues and organs. Gene-targeting studies and expression analyses have identified several pathways, including Wnt, Nodal and bone morphogenetic protein (BMP) signaling, which in a coordinated manner control early steps of embryogenesis and progressively dictate cell fates, from gastrulation and germ layer formation to the differentiation and specialization of tissues[26].
These key events can be recapitulated using hESCs *in vitro*, which requires the cooperative action of the same signaling pathways that govern embryogenesis. Accordingly, differentiation protocols using pluripotent stem cells progress through a primitive streak-like phase, followed by germ layer formation and tissue specification[10,27]. Resulting differentiated cell populations are validated based on the expression of marker genes and physiological characteristics that identify fetal or adult cell populations *in vivo*[27]. Furthermore, in defined protocols exploiting embryonic signaling pathways, pluripotent stem cells give rise to specialized cells that functionally integrate into host tissue upon transplantation[27]. These studies show that differentiation of pluripotent stem cells mirrors the key events taking place during embryogenesis, and thus serves as a relevant model to study human embryonic development.

1.1.4 Modeling developmental syndromes using pluripotent stem cells

Congenital defects arise as a consequence of perturbed formation of fetal tissues[28]; accordingly, the elucidation of disease mechanisms requires investigation of developmental systems. Differentiation of pluripotent stem cells recapitulates human embryogenesis, hence providing a suitable model for developmental syndromes in the dish[12]. Human iPSCs reprogrammed from patient-derived somatic tissue, or genetically modified hESC expressing disease-relevant mutations, help to decipher the molecular mechanisms that are involved in congenital syndromes and to establish screens for drug discovery[25,29,30]. These approaches have also served the elucidation of aberrant regulation in neurocristopathies, a group of congenital anomalies resulting from defects in a distinct progenitor cell population, the neural crest[31-34] (see also chapter **1.4.3**). As this embryonic lineage contributes to hundreds of derivatives in the body[35], modeling neural crest development with pluripotent stem cells is a prerequisite to understanding many human birth defects on a cellular and molecular level.

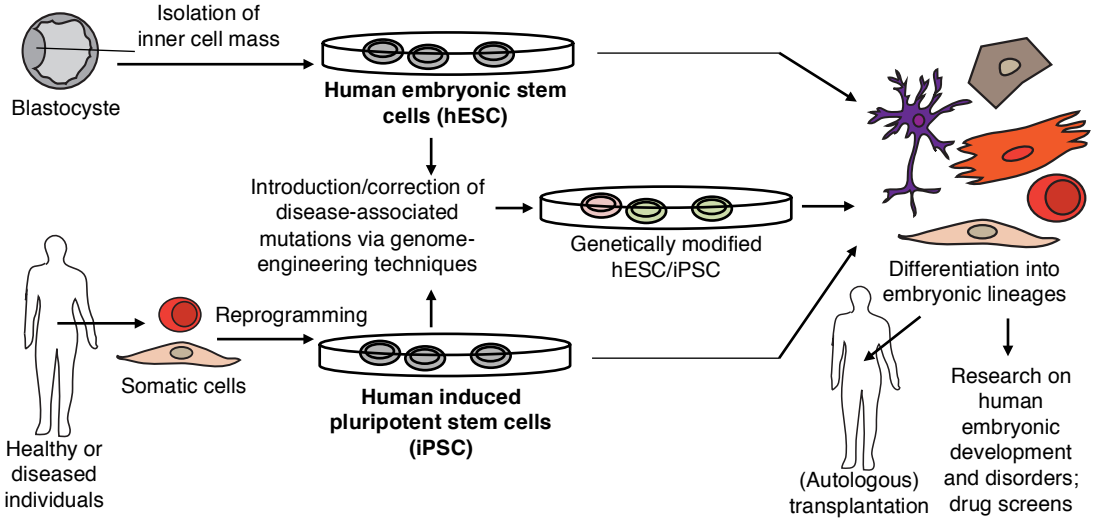

Figure 1. Generation, manipulation and application of human embryonic stem cells (hESCs) and induced pluripotent stem cells (hiPSCs).
hESCs are derived from the inner cell mass of surplus embryos obtained through *in vitro* fertilization techniques. iPSC with virtually equal developmental properties can be generated by introduction of pluripotency factors into adult, somatic cells, which induces reprogramming, resulting in a pluripotent state. Genetic manipulation via techniques like the CRISPR/Cas system allow for correction of disease-associated genes in patient-derived iPSC cells, or introduction of mutations into healthy donor-derived hESCs. Differentiation of genetically manipulated and control hESC and hiPSC lines can be applied to study (pathological) embryonic processes, perform drug screens and for cell-based therapies.

1.2 Epigenetic regulation in embryonic development

It has been thoroughly demonstrated that the regulation of human pluripotent stem cell differentiation involves changes of transcriptional programs; the regulatory network that regulates pluripotency diminishes during exit from this state while germ layer-specific regulators become activated. In multipotent precursors, which are able to commit to various terminal fates, transcriptional landscapes still harbor a certain degree of flexibility so they are to respond to specific guiding signals. However, genetic programs need to be consolidated, as cells have to remember past fate choices even after the signals that initiated them are gone. These processes finally result in tissue-specific

gene regulatory networks, in which pluripotency genes and factors associated with alternative lineages are consistently turned off.
An important question therefore is which and how regulatory factors manipulate and maintain transcriptional programs. The best understood modality is via the binding of transcription factors (TFs) to regulatory elements of genes, which leads to their activation or repression through interactions with the transcriptional machinery. Nevertheless, epigenetic mechanisms are also fundamentally important by shaping and stabilizing expression programs, resulting in poising, long-term activation or silencing of genes. These processes involve modifications of the chromatin, the complex of DNA, proteins and RNAs (**Fig. 2**). Methylation of the DNA, covalent modification of histone tails, the conformational status of chromatin, and small interfering RNAs are primary epigenetic mechanisms that modulate gene expression[36-38]. Certain groups of proteins, named epigenetic factors, mediate these processes by remodeling chromatin, reading and interpreting epigenetic marks and catalyzing nascent or removing existing modifications[39] (**Fig. 2**). In accordance with their functions, epigenetic factors have been shown to re-arrange chromatin landscapes and thereby to regulate cellular identities and to ensure lineage fidelity. These activities present so-called 'epigenetic barriers' that have to be surmounted in order to switch cellular fates[40].

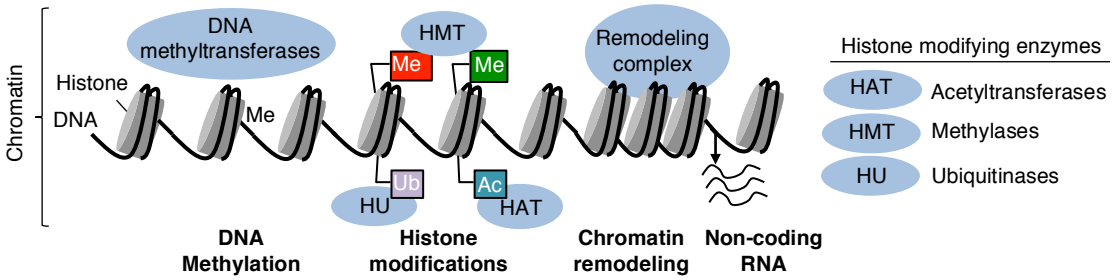

Figure 2. Examples of epigenetic mechanisms that regulate chromatin structure.
Methylation of DNA mediated by methyltransferases, modification of histone tails including methylation, acetylation and ubiqutination catalyzed by different sets of histone-modifying enzymes, remodeling of chromatin by specific remodeling complexes, and non-coding RNAs are involved in establishing chromatin landscapes that regulate transcription. Modified from[36].

1.2.1 Epigenetic regulation in embryonic syndromes

Many congenital disorders are associated with mutations in chromatin writers and remodeling complexes (selected examples in **Table 1**). For instance, haploinsufficiency of the chromatin remodeler *CHD7* leads to CHARGE syndrome[33,34,41], and dominant mutations of the transcriptional co-activator CREB-binding protein CBP are manifested in Rubinstein-Taybi-Syndrome[42]. Interestingly, in many cases, mutations in epigenetic factors that lead to congenital disorders can also promote tumor formation if they occur in somatic tissues, which is thought to involve misregulation of transcriptional networks, resulting in overactivation of proliferative programs[43] (**Table 1**). The group of genes that exhibit this dual functionality includes an important set of epigenetic factors, the Polycomb proteins, which are essential for embryonic development and pluripotent stem cell differentiation[44-46]. This underscores the importance of epigenetic processes in the regulation of development.

Table 1. Examples of chromatin modifiers implicated in congenital syndromes and tumorigenesis. MRS, mental retardation syndrome; HAT, histone acteyltransferase; HDAC, histone deacetylase; HMT, histone methyltransferase; HDMT, histone demethylase; STAGA, SPT3/TAF9/GCN5 transcription coactivator complex, SWI/SNF, SWItch/Sucrose Non Fermentable chromatin remodeling complex; CHD, chromodomain helicase DNA-binding protein complex, GOF, gain-of-function; LOF, loss-of-function. From[47,48].

Gene	Class	Function/ Complex	Germline/ *de novo* mutations	Somatic mutations
CREBBP/P300	Histone modifiers	HAT	Rubinstein-Taybi Syndrome 1/2	B cell/follicular lymphoma, bladder cancer, ...
HDAC4		HDAC	Brachydactyly-MRS	Breast adenocarcinoma
MLL2		HMT	Kabuki syndrome 1	Non-Hodgkin lymphoma
EZH2		HMT	Weaver syndrome 2 (WVS2)	GOF: Solid tumors and Non-Hodgkin lymphoma; LOF: myeloid malignancies, ...
NSD1		HDMT	Beckwith–Wiedemann syndrome/ Sotos syndrome/ Weaver syndrome 1	Acute myeloid leukemia, endometrial carcinoma, melanoma, myeloma, ...
ATXN7	Chromatin remodeler	STAGA-HAT	Spinocerebellar ataxia 7	Breast cancer
ATRX		SWI/SNF	Alpha-thalassemia X-linked MRS	pediatric glioblastoma, pancreatic neuroendocrine tumours
CHD7		CHD	CHARGE-syndrome	gastric, colorectal, prostate, breast, bladder cancers

1.2.2 Keeping genes in check: Polycomb group proteins

Mutations in Polycomb group (PcG) genes were first described in the fruit fly (*Drosophila*), where they alter body segmentation, a phenomenon called homeotic transformations[49]. This phenotype is caused by de-repression of *Homeobox* (*Hox*) genes, factors that are important for anterior-posterior body patterning, and which are normally under tight spatiotemporal control by the PcG proteins. The connection to different regulatory mechanisms, including modification of local chromatin structure up to global genome architecture, have shown that PcG factors are evolutionary conserved regulators in gene silencing involved in X chromosome inactivation, genomic imprinting, pluripotency, cell cycle control and cancer[46,50].

Mammalian PcG proteins assemble in two major complexes. Polycomb repressive complex 2 (PRC2) is responsible for mono-, di- and tri-methylation of Lysine 27 in Histone 3[51,52]. The mammalian complex consists of three core members: enhancer of zeste (EZH1 or EZH2), which catalyzes methylation, embryonic ectoderm development (EED) and suppressor of zeste (SUZ12), both of which are essential co-factors to the methylation reaction[50]. Various accessory subunits further regulate PRC2 activity[50]. H3K27me3 at gene bodies and regulatory regions is associated with compaction of chromatin and reduced RNA Polymerase II binding, leading to stable silencing of marked genes[53].

While PRC2 is highly conserved from the fruit fly to mammals, the other repressive complex, PRC1, has undergone immense diversification during evolution[54]. Six human

PRC1 complexes have been described[55], which assemble around the core members Ring finger protein 1 A/B (RING1A or B) and one of six Polycomb group ring finger (PCGF1-6) proteins. They are classified into canonical PRC1, characterized by the presence of one chromobox protein CBX, and non-canonical complexes[56]. The catalytically active RING1 is a E3 ubiquitin ligase of Histone 2A at Lysine 119 (H2AK119), a mark that is thought to induce chromatin compaction and gene repression[50,56].
CBX proteins interact with H3K27me3 and recruit canonical PRC1 complexes, thereby 'reading' the epigenome and instructing ubiquitination of H2AK119 in a PRC2-dependent manner[57] (**Fig. 3A**). This hierarchical model – first PRC2 and then PRC1 – has been challenged by the finding of non-canonical PRC1 complexes that do not require PRC2 activity to mediate H2AK119 ubiquitination[57,58]. Quite the contrary, PRC1.1, PRC1.3 and PRC1.5 can recruit PRC2 subunits and promote trimethylation of H3K27me3[59,60](**Fig. 3A**). Moreover, several studies have shown that both complexes can engage each other in a context-dependent manner, and PRC complexes act cooperatively as well as independently[50].

1.2.3 Trithorax proteins antagonize Polycomb function

While PcG factors function as main epigenetic repressors, the Trithorax group (TrxG) proteins are their positive counterparts. In the fruit fly, TrxG complexes bind to a set of DNA elements that also recruit PcG complexes, and antagonize PcG activity to maintain active transcriptional states[51].
Comparable to the PcG, TrxG factors assemble in multiprotein complexes of various flavors. The most important players in transcriptional activation and maintenance are the 'switch/sucrose non-fermentable' (SWI/SNF) and the 'Complex proteins Associated with Set 1' (COMPASS) complexes[50]. The human analogs to SWI/SNF, the 'BRG1-or HBRM-associated factors' (BAF) and the 'polybromo-associated BAF' (PBAF) complexes, are nucleosome remodeling factors that regulate the chromatin structures of their target genes[61].
The initial COMPASS complex, which diverged to several non-redundant COMPASS-like complexes in mammals, counteracts PcG activity by mediating H3K4 methylation. SET1-COMPASS catalyzes bulk trimethylation at active promoters (**Fig. 3B**). H3K4me3 however can also be catalyzed independently of transcription and may not be crucial for initial activation, but rather supports the memory of active states[51]. Different mammalian 'mixed lineage leukemia' (MLL) proteins, of which MLL1 is orthologous to *Drosophila*'s Trx, confer diverse functions to the COMPASS-like complexes[50]. MLL1-COMPASS-like methylates only specific loci including the *Hox* genes, and MLL2-COMPASS-like complexes are associated with H3K4 trimethylation of 'bivalent' genes (**Fig. 3B,** see also next chapter). MLL3/4-COMPASS-like are monomethyltransferases for H3K4 at enhancers, short DNA sequences that serve as binding platform for transcription factors and other regulatory proteins to enhance transcription of nearby genes[62] (**Fig. 3B**).
Of note, histone methylases and demethylases that associate with PcG or TrxG complexes respectively antagonize each other[63,64]. Similarly, PcG-mediated chromatin compaction hinders SWI/SNF-mediated chromatin remodeling[65]. These opposing functions result in a balanced system that can react to new transcriptional stimuli, and coordinate systems like the rapidly changing expression networks in embryogenesis.

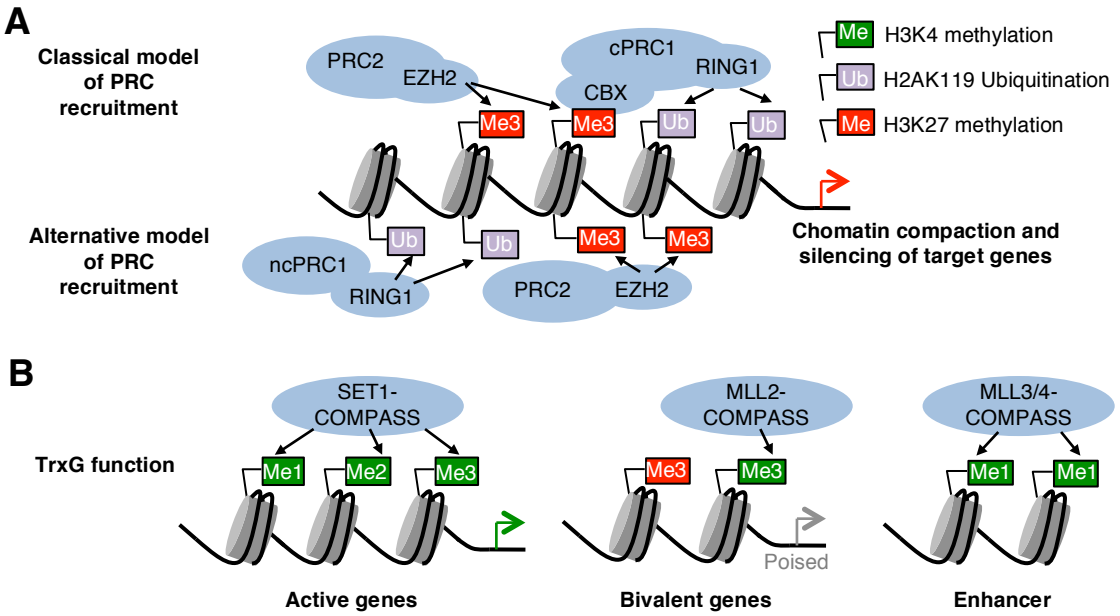

Figure 3: Recruitment and opposing functions of PcG and TrxG complexes.
(A) Mutual targeting of Polycomb repressive complexes (PRCs) to chromatin results in chromatin condensation and transcriptional repression. Recruitment can occur via PRC2-mediated H3K27me3 modifications that recruit CBX of canonical PRC1 (cPRC1) complexes ("classical model"), or via interaction of PRC2-complexes with H2AK119Ub that is placed by the RING1 enzyme in noncanonical PRC1 (ncPRC1)-complexes ("alternative model"). SUZ12, EED and EZH2 (catalytical subunit) are PRC2 core members. **(B)** Different TrxG complexes methylate H3K4 at regulatory regions. Methylation of promoter regions is catalyzed by SET1-COMPASS, which effects all degrees of H3K4 methylation and contributes to active transcription, and by MLL2-COMPASS, which is involved in bivalent states. MLL3/4- COMPASS complexes monomethylate H3K4 at enhancers, which facilitates their activation. After[50].

1.2.4 Polycomb and Trithorax coordinate developmental gene control

During embryonic development, the antagonistic functions of PcG and TrxG complexes stabilize the cascades of transcription programs, and loss of PRC1 or PRC2 factors results in precocious, impaired or biased differentiation of pluripotent stem cells[66,67]. The majority of developmental regulators and enhancers exhibit a 'bivalent' state in pluripotent stem cells, characterized by the presence of both repressive (H3K27me3) and permissive (H3K4me3, or H3K4me1 in the case of enhancers) histone marking, which is mediated by PcG and MLL2 complexes[62] **(Fig. 4)**. This results in a 'steady-state' that allows for immediate activation upon beginning of differentiation[68]. Ubiquitination by RING1B also seems to be involved in setting up bivalent chromatin states, and both PRC1 and PRC2 cooperate in silencing developmental regulators like the *Hox* genes and other transcription factors families including the *Pax, Six, Fox* and *Sox* genes in pluripotent stem cells[37,66,69,70]. Factors that are needed to maintain the undifferentiated state of the cell are expressed and embedded in an active chromatin structure, characterized by occupation of promoters by H3K4me3 and a relaxed chromatin conformation **(Fig. 4)**.
After induction of differentiation and upon lineage commitment, repression of lineage-specific regulators is released, and pluripotency genes and loci associated with alternative fates are silenced **(Fig. 4)**. How the necessary re-arrangement of PcG and

TrxG complexes is regulated still remains largely elusive, but variation in complex assembly is known to take part in this well-orchestrated process. The CBX7 subunit is expressed in pluripotent stem cells, and paralogs CBX8/2/4 replace it within the PRC1 complex in differentiated cells[71,72]. Similar mechanisms are pertinent for the PCGF proteins, as well as the switch from EZH2 to EZH1 during differentiation[50]. Importantly, also accessory proteins and co-factors facilitate specific targeting of the PcG complexes and contribute to differential regulation of transcription during lineage commitment.

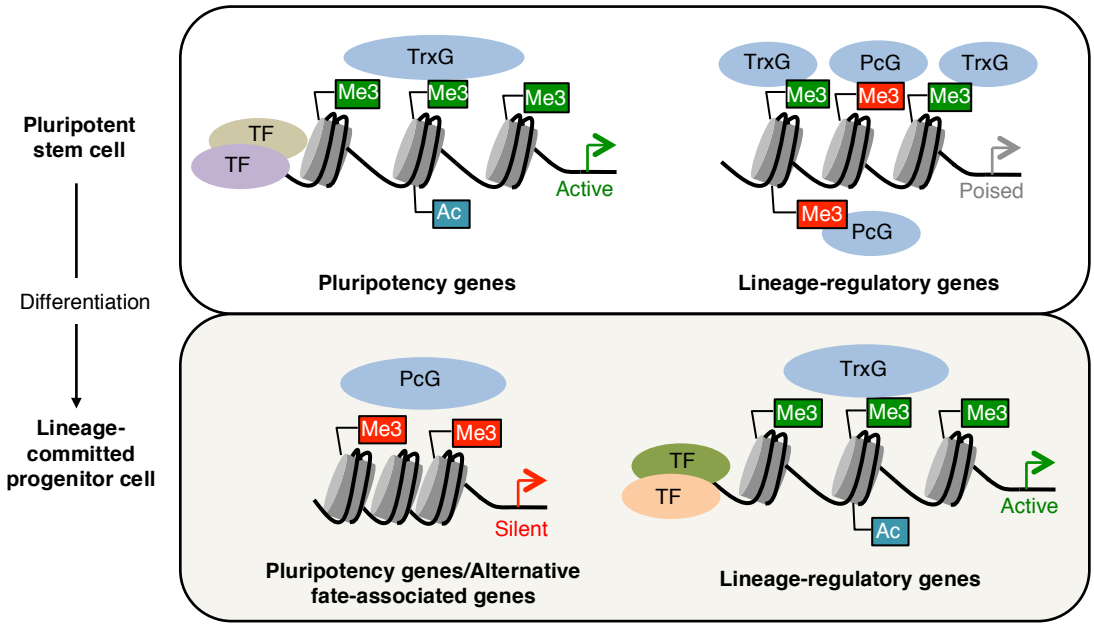

Figure 4. TrxG and PcG complexes control chromatin structures in pluripotent stem cells and upon lineage committment.
In the undifferentiated stage, pluripotency genes are actively transcribed by association with TrxG and relaxed histone states (H3K4me3, H3 acetylation), whereas lineage-regulatory genes are in a poised or bivalent mode, marked by transcription-permissive (H3K4me3) and repressive histone marks (H3K27me3) and by co-localization of PcG and TrxG complexes. This state is resolved to either repression or activation depending on the lineage choice, paralleled by repression of pluripotency. Upon transcription factor-mediated induction of expression, TrxG complexes in cooperation with accessory co-factors maintain the active transcription by establishing a permisse histone landscape (H3K4me3, H3 acetylation, relaxed chromatin conformation). The absence of inductive signals results in occupation of genes with PcG complexes and co-factors that generate repressive histone structures (H3K27me3, histone deacetylation, chromatin compaction).

Taken together, the TrxG and PcG proteins form a regulatory nexus that memorizes transcriptional changes, turning TF-induced regulations into epigenetic landscapes that last beyond mitosis and ensure lineage fidelity during embryonic differentiation. The discovery of additional co-factors that interact with both groups and balance their functions should provide further explanations on how their antagonistic functions are integrated.

1.3 Mediators between repression and activation: *Additional sex combs* genes

The *Additional sex combs (Asx)* gene was classified in *Drosophila* as dual co-factor of PcG and TrxG proteins, since mutations in *Asx* induce anterior and posterior transformations in the same embryo[73,74]. Indeed, Li *et al.* reported transient interaction of a bipartite motif of Asx with both the SET domains of Trx and the PcG factor E(z), which enables target-specific regulation of H3K4me3 and H3K27me3 by Asx[75,76]. Asx shares several characteristics with PcG proteins, namely a subset of genomic targets, a similar protein structure and a ubiquitous developmental expression pattern; however, *Asx* target gene regulation is tissue-specific, which is unusual for PcG factors[77,78]. Hence, Asx seems to play context-dependent roles in the integration of activating and repressive epigenetic mechanisms. The important regulatory functions of Asx are highlighted by its evolutionary conservation and diversification to several paralogs with different structures, expression patterns and functions.

1.3.1 Structural properties of the *Additional sex combs-like* family

Three genes constitute the human *ASXL* family: *ASXL1* and *ASXL2,* which are located within syntenic genomic regions (*DNMT3B-ASXL1-KIF3B* and *DNMT3A-ASXL2-KIF3C*)[79] and are transcribed to similarly sized proteins (1541 and 1435 amino acids, respectively), and *ASXL3*, which encodes for a protein of 2248 amino acids (**Fig. 5**).
The *ASXL* genes share similar transcript architectures of 13 (*ASXL1, ASXL2*) or 12 (*ASXL3*) exons, respectively, and encode for isoforms through alternative splicing. This includes not yet annotated exons[1], which can result in the production of conserved circular isoforms in the case of *ASXL1*[80]. Usage of alternative polyadenylation sites predicts expression of three *ASXL1* transcripts of 4925, 5976 and 6864 bp, however, a highly expressed 8 kb isoform was detected in human adult tissues, as well as a 6 kb form and a 5 kb transcript, which was detected only in the testis[81]. ASXL proteins show a high degree of conservation of several structural and functional domains, namely the N-terminal ASXN domain, the ASXH and ASXM domains and the C-terminal plant homeodomain (PHD, **Fig. 5**). The ASXH domain and the plant homeodomain (PHD) are conserved in the *Drosophila* Asx protein[79], while its 'AT hook' DNA binding motif was not passed on to mammalian ASXLs[78,81] (**Fig. 5**).
In silico analysis of the ASXL proteins predicts N-terminal globular domains coined HARE-HTH, which contain forkhead domains that were suggested to bind DNA similarly to the FOXO1 protein[82,83], however, they have not been functionally validated yet. The ASXH region harbors two potential nuclear receptor (NR) binding motifs (LXXLL) which are presumptively inactive[84], a DEUBAD domain that enables binding of ASXL members to the BRCA1-associated protein 1 (BAP1)[82,85], and overlaps with binding regions of several other epigenetic regulators (HP1, NCOA1, LSD1, the Cohesin Core complex, **Fig. 5).** Notably, the HP1 binding motif is absent in ASXL2. A further NR binding motif that mediates interaction with several NRs in complex with their respective ligands is situated towards the C-terminus of the ASXL proteins within the ASXM2 domain[79]. The PHD finger at the very C-terminus of all ASXL proteins is highly conserved. PHD domains are typically found in chromatin-associated proteins, where they interact with methylated or acetylated H3 histones[86]. The conformation of the ASXL PHD finger theoretically allows binding of internal histone tails such as K27[83], although exact targeting sites and mechanisms have yet to be investigated.

Proteolytic degradation of ASXL1 is promoted through several PEST sequences[81,87] and via ubiquitination of K351, which has to be erased by the de-ubquitinating enzyme USP7 to enhance ASXL1 protein levels[88]. Several conserved putative nuclear localization signals (NLS) provide a mechanism for the transportation of ASXLs to the nucleus[81].
Given their diverse interaction capacities, mammalian ASXL proteins are considered epigenetic scaffolds that recruit other enzymes to target sites and transduce signals mediated by nuclear hormone receptors, integrating them with the epigenetic and transcriptional landscape.

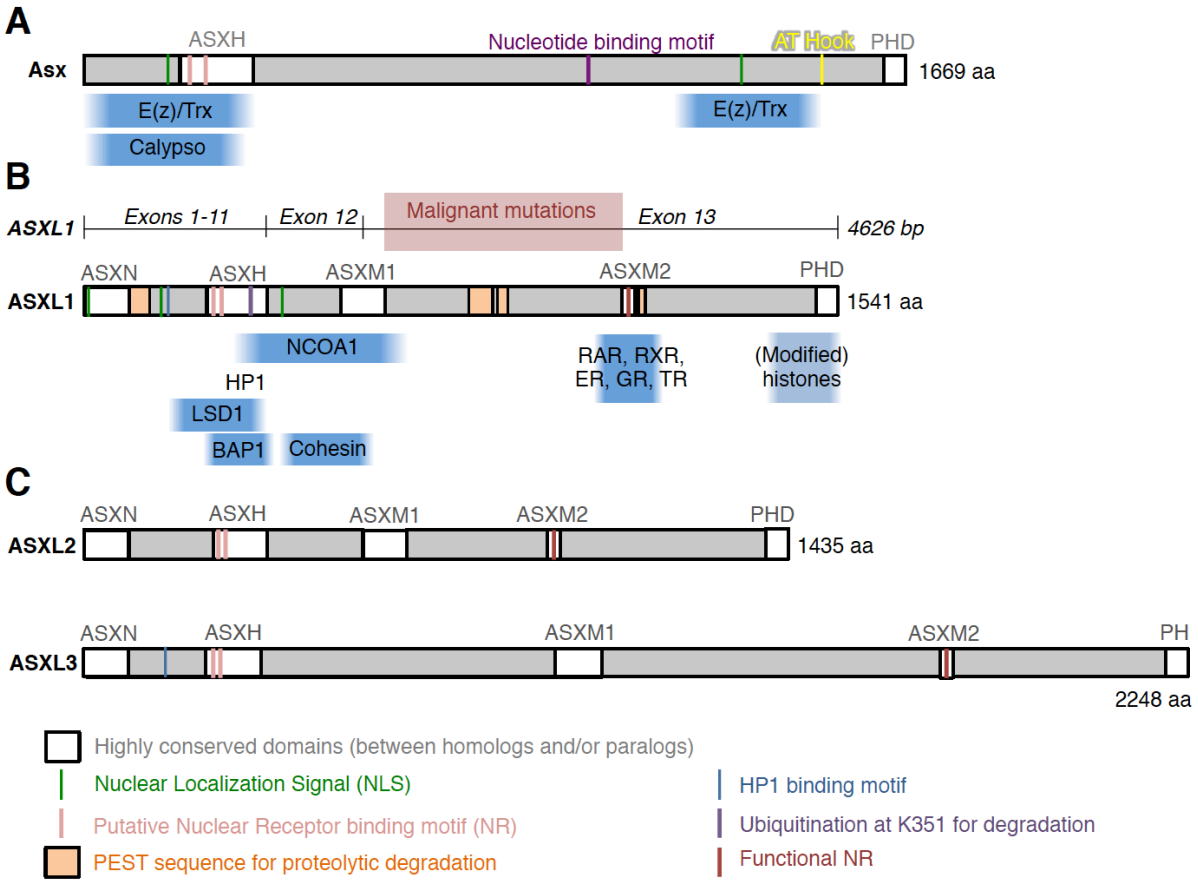

Figure 5. Asx and the ASXL proteins.
Structure of Drosophila Asx **(A)** and human ASXL1 gene and protein **(B)** and ASXL2/3 proteins **(C)** with annotated domains. White boxes in Asx indicated domains that are conserved in mammalian ASXLs, and white domains in ASXL1 are shared with ASXL2 and ASXL3 proteins. Known interaction partners are shown in blue at the respective binding sites in Asx/ASXL1. The large terminal exon of the human *ASXL1* transcript includes a mutation 'hotspot' (pale red box), in which the majority of mutations that have been associated with leukemia and developmental syndromes are found. ASXN contains a HARE-HTH motif proposed to function in DNA binding. The ASXH domain harbors a DEUBAD domain present in all ASXL proteins. Histone binding of the PHD finger was not directly shown but inferred from sequence comparisons. NLS and PEST sequences of ASXL2 and ASXL3 were not determined. From[78,79,81,83-85,88-90].

1.3.2 ASXL proteins recruit binding partners and regulate transcription

1.3.2.1 Nuclear hormone receptors and Cohesin

NRs are a family of transcription factors that complex with small molecule ligands including steroid hormones and retinoids, bind to responsive DNA elements and regulate transcription of their target genes. Thereby, they are involved in different processes of embryonic vertebrae development, cellular metabolism and homeostasis, and cancer[91-93].

Studies reporting on the interaction of ASXL proteins with several types of ligand-bound NRs though specific motifs in the ASXM2 domain, which is not present in *Drosophila* Asx, offered new insights on how NR-initiated transcriptional regulation can be sustained by chromatin modifications[84]. ASXLs seem to act as regulatory switches that specifically assemble transcription factors and repressive or activating histone modifiers at target promoter regions in a context-dependent manner.

In cell lines, ASXL1 was shown to enhance the transcriptional activity of the Retinoic Acid Receptor (RAR) – Retinoic X Receptor (RXR) complex, supposedly via binding and recruitment of the histone acetyltransferase NCOA1 to target promoters[84] (**Fig. 6A**). By contrast, the transcriptional activity of a different NR, peroxisome proliferater-activated receptor γ (PPARγ), is repressed in association with ASXL1. This occurs via ASXL1-mediated recruitment of Heterochromatin protein 1 (HP1), a factor shown to lock condensed chromatin[94], and is accompanied by an increase in H3K9 trimethylation[95] (**Fig. 6A**). Interestingly, ASXL2, which lacks the HP1 binding motif, increases the transcriptional activity of the NRs PPARγ, RAR and also the estrogen receptor[95,96], whereas ASXL3 with a retained HP1 binding box was found to repress the activities of RARα, the liver X receptor α and the thyroid receptor α[95,97]. PPARγ is associated with ASXL2 at selected promoter regions together with the TrxG protein MLL1, which is accompanied by locally increased levels of H3K9ac and H3K4me3. These reports demonstrate the opposing functions of ASXL1/ASXL3 and ASXL2 at a specific subset of shared target genes[95].

A recent study further extended the list of ASXL1-binding proteins by core members of the Cohesin complex, which function in separation of sister chromatids during mitosis[98], and it was suggested that via recruitment of Cohesin members, ASXL1 plays an important role in this process[90].

1.3.2.2 Interaction with Polycomb repressive complex 2

Despite the multitude of regulatory functions, members of the ASXL family are generally considered PcG co-factors. In fact, several reports have confirmed the integral function of ASXL1, and partially also of ASXL2, in recruitment of the PRC2 complex to promote global or local deposition of repressive H3K27me3 marks and gene silencing[99-103] (**Fig. 6B**).

In human leukemia cells, ASXL1 loss or knockdown leads to reduction in H3K27me3 levels at transcriptional start sites (TSSs) of predominantly bivalent genes, gene bodies and large H3K27me3 regions, and to de-repression of *HOXA* genes[99]. This effect is more pronounced upon complete knockout of *Asxl1* in hematopoietic lineages in mice[100,104]. Shown not to be mediated by transcriptional repression of the PRC2 complex, binding of EZH2 to *HOXA* genes is dramatically decreased when ASXL1 is downregulated or absent. The *HOX* loci, as well as other CpG-rich TSSs of PcG target genes, are co-bound

by ASXL1. Together with the observation that re-introduction of ASXL1 in knockdown cells or enhanced endogenous ASXL1 levels lead to an increase in H3K27me3 marks, these findings confirm a role of ASXL1 in the recruitment of EZH2 to target sites and promoting H3K27 trimethylation[88,99]. Of note, *Asx*^{Null} *Drosophila* embryos do not exhibit reduction in bulk H3K27me3 levels[105], although Asx has been shown to regulate H3K27me3 at target genes[75]. It is therefore suggested that Asx/ASXLs are involved in PcG recruitment in distinct cell types and/or at specific loci. Direct binding of ASXL1 to core PRC2 members EZH2 and SUZ12, but not to PRC1 members, was detected in hematopoietic and HEK293T cells[99].

ASXL2 loss also results in slight reductions of H3K27me3 levels, decreased PRC2 binding and de-repression of selected genes[103], which do however not include *Hox* genes in *Asxl2*-Null mouse hearts[102]. Interestingly, these effects are accompanied by increased deposition of H3K27me2, which supports a model of unspecific PRC2 binding and mono- and di-methylation of H3K27 by Ezh2, while efficient trimethylation requires tethering of the PRC2 complex through Asxl2[50,102]. This interaction however seems to be indirect or transient[103,106].

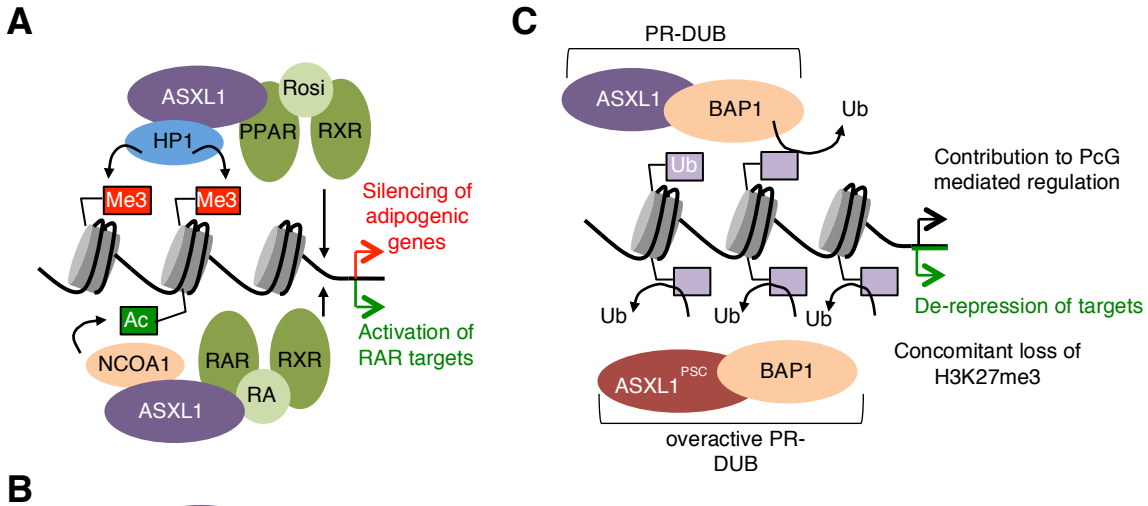

Figure 6. The diverse functionality of ASXL1 in transcriptional regulation relies on its association with nuclear receptors and enzymes.
(**A**) ASXL1 can bind several nuclear hormone receptors via its ASXM2 domain. In HEK293 and mouse preadipocyte fibroblasts, the association of ASXL1 with the peroxisome proliferator-activated receptor γ (PPAR) - retinoic x receptor (RXR)- complex in the presence of rosiglitazone (Rosi) inhibits the activation of adipogenic target genes through recruitment of heterochromatin protein-1 (HP1), which trimethylates H3K9. Conversely, binding of ASXL1 to the retinoic acid receptor (RAR)-RXR complex in the presence of retinoic acid (RA) results in activation of RA-target genes in HeLa cells, as ASXL1 additionally recruits the histone acteyltransferase NCOA1. (**B**) ASXL1 can recruit Polycomb-repressive complex 2 (PRC2) subunits EZH2 and SUZ12, which is important for H3K27me3 placement and silencing of bound targets. **(C)** The Polycomb repressive de-ubiqutination complex (PR-DUB), composed of ASXL1 and the de-ubiqutinase BAP1, is involved in PcG-mediated transcriptional regulation through removal of ubiquitin marks at H2AK119. Truncated variants of ASXL1 (ASXL1^{PSC}), which can be the result of mutations in leukemia cells, enhance the de-ubiqutinating activity of PR-DUB, resulting in loss of H2AK119 and H3K27me3, and gene de-repression. **(A-C):** from[69,84,95,99,100,107].

1.3.2.3 Formation of the PR-DUB complex

ASXL proteins act as regulatory switches also by regulating the Polycomb repressive de-ubiquitinating complex (PR-DUB). Scheuermann and colleagues coined this name in 2010, when they discovered the interaction between *Drosophila's* Asx and calypso, a histone de-ubiquitinating enzyme, which is conserved in the mammalian ASXL1-BAP1 complex[105]. BAP1 is a member of a family of ubiquitin carboxy-terminal hydrolases that act as ubiquitin proteases on diverse substrates in different cellular processes[108], and it is essential for mouse embryonic development[109].

By specifically erasing H2AK119Ub marks (**Fig. 6C**), the PR-DUB complex counteracts ubiquitination catalyzed by the RING1 enzyme in PRC1, a mark that is involved in chromatin compaction, gene silencing and recruitment of PRC2 complexes as mentioned earlier. Surprisingly, PR-DUB activity is nevertheless required for PcG-mediated silencing of *Hox* genes, as well as for their activation, and the complex is bound at regulatory regions of many PcG targets irrespective of their transcriptional status[105]. These seemingly contradictory observations imply an intricate balancing mechanism, which requires both ubiquitination and de-ubiquitination at least in the context of *Hox* gene regulation[105,110].

Knockout and Knockdown studies indicate that the roles of Asx/ASXLs in the PR-DUB complexes reside in the stabilization of calypso/BAP1 protein levels[105,111], and in facilitating the interaction of the catalytically active center of BAP1 with its substrate, thus enhancing the reaction[85]. All human ASXL paralogs can associate with BAP1, and their DEUBAD domains (**Fig. 5**) activate the de-ubiqutinating reaction [85,106,109,112,113]. ASXL1 and ASXL2 form mutually exclusive PR-DUB complexes that might be redundant, since in HeLa cells, only knockdown of both *ASXL1* and *ASXL2* leads to significant increase in H2AK119Ub levels, and not all *Asxl1* Knockout studies report alterations in H2AK119Ub levels[104,111]. BAP1 also positively affects expression and protein levels of ASXL1 and ASXL2[88,111], and although it was suggested that this does not occur through de-ubiqutination of the proteins themselves, this point might require further analysis[88]. BAP1 assembles additional proteins including HCF1, a transcriptional co-regulator, OGT, KDM1B, FOXK1/2 and YY1[109,114], and may thus form a platform for different co-factors with diverging functions.

Interestingly, mutant variants of the ASXL1 protein can arise as a consequence of leukemia-promoting mutations, which generate premature stop codons (PSC) in the *ASXL1* transcript[69,88]. These truncated forms (ASXL1^{PSC}) can bind to BAP1 and strongly stimulate the catalytical function, resulting in massive de-ubiquitination and concomitant reduction in H3K27me3 levels (**Fig. 6C**). These findings provide a novel mechanism for transcriptional dysregulation in myeloid malignancies[69].

1.3.3 ASXLs in embryonic development

Regulation of *Hox* genes is an important task of Asx during *Drosophila* embryogenesis[78], and an evolutionary conserved developmental function that expanded to other genes and organs with the diversification of the ASXL family in mammals.

This is evident by the expression of all *Asxl* paralogs during mouse embryonic development[115]. Specifically, *Asxl1* and *Asxl2* transcripts are expressed in the egg and in the pre- and the postimplantation embryo, and are presumably regulated in a coordinated manner, whereas the expression of *Asxl3* is restricted to mid-gestation and to post-natal pups at low levels[115]. Expression of *Asxl1* and *Asxl3*, albeit the latter in

lower levels, in neuroectodermal tissues suggest a role in brain and/or eye formation, which is supported by the complete absence or reduced size of eyes in *Asxl1* null mice[100,116]. These mutants exhibit embryonic lethality on a pure inbred background, with resorbed embryos found as early as day 12.5 of gestation, whereas homozygous progeny of mixed background die postnatally at day 3. They show reduction in body size, decreased kidney size, reduced thymus and testis weight, splenomegaly, defects in lung maturation, cleft palate, skeletal transformations and reduced skull size[100,107,116-118]. Heterozygous animals displayed craniofacial features in 35 % of cases in one study[100]. In accordance with positive and negative misregulation of *Hox* genes, both *Asxl1* and *Asxl2* null embryos exhibit mild anterior and posterior transformations, visible in skeletal abnormalities[100,116,119]. Notably, also ASXL3 seems to be involved in the regulation of *HOX* genes, as seen in *ASXL3*-deficient human fibroblasts[112].
Asxl1 seems to be important for self-renewal of hematopoietic stem cells as well as erythroid development and terminal maturation, presumably via regulating PcG-mediated histone modifications[100,104]. *Asxl2* takes over non-redundant functions in the maintenance of hematopoietic stem and progenitor cells[103], whereas *Asxl3* is not expressed during hematopoiesis[120]. Apart from the hematopoietic lineage, *Asxl1* seems to regulate the self-renewal of skeletal stem cells, and *Asxl1* ablation skews their differentiation from osteoblasts to adipocytes[118]. This contrasts *in vitro* studies, which reported repression of adipocyte fate by *Asxl1*, and activation of adipogenesis by *Asxl2* in pre-adipocyte murine cell lines[95].
Furthermore, both *Asxl1* and *Asxl2* are important for different aspects of heart development. Depletion of *Asxl2* or *Asxl1* leads to heart defects of different penetrance and pathologies, and each gene cannot compensate for mutations in the other paralog[107,119]. Asxl2-mediated recruitment of PRC2 to promoters of specific cardiac genes and their repression via maintenance of H3K27me3 marks seems to be involved both in embryonic heart formation and adult heart function[102,106,119]. In general, *Asxl2* null mice exhibit less severe phenotypes compared to *Asxl1* null mutants, with reduced body size and perinatal death[102,107,119]. Some features in *Asxl2* null mice were attributed to regulation of skeletal homeostastis, as it was proposed that Axl2 regulates osteoclastogenesis[96,121], which is the generation of bone-absorbing cells from hematopoietic progenitor cells[122].
Taken together, animal models revealed roles of *Asxls* in regulation of fetal development, specifically *Hox* genes, craniofacial development, proliferation and differentiation of progenitor and stem cells in the hematopoieitic system and in the lung, kidney development, heart and bone formation, adipogenesis and lipid and insulin homeostasis. These findings mainly stem from analyses in mouse models. The functions of ASXL proteins in human cell systems have not been investigated thus far, although the involvement of *ASXL* genes in human diseases suggests important functions in development and tissue homeostasis.

1.3.4 Mutations in *ASXL* genes cause human diseases

1.3.4.1 ASXL genes and cancer

The contribution of *ASXL* genes to the control of proliferative processes[100,103,113,118] is evident from their involvement in tumorigenesis[79].
ASXL1 is among the most frequently mutated genes in all types of malignant myloid diseases[123,124]. Strikingly, the exclusively heterozygous mutations predominantly reside

in the last exon of *ASXL1*, indicating a 'mutation hotspot' (see highlighted region in **Fig. 5A**). They are predominantly frameshift or nonsense and thus generate PSCs, which implies production of a truncated protein, excluding the functional NR binding motif as well as the putative histone-interacting PHD domain[79]. Nevertheless, the exact pathogenic mechanism has not yet been clarified. It was suggested that rapid degradation of mutant *ASXL1* isoforms results in loss of *ASXL1* expression in cell lines derived from myeloid leukemia patients[99,125]. However, new data links putative *ASXL1* truncating mutations to PcG misregulation. One study reported that truncated *ASXL1* variants are not degraded but are in fact as stable as the long, native *ASXL1* transcript in leukemia cell lines[126]. When ectopically expressed, ASXL1 variants encompassing the N-terminal 635 or 646 amino acids inhibit hematopoietic differentiation in precursor cells and act as drivers of myelodysplastic syndrome in mice[101]. On the molecular level, the truncated isoform leads to global reduction in H3K27me3 levels and upregulation of PRC2 target genes, including the posterior *HOXA* genes, which supports the hypothesis that truncated ASXL1 proteins are dominantly acting and hamper EZH2 recruitment or function.
A different hypothesis was brought forward by Balasubramani *et al*, who noted that exogenous truncated ASXL1 expression promotes global reduction of H2AK119Ub, which is indicative of increased activation of the PR-DUB complex. This was followed by a reduction in H3K27me3 levels and skewed differentiation in hematopoietic precursor cells[69]. The temporal order of histone modification events suggests that the loss of H2AK119Ub signals might hinder recruitment of PRC2 complexes. Recent studies that expressed truncated Asxl1 in mouse models have confirmed a dominant effect of the mutant protein in the progression to myeloid malignancies in cooperation with additional factors[127,128].
Regarding mutations in the other *ASXL* paralogs that were linked to tumorigenesis, no studies exist on their molecular mechanisms. Mutations in *ASXL2* were identified in myelodysplastic syndrome and acute leukemia as the second most frequent hit after the *KIT* gene, both in pediatric and adult cases[129]. *ASXL3* mutations were described in various malignancies, but rarely in myeloid disorders[129,130].
In conclusion, perturbation of *ASXL* function in somatic tissues can contribute to cancer progression, potentially via the production of dominant protein isoforms.

1.3.4.2 Bohring-Opitz syndrome

In 2011 and 2012, two exome-sequencing studies identified heterozygous, truncating mutations in the *ASXL1* gene as a cause for Bohring-Opitz-Syndrome (BOS), a human congenital defect described initially in 1975[131-135]. The characteristic symptoms that clinically define BOS include microcephaly and trigonocephaly, severe feeding difficulties, craniofacial dysmorphisms, intrauterine growth restriction, severe developmental delay, intellectual disabilities, and a specific limb posture with contractures of the upper limbs[131,132,136] (BOS posture; **Fig. 7 A-C**, **Table 2**). Craniofacial features comprise prominent eyes, an abnormal, and less commonly cleft palate, retrognathia (overbite), anteverted nares, nevus flammeus (port-wine-stain) on the forehead, upslanted palpebral fissures (upslanted eyes) and rarely ocular hypertelorism (wide-set eyes) (**Fig. 7 A-B**, **Table 2**). Further symptoms found at varying penetrance in the patients are vision impairment and ophthalmic features, seizures, episodes of sleep apnea, brain malformations including Dandy-Walker malformation and agenesis of

the corpus callosum, cyclic vomiting, genital abnormalities and heart defects[131,132,136,137]. Thus, neonatal presentation is variable, which renders initial diagnosis challenging. Interestingly, BOS cases show comparable frequencies of symptoms irrespective of the presence of absence of *ASXL1* mutations, which implies a commonality of the underlying molecular pathways. However, hypertrichosis/hirsutism, *i.e.* abnormal hair growth, and myopia are strongly correlated with perturbation of the *ASXL1* locus, suggesting an exclusive link[134,137].

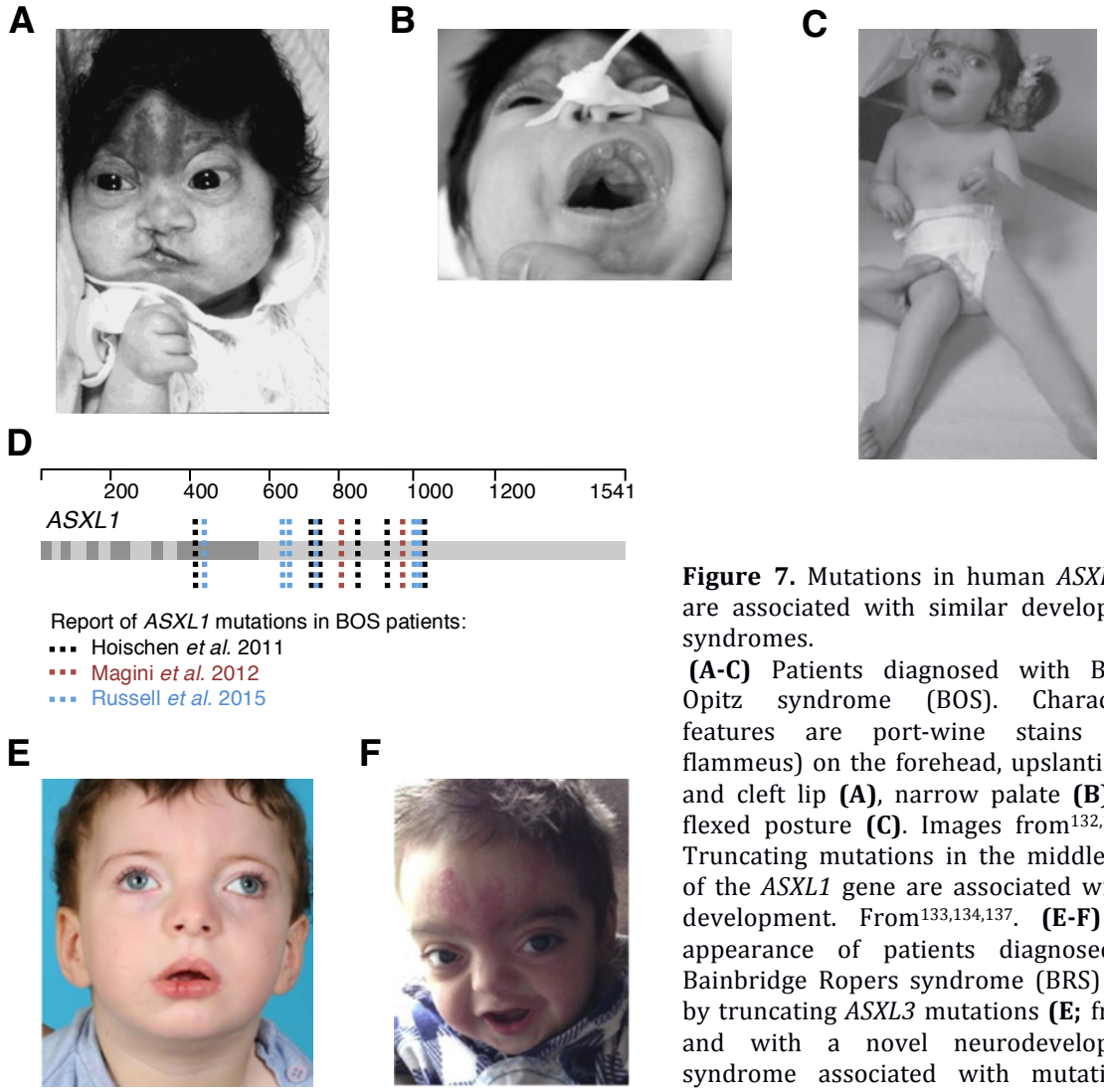

Figure 7. Mutations in human *ASXL* genes are associated with similar developmental syndromes.
(A-C) Patients diagnosed with Bohring-Opitz syndrome (BOS). Characteristic features are port-wine stains (nevus flammeus) on the forehead, upslanting eyes and cleft lip **(A)**, narrow palate **(B)** and a flexed posture **(C)**. Images from[132,135]. **(D)** Truncating mutations in the middle region of the *ASXL1* gene are associated with BOS development. From[133,134,137]. **(E-F)** Facial appearance of patients diagnosed with Bainbridge Ropers syndrome (BRS) caused by truncating *ASXL3* mutations **(E;** from[138]), and with a novel neurodevelopmental syndrome associated with mutations in *ASXL2* **(F;** from[139]).

BOS patients are at high risk of death during early infancy, which is mainly caused by recurrent respiratory infections[137]. These, together with persistent feeding difficulties observed in all patients, require repeated hospitalizations[137]. While these symptoms generally improve with age, the specific BOS posture impedes or entirely prevents for patients to sit or walk on their own, and severe intellectual disabilities contribute to the lack of speech and reduction in purposeful movements[132,137].
To date, there are 51 BOS cases documented in the literature, of which 17 were tested positive on *ASXL1* mutations[133,134,137]. Strikingly, similar to the myeloid diseases, all of

these mutations are frameshift or PSC-gain and lie in the penultimate or last exon of *ASXL1* (**Fig. 7D**), suggesting similar mechanisms. Although leukemia was not reported in any of the BOS patients with *ASXL1* mutations so far, Wilms tumor developed in the kidneys of two patients[137]. This is noteworthy since murine Asxl1 binds to Wtip, the Wilms tumor 1-interacting protein[117]. As described above, *Asxl1* null mice show partial phenotypic overlap with human BOS symptoms, including low birth weight, craniofacial features and heart defects[100,107,118]. However, it is not yet clear whether BOS-causing mutations result in *ASXL1* loss of function or a dominant functionality of the truncated protein. The pending clarification of a molecular etiology is of special importance, as the other *ASXL* family members are likewise implicated in congenital malformations.

1.3.4.3 ASXL2- and ASXL3-associated human disorders

Two human syndromes with manifestations resembling those of BOS have been attributed to mutations in *ASXL2* and *ASXL3*[139,140].

Bainbridge-Ropers syndrome (BRS) is clinically defined by the presence of mild craniofacial dysmorphisms, absence of speech, hypotonia, developmental delay, failure to thrive and severe feeding difficulties, intrauterine growth restriction, and gastrointestinal symptoms, and has been linked to exclusively truncating mutations in the penultimate or last exon of *ASXL3*[112,138,140] *(***Fig. 7E, Table 2***)*. In total, 29 BRS patients have been described to date with mutations in the *ASXL3* locus, and they show variable degrees of symptomatic severity, also including less prominent features as slender habitus, little facial expression, mild autism, sleeping disorders and very rarely trigonocephaly[112,138,140-143]. Arguing for a role in neuronal development, missense mutation in *ASXL3* have also been described in individuals with autism spectrum disorders[144].

Most recently, a novel neurodevelopmental syndrome, hereafter termed NDS, was defined by a distinct set of symptoms and presence of heterozygous truncating variants in the penultimate or last exon of *ASXL2*[139]. The six patients presented variable developmental and intellectual impairments, macrocephaly, specific facial features, congenital heart disease, feeding difficulties and hypotonia *(***Fig. 7F, Table 2***)*.

It is striking that all known *ASXL*-related congenital disorders are associated with mutations in analogous regions, which suggests a common pathological mechanism. One group reported reduced *ASXL3* expression in BRS patient-derived fibroblasts, coupled to increased H2AK119Ub levels due to impaired PR-DUB activity[112]. On the other hand, both the wildtype and mutant alleles of *ASXL2* and *ASXL3* were reported to be expressed at equal levels in NDS- and BRS patient-derived cells, respectively, in other studies[139,140]. This argues against loss-of-function variants and suggests common pathogenic mechanisms.

The intricate chromatin-related molecular coupling behavior of ASXLs likely contributes to the broad spectrum of symptoms and affected tissues in these human disorders. Conceivably, *ASXL* mutations might also perturb the development of embryonic cell types that contribute to a broad variety of adult tissues. The neural crest constitutes a candidate cell population in this context, as it is multipotent and involved in many common birth defects including craniofacial dysmorphisms.

Table 2. Main clinical features of human diseases associated with mutations in *ASXL* genes. NA, not available/unknown. From[137,139].

	Bohring-Opitz Syndrome (BOS)	**Bainbridge-Ropers Syndrome (BRS)**	**ASXL2-associated syndrome**
Gene mutation	Truncating mutation in ***ASXL1***	Truncating mutation in ***ASXL3***	Truncating mutation in ***ASXL2***
Prenatal	IUGR	IUGR	no findings
Growth parameters	Severe growth retardation, microcephaly	Severe growth retardation, microcephaly	Variable, macrocephaly
Nutrition	Severe feeding difficulties	Severe feeding difficulties	Only neonatal problems
Hypotonia	Present	Present	Present
Intellectual disabilities	Severe	Severe	Variable, from moderate to severe
Seizures	Present	NA	Variable
Brain MRI	Brain abnormalities (Dandy Walker malformation, agenesis of corpus callosum)	Brain abnormalities (Dandy Walker malformation, white matter volume loss)	Brain abnormalities (white matter volume loss)
Craniofacial features	Trigonocephaly, prominent eyes, ocular hypertelorism, retrognathia, low-set posteriorly rotated ears, high narrow palate, cleft palate, upslanting palpebral fissures, prominent forehead	Prominent eyes, ocular hypertelorism, arched eyebrows, anteverted nares, low-set posteriorly rotated ears, high narrow palate, high and broad forehead	Prominent eyes, ocular hypertelorism, low-set posteriorly rotated ears, broad nasal tip, ptosis of eyelids, arched eyebrows, epicanthal folds
Hair/Skin	Nevus flammeus, hypertrichosis	deep palm creases, hypertrichosis	Deep palm creases, nevus flammeus
Skeleton	Scoliosis, ulnar deviation of hands, flexed wrists and elbows	Ulnar deviation of hands	Variable (advances bone age, fractures, fusions, scoliosis)
Heart	Atrial and ventricular septal defects	Patent ductus arteriosus	Atrial septal defects
Eyes	Myopia, retinal/optic-nerve abnormalities, strabismus	-	-
Infections	Recurrent infections	-	-

1.4 The neural crest: A versatile embryonic cell population

The neural crest (NC) is a multipotent, transient embryonic cell population that only exists in vertebrates[145]. After establishment of their NC identity, cells migrate over long distances in the embryo, invading various organs and differentiating into a plethora of cell types, including striated muscle, dermis, cartilage and bone of the skull, odontoblasts that contribute to the teeth, all pigment cells except those arising from the retina, sensory neurons and enteric ganglia in the peripheral nervous system, adrenal and other endocrine cells, smooth muscles, adipocytes and connective tissue supporting

the function of thymus, the thyroid glands, the outflow tract of the heart and the branchial vascular sector[35,146,147]. No other embryonic lineage generates such a diverse spectrum of derivatives[35]. This enormous developmental potential demands tight control of NC induction, proliferation, migration and terminal differentiation; otherwise, perturbations of NC development lead to congenital defects[146]. Studies in *Xenopus*, chicken, qail, zebrafish and mouse embryos have provided initial insights into a generally conserved transcriptional network regulating the different steps of NC development.

1.4.1 The transcriptional network directing neural crest identity

NC progenitors arise in an area between the neural plate, which is the precursor of the central nervous system, and the adjacent ectoderm during early gastrulation[148]. This region, termed the neural plate border (NPB), is formed by a combination of signals derived from interactions between the neural plate, the non-neural ectoderm and the underlying paraxial mesoderm, and include intermediate levels of BMP signaling together with high levels of Fibroblast Growth Factors (FGF), Wnt, RA and Notch signaling[149] (**Fig. 8A**). Interestingly, binding sites for WNT and BMP-signaling effectors were identified at human NC cell enhancers, suggesting conservation of instructive mechanisms during NC fate decisions[150].

Integration of these different signals induces the expression of the so-called NPB specifiers, which include *Tfap2, Msx1, Zic1, Gbx2, Pax3/7, Dlx5/6, Gata2/3, Foxi1/2* and *Hairy2*[151]. They form a self-maintaining regulatory network that confers NPB identity, separating future NC from the neighboring central nervous system. The NPB specifiers, most importantly *Pax3/7, Msx1* and *Zic1,* in concert with reiterated signaling by the above-mentioned pathways activate the next set of regulatory factors, the NC specifiers[151] (**Fig. 8A**).

The NC specification module includes *c-Myc, Ets1, FoxD3, Tfap2a, Snail1/2, Id*, and the *SoxE* family members (mainly *Sox9* and *Sox10*); importantly, the majority of NPB and NC specifiers were confirmed to be important for human NC formation *in vitro* as well[150,152,153]. Thus, at the time the neural tube closes, nascent NC cells situated at the dorsal neural folds are identified by robust expression of an autoregulatory and interconnected combination of factors centered around *FoxD3, Snail1/2* and *Sox8/9/10*[151]. Of note, expression of several NPB specifier genes can be maintained at this stage, e.g. *Zic1, Tfap2a* and *Msx1*[151]. The NC specifying network has two main functions: maintaining the developmental plasticity of the NC population, and initiating the next step of NC development, their emigration[149] (**Fig. 8A**).

Delamination of NC cells from the neuroepithelium requires enormous transcriptional and structural changes that start the migratory program via an epithelial-to-mesenchymal transition (EMT). The global *E-Cadherin* to *N-Cadherin* switch in pre-migratory cells[154], mediated by the combinatorial action of NC specifiers in combination with Wnt signaling, is one of the main drivers of EMT, delamination and dispersion of NC cells[151,155,156]. Among the few studies on epigenetic regulation of NC development[150,157-159], it was shown that the PRC2 complex is recruited by Snail2 and important for *E-Cadherin* downregulation in *Xenopus*[160], while the PBAF remodeling complex in cooperation with CHD7 promotes transcription of important TFs, including *SOX9* and *TWIST1,* to activate the migratory program in human NC cells[33]. Essentially, interactions within the migratory module of the NC regulatory network equip NC cells with the

molecular machinery needed for migration, invasion, remodeling of the extracellular matrix and activation of distinct differentiation programs[161] (**Fig. 8A**).

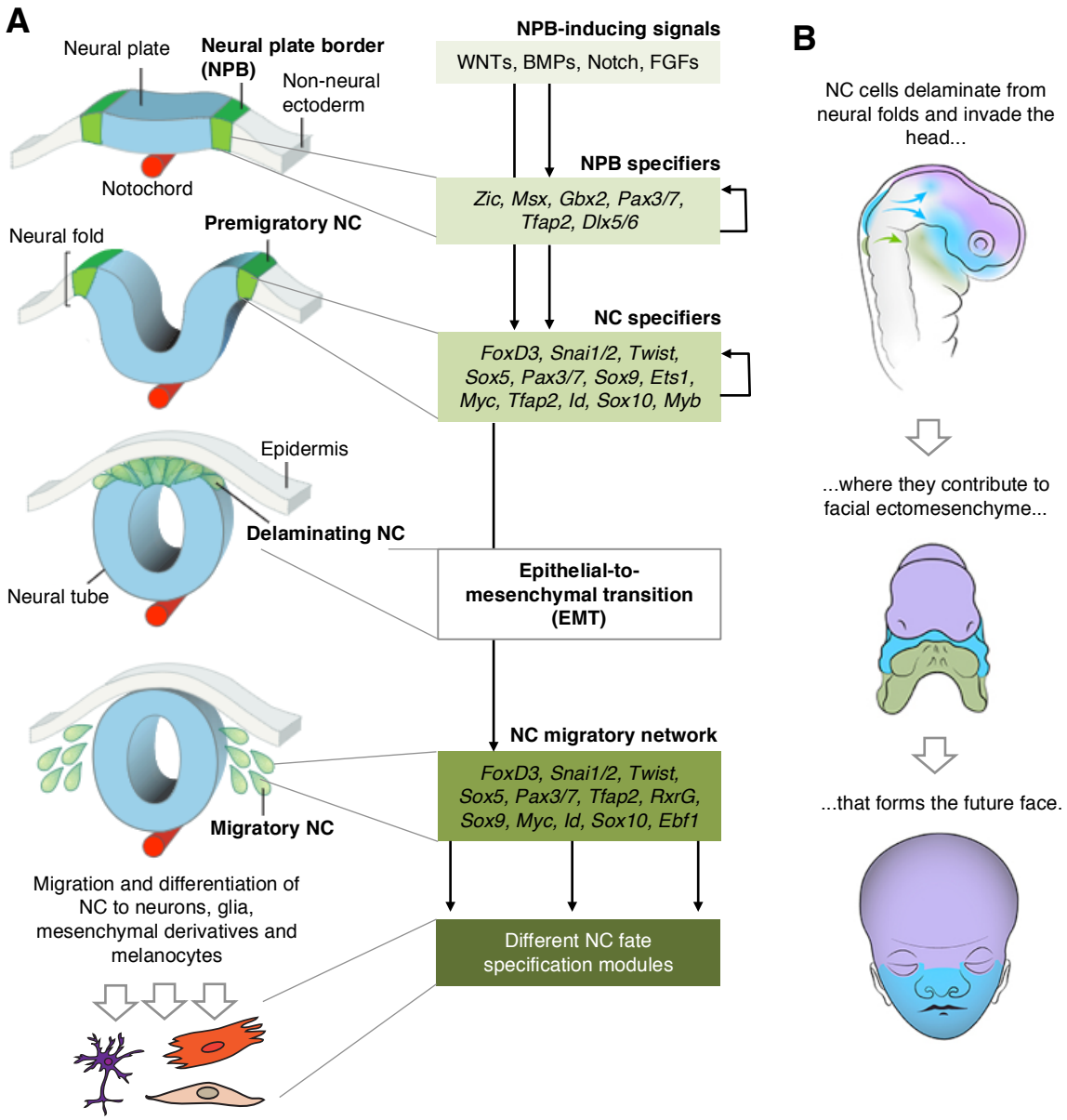

Figure 8. Neural crest (NC) development and contribution to craniofacial tissues. **(A)** NC development occurs in several steps, which are characterized by expression of different modules of a gene regulatory network in *Xenopus*, zebrafish and chicken. Signaling pathways, including WNT, BMP, Notch and FGF, induce the formation of the neural plate border (NPB), which is characterized by the expression of NPB specifiers. This set of genes, together with reiterated WNT and FGF signaling pathways, activates the NC specifier module, which is responsible for equipping premigratory NC cells with a molecular toolset for their delamination from the dorsal neural tube. This includes an epithelial-to-mesenchymal transition (EMT) and activation of the NC migratory expression module. After migration and invasion of target organs, post-migratory NC cells differentiate into a variety of derivatives, depending on external stimuli that modulate internal differentiation programs. From[158]. **(B)** Different NC subpopulations (highlighted by different colors), reflecting regionalization of the body axis, emigrate from their position of birth at the neural folds. Cranial NC cells migrate into the head region and organize the formation of craniofacial structures, which are colored depending on the NC population that contributed to their development. From[162].

1.4.2 The fate of neural crest cells

Even after delamination, the majority of NC cells maintain multipotency[163]. While migrating, NC cells encounter environmental cues presented by surrounding tissues, which cooperatively with cell-intrinsic properties dictate their terminal identity by activation of tissue-specific regulatory networks[164]. The diversification of NC cells is also guided by already active transcription and signaling networks, including *Sox10* and Wnt signaling, which promote the derivation of neurons, glia and melanocytes from NC cells[165], while BMP signaling is involved in their differentiation to smooth muscle cells, and also in the formation of the autonomous nervous system[166].
Two major subpopulations, cranial and trunk NC cells, emigrate from the neural tube and contribute to overlapping, but also distinct sets of derivatives. Trunk NC cells colonize the entire gut wall, forming all neurons of the enteric system[166], and also contribute to the sympathetic ganglia and the dorsal root of the peripheral nervous system[167].
The cranial NC populates the developing pharyngeal arches and the head region, contributing to formation of heart (vagal NC subpopulation), thymus and craniofacial structures[158]. NC-derived ectomesenchyme forms the future face and head in an intricate process of continuous interactions between multiple other ectodermal, mesodermal and endodermal cell populations[162,168,169] (**Fig. 8B**). Frontal bone formation from the cranial NC is driven by FGF, canonical WNT and sonic hedghehog (SHH) signaling and other molecules, as well as *Msx2, Tfap2a* and *Sox10* expression[170-172]. The NC also contributes to smooth muscles, cartilage, pigment cells and blood vessels of the face, strongly influencing the facial appearance[173]. In accordance, mutations in genes that are important for NC development result in congenital birth defects including craniofacial abnormalities[172].

1.4.3 Neurocristopathies

Abnormal development of the NC in response to genetic mutations that affect NC proliferation, migration, survival or differentiation leads to organ and tissue defects that are collectively termed neurocristopathies[35,146]. Among the most frequent pathologies in this group are DiGeorge's syndrome, Goldenhar's syndrome, Waardenburg's syndrome, CHARGE syndrome and Treacher Collins syndrome[35,146]. Mutations in known NC specifier genes are often observed in these disorders, and correspondingly to the diverse array of NC derivatives, common symptoms include lack of outflow tract septation, partial lack of enteric ganglia (aganglionosis), hearing loss, mandible defects, cleft palate and pigmentation defects[35].
CHARGE, which is an acronym for the characteristic symptoms (colonoma of iridis, heart defects, atresia choanae, retarded growth, genital hypoplasia, ear anomalies) observed in this syndrome, is attributed to mutations in *CHD7*[41,174]. This chromatin modulator cooperates with SOX2, SOX9 and SOX10 in regulating NC specification[33,175], and loss of *CHD7* in human pluripotent stem cells leads to defective delamination and migration, and reduced motility of derived cranial NC cells[33,41]. Impaired migration of NC cells is also implicated in Hirschsprungs disease, where a lack of enteric NC results in reduced innervation of the intestine[35]. Furthermore, neurocristopathy-related mutations often manifest in abnormalities of the craniofacial skeleton through defective patterning of cranial NC cells, as seen in Treacher Collings syndrome[172].

It was estimated that over 500 mendelian congenital disorders likely involve NC perturbation[150], which makes the case for the importance of understanding human NC development.

1.4.4 *In vitro* generation and maintenance of human NC cells

The vast majority of knowledge on the factors that drive and regulate NC development is extrapoplated from animal models to the human case. While many interactions and instructive signals are conserved, mammalian evolution is undoubtedly accompanied by shuffling of regulatory networks[176]. Hence, to better understand human NC specification, differentiation and related pathologies, NC developmental processes have to be investigated in cell culture experiments.

Differentiation of hESC or hiPSC to migratory NC cells *in vitro* follows the same gene cascades that also regulate embryonic NC development, confirming the conservation of master regulators including *PAX3, TFAP2A, ZIC1, TWIST1, SNA1, SLUG, MSX1/2* and *SOX10*[150,152,153,177,178]. Approaches are generally based on defined culture conditions, and initial protocols made use of unspecific instructive signals by stromal feeder cells[179,180]. Several feeder-free systems rely on variations of N2 (/B27) medium complemented with BMP and Transforming Growth Factor β (TGFβ) inhibitors, WNT activation and/or addition of FGF and Epithelial Growth Factor (EGF), some of these via formation of neural rosettes or neurospheres that resemble neural tube structures[33,34,181-183]. Isolation of pure NC populations from heterogeneous neural precursor cultures is based on the expression of conserved markers including *TFAP2A, POU4F1, SOX10, p75* and *HNK1*, although it was reported that *HNK1* does not label all migratory cells in human embryos[184]. The identity of *in vitro* generated NC cells is furthermore confirmed via terminal differentiation into their derivatives, as well as in grafting experiments that confirm *in vivo* migration capabilities[179,185].

Generation of human NC cells *in vitro* has been proven to be a very useful tool to model neurocristopathies like CHARGE syndrome, understanding molecular etiologies and identifying new targets for therapeutic intervention[33,34]. Furthermore, the differentiation of patient-derived iPSC, corrected for their disease-specific mutations, offers the possibility to modulate or restore diseased tissues through autologous transplantation[172,186,187]. Just recently, tissue-engineered human small intestine models were repopulated with enteric NC cells derived from human pluripotent stem cells, resulting in functional innervation, which demonstrates the feasibility of regenerative therapies in disorders like Hirschsprung's disease[188].

In all, future work on human NC derivation *in vitro* will likely give new insights in normal and pathological NC development, and should meet the challenges of safe derivation and efficient homing and function of NC cells in target tissues to enable their use in human therapies.

1.5 Aim and impact of this work

During the last years, an increasing list of human congenital syndromes has been attributed to perturbations in *ASXL* genes. While this indicates consistency with findings on Asx(l) functions during mouse and fly development, there is a lack of corresponding studies elaborating on possible developmental roles of the human counterparts.
Based on the symptoms linked to heterozygous mutations in *ASXL* genes and their embryonic origin and impact on prenatal growth and morphogenesis, I hypothesize that ASXL proteins occupy fundamental positions in the orchestration of early human developmental programs. Therefore, I seek to identify how ASXL1 contributes to the commitment and maturation of embryonic lineages on the cellular and molecular level. My focus is set on *ASXL1* firstly because BOS is relatively severe, and secondly due to its manifold functions in transcriptional regulation. How these are involved in the pathogenesis of BOS is currently not known, and I want to clarify whether and how reduction in *ASXL1* levels or dominant mutant variants contribute to the emergence of BOS symptoms.
Findings from this work might likewise be relevant to hematological disorders, since truncating mutations in *ASXL1* are causative to BOS as well as human leukemias. Some advances were already made in the context of tumorigenesis, suggesting that malignant processes might arise from perturbed regulation of ASXL1 with PRC2 and PR-DUB. Developmental tasks of these complexes have been predicted before[105], and can be inferred from embryonic defects in Polycomb mutants[189]. This motivates my investigations on PRC2- and BAP1-associated functions of ASXL1 during differentiation of embryonic lineages.
Prior to this undertaking however stands the identification of embryonic tissues that are influenced by ASXL1 regulation. Craniofacial features in BOS conceivably argue for an involvement of the NC, and this hypothesis is compliant with published expression patterns of *Asxl1* in murine NC-associated tissues[115]. I want to scrutinize an involvement of *ASXL1* and BOS-associated *ASXL1* mutations in NC development as a conceivable mechanism underlying the congenital birth defects in BOS patients. Potential findings might furthermore expand the still very limited knowledge of epigenetic regulation during NC specification and differentiation[157].
In summary, I define the purpose of the following work as an attempt to advance insights into ASXL1 regulation of differentiation: in i) normal and ii) BOS-associated pathological development of embryonic lineages, specifically the NC, and iii) Polycomb-mediated epigenetic regulations involved therein. Thus, this study should stand as a paradigmatic case for pathological development arising from *ASXL* mutations, and my endeavors should be an important foundation for future research on therapeutic intervention in related disorders. On a more basic level, ASXLs might be important regulatory factors that integrate positive and negative signals during lineage commitment and confer specificity to PcG-associated regulations. Novel findings should thus add to the understanding of the mechanisms that control human embryonic development and NC development, which is fundamental to the development of safe cell-based therapies in the culture dish.

2. Materials and methods

2.1 Materials

2.1.1 Cell culture media, supplements and small molecule inhibitors

Reagents are further specified in the respective sections of the experimental procedures where they were applied. Reagents and supplies routinely used in cell culture are listed in **Table M1** below.

Table M1. Media, supplements and equipment used in cell culture experiments. cat. #, catalogue number.

Reagent	cat. #	Supplier
2-Mercaptoethanol	31350-010	Life Technologies
Accutase	A6964-100ML	Sigma-Aldrich
B27 Supplement	17504044	Life Technologies
BMP-2 (recombinant)	0120-02-10	PeproTech
Bovine Serum Albumin (BSA), Cell Culture Grade	10773877	Thermo Fisher Scientific
Cell scraper	sc-213230	Santa Cruz
CHIR99021	4953/50	R&D Systems
Collagenase, type IV	17104019	Life Technologies
Cryotubes	10577391	Thermo Fisher Scientific
DMEM	21969035	Life Technologies
DMEM/F12	11320074	Life Technologies
DMSO	D5879-100ml	Sigma-Aldrich
Dorsomorphin	3093	Tocris
Doxycycline hydrochloride	D9891-1G	Sigma-Aldrich
EGF	E9644-.2MG	Sigma-Aldrich
Fibronectin from human plasma	F1056-1MG	Sigma-Aldrich
Gelatin, powdered, pure Ph. Eur., NF	A1693.0500	AppliChem
Geltrex Basement Membrane Matrix	A1413302	Life Technologies
Gentle Cell Dissociation Reagent	7174	STEMCELL technologies
GlutaMAX, 100X	35050038	Life Technologies
HyClone™ Fetal Bovine Serum (South America), Research Grade	SV30160.03 LOT #RZB35918	GE Healthcare
Insulin	12585014	Life Technologies
Knockout-Serum Replacement (KSR)	10828028	Thermo Fisher Scientific
Matrigel-Matrix	354230	Corning
MEM Non-Essential Amino Acids Solution (NEAA, 100X)	11140050	Thermo Fisher Scientific
mFreSR™	5855	STEMCELL technologies
Millex-GP Syringe Filter Unit, 0.22 µm, polyethersulfone, 33 mm, gamma sterilized	SLGP033RS	Merck Millipore
mTeSR1 medium	5850	STEMCELL technologies
N2 Supplement	17502048	Life Technologies
Neurobasal Medium	21103049	Life Technologies
Phosphate-buffered Saline (PBS), 1x	14190094	Life Technologies
Penicillin-Streptomycin	15070063	Life Technologies
Recombinant Human FGF-basic (154 a.a.; bFGF/FGF-2)	100-18B	Peprotech
StemMACS iPS-Brew XF	130-104-368	Miltenyi Biotec
StemMACS SB431542 in Solution	130-106-543	Miltenyi Biotec
Trypsin-EDTA (0.25%), phenol red	25200056	Thermo Fisher Scientific
Y-27632 dihydrochloride (ROCKi)	1254/10	R&D Systems
µ-Slide 8 Well, ibidi-treat	80826	Ibidi

2.1.2 Cell lines

Two different human embryonic stem cell lines, H9 (WA09) and HUES9 iCas9[190] were used in this work as control lines and for genetic engineering purposes as outlined in the respective methods sections below. The iCas9 line bears a genomic integration of the endonuclease Caspase 9 (Cas9), expression of which can be induced by administration of doxycycline (DOX) to the culture medium[190] .
For comparison to the BOS patient-derived iPSC that were generated during this study (see section **2.2.2**), two control hiPSC lines were applied. These were generated by E. Rusha and Dr. Pertek at the hiPSC Core Facility of the Helmholtz Center Munich, Germany via reprogramming of fibroblasts from a healthy 2-year-old donor using modified mRNA (for details on the reprogramming method, see[191]), and via reprogramming of B-lymphocytes derived from a healthy 12-year-old donor via 4-in-1-mini-intronic plasmids[17].

2.1.3 Chemicals

All chemicals were of reagent grade; routinely used reagents are denoted in **Table M2** below.

Table M2. Chemicals, reagents and solutions routinely used in this study.

Reagent	cat. #	Supplier
16% Formaldehyde (w/v), Methanol-free	10321714	Thermo Fisher Scientific
2-Mercaptoethanol	M3148	Sigma-Aldrich
Albumin from bovine serum (BSA)	A9647-10G	Sigma-Aldrich
Ampicillin sodium salt	A-166	Sigma-Aldrich
Biozym LE Agarose	840004	Biozym
Boric acid, electrophoresis grade	15166.02	Serva Electrophoresis
DAPI Nuclear Staining Dye	1351303	Bio-Rad Laboratories
DNA Gel loading dye, 6x	R0611	Thermo Fisher Scientific
Dynabeads(R) Protein A for Immunoprecipitation	10001D	Life Technologies
EDTA Dinatriumsalz Dihydrat >99%	X986.1	Carl Roth
EGTA	3054.1	Carl Roth
Ethanol, 99.8%	9065.2	Carl Roth
Ultra pure glycerol	15514011	Thermo Fisher Scientific
Glycine	23391.02	Serva Electrophoresis
HEPES, 1M Buffer Solution	15630122	Life Technologies
Isopropanol	6752.2	Carl Roth
Potassium hydroxide (KOH)	6751	Carl Roth
Lithium chloride (LiCl)	62480-500G-F	Sigma
Lithium Acetate dihydrate, 98%	15157442	Thermo Fisher Scientific
Methanol	45631.02	Serva Electrophoresis
Magenesium chloride (MgCl2)	KK36	Carl Roth
Na-deoxycholate	D6750-10G	Sigma-Aldrich
NaHCO3	S5761	Sigma-Aldrich
Tergitol type NP-40 70% solution	NP40S	Sigma-Aldrich
Nuclease-free water (H2O)	AM9932	Life Technologies
Phenylmethylsulfonylfluorid (PMSF)	6367,1	Carl Roth
Powder Milk, blotting grade	T145.1	Carl Roth
Protease Inhibitor Cocktail Set III, EDTA-Free	539134	Merk Millipore
Ribonucleic acid, transfer from bakers yeast (tRNA)	R5636-1ML	Sigma-Aldrich
SDS Solution, 20 %	20768.02	Serva Electrophoresis
Sodium Chloride (NaCl)	P029.2	Carl Roth

SYBR® Safe DNA Gel Stain	5001208	Life Technologies
TE buffer, pH 7.4, RNAse free	93302	Sigma-Aldrich
TRIS PUFFERAN®	5429.3	Carl Roth
Triton™ X-100	X100-500ML	Sigma-Aldrich
Tween(R)-20	P9416	Sigma-Aldrich

2.1.4 Kits

Kits that were routinely used in this study are listed in **Table M3** below.

Table M3. Kits routinely used in this study.

Kit	cat. #	Supplier
GeneJET Plasmid Miniprep Kit	K0502	Fermentas
P3 Primary Cell 4D-Nucleofector® X Kit	V4XP-3024	Lonza
PureLink HiPure Plasmid Filter Maxiprep Kit	K210017	Life Technologies
QIAprep Spin Miniprep Kit	27104	Qiagen
QIAquick PCR Purification Kit	28104	Qiagen
QIAquick Gel Extraction Kit	28704	Qiagen
RNA 6000 Pico kit	5067-1513	Agilent
RNeasy MinElute cleanup kit	74204	Qiagen
RNeasy Mini Kit	4104	Qiagen

2.1.5 Enzymes

Unless otherwise noted, enzymes were used in the provided buffers, and are either denoted in **Table M4** below or in the respective sections of the experimental procedures where they were applied.

Table M4. Enzymes or enzyme master-mixes routinely used in this study. NEB, New England Biolabs

Enzyme/ Enzyme Mix	cat. #	Supplier
BsaI	R0535 S	NEB
EcoRI-HF	R3101	NEB
Gibson Assembly Master-Mix	E2611 L	NEB
Pfu DNA Polymerase, recombinant	EP0501	Thermo Fisher Scientific
Power SYBR® Green PCR Master Mix	4367659	Thermo Fisher Scientific
Proteinase K Solution 20 mg/ml	AM2546	Life Technologies
Q5® High-Fidelity 2X Master Mix	M0492	NEB
Quick Ligation™ Kit	M2200 L	NEB
RNase A (20 mg/ml)	12091021	Life Technologies
SuperScript® III First-Strand Synthesis System for RT-PCR	18080051	Life Technologies
T4 DNA Polymerase (T4)	M0203	NEB
Taq PCR Master Mix Kit	201445	Qiagen
TaqMan® Gene Expression Master Mix	4369016	Thermo Fisher Scientific
TopTaq Master Mix Kit	200403	Qiagen
TURBO DNase 2U/µl	am2238	Life Technologies
*Xho*I (NEB)	R0146S	NEB

2.1.6 Oligonucleotides

Oligonucleotides used for cloning, CRISPR/Cas experiments, quantitative real-time PCR (qPCR) and reverse transcription PCR (RT-PCR) were purchased from Sigma-

Aldrich/Merck (St. Louis, USA), and sequences are listed in the respective sections of the experimental procedures. Primers were designed using the Primer3web software version 4.1.0[192].

2.1.7 Antibodies

Table M5. Antibodies used in thus study. ICC, Immunocytochemistry; WB, Western Blot; ChIP, Chromatin immunoprecipitation; Co-IP, Co-immunoprecipitation.

Target/Clone	Application	Dilution	cat. #	Supplier
Oct4	ICC	1:400	2840 (C30A3)	Cell Signaling
Sox2	ICC	1:200	2748	Cell signaling
Nanog	ICC	1:200	ab21603	Abcam
Lin28a	ICC	1:200	3978 (a177)	Cell Signaling
TFAP2A	ICC	1:200	sc-184X	Santa Cruz
Sox9	ICC	1:100	-	obtained from Prof. Dr. Götz
SOX10 MAb (Cl 20B7)	ICC	1:100	MAB2864	R&D
Ki67	ICC	1:500	-	obtained from Prof. Dr. Götz
Anti-human CD57/HNK-1, Cl. VC1.1	ICC	1:1000	C6680-50TST	Sigma
hNGF R/p75 NTR MAb (Cl 74902)	ICC	1:100	MAB367	R&D
Alexa Fluor 594 anti-rat IgG	ICC	1:1000	A-11007	Invitrogen
Alexa Fluor 488 anti-rabbit IgG	ICC	1:1000	A-21206	Invitrogen
Alexa Fluor 488 anti-mouse IgG	ICC	1:1000	A-21202	Invitrogen
Alexa Fluor 647 anti-mouse IgG	ICC	1:1000	A-21235	Invitrogen
Alexa Fluor 594 anti-rabbit IgG	ICC	1:1000	A-21207	Invitrogen
ASXL1 (clone 12F9)	ICC	1:2	-	this study/E. Kremmer
ASXL1 (clone 4F6)	WB	1:10	-	this study/E. Kremmer
ZIC1	WB	1:400	AF4978-SP	R&D
H2A	WB	1:5000	GTX129418	GeneTex
Ubiquityl-Histone H2A (Lys119)	WB	1:2000	8240	New England Biolabs
H3K27me3	ChIP and WB	1:750	C15410069	Diagenode
ACTIN	WB	1:1000	3700	Cell Signaling
mouse anti-rat IgG (isotype IgG2a), HRP-conjugated	WB	1:1000	-	Dr. Kremmer
Goat anti-mouse IgG HRP-conjugated	WB	1:30,000	115-035-003	Dianova/Jackson
Goat anti-rabbit antibody, HRP-conjugated	WB	1:30,000	111-035-045	Dianova/Jackson
rabbit IgG isotype control	ChIP, Co-IP	5 µl/IP	GTX35035	GeneTex
EZH2	Co-IP	10 µl/IP	39934	Active Motif

2.1.8 Software

Table M6. Software routinely used for analyses or visualization of results in this study.

Software	Supplier
ApE - A plasmid Editor v2.0.46	M. Wayne Davis
Genomatix Software Suite v3.10	Genomatix AG
R v3.3.2	The R foundation for Statistical Computing (R Core team 2014)
Image Lab v5.2.1	Bio-Rad Laboratories
Fiji/ImageJ v2.0.0	National Institutes of Health NIH, USA
Excel (for mac 2011) v14.0.0	Microsoft Corporation
Integrative Genomics Viewer v2.3.98	Broad Institute, USA

2.2 Experimental procedures

2.2.1 Maintenance of pluripotent stem cell lines

Routine passaging and maintenance of pluripotent stem cells was performed essentially as described before[193], for details and modifications see below.

2.2.1.1 Cultivation

All iPSC and hESC lines were cultivated in mTeSR1 medium (STEMCELL technologies) or StemMACS iPS-Brew XF (Miltenyi Biotec), each prepared according to the manufacturer's specifications with addition of 1% Penicillin-Streptomycin (Pen-Strep, Life Technologies). Cells were maintained as feeder-free cultures on 6-well and 10 cm cell cultures plates that had been coated for >15 min with Matrigel (Corning) or Geltrex (Life Technologies), respectively, according to the manufacturer's specifications. Cells were maintained in a HERAcell 240i incubator at 37 °C and 5 % CO_2.

2.2.1.2 Passaging

Routine passaging was performed by washing of cells with phosphate-buffered saline (PBS; Life Technologies), followed by harvesting of cells after 40-60 min incubation at 37 °C with a filtered 2 mg/ml Collagenase Type IV (Life Technologies) solution in DMEM/F12 (Life Technologies). The collagenase solution was quenched with fresh medium and detached colonies were collected by precipitation, resuspended in fresh culture medium, broken to smaller pieces by pipetting with a 1 ml pipette and transferred to plates at roughly 1:5-1:10 dilution.

2.2.1.3 Freezing and thawing of pluripotent stem cells

All centrifugation steps were performed at room temperature (RT) for 3 min and 200x*g* on a Megafuge 40R centrifuge (Thermo Fisher Scientific).
Freezing of cells was performed by washing one confluent 6-well with PBS followed by 10 min incubation with 1 ml Accutase (Sigma-Aldrich), which was then quenched with 3 ml of fresh medium and detached cells were harvested via centrifugation. Cell pellets were resuspended in mFreSR (STEMCELL technologies), transferred to cryotubes (Thermo Fisher Scientific, cat. #375418) and cooled to -80°C in freezing containers (Thermo Fisher Scientific, cat. #5100-0001). After 24 hours cells were transferred to liquid nitrogen.
For thawing, cells were taken from liquid nitrogen, quickly thawn in a water bath at 37 °C, resuspended in fresh culture medium, centrifuged and the supernatant was discarded. Cells were taken up in medium and plated as described before.

2.2.2 Generation of induced pluripotent stem cell (iPSC) lines

2.2.2.1 Isolation of patient-derived fibroblasts (BOS fibroblasts)

Informed consent on the donation of patient specimens was given in the study that initially described the two patients #1 (female, 6 years) and #2 (male, 10 years), which harbor heterozygous mutations in the ASXL1 locus, c2407_2411del5 (#1) and c2893C>T

(#2), respectively[134]. Patient material was obtained in collaboration with Prof. Giovannucci Uzielli (University of Florence, Italy) and Dr. Magini (S. Orsola-Malpighi University Hospital, Bologna, Italy). The skin biopsies were dissociated using a scalpel, and plated in fibroblast medium (**Table M11**) on cell culture plates that had been coated with a 0.1 % gelatine solution (AppliChem). After approximately 2 weeks, fibroblasts began to grow out of specimens, and the biopsy tissue was removed from the well upon confluency. Fibroblasts cultures were passaged by treatment with 0.5 ml of 0.25 % Trypsin-EDTA (Life Technologies) for up to 5 minutes at 37 °C, followed by collection of detached cells in fresh medium, centrifugation for 3 min at 300x*g* and transfer onto 0.1 % gelatine-coated plates in fresh medium. Fibroblast lines #1 and #2 were expanded and after images were captured, the cultures were either stored frozen in liquid nitrogen, as described above, in fibroblast freezing medium [90% fetal bovine serum (FBS, HyClone, GE Healthcare) and 10 % DMSO (Sigma-Aldrich)], or subjected to reprogramming via modified mRNA or episomal plasmids.

2.2.2.2 Modified mRNA-mediated reprogramming

Reprogramming of BOS fibroblast lines, using a cocktail of modified mRNAs (*OCT4, SOX2, LIN28A, CMYC* and *KLF4* mmRNAs), was performed to generate BOS-iPSC lines #1-0 and #2-0, respectively, by E. Rusha and Dr. Pertek at the hiPSC Core Facility, Helmholtz Center Munich, Germanys as described in[191]. The mmRNAs were provided by the RNA CORE unit of the Houston Methodist Hospital and contained the following modifications: 5-Methyl CTP, a 150 nt poly-A tail, ARCA cap and Pseudo-UTP.

2.2.2.3 Episomal-based reprogramming

Episomal-mediated reprogramming was performed on BOS fibroblast lines to generate BOS-iPSC lines #1-1 and #2-1, respectively, by E. Rusha and Dr. Pertek at the hiPSC Core Facility of the Helmholtz Center Munich, using a protocol based with slight modifications on[17].

2.2.3 Generation of *ASXL1*$^{PSC/PSC}$ hESC lines via CRISPR/Cas

The *ASXL1* locus was modified in iCas9 hESC, as the DOX-inducible Cas9 expression in combination with introduction of gRNAs allows for simple genetic engineering according to the CRISPR/Cas system. Deletions of around 500 bp were introduced that should i) be detectable via PCR and ii) result in truncating mutations corresponding to *ASXL1* mutations reported in BOS patients[134].

2.2.3.1 gRNA design and vector construction

A pair of gRNAs flanking the region bp 2436-2877 of the human ASXL1 transcript, thus located within the BOS 'mutation hotspot' (**Fig. 7D**), was selected using the MIT CRISPR design webpage (http://crispr.mit.edu), and sense/antisense oligonucleotides were designed according to published instructions[194]:
gRNA 1: CCATTGTCTGCAGGAACGGT (target locus: chr20:32435128)
gRNA 1-sense: CACCGCCATTGTCTGCAGGAACGGT
gRNA 1-antisense: AAACACCGTTCCTGCAGACAATGGC

gRNA 2: AGTGAAGTAAGGCTGTCAAG (target locus: chr20:32435569)

gRNA 2-sense: CACCGTGGACTGTGCCATCTCGAGG
gRNA 2-antisense: AAACCCTCGAGATGGCACAGTCCAC

The sense and antisense strand were annealed for integration into expression vectors as follows: gRNA oligonucleotides were resuspended in TE to a final concentration of 1 µg/µl, and 1 µl of each gRNA and reverse compliment fragment were combined in 100 µl TE. The mixtures were denatured in a Mastercycler nexus (Eppendorf) for 5 min at 100°C, with subsequent temperature decline of 5 °C/minute to allow for annealing of complementary gRNA fragments. The resulting doublestrand gRNAs were ligated into the pBS/U6 Vector (obtained from Dr. Modic, Helmholtz Center Munich) using the Quick Ligation™ Kit (NEB) according to the manufacturer's instructions. 1 µl of the ligation mix was transformed into competent *E. coli*, followed by plasmid isolation, confirmation of correct integration via Sanger sequencing using the 'U6 forward' primer (5'-3': GAGGGCCTATTTCCCATGATTCC) and plasmid purification, all as described in sections **2.2.6.3** and **2.2.8.4**.

2.2.3.2 Manipulation of the ASXL1 locus in iCas9 and isolation of clones

iCas9 hESC were electroporated with 3 µg of each purified gRNA expression plasmid as described in the next section. Cas9 expression was induced after nucleofection by addition of 1 µg/ml DOX (Sigma-Aldrich) for 48h. To allow for isolation of clones, electroporated cells were detached and harvested by Accutase treatment as described before and the resulting single cell suspension was plated at low density on Matrigel-coated 15 cm plates in mTeSR1 medium, adding 10 µM ROCKi (Y-27632; R&D Systems) for 48 h. A subset of the culture was subjected to bulk genomic DNA isolation and PCR for detection of deletions as described below. After approximately 10 days, single colonies were isolated via picking into Matrigel-/Geltrex-coated 96 well plates using a 200 µl-pipette. Clones in 96-well plates were passaged via treatment with 50 µl Gentle Cell Dissociation Reagent (STEMCELL Technologies) per well, followed by disruption of colonies through vigorous pipetting, and transfer of cell suspensions to new plates at 1:3 dilution in medium containing 10 µM ROCKi. To detect genetic manipulation of single clones in 96-well plates, cells were washed with PBS, and subjected to genomic DNA isolation, followed by PCR using 'ASXL1-GT' primers (5'-3'; forward: GAGCACCCCTGGAAAGTGTA; reverse: TGCTTCAGAGTCTCCGTTGA) and analysis of PCR products via agarose gel electrophoresis, all as described in sections **2.2.9** and **2.2.8.1**. Upon confirmation of excision of approximately 500 bp within the genomic *ASXL1* locus, PCR fragments were isolated as described in section **2.2.8.2**. Deletion was confirmed via Sanger sequencing (see section **2.2.8.4**) using the 'ASXL1-GT' forward primer and correct homozygous clones were maintained as individual *ASXL1*$^{PSC/PSC}$ hESC lines on 6-well plates.

2.2.3.3 Nucleofection

Cultures of approximately 80 % confluency were dissociated and harvested using Accutase as described above, and cell numbers were counted using a Neubauer Chamber. 1 x 106 cells were nucleofected with 6 µg of DNA in total on a 4D NucleofectorTM System (Lonza) using the CB-156 program and the P3 Primary Cell 4D-Nucleofector X Kit (Lonza) according to the manufacturer's specifications. Cells were re-plated on a Matrigel/Geltrex-coated well of a 6 well plate in pre-warmed mTeSR1 and 10 µM ROCKi (only added for the first 24 hours). Subsequently, cells were subjected to

selection or single cell dissociation depending on the application as described in respective sections.

2.2.4 Generation of PB-*ASXL1*^{PSC}, PB-*ASXL1*^{FL} and PB-*ZIC1* hESC overexpression lines

2.2.4.1 Construction of vectors

For the construction of overexpression vectors, several fragments per vector were amplified via PCR and isolated as described in sections **2.2.8.1** and **2.2.8.2**. The primers and templates used for amplification are listed in **Table M7**. The PiggyBac backbone (SRF-PB#9) was obtained from Dr. Shaposhnikov (Helmholtz Center Munich), and harbors an eGFP coding sequence followed by a P2A cleavage signal upstream of the inserted sequence, which allows for cleaving of translated GFP and ASXL1/ZIC1 peptides. The backbone furthermore contains a tetracycline-inducible promoter system, a Hygromycin resistance gene and a transposon, which enables genomic integration upon co-transfection with a transposase plasmid.
Purified fragments were ligated to final constructs using the Gibson Assembly Master-Mix (NEB) according to the manufacturer's instructions; amounts used for each fragment are given in **Table M7**. 3 µl of each ligation mixture were transformed into competent bacteria; plasmids were isolated, analyzed for correct construction via sequencing and purified, all as described in sections **2.2.8.3** and **2.2.8.4**.

Table M7. Primers and fragments used to construct overexpression vectors.
G.A., Gibson Assembly; SRF-PB#9 from Dr. Shaposhnikov. * cat. #BC104848-seq-TCHS1003-GVO-TRI.

Vector	Fragments (length); pmol used in G.A.	Primers used for amplification of fragments (5′-3′);	Template
PB-*ASXL1*^{PSC}	Fragment 1 (3669 bp); 0.2 pmol used	Forward (for): cttacttcactctggactgtgccatcttaactgcagcgcggggatctcatgctgg reverse (rev): 'PB-rev' tggagctcccgtgaggcgtgcttgtcaatgcggtaagtgt Touchdown-PCR from 72 °C to 60 °C (1 °C/cycle)	SRF-PB#9
	Fragment 2 (4486 bp); 0. 2 pmol used	for: acacttaccgcattgacaagcacgcctcacgggagctcca rev: ggtgaacagctcctcgcccttgctcaccatggatccgagctcggtaccaagctta Touchdown-PCR from 72 °C to 60 °C (1 °C/cycle)	SRF-PB#9
	Fragment 3 (747 bp); 0.2 pmol used	for: 'eGFP-for' aaacttaagcttggtaccgagctcggatccatggtgagcaagggcgaggagctgt rev: gcgctccttcttcttcttctgtttgtccttcttgtcgtcatcgtctttgtagtc Touchdown-PCR from 72 °C to 60 °C (1 °C/cycle)	SRF-PB#9
	Fragment 4 = *ASXL1* transcript, N-terminal 2892 bp); 0.2 pmol used	for: 'ASXL1-for' cccatggactacaaagacgatgacgacaagaaggacaaacagaagaagaagaag rev: gaactccagcatgagatccccgcgctgcagttaagatggcacagtccagagtga	H9 hESC-derived cDNA
PB-*ASXL1*^{FL}	Fragment 5(3669 bp); 0.05 pmol used	for: ctctgtgtattgtgccttgtggtgagataactgcagcgcggggatctcatgctgg rev: 'PB-rev'	SRF-PB#9
	Fragment 6	See Fragment 2	SRF-PB#9
	Fragment 7	See fragment 3	SRF-PB#9
	Fragment 8= *ASXL1* transcript, 4656 bp)	for: 'ASXL1-for' rev: gaactccagcatgagatccccgcgctgcagttatctcaccacaaggcacaatac	H9 hESC-derived cDNA

PB-*ZIC1*	Fragment 9 (3669 bp); 0.05 pmol used	for: ttaacgaatggtacgtttaactgcagcgcggggatctcatgctgg rev: 'PB-rev' Tm : Touchdown-PCR from 72 °C to 60 °C (1 °C/cycle)	SRF-PB#9
	Fragment 10	See Fragment 2	SRF-PB#9
	Fragment 11 (747 bp); 0.02 pmol used	for:'eGFP-for' rev: gggccggcgtccaggagcatcttgtcgtcatcgtctttgtagtc Tm : Touchdown-PCR from 72 °C to 60 °C (1 °C/cycle)	SRF-PB#9
	Fragment 12 = *ZIC1* transcript (1344 bp); 0.05 pmol used	for: cccatggactacaaagacgatgacgacaagatgctcctggacgccgg rev: gaactccagcatgagatccccgcgctgcagttaaacgtaccattcgttaaaattggaag; Tm=65 °C	ZIC1 cDNA, Biocat*

Sequencing of constructs was performed using following primers (5'-3'):

ASXL1^{PSC} construct	*ASXL1*^{FL} construct	*ZIC1* construct
1: gtcagcccacttaccagatatgc	1: tctatggcagtggtgacctc	1: aacgtggtcaacgggcag
2: ggcttcattagacccacagc	2: tccacacctgaatcctcacc	2: gcagcatagtgctccgaacg
3: ctgctgctggaagtgtgatg	3: tcgcagacattaaagcccgt	
4: gaggaggagaggggttgttt	4: ccagtgacaaatcccattacatcc	

2.2.4.2 Generation of stable overexpression lines

The PB- *ASXL1*^{PSC} construct was introduced into iCas9 (=control) hESC, the PB- *ASXL1*^{FL} construct was introduced into H9 hESC, and PB- *ZIC1* was introduced into control hESC and *ASXL1*$^{PSC/PSC}$ hESC, all via nucleofection as described in section **2.2.3.3**. For each nucleofection, 3 µg of a plasmid expressing the PiggyBac transposase (obtained from Dr. Shaposhnikov) was co-transfected. Stably integrated clones were selected by 2 weeks' treatment with 50 µg/ml Hygromycin B (Thermo Fisher Scientific, cat. # 10687010). To initially test for successful integration, overexpression was induced in PB-A*SXL1*^{PSC}, PB-*ASXL1*^{FL} and PB-*ZIC1* hESC via treatment with 1 µg/ml DOX for 24h, and eGFP expression was assessed via fluorescence microscopy. Expression of truncated or endogenous *ASXL1* or *ZIC1* was tested by qPCR and RT-PCR using *ASXL1* primers/taqman probes and *ZIC1* primers, respectively (**Table M10**), Western blotting and immunocytochemistry (for antibodies see **Table M5**), all as described in sections **2.2.10**, **2.2.12** and **2.2.13**.

2.2.5 Generation of hESC reporter lines GFP-*ASXL1*$^{PSC/PSC}$ and GFP-control

ASXL1$^{PSC/PSC}$ and control hESC lines were transfected as described above with 3 µg of the plasmid expressing the Piggybac transposase together with a PiggyBac vector harboring an eGFP expression cassette under the constitutively active CAG promoter (vector obtained from D. Shaposhnikov). 4 days after transfection, homogenous cultures of eGFP-expressing cells were obtained by fluorescence-activated cell sorting (FACS) as described in the next section.

2.2.5.1 Flourescence activated cell sorting (FACS)

Each one well of transfected and untransfected cells were dissociated with 1 ml 0.25 % trypsin and harvested by centrifugation as described above. Cells were then resuspended in 1 ml PBS containing 4 % FBS and 5 mM EDTA (Carl Roth), filtered through a 35 µm cell strainer (Corning, cat. #352235) and analyzed on a FACS ARIA III

(BD Biosciences). For sorting, cells were first gated using SSC-A (side scatter-area) against FSC-A (forward scatter-area) according to morphology of the population, and doublets were exluded according to FSC-W (forward scatter-width) against FSC-A (forward scatter-area). Gating of positive cells was performed with non-transfected cells serving as a negative control. eGFP-positive cells were sorted into fresh mTeSR1 medium containing 10 µM ROCKi, 2 % Pen-Strep and 1:100 Fungizone ® Antimycotic (Thermo Fisher Scientific, cat.# 15290-018), plated and maintained as described earlier.

2.2.6 Differentiation of human pluripotent stem cells

2.2.6.1. Short-term differentiation

For short-term undirected differentiation or germ layer induction, hESC lines were dissociated using Accutase and plated at 250,000 cells per well of a 6-well plate with 10 µM ROCKi in mTeSR1medium, which was replaced 24 h later with FBS-Diff, KSR-Diff, 2SMADi, CHIR or ACTIVIN A medium (see **Table M11**). Cells were harvested after 24 h or 5 days and subjected to RNA isolation, reverse transcription and qPCR as described in section **2.2.10**, for primers see **Table M10**.

2.2.6.2 Neural crest (NC) differentiation

Cells were subjected to NC differentiation 5-7 days after passaging and differentiation was performed according to Bajpai *et al.*[33].
On day 0, cells of one well (6-well plate) or one 10 cm-plate were treated with Collagenase solution as described before, and fully detached colonies were harvested in 2-4 ml of PBS, followed by an additional washing step in PBS. Pellets were carefully resuspended twice in 1 ml of prewarmed NC-induction medium (**Table M11**) using a 1 ml pipette to generate spheres of medium size, which were transferred to one well of a uncoated 6-well plate containing 3 ml of prewarmed NC induction medium, and cultures were kept at 37 °C. This basic protocol was modified according to experimental conditions: for ChIP-qPCR and RNA-seq, spheres were generated and maintained on uncoated 10 cm plates. For overexpression studies, NC differentiation was performed in uncoated 24-well plates to allow for easier quantification of spheres. Overexpression of PB-*ASXL1*^{PSC} and PB-*ZIC1* constructs in stable cell lines was induced via addition of 1 µg/ml DOX from day 1-7 (PB-*ASXL1*^{PSC}) or day 3/4-7 (PB-*ZIC1*).
From day 1-4, medium was changed daily to remove apoptotic cells and debris. For this, spheres were collected via precipitation, medium was aspirated and spheres were carefully resuspended in fresh NC induction medium and transferred back to culture plates. Differentiation cultures were not examined or handled on days 5 and 6 (except for transplantation experiments, see section **2.2.16.1**) to ensure undisturbed adhesion of neuroepithelial structures (neurospheres) to the plates. On day 7, attachment of neurospheres was assessed in brightfield microscopy (see section **2.2.7.7**). From day 7 onward, medium was changed every other day until plates were confluent (usually around day 11-15). Residual neurospheres were removed via aspiration, cells were washed with PBS and treated with 0.5 ml Accutase for 5 minutes at 37 °C. 2-4 ml of prewarmed NC-Maintenance medium (**Table M11**) were added to the well to quench the Accutase solution, followed by pipetting to dissociate NC cells, and 0.5-1 ml of the cell dispersion were added onto a well that had been coated with a 5 µg/ml fibronectin (Sigma-Aldrich) solution in PBS and contained prewarmed NC-Maintenance medium. NC

cultures were passaged and maintained in this way in NC-Maintenance medium on fibronectin-coated plates for 2-4 passages, when the medium was replaced by NC-Maintenance + BC (**Table M11**). Thus, NC cultures could be maintained for around 10-15 passages, before they ceased to proliferate.
To determine expression of NC markers and *ASXL1-3*, NC differentiation cultures were harvested at different timepoints during differentiation and subjected to further analyses as described in chapter **2.2.7.6**.

Table M11. Cell culture media used in differentiation experiments and for fibroblast lines.

Name	Base	Supplements
Fibroblast medium	DMEM	10 % fetal bovine serum, 1 % NEAA, 1 % GlutaMAX, 1 % Pen-Strep
FBS-Diff	DMEM/F12	10 % fetal bovine serum, 1 % NEAA, 1 % GlutaMAX, 0.2 % 2-mercaptoethanol (Life Technologies), 1 % Pen-Strep
KSR-Diff	DMEM/F12	20 % Knockout Serum Replacement, 1 % NEAA, 1 % GlutaMAX, 0.2 % 2-mercaptoethanol, 1 % Pen-Strep
2SMADi	50 % DMEM/F12, 50 % Neurobasal medium	0.5 x N2, 0.5 x B27, 10 µM SB431542, 5 µM Dorsomorphin
CHIR	DMEM/F12	1 % B27, 5 µM CHIR99021
ACTIVIN A	DMEM/F12	1.5 % FBS, 100 ng/ml Activin A
NC-Induction	50 % DMEM/F1, 50 % Neurobasal medium	0.5 % N2, 0.5 % B27, 0.5 % GlutaMAX, 1 % Pen-Strep, 20 ng/ml bFGF, 20 ng/ml EGF, 5 µg/ml insulin
NC-Maintenance	as above	0.5 % N2, 0.5 % B27, 0.5 % GlutaMAX, 1 % Pen-Strep, 20 ng/ml bFGF, 20 ng/ml EGF, 1 mg/ml BSA (Thermo Fisher)
NC-Maintenace +BC	as above	as above, + 50 pg/ml BMP-2 and 3 µM CHIR99021

2.2.6.3 Differentiation of NC cells to mesenchymal stem cells (MSCs) and derivatives

NC cells of passage 2-6 were treated with Accutase as described above, diluted using StemMACS MSC Expansion Medium (human, Miltenyi, cat. #130-091-680), transferred to uncoated wells of a 6-well plate and kept in StemMACS MSC Expansion Medium. Change in morphology was visible directly after passaging, and after 7 days, cells displayed a homogenous, spindle-shaped morphology. NC-derived MSC were passaged using 0.05 % Trypsin-EDTA (Thermo Fisher Scientific, cat. #25300054). At passage 2-3, the cells were subjected to flow cytometry analysis or osteoblast/adipocyte differentiation on 24-well plates via treatment with StemMACS MSC Expansion Medium (= negative control), StemMACS OsteoDiff Media (human, Miltenyi, cat. # 130-091-678) or StemMACS AdipoDiff Media (human, Miltenyi, cat. # 130-091-677) for 21-26 days.

2.2.7 Analysis of undifferentiated and differentiated cell lines

2.2.7.1 Assessment of morphology and eGFP expression

Image capture and visual examination of cultures in brightfield and fluorescence microscopy was performed on a Leica DMIL LED microscope using the ICC50 HD or DFC 450C camera.

2.2.7.2 Analysis of nonsense-mediated decay in BOS-iPSC

Undifferentiated iCas9 hESC (=Control hESC) and BOS-iPSC were treated with 100 µg/ml cycloheximide (Sigma-Aldrich, cat. #C7698) for 6 h, and then subjected to RNA isolation, reverse transcription, qPCR and RT-PCR as described in section **2.2.10**, using primers listed in **Table M8**:

Table M8. Primers used for RT-PCR nonsense-mediated decay experiments (5'-3').

Target	forward primer	reverse primer
Caspase-2	gttacctgcacaccgagtcacg	gcgtggttctttccatcttgttggtca
B2M (β-Globulin)	ctcacgtcatccagcagaga	tctttttcagtgggggtgaa
ASXL1-Exon 1	ggacaaacagaagaagaagaagga	tgcctctatgacctgcagaa
ASXL1-Exon 12-A	tcgcagacattaaagcccgt	agctctggacatggcagttc
ASXL1-Exon 12-B	agttgggaccaagcacaaac	aagtgacccaccagttccag

2.2.7.3 Sequencing of ASXL1 transcripts in BOS-iPSC

To determine whether mutant alleles were transcribed to stable mRNA in undifferentiated BOS-iPSC #1-0 and #2-0, these lines were subjected to RNA isolation, reverse transcription and RT-PCR as described in chapter **2.2.10**. Following primers were used to amplify target regions from cDNA (5'-3'):
For: TCGCAGACATTAAAGCCCGT
Rev: CAGAGGCTGTATCCGTGGA
PCR products were isolated using the QIAquick PCR Purification Kit (Qiagen) according to the manufacturer's specifications and subjected to Sanger sequencing (using primer GAGCACCCCTGGAAAGTGTA) and analyzed on the presence of patient-specific mutations (see chapter **2.2.8.4**).

2.2.7.4 Analysis of HOX gene induction

H9 hESC, control hiPSC and BOS-iPSC were kept in mTeSR1 in 6-well plates, and retinoic acid (Sigma-Aldrich, cat. #R2625) in DMSO was added to the cultures to final concentrations of 0.5, 1, 2.5 and 5 µM, using DMSO-treated cultures as negative control. Cells were imaged and harvested after 24 h and subjected to RNA isolation and qPCR (see section **2.2.10**) using primers stated in **Table M9** below.

Table M9. Primers used for HOX gene detection (5'-3').

Target	forward primer	reverse primer
HOXA1	cccaaaacagggaaagttggagag	cgcgcgtcaggtacttgttgaag
HOXA2	cctcagccacaaagaatccctg	ctccacccttcggggtctg
HOXA3	cagctcatgaaacggtctgcg	cgcacactctgacaggggtttg
HOXA4	catgtcagcgccgttaaccc	cgccgggtcaggtatcgattg
HOXA5	ctgcacataagtcatgacaacataggc	ctgcgggtcaggtaacggttg
HOXB1	caagacagcgaaggtgtcagag	ggcccggctcaggtacttg
HOXB2	ctgcagatggcctgggactg	ccttctccagttccagcagc
HOXB4	gagcacggtaaaccccaattacg	gccgtgtcaggtagcggttg
HOXB5	cacatcagccatgatatgaccgg	gtgggcgatctcgatgcg

2.2.7.5 Cell density assays

Control hiPSC, control hESC or BOS-iPSC were dissociated using Accutase as described before, counted using a Neubauer Chamber and seeded at different densities as single cells in fresh medium containing 10 µM ROCKi. After 24 h, 48 h or 96 h, cells were subjected to expression analysis as described in the next section.

2.2.7.6 Transcript and protein analysis in control and mutant cell lines

Expression of pluripotency factors, germ layer markers, NC markers or *ASXL* genes was detected via transcriptional and/or protein expression analysis in undifferentiated lines and NC cultures derived thereof. For stable overexpression lines, induction of constructs via 1 µg/ml DOX treatment was usually performed for 24 h prior to sample collection and analysis, unless stated otherwise.
For transcriptional analyses, cell cultures were subjected to RNA isolation and qPCR/RT-PCR/microarray/RNA-seq, as described in section **2.2.10**, primers and probes are listed in **Table M10**. For Western Blot, adherent cells were washed once with PBS, harvested in PBS using a cell scraper (Santa Cruz) to lift off colonies, and collected via centrifugation at 500x*g* for 5 min at 4 °C. Neurospheres in NC differentiation cultures were collected directly via centrifugation, and washed once in PBS. Cell pellets were stored at -80 °C and then subjected to protein extraction and Western Blot as described in chapter **2.2.13**; antibodies used for detection are listed in **Table M5**. For immunocytochemistry, cells were plated as single cells, using Accutase, onto µ-Slide 8 Well chambers (Ibidi). After 2-4 days, cultures were fixed and stained as described in section **2.2.12**, using antibodies listed in **Table M5**.

2.2.7.7 Analysis of neurosphere attachment

Assessment of NC differentiation via quantification of neurospheres was performed at day 7 or at day 8 of the protocol via brightfield microscopy. Neurospheres were classified into three categories: attached neurospheres that showed delamination of prospective NC cells (=delaminating neurospheres), attached neurospheres without outgrowth, and floating neurospheres. If feasible, neurospheres of all three categories were counted per cell line, and the number of delaminating neurospheres in percent of the total number of neurospheres derived from the respective cell line was determined. Otherwise, the number of delaminating neurospheres derived from BOS-iPSC or *ASXL1*$^{PSC/PSC}$ hESC was directly compared to the number of delaminating neurospheres in control hiPSC or control hESC-derived NC cultures, respectively. Furthermore, total number of neurospheres derived from *ASXL1*$^{PSC/PSC}$ and control hESC were determined.

2.2.7.8 Flow cytometry analysis of MSC cultures

Flow cytometry analysis of MSC cultures was performed by V. Rishko (Helmholtz Center Munich) using the MSC phenotyping kit (Miltenyj Biotec, #130-095-198) according to the manufacturer's specifications on a FACS ARIA III (BD Biosciences), with subsequent analysis using the FlowJo X 10.0.7r2 software. For controls, MSC cultures were incubated with isotype control cocktail from the kit.

Table M10. Primers and probes used for analysis of cell lines on pluripotency markers, germ layer and NC specifiers, and *ASXL* genes (5'-3'). * detection of full-length *ASXL1* in BOS-iPSC

Name	application	forward primer	reverse primer
ASXL1-Taqman	qPCR	TaqMan Gene Expression Assay ID: Hs00392415_m1, LT	
ASXL1-FL	RT-PCR*	aaggacaaacagaagaagaagaag	ttatctcaccacaaggcacaatac
ASXL1	qPCR	gccacaggtcaaatgaagc	ggtccgagagttgatcagg
ASXL2	qPCR	ctaaagcaggcgctaaagc	gctttgacagtctttagtgag
ASXL2-Taqman	qPCR	TaqMan Gene Expression Assay ID: Hs00827052_m1, LT	
ASXL3	qPCR	catacgtttgcttccttacct	acttcccatctgcctatcc
ASXL3-Taqman	qPCR	TaqMan Gene Expression Assay ID: Hs00296943_m1, LT	
CER1	qPCR	caggacagtgcccttcagcca	acagtgagagcaggaggtatgg
E-CAD	qPCR	gcctcctgaaaagagagtggaag	tggcagtgtctctccaaatccg
FOXA2	qPCR	gggagcggtgaagatgga	tcatgttgctcacggaggagta
GAPDH	qPCR	TaqMan Gene Expression Assay ID: Hs02758991_g1, LT	
GAPDH	qPCR	tgcaccaccaactgcttagc	ggcatggactgtggtcatgag
GBX2	qPCR	gcggaggacggcaaaggcttc	gtcgtcttccacctttgactcg
GDF3	qPCR	gtctcccgagacttatgctacg	agtagaggagcttctgcaggca
HNK1	qPCR	gaaagcagcctccttcgagaac	cctcattcaccagcactggctt
MESP1	qPCR	ctgcctgaggagcccaagt	gcagtctgccaaggaacca
N-CAD	qPCR	cccacaccctggagacattg	gccgctttaaggccctca
NANOG	qPCR	TaqMan Gene Expression Assay ID:Hs04260366_g1, LT	
Nestin	qPCR	gtctcaggacagtgctgagccttc	tcccctgaggaccaggagtctc
OCT4	qPCR	TaqMan Gene Expression Assay ID:Hs00999632_g1, LT	
p75	qPCR	cctcatccctgtctattgctcc	gttggctccttgcttgttctgc
PAX3	qPCR	ggctttcaaccatctcattcccg	gttgaggtctgtgaacggtgct
PAX6	qPCR	gcggagttatgatacctacacc	gaaatgagtcctgttgaagtgg
SNAI2	qPCR	atctgcggcaaggcgttttcca	gagccctcagatttgacctgtc
SOX10	qPCR	atgaacgccttcatggtgtggg	cgcttgtcactttcgttcagcag
SOX17	qPCR	ggcgcagcagaatccaga	ccacgacttgcccagcat
SOX2	qPCR	TaqMan Gene Expression Assay ID:Hs01053049_s1, LT	
SOX9	qPCR	aggaagctcgcggaccagtac	ggtggtccttcttgtgctgcac
T	qPCR	caacctcactgacggtgaaaaa	acaaattctggtgtgccaaagtt
TFAP2A	qPCR	gacctctcgatccactccttac	gagacggcattgctgttggact
ZIC1	qPCR	gatgtgcgacaagtcctacacg	tggaggattcgtagccagagct

2.2.7.9 Oilred O/Alizarin Red staining of adipocytes and osteoblasts

For detection of calcium-containing osteoblast cells derived from MSCs, Alizarin Red staining was perfomed as follows: Cells were washed twice in 2 ml of PBS and then fixed for 30 min at RT in 10 % Formalin (neutral buffered, Sigma-Aldrich cat. #HT501128), followed by two washing steps in 2 ml de-ionized water each. Cells were stained with 1 ml of a filtrated Alizarin red staining solution [20mg/mL Alizarin red S (Carl Roth, cat. #0348.1) in de-ionized water] for 45 min at RT, washed four times with 1 ml de-ionized water and imaged in 1 ml PBS.

For evaluation of adipogenic differentiation of MSCs, Oil Red O staining was performed as follows: Cells were washed twice in 2 ml PBS and fixed for 30 min in 10 % Formalin as before. Subsequently, cells were washed twice with 2 ml of tap water and fixed for 5 min with 1 ml of 60 % 2-propanol at RT, which was then replaced by 1 ml of a filtrated

Oil Red O working solution [1.8 mg/ml Oil Red O (Sigma-Aldrich cat. #O0625) in de-ionized water, diluted from a stock solution in 2-propanol]. After 10 min incubation at RT, cells were washed twice with 2 ml of PBS, and afterwards stained with 1 ml of filtrated Mayer's Hematoxylin solution (Sigma, cat. #MHS1) for 5 min at RT. Cells were then washed twice with 2 ml of tap water and imaged in 1 ml PBS.

2.2.8 Molecular cloning procedures

2.2.8.1 PCR and agarose gel electrophoresis

Amplification of DNA fragments for construction of vectors was performed using the Q5® High-Fidelity 2X Master Mix (NEB) according to the manufacturer's specifications, either in a final volume of 25 µl for detection on agarose gels, or in a final volume of 50 µl for subsequent isolation of PCR fragments. Annealing temperatures, primers and templates are given in the respective sections.
Amplification of genomic target regions in samples derived from CRISPR-targeted hESC clones, mouse or zebrafish for genotyping purposes, or from bacterial colonies to confirm successful transformation of plasmids, was performed using the TopTaq Master Mix Kit (Qiagen) according to the manufacturer's specifications at an annealing temperature of 60 °C. 1 µl of genomic DNA was added to the PCR reaction mixture in a final volume of 20 µl; alternatively for bacteria colony PCR, material of one colony was transferred into the well of a 96-well PCR plate containing 20 µl of the pre-made PCR reaction mixture using a 200 µl pipette tip.
DNA Gel loading dye (Thermo Fisher Scientific) was added to PCR products, which were separated on 1% agarose gels containing SYBR® Safe DNA Gel Stain (1:20,000; Life Technologies) in LAB buffer (10 mM lithium acetate, 10 mM boric acid in dH_2O) at 200 V and visualized on the ChemiDoc™ MP System (Bio-Rad Laboratories).

2.2.8.2 Isolation of PCR products

PCR fragments were isolated via two different methods. If gel electrophoresis confirmed amplification of one specific product, PCR products were isolated using the QIAquick PCR Purification Kit (Qiagen). If PCR resulted in detection of several products, the band of expected size was excised from the agarose gel and subjected to DNA isolation using the QIAquick Gel Extraction Kit (Qiagen). Isolated PCR products were stored at -20°C.

2.2.8.3 Transformation and plasmid isolation

NEB® 5-alpha Competent *E. coli* (High Efficiency, NEB, cat. #C2987) where transformed with DNA/ligation mixture (see respective sections) according to the manufacturer's specifications. 50 µl of transformed bacteria were plated on a pre-warmed Luria Bertani (LB) agar plate containing 50 µg/ml ampicillin and incubated at 37 °C overnight. Colonies were picked into 3 ml LB medium containing 50 µg/ml ampicillin and again incubated at 37 °C overnight. Plasmid DNA was isolated using either the GeneJET Plasmid Miniprep Kit (Fermentas) or the QIAprep Spin Miniprep Kit (Qiagen) according to the manufacturers' instructions. Plasmids were then subjected to Sanger sequencing (chapter **2.2.8.4**) to confirm correct integration/construction. Upon validation, cultures were used to inoculate 100 ml LB medium containing 50 µg/ml ampicillin, incubated at 37 °C overnight, and plasmids were isolated using the PureLink HiPure Plasmid FP

Maxiprep Kit (Life Technologies) according to the manufacturer's instructions. Subsequent to the last ethanol purification step, plasmids were resuspended in sterile dH_2O, concentration was measured using the Nanodrop ND-1000 system, and plasmids were stored at -20°C.
LB medium: 16 g/l Trypon/Pepton from Casein (Roth cat. # 8952.2), 5 g/l yeast extract (Roth, cat. # 2363.2) and 10 g/l NaCl (Roth, cat. # P029.2)
LB agar plate: LB medium + 15 g/l agar (Agar-Agar, Carl Roth cat. # 5210.2)

2.2.8.4 Sanger sequencing

Isolated PCR fragments or plasmids were subjected to Sanger Sequencing at GATC Biotech (Konstanz, Germany), and analysis of sequences to validate correct construction/integration was performed using the ApE (A plasmid Editor, v2.0.46) software.

2.2.9 Genomic DNA isolation

Genomic DNA isolation was performed using the QuickExtract DNA Extraction Solution 1.0 (Biozym, cat. #101098) according to manufacturer's instructions, and extracted DNA was stored at -20°C. Below, the specification for different applications are given:
96-well plates: 10 µl of DNA Extraction Solution/well
Bulk cell pellets: 50-200 µl of DNA Extraction Solution/pellet
Zebrafish fin tips/mouse tail tips: 30 µl of DNA Extraction Solution/sample

2.2.10 Transcription analyses

2.2.10.1 Isolation of RNA

Lysis of samples was performed in 350 or 600 µl RLT buffer (supplied with the RNeasy Mini Kit, Qiagen) that was either i) added directly onto adherent cells grown in 24- or 6-well cell culture plates, ii) added to cell pellets that had been harvested via Accutase or Trypsin treatment as described before, iii) added to neurospheres collected via centrifugation, or iv) added to zebrafish samples. In all cases, homogenization was performed via pipetting or forcing of lysed samples through a 0.50 x 16 mm needle (Omnifix®-F fine dosage syringe Omnilab cat. #5421735). Homogenized samples in RLT buffer were either stored at -80°C, or directly subjected to RNA isolation, which was performed using the RNeasy Mini Kit (Qiagen) according to the manufacturer's instructions. Isolated RNA was stored at -80°C.

2.2.10.2 Reverse transcription

RNA concentration was measured using the Nanodrop ND-1000 system. For all samples of one experiment, similar RNA concentrations (100-800 ng) were reverse transcribed using the SuperScript® III First-Strand Synthesis System (Life Technologies) with oligo dT primers according to manufacturer's instructions.

2.2.10.3 RT-PCR

The Taq PCR Master Mix Kit (Qiagen) was used according to the manufacturer's instructions to amplify target regions from 1 µl oligodT-amplified cDNA. Products were visualized via agarose gel electrophoresis as described for PCR products.

2.2.10.4 qPCR

Power SYBR® Green PCR Master Mix (Life Technologies) or TaqMan® Gene Expression Master Mix (Life Technologies) were used for qPCR on a QuantStudio 12k Flex (Life Technologies) according to the recommended cycling conditions. Reaction mixtures per sample were:

	SYBR® Green qPCR	TaqMan® qPCR
Master Mix	4.5 µl	5 µl
Primer mix (5µM)/probe	1 µl	0.5 µl
cDNA	0.5 µl	0.5 µl
H_2O	3.5 µl	4 µl

Primers are indicated in the respective sections and in **Table M10**. Relative expression level was calculated as follows: Ct values were first normalized to the respective Ct values of housekeeping gene *GAPDH*, then, resulting delta Ct values of treated cells or BOS lines were compared to control cells or untreated cells, as denoted in the respective charts, according to the following formula:

$$\text{Relative expression level (mutant compared to control)} = 2^{-(\text{delta Ct(mutant)} - \text{delta Ct(control)})}$$

2.2.10.5 Microarray in iPSC lines

For microarray analysis, RNA was isolated from BOS-iPSC lines #1-0 and #2-0 (three passages per line), H9 hESC (three passages), mmRNA-derived control hiPSC (two passages) and fibroblasts #1 and #2 (three wells per line) as described in chapter **2.2.10.1**. RNA quality was assessed with the RNA 6000 Pico Kit (Agilent) on an Agilent 2100 Bioanalyzer and subjected to cDNA preparation with the Ovation® Pico WTA System V2 (NuGEN, cat. #3302-60) and the Encore™ Biotin Module (NuGEN, cat. #4200-60) according to the manufacturer's specifications. Hybridization onto GeneChip® Human Gene 2.0 ST Arrays (Affymetrix, cat. #902113) and subsequent scanning was performed with the GeneChip® Hybridization, Wash, and Stain Kit (Affymetrix, cat. #900720) according to the supplied protocol.
For data analysis, CEL files were processed, normalized and run quality assessed using the Expression Console software (Build 1.3.1.187, Affymetrix), which was also used to build Principal Component Analysis (PCA) plots. Annotated expression files were then analysed using the CARMAweb software (v1.5, Medical University Innsbruck), available under *https://carmaweb.genome.tugraz.at/carma/*. Differentially expressed genes were determined using moderated t-statistics (limma package), with correction for multiple testing according to the Benjamini & Hochberg method. A gene was considered to be differentially expressed if its corrected p-value BH was below a threshold of 0.1 (false discovery rate <10%), with a linear fold-change >2. Resulting gene sets were subjected to literature-based tissue enrichment analysis using the GeneRanker tool within the Genomatix Software Suite v3.10.

2.2.10.6 Sequencing of total RNA in NC cultures

A subset of material collected from day 7 NC cultures in section **2.2.14** (ChIP-qPCR) was used for RNA extration using the RNeasy Mini Kit as described above. RNA quality was assessed using the RNA 6000 Pico Kit (Agilent) on an Agilent 2100 Bioanalyzer. Per RNA-seq library, 1 µg of RNA was treated with RiboZero Gold (Human/Mouse/Rat) kit (Illumina, cat. #RS-122-2301) to remove ribosomal RNA, followed by RNA cleanup using the RNeasy Minelute RNA cleanup kit (Qiagen). Sequencing libraries were prepared using the TruSeq Stranded total RNA LT kit (Illumina, cat. #RS-122-2301) according to the supplied protocol, including 11 cycles of PCR followed by purification with Agencourt Ampure XP beads (Beckman-Coulter, cat. #A63881). Libraries were again evaluated on the Bioanalyzer using the DNA 1000 kit (Agilent, cat. #5067-1504). DNA concentration was measured using a Qubit dsDNA HS Assay Kit (Life Technologies, cat. #Q32854), libraries were pooled and diluted stepwise to 2 nM according to the manufacturer's instructions and subjected to single-end sequencing for 75 cycles on a NextSeq with the NextSeq 500/550 v2 reagent cartridge (Illumina, cat. #FC-404-2005).
Quality of the sequencing run was confirmed via QC reports on the Illumina BaseSpace platform and the FastQ tool provided on the Galaxy platform[195]. Reads were mapped to the hg19 genome using TopHat and read count was performed by Dr. Simon (Helmholtz Center Munich, Germany) using the featureCounts (v1.5.0) function of the Subread package[196] and the hg19 human gene annotation. Differential gene expression analysis was performed with the DESeq2 package[197] in R v3.3.2; genes with a maximum read count of zero were considered to be non-expressed and thus removed from further analysis. PCA Plots and Volcano Plots were built using the ggplot2, dplyr and ggrepel packages in R, respectively. To characterize misregulated gene sets, the list of significantly downregulated transcripts (padj<0.05) was submitted to the Genomatix Software Suite GeneRanker Analysis as described above.

2.2.11 Generation of monoclonal antibodies

2.2.11.1 Cloning of expression constructs

To construct vectors expressing N-terminal *ASXL1* or *ASXL2* fragments that were used for immunization or validation of specific antibodies, respectively, a ligase-independent cloning (LIC)-approach was followed based on a protocol supplied by Dr. Geerlof (Helmholtz Center Munich). Reaction mixtures prepared at different steps of the LIC protocol are denoted in **Table M12**.
First, the pETM13/LIC plasmid, which contains a C-teminal His_6-tag (Dr. Geerlof), was linearized via *BsaI* (NEB) treatment for 1 h at 50 °C (Step 1). The linearized plasmid was isolated via gel purification as described in chapter **2.2.8.2**, and treated with T4 DNA Polymerase (T4; NEB) for 30 min at RT (Step 2). The Polymerase was afterwards heat-inactivated at 75°C for 20 min.
The *ASXL1* (bp 1-1854 = aa 1-618) and *ASXL2* (bp 1-1983 = aa 1-661) inserts were amplified from H9 hESC-derived cDNA via PCR (Step 3) using following primers (5′-3):

ASXL1-AB-for: AAGAAGGAGAACAACCATGAAGGACAAACAGAAGAAGAAGAAG
ASXL1-AB-rev: GACCCGACGCGGTTTTAATGTCTGCGAGGGTCC
ASXL2-AB-for: AAGAAGGAGAACAACCATGAGGGAAAAGGGACGTAG
ASXL2-AB-rev: GACCCGACGCGGTTTTGATGTCTGCAAGAGTTCTG

Cycling conditions were as follows:

Step	Time	Temperature	Cycles
Denaturation	2 min	95°C	1
Denaturation	30 sec	95°C	
Annealing	30 sec	60°C	30
Extension	4 min	72°C	
Extension	10 min	72°C	1

PCR products were analyzed on agarose gels, extracted and purified as described before. The inserts were then treated with T4 (Step 4) under the same conditions as in Step 2. Ligation of T4-treated inserts and plasmid (Step 5) were performed for 5 min at 22 °C and terminated via addition of addition of 1 µl EDTA (25 mM) for 5 min at 22 °C.

Table M12. Reaction mixtures applied at different steps 1- 5 of the LIC procedure. * supplied with enzymes; **Thermo Fisher Scientific cat. #R0181, *** Life technologies, cat. #18080051

1. Linearization of pETM-13/LIC	**2. T4 treatment of linearized pETM-13/LIC**	**3. PCR amplification of the insert**	**4. T4 treatment of insert**	**5. Annealing of insert and pETM-13/LIC**
5 µl 10X NEB buffer 3*	2 µl 10X NEB buffer 2*	5 µl 10X Pfu polymerase buffer	2 µl 10X NEB buffer 2*	1 µl T4-treated vector DNA
5 µg pETM-13/LIC vector DNA	600 ng *BsaI*-digested pETM-13/LIC	0.5 µl forward and reverse primer (100 pmol/µl)*	0.2 pmol PCR product	2 µl T4-treated insert DNA
2.5 µl *BsaI* (10 units/µl)	0.5 µl dTTP (100 mM)**	100 ng dNTPs (10 mM each)	1 µl DTT (100 mM)	
ad 50 µl with dH2O	1 µl DTT (100 mM)***	2 µl cDNA	0.5 µl dATP (100 mM)**	
	0.2 µl 100x BSA	1 µl Pfu DNA polymerase (2.5 units/µl)	0.2 µl 100X BSA	
	0.4 µl T4 DNA polymerase (3 units/µl)	ad 50 µl with dH2O	0.4 µl T4 DNA polymerase (3 units/µl)	
	ad 20 µl with dH2O		ad 20 µl with dH2O	

1 µl of ligation mixture per construct were used for transformation into competent bacteria, and colony-PCR was performed using 'ASXL1-AB' and 'ASXL2-AB' primer pairs to determine successfully transformed bacteria clones, which were used for plasmid isolation, all as described in sections **2.2.8.1** and **2.2.8.3**, and three purified plasmids per clone were subjected to Sanger sequencing (see **2.2.8.4**) to confirm correct integration of the *ASXL1/ASXL2* inserts and presence of the His_6-tag using following primers (5′-3′):

T7 primer (provided by GATC Biotech): TAATACGACTCACTATAGGG
pETM13-rev: TTGTTAGCAGCCGGATCTC
Sequencing of *ASXL1* (central part): CTGCATCAGGGTTCTCGG
Sequencing of *ASXL1* (3' end): GCCCACTAAAGAGGAGCC
Sequencing of *ASXL2* (central part): GATGGACAGACAGGCAGC
Sequencing of *ASXL2* (3' end): CCAGCAGCCATTTCAGGT

2.2.11.2 Protein expression and purification

Correct pETM-13/LIC-*ASXL1* and pETM-13/LIC-*ASXL2* constructs were used for expression and purification of N-terminal ASXL1 and ASXL2 fragments by Dr. Geerlof in the Protein Expression and Purification Core Facility at the Helmholtz Center Munich.

2.2.11.3 Antibody production

50 µg purified His-tagged human ASXL1 protein was used by Dr. Elisabeth Kremmer, Dr. Regina Feederle and Andrew Flatley in the Monoclonal Antibody Core Facility of the Helmholtz Center Munich to generate monoclonal antibodies in rat hybridoma cultures, according to their published method[198], providing clones that detected the ASXL1 fragment, but not the ASXL2 fragment in enzyme-linked immunosorbent assays (ELISA). I validated these clones further by Western blot analysis (see chapter **2.2.13**) on H9 hESC and induced PB-*ASXL1*^{PSC} and PB-*ASXL1*^{FL} hESC. Experiments in this study were performed with hybridoma culture supernatants of clones 12F9 and 4F6 (both rat IgG2a/k).

2.2.12 Immunocytochemistry

Cells were fixed with 4% formaldehyde/PBS for 10-15 min at RT and permeabilized and blocked using 0.1 % Triton X-100 (Sigma-Aldrich), 3 % donkey serum (Biowest, cat. #S2170-500) and 0.1 % bovine serum albumine (BSA; Sigma-Aldrich) in PBS for 25 min at RT. Primary and secondary antibodies were diluted to working concentrations in 1% BSA/0.1 % Triton X-100/PBS. Primary antibody was incubated overnight at 4 °C, secondary for 1 hour at RT (for antibodies, see **Table M5**). Specimens were washed with PBS containing DAPI (Bio-Rad Laboratories) before mounting in Aqua-Poly/Mount (Polysciences, cat. #18606-20). Images were obtained using a Zeiss Axiovert 200M epifluorescent microscope.

2.2.13 Western Blotting

Total protein lysates were prepared via lysis of cell pellets in RIPA buffer (50 mM TrisHCl, pH8.0; 150 mM NaCl; 1 % Triton X-100; 0.5 % Na-Deoxycholate; 0.1 % SDS) containing Protease Inhibitor Cocktail Set III (Merck Millipore). After addition of 2x Laemmli Sample Buffer (Bio-Rad Laboratories, cat. #161-0737) supplemented with 10 % 2-mercaptoethanol (Sigma-Aldrich), samples were heated to 95°C for 5 min and subsequently separated via SDS PAGE on Mini-PROTEAN TGX Stain Free Gels, 4-15% gels (Bio-Rad Laboratories, cat. # 456-8086) using SDS running buffer (25 mM Tris, 192 mM glycine, 0.1 % SDS) in a Mini Trans-Blot Cell (Bio-Rad Laboratories). The Trans-Blot Cell was also used for subsequent wet blotting on nitrocellulose membranes (Bio-Rad Laboratories, cat. #162-0115) in blotting buffer (25 mM Tris, 92 mM glycine, 20 % methanol, 0.1 % SDS). Following 3x 5 min washing steps in TBS-T (20 mM Tris, 150 mM NaCl, 0.1 % Tween-20), membranes were blocked for 1 h in 5 % milk powder (Carl Roth) in TBS-T and afterwards incubated with primary antibodies (see **Table M5**) diluted to working concentrations in 5% milk powder in TBS-T at 4 °C overnight. After 3x 5 min TBS-T washing steps, membranes were incubated with HRP-coupled secondary antibodies (see **Table M5**) in 5 % milk powder in TBS-T, washed four times in TBS-T for 15 min each and activated for 1 min using Clarity Western ECL Substrate (Bio-Rad

Laboratories, cat. #170-5060) on the ChemiDoc™ MP System (Bio-Rad Laboratories). Intensities of analyzed proteins were normalized to respective Actin band intensities using Image Lab v5.2.1 to determine relative protein levels.

2.2.14 Chromatin immunoprecipitation followed by qPCR (ChIP-qPCR)

ChIP-qPCR was performed essentially as described by Krendl *et al.*[199]; details and slight modifications are outlined below. The compositions of buffers and solutions are listed in **Table M14**. All steps were performed on ice unless otherwise noted.

2.2.14.1 Preparation of chromatin

NC cultures for ChIP analysis were derived from control hESC and *ASXL1*$^{PSC/PSC}$ hESC (clones A, C, and D) at day 7 of three independent differentiation experiments (three 10 cm-plates per replicate). For harvesting of the cultures, which contained both neurospheres and adherent cells, neurospheres were first collected from the culture plates, and both neurospheres and adherent cells were washed with PBS. Subsequently, neurospheres were transferred back to the plates and cells were dissociated with 0.25 % Trypsin-EDTA and harvested via centrifugation as described before.
Pellets were resuspended in a solution of 10 ml cold DMEM/F12 with 1 ml of freshly prepared crosslinking solution. Crosslinking was performed for 10 min in at RT under constant shaking (30 rpm on a Polymax 1040, Heidolph) and stopped by addition of glycine at a final concentration of 0.125 M. Fixed cells were harvested via centrifugation at 2000x*g* for 5 min at 4 °C, and each pellet was resuspended in 5 ml ice cold PBS containing 50 µl 100 mM PMSF and collected as before. This washing step was repeated once, and pellets were flash frozen in liquid nitrogen and stored at -80 °C until proceeded further.
For lysis, cell pellets were thawn on ice for 1 h and resuspended in 500 µl LB1 freshly supplemented with protease inhibitor (1X), followed by incubation on a rotating wheel for 10 min at 4 °C. Cells were collected via centrifugation at 2000x*g* for 5 min at 4 °C, and each pellet was resuspended in 500 µl LB 2 freshly supplemented with protease inhibitor (1X), followed by incubation and collection as before. Pellets were then resuspended in 120 µl LB3 and transferred into Bioruptor® Microtubes (Diagenode, cat. #C30010016) and sonicated in 200 µl LB3 for 10 min on the Bioruptor® Pico (Diagenode).

2.2.14.2 Pre-treatment of magnetic beads

For 10 pre-clearing reactions, 1 ml TE buffer (Sigma-Aldrich) supplied with 1 mg denaturated tRNA (Sigma-Aldrich) and 20 µg of rabbit IgG isotype control (**Table M5**) was used to resuspend 200 µl Dynabeads(R) Protein A for Immunoprecipitation (Life Technologies) after bead storage solution had been discarded on a MagnaRack™ Magnetic Separation Rack (Thermo Fisher Scientific). The pre-clearing-bead mixtures were incubated on a rotating wheel at 4 °C overnight and subsequently, pre-clearing beads were washed three times with each 1 ml WB1 for 5 min on a rotating wheel at 4 °C. Afterwards, pre-clearing beads were resuspended in 200µl TE buffer.
For each ChIP reaction, 20 µl Dynabeads were incubated with 100 µg BSA and 200 µg denaturated tRNA in 1 ml TE on a rotating wheel overnight at 4 °C. On the next day, blocked beads were washed three times with WB1 as described before and resuspended in 20 µl TE per ChIP.

2.2.14.3 Chromatin immunoprecipitation

Per sample, 10 µl (5 %) of sheared chromatin was stored as input sample at -80 °C, and the remaining chromatin was diluted to 2 ml in ChIP dilution buffer. 100 µl pre-clearing beads (see above section) were added and the mixtures were incubated for 2 hours at 4 °C on a rotating wheel. Thus pre-cleared chomatin was collected and divided into two aliquots per sample, to which 2 µl rabbit IgG control antibody or 1.4 µl H3K27me3 antibody (**Table M5**) were added, respectively, and incubated on a rotating wheel at 4 °C overnight. Then, each ChIP reaction was incubated with 20 µl blocked beads (see above section) for 3 hours at 4 °C on a rotating wheel. Chromatin-bound beads were washed according to the following steps, each performed for 5 min at 4 °C on a rotating wheel:
2 x WB1
1x WB2
1x WB3
2x WB4
Antibody-bound chromatin was then eluted twice from the beads via incubation with first 130 µl, then 100 µl Elution buffer/sample under constant shaking at 1,400 rpm (on a Thermomixer Comfort, Eppendorf) for 15 min at 65 °C, and supernatants of the two elution rounds were combined. Input samples were thawn, filled up to 230 µl with Elution buffer and treated along with the ChIP samples. All samples were filled up with TE to a volume of 300 µl and incubated with 200 µg/ml RNase A (Life Technologies) for 45 min at 37 °C. Then, sodium chloride and 3 µl Proteinase K (Life Technologies) were added to final concentrations of 150 µM and 260 µg/ml, respectively, and samples were de-crosslinked under occasional shaking (15 min per hour) at 600 rpm and 65 °C overnight. ChIPed DNA was purified with the QIAquick PCR Purification Kit according to the manufacturer's specification and used to quantify the enrichment of H3K27me3 over input samples as described below.

Table M14. Buffers used for ChIP. WB, Wash buffer; LB, Lysis buffer.

Name	Composition
Crosslinking solution	50 mM Hepes/KOH, 100 mM NaCl, 1 mM EDTA, 0.5 mM EGTA, 11% Formaldehyde
WB 1	50 mM Tris.HCl pH 8.8, 0.1% SDS, 0.1% Na-Deoxycholate, 1% Triton X-100, 150 mM NaCl, 1 mM EDTA, 0.5 mM EGTA
WB 2	WB2, 50 mM Tris.HCl pH 8.0, 0.1% SDS, 0.1% Na-Deoxycholate, 1%, Triton X-100, 500 mM NaCl, 1 mM EDTA and 0.5 mM EGTA
WB 3	50 mM Tris.HCl pH 8.0, 250 mM LiCl, 0.5% Na-Deoxycholate, 0.5% NP-40, 1 mM EDTA and 0.5 mM EGTA
WB 4	50 mM Tris.HCl pH 8.0, 10 mM EDTA and 5 mM EGTA
LB 1	50 mM Hepes/KOH, 140 mM NaCl, 1 mM EDTA, 10% glycerol, 0.5% NP-40, 0.25% Triton X-100
LB 2	10 mM Tris.HCl, 200 mM NaCl, 1 mM EDTA, 0.5 mM EGTA
LB 3	10 mM Tris.HCl, 100 mM NaCl, 1 mM EDTA, 0.5 mM EGTA, 0.1% Na-Deoxycholate, 0.5% N-lauroylsarcosine, 0.1% SDS
ChIP dilution buffer	50 mM Tris.HCl pH 8.0, 167 mM NaCl, 1.1% Triton X-100 and 0.11% Na-Deoxycholate
Elution buffer	1% SDS, 0.1 M NaHCO3

2.2.14.4 Primer design, qPCR and enrichment analysis

Primers for the *ASXL1, ASXL3, ZIC1/ZIC4, FOXP2* and *HOXB2* loci were designed to span 80-150 bp regions that showed an enrichment for H3K27me3 in H1 hESC according to ENCODE data[200], using Primer3Plus (*http://primer3plus.com/cgi-bin/dev/primer3plus.cgi*). Quantitative detection of target loci by selected primers was tested in SYBR® Green qPCR (see chapter **2.2.10.4**) on gDNA at concentrations of 0.6, 3, 15, 75, 150 and 300 ng/µl. Primer pairs that were used in SYBR® Green qPCR on input samples and IgG control/H3K27me3 ChIP samples are shown in **Table M13**. Primers for the detection of the *ACTIN (ACTB)* locus (negative control) were obtained from and validated by Dr. Krendl[199].

Table M13. Primers used for detection of H3K27me3 enrichment in ChIP samples (5′-3′). *from[199]

Name	forward sequence	reverse sequence	genomic location
ZIC1-ChIP-Ex1	aacgtggtcaacgggcag	gcagcatagtgctccgaacg	chr3:147128490+147128671
ZIC4-ChIP-Ex3	gggaaaggacaagggaaggg	aacaggccaaccacatttgc	chr3:147113701+147113827
FOXP2-ChIP-Promoter	cgactgagatgtcctttcgc	cgttttggtgaaattcgcagc	chr7:113723769+113723850
FOXP2-ChIP-Intron	taaccgtgcacagggatgac	gcgacctctctaaagcggaa	chr7:113727353+113727474
ACTB-ChIP*	aacggcagaagagagaacca	aagatgacccaggtgagtgg	chr7:5568699+5568803
HOXB2-Intron-ChIP	tctctagtctacagccccgg	ggatctgaggttccggcg	chr17:48543918+48544024
ASXL1-ChIP-Intron1	tctaacggttctgcacctgg	cccagggtcataaacacccg	chr20:32360403+32360545
ASXL3-ChIP-Intron1	gttcggcgtttgtgagttcaa	cacagacacgcaaccaccta	chr18:33579112+33579216

For enrichment analysis, first, input Ct values were adjusted according to the dilution factor (20x), then, the mean Ct of 2 technical replicates per sample and primer was compared to the adjusted input value using the following formula:

$$\text{Enrichment (in \% input)} = 100 \times 2^{-(\text{Ct (IP sample)} - \text{Ct (adjusted input)})}$$

H3K27me3 antibody specificity was validated via high enrichment in repressed *HOXB2* locus, and low enrichment for H3K27me3 at the *ACTINB* locus.

2.2.15 Co-Immunoprecipitation

Nuclear lysates of neurospheres derived at NC differentiation day 3 from PB-*ASXL1*^{PSC} with or without DOX treatment were prepared and subjected to co-immunoprecipitation using EZH2 and IgG control antibodies (**Table M5**) with the Nuclear Complex Co-IP Kit (Active Motif, cat. # 54001) according to the manufacturer's instructions, and detection was performed via Western Blot, using ASXL1 and EZH2 antibodies (**Table M5**), as described in section **2.2.13**.

2. 2.16 Chicken experiments

Experiments were carried out in collaboration with Dr. Rada-Iglesias at the CMMC (Cologne, Germany). According to German animal care guidelines, no IACUC (Institutional Animal Care and Use Committee) approval was necessary to perform chicken embryo experiments. White fertilized chicken eggs (*Gallus gallus domesticus*)

were obtained from a local breeder (LSL Rhein-Main) and incubated at 37 °C and 80% humidity until reaching desired stages as determined according to Hamburger and Hamilton (HH)[201].

2.2.16.1 In ovo transplantation of neurospheres and analysis of emigration

Neurospheres, which I derived from GFP-*ASXL1*$^{PSC/PSC}$ and GFP-control lines at day 5 of NC differentiation, were inserted in the developing anterior neural region (i.e. hindbrain) of chicken embryos at the 8-10 somite stage (HH10) by Dr. Rehimi (CMMC Cologne). The operated eggs were re-incubated until stage HH22, when the embryos were isolated and analyzed under a fluorescence stereo microscope (Olympus SZX 16).
The distance between transplanted neurospheres and furthest migrated cells, the diameter of transplanted neurospheres and the total number of emigrated cells were determined using the Fiji/ImageJ software[202].

2.2.16.2 In ovo electroporation of truncated ASXL1 overexpression constructs

For overexpression experiments in chicken embryos, the truncated chicken (*Gallus gallus*) *ASXL1* cDNA sequence (Gg-*ASXL1*^{PSC}; N-terminal 2445 bp) and the truncated human *ASXL1* cDNA sequence (*hASXL1*^{PSC}; N-terminal 2892 bp) were each cloned into the pCIG vector harboring a *GFP* coding sequence coupled to the T2A cleavage signal (obtained from Dr. Rehimi).
5 µg of the pCIG vector were linearized using 20 Units of *EcoRI*-HF and *XhoI* (NEB) according to the supplier's specifications, and purified with the QIAquick PCR Purification Kit. Gg-*ASXL1* and h*ASXL1* fragments were amplified from chicken (obtained from Dr. Rehimi) or human cDNA (control hESC-derived) via RT-PCR as described in section **2.2.10.3**, using following primers (5'-3'):

Gg-*ASXL1*^{PSC} -pCIG-for
TCTCATCATTTTGGCAAAGAATTGCTCGAGGCCACCATGAGGGAGATGAAGCAGC
Gg-*ASXL1*^{PSC} -pCIG-rev
AGGGGCGGATCCCCCGGGCTGCAGGAATTCTTAGAGTTCTGACACAACCCTGC

hASXL1^{PSC} -pCIG-for
TCTCATCATTTTGGCAAAGAATTGCTCGAGGCCACCATGAAGGACAAACAGAAGAAGAAGAAG
hASXL1^{PSC} -pCIG_EX-rev
AGGGGCGGATCCCCCGGGCTGCAGGAATTCTTAAGATGGCACAGTCCAGAGTGA

PCR products were purified using the QIAquick PCR Purification Kit. 100 ng linearized pCIG vector (0.024 pmol) were mixed with either 78 ng Gg-*ASXL1*^{PSC} or 94 ng h*ASXL1*^{PSC} fragment (0.048 pmol each), and ligated using the Gibson Assembly Master Mix (NEB). Transformation into competent bacteria and colony-PCRs were performed as described in chapters **2.2.8.1** and **2.2.8.3**, using following primer combinations (5'-3'):

pCIG- Gg-*ASXL1*^{PSC} construct: Gg-*ASXL1*^{PSC} -pCIG-for + ATCCTCACCCCTGTTTCGTT

pCIG- *hASXL1*^{PSC} construct: *hASXL1*^{PSC} -pCIG-for + CTGCTGCTGGAAGTGTGATG

Positive bacteria clones were subjected to plasmid preparation and confirmation of constructs by Sanger sequencing, all as described in sections **2.2.8.3** and **2.2.8.4**, using following primers (5'-3'):

pCIG- Gg-*ASXL1*^{PSC} construct
1: ATCCTCACCCCTGTTTCGTT
2: CCAGATATGCCCCAGGATCA

pCIG- *hASXL1*^{PSC} construct
1: CTGCTGCTGGAAGTGTGATG
2: GTCAGCCCACTTACCAGATATGC
3: GAGGAGGAGAGGGGTTGTTT
4: GGCTTCATTAGACCCACAGC

Injections of correct pCIG- Gg-*ASXL1*^{PSC} and pCIG-h*ASXL1*^{PSC} constructs into the target site of the developing brain and neural tube of HH9-10 chicken embryos, followed by electroporation and imaging at developmental stages HH19 and HH24, were carried out by Dr. Rehimi. For control experiments, the pCIG vector expressing only GFP was electroporated.

2.2.17 Mouse experiments

The *Asxl1*$^{tm1a(EUCOMM)Wtsi}$ mouse strain (*Mus musculus*), described by McGinley *et al.*[107], was maintained on a C57BL/6NCrl background. Evaluation of this genetically modified line (Abschlussbeurteilung genetisch veraenderter Zuchtlinien) did not indicate a burden according to the German legal guidelines. Mouse husbandry and experiments were performed at the Helmholtz Center Munich respecting animal welfare in accordance to European Directive 2010/63/EU.

2.2.17.1 Breeding, genotyping and phenotypes

Breeding of heterozygous carrier mice, as determined by genotyping for each generation, to C57BL/6NCrl wildtype (wt) mice was performed for ten generations to ensure generation of congenic animals[203].
Genotyping was performed on animals at postnatal day P20-22. Genomic DNA was extracted from ear punch biopsies and the *Asxl1* target region was amplified by PCR, all as described in sections **2.2.9** and **2.2.8.1**, via combination of following primers (strategy and primers supplied by the EuMMCR at the Helmholtz Center Munich):

Detection of reporter construct knockin: CAACGGGTTCTTCTGTTAGTCC
Asxl1-for: ATATACTTGGTTACACTCGGAGGC
Asxl1-rev: CTCCTCTAATTCATTTCCAAACCAGG

The presence of two bands in agarose gel electrophoresis allowed for the identification of heterozygous animals, as opposed to the generation of one PCR product in wt animals. Occasionally (<1 pup per litter), one of the following phenotypes was observed in heterozygous animals: unilateral microphthalmia, anaphthalmia or cataracts and reduced birth weight, and phenotypic mice and wt littermates were imaged.

2.2.17.2 LacZ staining of whole-mount mouse embryos

As the *Asxl1*$^{tm1a(EUCOMM)Wtsi}$ mouse strain carries a *lacZ* reporter within the endogenous *Asxl1* locus, X-Gal stainings were performed on whole-mount embryos to assess *Asxl1* expression patterns *in vivo*. Composition of used buffers and solutions are listed in **Table M15**.
One timed pregnancy (heterozygous x wt mating) was terminated via cervical dislocation 11 days after a mating plug was observed (corresponding to embryonic day

E11.5), and embryos were prepared in cold PBS. Tail tips were separated and subjected to genotyping as described above, and embryos were fixed in LacZ Fix at RT for 30 min. Followed by 3x 5 min of washing in LacZ Wash buffer, embryos were stained for 3 h in LacZ Stain at 37 °C in darkness. Subsequently, embryos were washed for 3x 15 min in LacZ Wash buffer and fixed overnight at 4 °C (in darkness) using lacZ Fix. Embryos were then transferred to 4 % PFA and imaged on a Zeiss Stereo Lumar.V12 microscope.

Table M15. Buffers and solutions used for X-Gal stainings.

Name	Composition
LacZ Fix	4 % Paraformaldehyd, 5 mM EGTA (pH 7.4), 2 mM $MgCl_2$ in PBS (pH 7.4)
LacZ Wash	2 mM $MgCl_2$, 0.02 % NP-40 in PBS (pH 7.4)
LacZ Stain	1 mM Ferrocyanide (Sigma-Aldrich, cat. #P9387), 1 mM Ferricyanide (VWR International, cat. #0713), 1 mg/ml X-β-Gal (Carl Roth, cat. #2315.2) in LacZ Wash

2.2.18 Zebrafish experiments

Zebrafish experiments were carried out in collaboration with Dr. Hernan Lopez-Schier (Helmholtz Center Munich).
All experiments were approved by the government of Upper Bavaria (Regierung von Oberbayern, Munich, Germany; Tierversuchsvorhaben Gz.: 55.2-1-154-2532-202-2014) and were performed in accordance with animal protection standards. The zebrafish (*Danio rerio*) wt line AB was used. Zebrafish embryos and larvae were kept at 28.5 °C and were staged according to Kimmel *et al.*[204].

2.2.18.1 Transcription analysis in zebrafish embryos and larvae

Zebrafish wt embryos were collected at different developmental stages and 2-10 embryos per stage and replicate were euthanized via transfer to liquid nitrogen. Subsequently, RNA extraction was performed using the RNeasy Micro Kit (Qiagen, cat. #74004) according to the manufacturer's specifications. Isolated RNA was subjected to reverse transcription and qPCR/RT-PCR as described in section **2.2.10**, using primers denoted below:

RT-PCR
asxl1 (Exon 5-10)-forward: AACAGCATCCACCACATCAA -reverse: ACATCTCCAGCTTCGCTCAT
asxl2 (Exon 5-9)-for: GCAGCAAACTCATGTCTCCA -rev: CCTTCAAGGCTCCATCCATA
gapdh for: GTGTAGGCGTGGACTGTGGT -rev: TGGGAGTCAACCAGGACAAATA

Power SYBR® Green qPCR:
asxl1-for: AACAGCATCCACCACATCAA -rev: AGGCACTGGAGGAAGTCTCA
asxl2-for: TGAGGGAACGACAGAAGAAGA -rev: CATGGGTGTGTTGGGGTACT
*elfa**-for: CTTCTCAGGCTGACTGTGC –rev: CCGCTAGCATTACCCTCC

**elfa* was selected as housekeeping gene as *gapdh* is not stably expressed in zebrafish embryos[205].

2.2.18.2 RNA in situ hybridization

To detect expression of *asxl1* and *asxl2* in zebrafish embryos, antisense RNA probes complimentary to the endogenous transcripts were generated and used for *in situ* hybridizations, alongside with sense probes as negative controls.

2.2.18.2.1 Generation of probes

Following primers were used to amplify each two fragments of zebrafish *asxl1* and *asxl2* transcripts in RT-PCR (see chapter **2.2.10.3**) from zebrafish cDNA (isolated at 6 hpf, 1 dpf, 2 dpf and 3 dpf):

asxl1 (Exon 5-10): see above*
asxl1 (Exon 1-2)-for: GGCTGTAGGAGCGACTGAAG -rev: TTGGGGCATCAGAAAAGTTC
asxl2 (Exon 5-9): see above
asxl2 (Exon 3-7): TGGCACTTCTCCTCTTGCTT -rev: GGCAGCGTTCACTCTTTTTC

*As this primer set amplifies two alternative *asxl1* transcripts, the larger fragment including the alternatively spliced exon was isolated.

PCR products were purified from agarose gels using the QIAquick Gel Extraction Kit. 50 ng of each fragment were treated with one unit of Taq Polymerase, according to the supplied protocol (Qiagen, cat. #201205), for 25 min at 72 °C to create 3'adenylation for cloning into the pCR™II-TOPO™ Vector with the TOPO™ TA Cloning™ Kit (Dual Promoter, Life Technologies, cat. #K461020) according to the manufacturer's specifications. Transformation, plasmid isolation and Sanger sequencing (using primers M13-FP: TGTAAAACGACGGCCAGT and M13-RP: CAGGAAACAGCTATGACC; GATC Biotech), were performed as described in sections **2.2.8.3** and **2.2.8.4**.
Correct clones were linearized using either *HindIII* or *EcoRV* (NEB, cat. #R0104 and R0195, respectively) according to the orientation of inserts, to allow for *in vitro* transcription of antisense and sense transcripts from the SP6 or T7 promoter present in the pCR™II-TOPO™ Vector. *In vitro* transcription was performed using the DIG RNA labeling Kit SP6/T7 (Roche/Sigma-Aldrich, cat. #11175025910) according to the manufacturer's instructions, followed by DNase I (Life Technologies) treatment at 37 °C for 30 min. RNA probes were purified LiCl/Ethanol precipitation as follows: To each transcription reaction, 80 µl TE, 10 µl of 4 M LiCl (Sigma) and 200 µl 100 % Ethanol (Carl Roth) were added, and precipitation was performed at -20 °C overnight. RNA was collected via centrifugation at 4 °C and 13,000 rpm in a tabletop centrifuge (Fresco 21, Thermo Fisher Scientific) for 20 min, pellets were washed once with 75 % Ethanol, centrifuged as before for 15 min and, after removal of ethanol, dried for 5 min at RT. Each pellet was resuspended in 12 µl RNase free TE buffer, and 1 µl was mixed with 9 µl RNAse-free water and 2 µl Ambion loading dye (Thermo Fisher Scientific, cat. #AM8546) and analyzed via gel electrophoresis for 5 min at 120 V. RNA probes were stored at -80 °C.

2.2.18.2.2 Hybridization and staining

All solutions and buffers are listed in **Table M16**.
Embryos of wt zebrafish were incubated in Petri dishes containing fish water and collected at 6 hpf, 36 hpf and 48 hpf. For latter stages, fish water was replaced with 0.0045 % 1-Phenyl-2-Thiourea (PTU) solution in 1x Danieau medium starting from the end of gastrulation in order to prevent pigmentation[206]. Embryos at 6 hpf were manually dechorionated using forceps. All embryos were fixed overnight in a freshly made 4% formaldehyde/PBS solution at 4 °C.
The next day, embryos were transferred to methanol (MeOH) in following steps (all RT incubation steps under constant shaking):

PBS-T	10 min
25% MeOH/75% PBS-T	5 min
50% MeOH/50% PBS-T	5 min
75% MeOH/25% PBS-T	5 min
100% MeOH	1 h at -20 °C

Subsequently, embryos were re-hydrated in following steps:

75% MeOH/25% PBS-T	5 min RT
50% MeOH/50% PBS-T	5 min RT
25% MeOH/75% PBS-T	5 min RT
100% PBS-T	3x 5 min RT

Proteinase K digestion (10 µg/ml in PBS) was performed at RT for 2 min (6 hpf embryos), 10 min (36 hpf) or 15 min (48 hpf). Embryos were washed twice in PBS-T for 5 min, re-fixed in 1 ml 4 % formaldehyde/PBS for 20 min at RT, and washed five times for 5 min in PBS-T. Embryos were then transferred to HM+ for 5 min at RT, then pre-hybridized in HM+ for 2 h at 67 °C. Per probe and stage, 500 µl HM+ plus 500 ng probe (*asxl1/asxl2*, antisense/sense) were combined and heated to 67 deg for 10 min. The HM+/probe mix was then added to embryos and hybridized overnight at 67 °C.
The following day, hybridized embryos were washed according to the following steps, for each probe/stage in 500 µl of the respective solutions:

100 % HM-	67 °C	5 min
75% HM-/25% 2xSSC	67 °C	15 min
50% HM-/50% 2xSSC	67 °C	15 min
25% HM-/75% 2xSSC	67 °C	15 min
2x SSC	67 °C	15 min
0.1x SSC	67 °C	2 x 30 min
75% 0.1x SSC/25% PBS-T	RT + shaking	10 min
50% 0.1x SSC/50% PBS-T	RT + shaking	10 min
25% 0.1x SSC/75% PBS-T	RT + shaking	10 min
PBS-T	RT + shaking	10 min

Washed embryos were transferred to 400 µl Blocking buffer for 2 h shaking at RT and afterwards incubated with 500 µl DIG antibody (supplied by Dr. Lopez-Schier) in Blocking buffer (1:2000) shaking at 4 °C overnight in darkness.
The following day, washes were performed as follows:

PBS-T	RT + shaking + darkness	3 x 10 min
PBS-T	RT + shaking + darkness	4 x 30 min
PBS-T	RT + shaking + darkness	4 x15 min
PBS-T	4 °C + shaking + darkness	overnight in 1500 µl

The following day, all washing and incubation steps were performed in darkness. Embryos were first incubated in 500 µl AP- buffer for 5 min at RT, then twice for 5 min in 500 µl AP+ buffer, and subsequently transferred to 12-well plates. 2 ml staining solution [1 ml AP+ plus 4.5 µl NBT (Sigma-Aldrich, cat. #N6876) and 3.5 µl BCIP (Sigma-Aldrich, cat. #B6149)] were added per well and incubated while shaking at RT. The reaction was monitored until the desired staining intensity was reached, and embryos

were washed 3x 5 min with PBS-T at 4 °C while shaking. The staining reaction was stopped by washing twice in PBS-T plus 1 mM EDTA at 4 °C. Embryos were imaged and stored in stop solution or glycerol.

Table M16. Buffers and solutions used for RNA in situ hybriziation in zebrafish embryos. Chemicals and reagents were obtained from Dr. Lopez-Schier, Helmholtz Center Munich.

Name	Composition
PBS-T	PBS + 0.2 % Tween-20
HM-	60 % formamide, 5 x SSC, 0.1 % Tween-20, 0.0092 M citric acid in H2O
HM+	HM- plus 50 µg/ml Heparin and 500 µg/ml tRNA (yeast)
Blocking buffer	2 mg/ml BSA and 1 % lamb serum in PBS-T
AP-	100 mM Tris.Hcl (pH 9.5), 100 mM NaCl, 0.1 % Tween-20 in H_2O
AP+	AP- plus 50 mM $MgCl_2$
20 x SSC	3 M NaCl, 300 mM Na3Citrate x2 H_2O; pH 7.0

2.2.18.3 Generation of zebrafish mutant via CRISPR/Cas

To generate truncating *asxl1* mutations in the zebrafish, insertions/deletions (indels) were generated in the center region of the zebrafish *asxl1* locus using the CRISPR/Cas technology. To optimize the injection procedure, first the *slc452* gene, which is disrupted in albino mutants, was targeted as pigmentation presented an efficient readout for successful CRISPR targeting.

2.2.18.3.1 Generation of gRNAs

gRNAs were designed using the MIT CRISPR design webpage as described in section **2.2.3.1**. Two gRNA sequences targeting exon 6 of the *slc45a*2 locus were selected, and one gRNA targeting exon 12 of *asxl1*. Oligonucleotides were designed to contain the gRNA sequence flanked by a T7 promoter and the gRNA scaffold, according to a published method[207], resulting in following antisense oligonucleotides (5′-3′, gRNA indicated in lower case):

slc45a2 (A)
AAAAGCACCGACTCGGTGCCACTTTTTCAAGTTGATAACGGACTAGCCTTATTTTAACTTGCTATTTCT
AGCTCTAAAACatatatggcagaagcagcctCTATAGTGAGTCGTATTACGC
slc45a2 (B)
AAAAGCACCGACTCGGTGCCACTTTTTCAAGTTGATAACGGACTAGCCTTATTTTAACTTGCTATTTCT
AGCTCTAAAACatcagaccggttcccaaaccCTATAGTGAGTCGTATTACGC

asxl1
AAAAGCACCGACTCGGTGCCACTTTTTCAAGTTGATAACGGACTAGCCTTATTTTAACTTGCTATTTCT
AGCTCTAAAACctgggcacgggcttgctgtgCTATAGTGAGTCGTATTACGC

The gRNA antisense oligonucleotides were annealed to the T7 primer (TAATACGACTCACTATAG) in TE buffer at a final concentration of 50 µM each for 5 minutes at 95 °C, then cooled to RT for 5 hours and diluted to 3 µM in TE buffer. 1 µl of the annealed mix was subjected to in vitro transcription with the MEGAshortscript™ T7 Transcription Kit (Thermo Fisher, cat. #AM1354) according to the supplied protocol (4 h incubation at 37 °C). gRNAs were treated for 15 min with TURBO DNase supplied with the kit, and extracted with phenol:chloroform (Roti®-

Phenol/Chloroform/Isoamylalkohol, Carl Roth, cat. #A156.3) followed by 2-propanol precipitation overnight at -20 °C according to the supplied protocol. The pellet was resuspended in 20 µl RNase-free H2O, aliquoted and stored at -80 °C. 1 µl per gRNA were analyzed via gel electrophoresis to exclude degradation.

2.2.18.3.2 Generation of Cas9 mRNA

The pCS2-Cas9-NLS plasmid[207], harboring a *Cas9* sequence fused to a nuclear localization signal (NLS) was obtained from Dr. Chapouton (Helmholtz Center Munich), with consent from Dr. Schmid, DZNE Munich, Germany.
According to the following reaction mixture, the pCS2-Cas9-NLS plasmid was linearized for 2 hours at 37 °C:

5 µl Buffer B (Supplied with *ApaI* enzyme)
12.5 µl pCS2-Cas9-NLS plasmid (= 5 µg)
5 µl *ApaI* (=50 units, Thermo Fisher, cat. #ER1411)
27.5 µl dH_2O

Linearization was confirmed on a 0.8 % agarose gel, and the linearized plasmid was in vitro transcribed using the SP6 mESSAGE machine Kit (Thermo Fisher #AM1340) followed by LiCl precipiation of the Cas9 mRNA overnight at -20 °C, all according to the supplied protocols. The pellet was resuspended in 20 µl RNase-free H_2O, of which 1 µl were analyzed via gel electrophoresis to exclude degradation.

2.2.18.3.3 Microinjection and analysis of targeted fish and mutants

gRNA and Cas9 mRNA were co-injected into one-cell stage zebrafish embryos using a Femtojet (Eppendorf). For each *slc45a2* gRNA, microinjections were performed according to two published methods:

	HW[208]	HR[207]
Cas9-NLS mRNA	300 ng/ul	0.5 µg/ul
gRNA	12.5 ng/ul	2.4 µg/ul
Injection volume	2 nl	2 nl

Embryos were assessed daily on a stereoscope, with uninjected siblings as controls, to identify perturbed pigmentation, indicating successful targeting of the *slc45a*2 locus.
According to these test experiments, *asxl1* gRNA was injected together with *Cas9*-NLS mRNA into zebrafish embryos using method 'HW'. Several injected founder embryos (1 dpf, with uninjected embryos as control) were subjected to genotyping as described below to confirm targeting of the *asxl1* locus, and the remaining injected fish were maintained. Adult founder fish were bred to wt fish, and the adult F1 generation was genotyped to detect heterozygous *asxl1* mutants. Heterozygous matings were then performed to generate heterozygous and homozygous F2 offspring, which was assessed for phenotypes and imaged on the Leica DMIL LED microscope. Phenotypes of F2 embryos and larvae were classified as normal, mild phenotype (slightly shorter tail or mild edema), pericardial edema, shortened/no tail (caudal truncations), and combined edema/no tail. Several embryos of each phenotype were subjected to genotyping as described below.

2.2.18.3.4 Genotyping of founder, F1 and F2 fish

Genomic DNA isolation was performed on single embryos that had been euthanized via freezing as described before, or on fin biopsies derived from adult fish anesthetized

using a 0.004 % MS-222 solution (Sigma-Aldrich, cat. #E10521), for the DNA extraction protocol see section **2.2.9**. The target region in *asxl1* was amplified via PCR as described in chapter **2.2.8.1** using following primers (5'-3'):

ZF-asxl1-GT-for: CTTCCTCTTCCTCCTCCAC
ZF-asxl1-GT-rev: CTGTAGTTGTGCTCCCGAC

PCR products were isolated using the QIAquick PCR Purification Kit and subjected to Sanger sequencing using primer 'ZF-asxl1-GT-for' (see chapter **2.2.8.4**). Results were analyzed for indel mutations and mutant sequences were transcribed *in silico* using the Ape software (see **Table M6**) to determine the putative effects of introduced mutations on expression of theoretical truncated asxl1 proteins.

2.2.19 Statistical analysis

Sample sizes are indicated in the respective figures and figure captions; values are expressed as mean +/- standard error of the mean as calculated with the Excel software (version 14.0.0 for Mac). For pairwise comparison of means, Shapiro-Wilk test was applied in R studio version 3.3.2 to evaluate normal distribution of samples, and if given, Welch's t-test was applied. Otherwise, Wilcox test was used to test for statistical significance.

2.2.20 Generation of charts and visualization of data from public databases

Boxplots, PCA plots and volcano plots were generated in R studio v3.3.2, all other charts were generated using the Excel software (version 14.0.0 for Mac).
ENCODE data[200] on H3K4me3-, H3K27me3- and EZH2-ChIP, as well as RNA-seq in H1 hESC, HSMM and NHEK cell lines were visualized on the IGV genome browser 2.3 or the WashU epigenome browser under *http://epigenomegateway.wustl.edu/browser/*, respectively.
Heatmaps displaying transcriptional data of the developing human brain were from: ©2010 Allen Institute for Brain Science. BrainSpan Atlas of the Developing Human Brain, available under: *http://www.brainspan.org/*.
The ASXL gene tree was generated with the Comparative Genomics tool of the Ensembl genome browser 91 under *https://www.ensembl.org/index.html*.
Annotation of functional protein domains in chicken and zebrafish ASXL proteins was extracted from data on the Uniprot database[209] under *https://www.uniprot.org/*.

3. Results

3.1. Expression of *ASXL* genes in pluripotency, differentiation and brain development

Despite mutations being involved in developmental syndromes, no studies examined the contribution of *ASXLs* to human embryonic development thus far. Focusing first on potential roles during progenitor commitment at the germ layer level, I evaluated transcriptional levels and histone marks of human *ASXL* genes during early differentiation of human pluripotent stem cells and analyzed datasets of human embryonic development in parallel.

As shown in **Fig. 9A**, transcripts of all three human paralogs *ASXL1*, *2* and *3* could be detected by RNA-seq in hESCs of the H9 line; while *ASXL1* and *ASXL2* were expressed at similar levels, *ASXL3* was detected at lower transcript numbers. This corresponded to RNA-seq data based on the H1 line (ENCODE project[200]; **Fig. 9B**). Interestingly, reviewing the ENCODE epigenome dataset revealed that the transcriptional start sites (TSSs) of both *ASXL1* and *ASXL3* exhibit H3K27m3 as well as H3K4me3 in H1 cells (**Fig. 9B**), reflecting a bivalent state characteristic of developmental regulators. The bivalent chromatin state of *ASXL1* is resolved to H3K4 trimethylation in two adult cell lines representing human skeletal muscle and epidermal keratinocytes, indicating that it is actively transcribed. Conversely, the TSS of *ASXL3* retains a bivalent status and *ASXL3* is not expressed in these somatic cell lines. The TSS of *ASXL2* is found in an H3K4 trimethylated state in undifferentiated cells as well as in selected somatic cell lines, and *ASXL2* is expressed in all these lines (**Fig. 9B**).

To analyze transcriptional dynamics during commitment to progenitors equivalent to the germ layer stage of development, I used diverse differentiation protocols. *ASXL1* and *ASXL2* levels increased after three days of growth in a medium that promotes spontaneous differentiation induced by withdrawal of basic FGF (bFGF), which was accompanied by a slight decline of *OCT4/POU5F1* expression (**Fig. 9C**). Induction of specific germ layer programs via BMP4 (mesoderm induction[210]), retinoic acid (RA; neural induction[211]) and Activin A (endoderm induction[212]) treatment, likewise induced upregulation of *ASXL1* and *ASXL2* (**Fig. 9C**). Murine *Asxl* genes are expressed in the embryonic brain[115], and intellectual deficits and microcephaly are observed in all BOS patients[89]. I therefore investigated the involvement of *ASXLs* in neuronal differentiation. Indeed, I noted strong induction of *ASXL1* in human neural stem cell cultures compared to undifferentiated cells, while the induction of *ASXL2* and *ASXL3* was considerably lower (**Fig. 9D,** RNA provided by Dr. Klaus, Helmholtz Center Munich). It should be mentioned that given the initial level of *ASXL1* in undifferentiated cells (**Fig. 9A**), these data indicate that *ASXL1* is highly expressed in neural stem cells. Analysis of published RNA-seq data that has been based on samples collected at different timepoints during neuronal differentiation[213] gave similar results: *ASXL1* was strongly upregulated already at day 11 of neuronal differentiation, prior to *PAX6,* the neuronal master regulator, and its levels were also maintained longer compared to *PAX6* upon passaging (**Fig. 9E**). *ASXL2* levels declined slightly during differentiation, while the *ASXL3* transcript was only detected at very low levels (**Fig. 9E**).

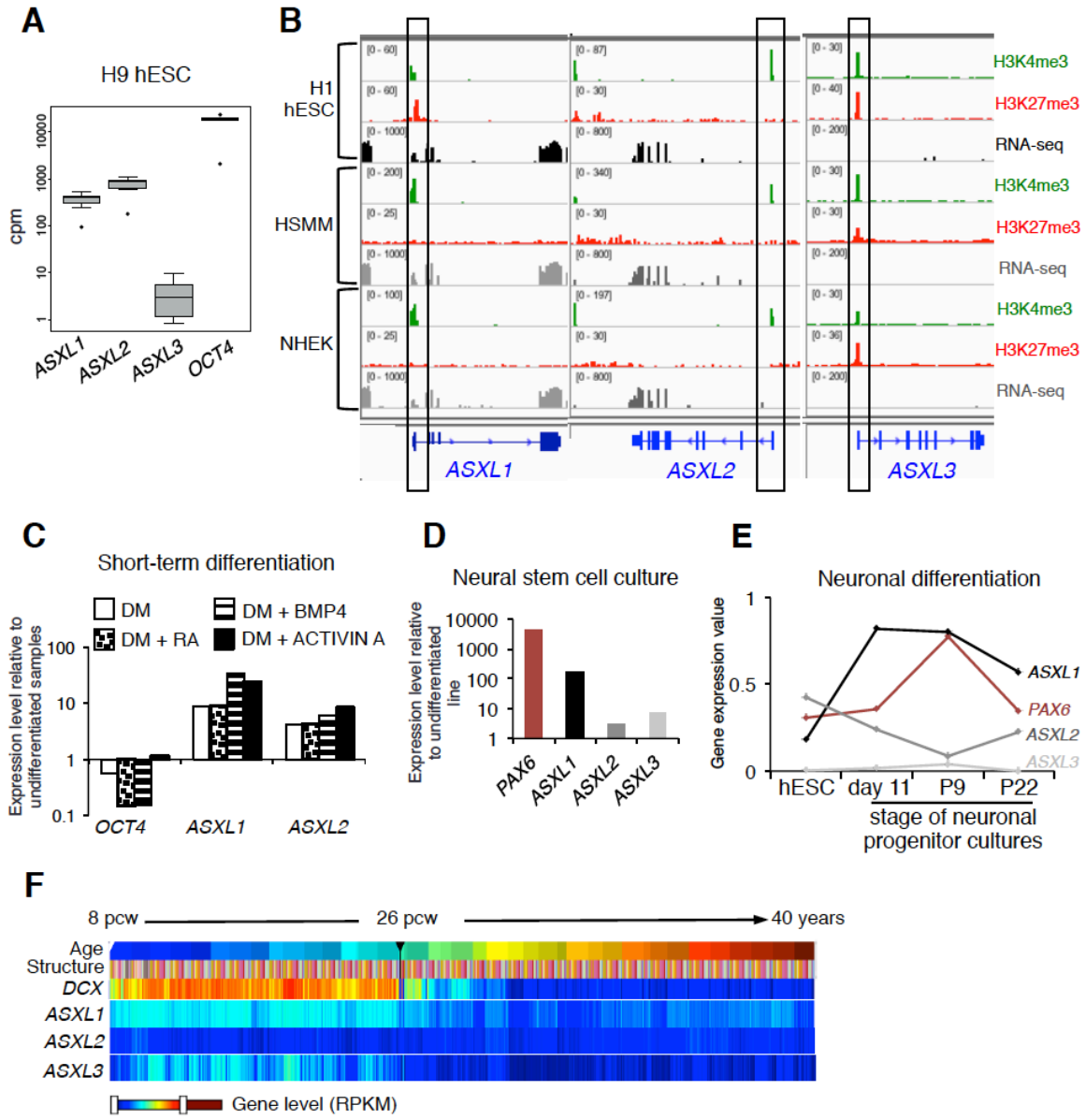

Figure 9. Regulation of *ASXL* paralogs during progenitor commitment from hESCs and human brain development.
(A) Transcript levels of *ASXL* genes and pluripotency factor *OCT4* in undifferentiated hESC; cpm, counts per million (n=8; RNA-seq data from[199]) **(B)** Transcript levels and histone modifications H3K4me3 and H3K27me3 at *ASXL* loci in H1 hESC and human cell lines HSMM (Human Skeletal Muscle and Myoblast) and NHEK (Normal Human Epidermal Keratinocytes). Data from the ENCODE project[200]. **(C)** qPCR analysis of *ASXL* genes and *OCT4* in H9 hESC samples treated with 50 ng/ml BMP4, 0.5 µM retinoic acid (RA), 5 ng/ml ACTIVIN A or solely FBS-containing differentiation medium (DM) for 72h. **(D)** Expression analysis of *ASXL* genes and *PAX6* in neuronal stem cell cultures derived from SH hiPSC (RNA provided by Dr. Klaus, Helmholtz Center Munich). **(E)** Transcription level dynamics during different steps of neuronal differentiation from H1 hESCs. [Raw data from[213]. Neuronal progenitor cells were obtained/maintained in N2B27 + Noggin (day 11) or N2B27 + 20 ng/ml bFGF and EGF (P9 and P22)]. **(F)** Spatiotemporal expression pattern of *ASXL* genes and *Doublecortin* (*DCX*), a regulator of neuronal progenitor migration, in human brain development; pcw, post-conceptional week. Image modified from *human.brain-map.org*.

A review of *in vivo* transcriptomics data from human brain tissues, sampled at different developmental stages from embryonic week 8 to 40 years of age, corroborated these findings (**Fig. 9F,** *human.brain-map.org*). *ASXL1*, and to a lesser extent *ASXL3,* are expressed during fetal brain development and display a spatiotemporal expression pattern resembling that of *Doublecortin (DCX)*, a microtubule-associated gene found in migrating neuronal progenitors[214] (**Fig. 9F**). In accordance with transcriptional analyses *in vitro*, *ASXL2* is expressed at relatively low levels in the developing and adult human brain (**Fig. 9F**).
Taken together, these data imply a role for *ASXLs* as developmental regulators, particularly of *ASXL1* (and *ASXL3*) in the formation and maturation of neuronal lineages.

3.2. Generation of human pluripotent stem cell-based models for BOS

According to the expression and upregulation of *ASXL* paralogs during hESC differentiation, which suggests an involvement during the specification and maturation of embryonic progenitors, mutations in *ASXL* genes might thereby negatively affect formation of fetal tissues. This could result in the congenital dysmorphisms that are observed in BOS, BRS, and the neurodevelopmental disorder associated with mutations in *ASXL2*. In order to investigate the pathogenesis and mechanisms pertinent to perturbation of developmental programs, I generated several human pluripotent stem cell-based models harboring *ASXL1* mutations.

3.2.1 BOS patient-derived human induced pluripotent stem cell lines (BOS-iPSC)

In collaboration with Prof. Giovannucci Uzielli (University of Florence, Italy) and Dr. Magini (S. Orsola-Malpighi University Hospital, Bologna, Italy), I obtained skin biopsies from two BOS patients, 5 and 7 years old, which harbor heterozygous mutations in *ASXL1*. Both mutations, p.Q803TfsX17 in the female patient #1 and p.R965X in the male patient #2, are located in the 'mutation hotspot' of the *ASXL1* coding region (**Fig. 7D**) and result in premature STOP codons[134] (PSCs; **Fig. 10A**). I derived fibroblasts from the patient skin explants (**Fig. 10B**), and with the help of Dr. Pertek and E. Rusha (Helmholtz Center Munich), I generated patient-specific human induced pluripotent stem cell lines (BOS-iPSC). Each line was reprogrammed separately by two different, integration-free methods: via introduction of modified mRNA[191] or 4-in-1 mini-intronic plasmids[17], resulting in four BOS-iPSC lines [female lines #1-0 (mmRNA) and #1-1 (4-in-1) and male lines #2-0 (mmRNA) and #2-1 (4-in-1), **Fig. 10B** and **Table 3**]. In comparison to control hiPSC lines, all four BOS-iPSC lines did not exhibit any apparent defect in self-renewal, morphology (**Fig. 10B**), or expression of pluripotency markers according to qPCR and immunocytochemistry with the exception of a slight upregulation of the *NANOG* transcript in BOS line #2-0 (**Fig. 10C** and **D**).

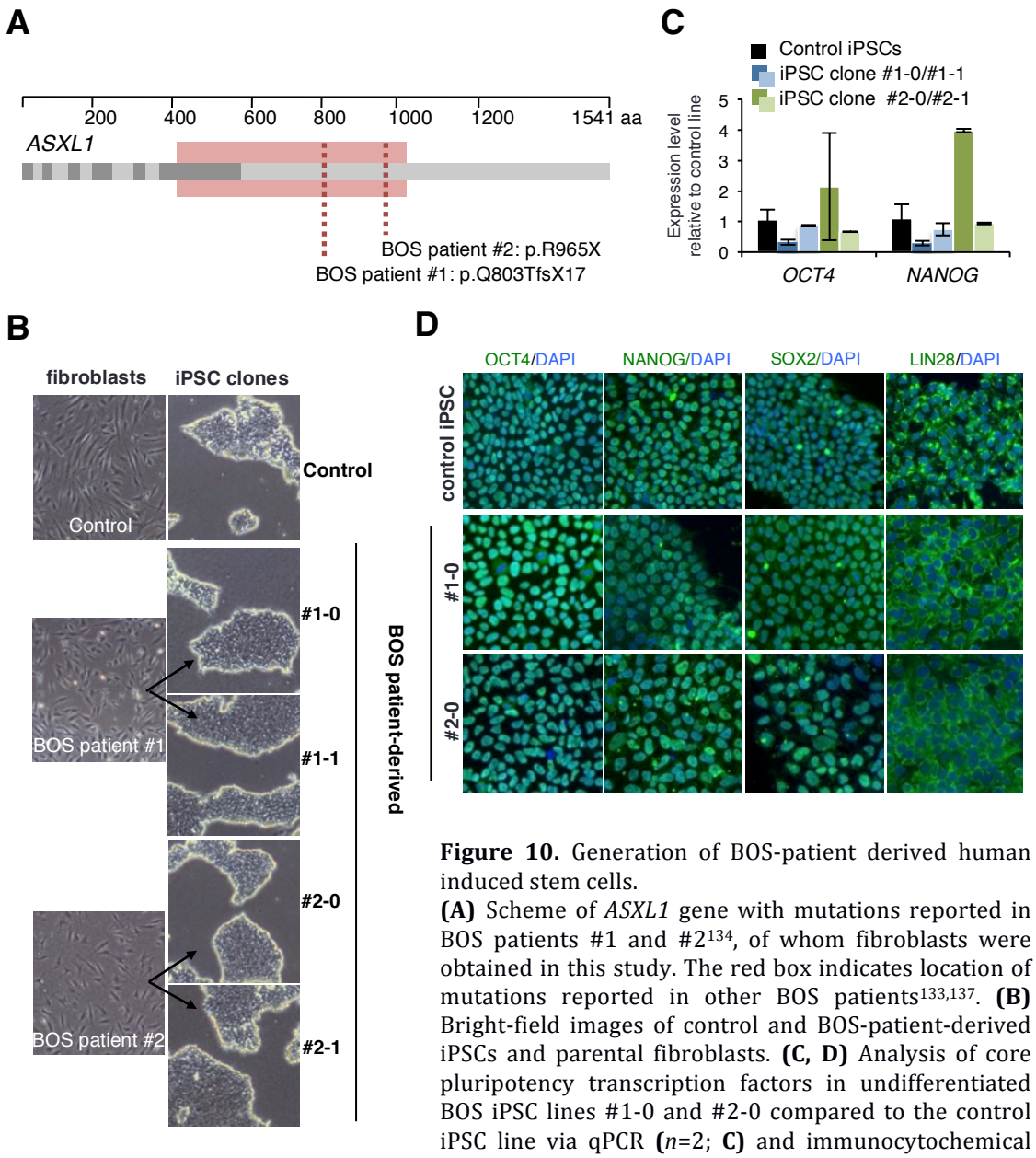

Figure 10. Generation of BOS-patient derived human induced stem cells.
(A) Scheme of *ASXL1* gene with mutations reported in BOS patients #1 and #2[134], of whom fibroblasts were obtained in this study. The red box indicates location of mutations reported in other BOS patients[133,137]. **(B)** Bright-field images of control and BOS-patient-derived iPSCs and parental fibroblasts. **(C, D)** Analysis of core pluripotency transcription factors in undifferentiated BOS iPSC lines #1-0 and #2-0 compared to the control iPSC line via qPCR (*n*=2; **C)** and immunocytochemical staining **(D)**.

3.2.2 Introduction of BOS-like *ASXL1* mutations to human embryonic stem cells

In order to generate isogenic human pluripotent stem cell models for BOS, I made use of a genetically modified HUES9 hESC line, which harbors an integrated tet-inducible Caspase 9 enzyme[190] (iCas9). To target *ASXL1* in this line, I electroporated two gRNAs and treated the cells with doxycycline (DOX) for 24 h. By subsequently raising clones, I was able to propagate a clone (clone A) with an excised region of 476 bp within the 'mutation hotspot' of *ASXL1* (**Fig. 11A**). I confirmed the deletion via amplification of the targeted area by PCR and subsequent sequencing (**Fig. 11B** and **C**; c.2419_2894del476). I expanded three additional clones of which two exhibited identical deletions on both *ASXL1* alleles (c.2419_2894del476, clones B

and C), and one compound heterozygous clone with a 475 bp deletion present on one copy, and an inversion of 476 bp on the other allele (c.2419_2893inv//c.2419_2893del475, clone D) (**Table 3**; no heterozygous clones were identified). Molecularly, these mutations corresponded to the genotype of BOS patient #1. The *ASXL1*$^{PSC/PSC}$ hESC clones did not show obvious defects in morphology (**Fig. 11D**), self-renewal or expression of pluripotency markers, as judged by immunocytochemistry and qPCR (**Fig. 11 E, F**).

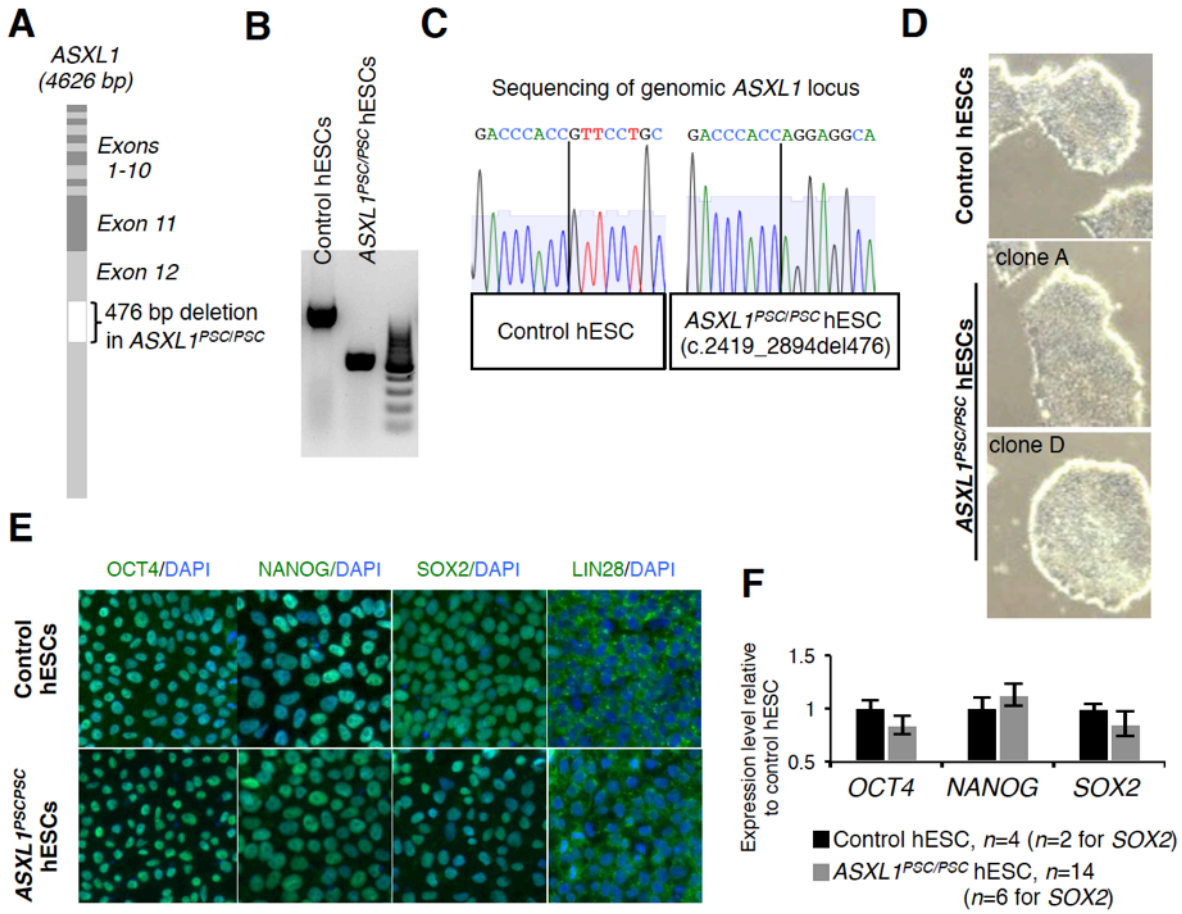

Figure 11. Generation of *ASXL1*$^{PSC/PSC}$ hESC lines carrying BOS-like truncating mutations in *ASXL1*. **(A)** Scheme of *ASXL1* locus, indicated is the CRISPR-mediated deletion introduced in *ASXL1*$^{PSC/PSC}$ hESC. **(B)** Amplification of the *ASXL1* locus via PCR confirms homozygous 476 bp deletion in ASXL1$^{PSC/PSC}$ hESC clone A (third lane showing a molecular marker). **(C)** Sanger sequencing of the *ASXL1* locus in *ASXL1*$^{PSC/PSC}$ hESC clone A and in control cells; the deletion start site is indicated. **(D)** Bright-field images of control hESC and *ASXL1*$^{PSC/PSC}$ hESC colonies. **(E, F)** Immunocytochemical staining **(E)** and qPCR analysis **(F)** of core pluripotency transcription factors in undifferentiated *ASXL1*$^{PSC/PSC}$.

3.2.3 Detection of overexpressed *ASXL1* variants by a novel antibody

The investigation of potential ASXL1 pathogenic isoforms required the generation of antibody tools to recognize full-length and N-terminal mutant ASXL1 variants. Using cDNA isolated from hESC as a template, I amplified both the full-length transcript of *ASXL1* (*ASXL1*^{FL}) and an N-terminal fragment encompassing bp 1-2892, and

introduced an artificial STOP codon at its 3' end to generate a transcript that equals the putative *ASXL1* mRNA variant expressed in BOS patient #2 (*ASXL1*^{PSC}, **Fig. 12A**).

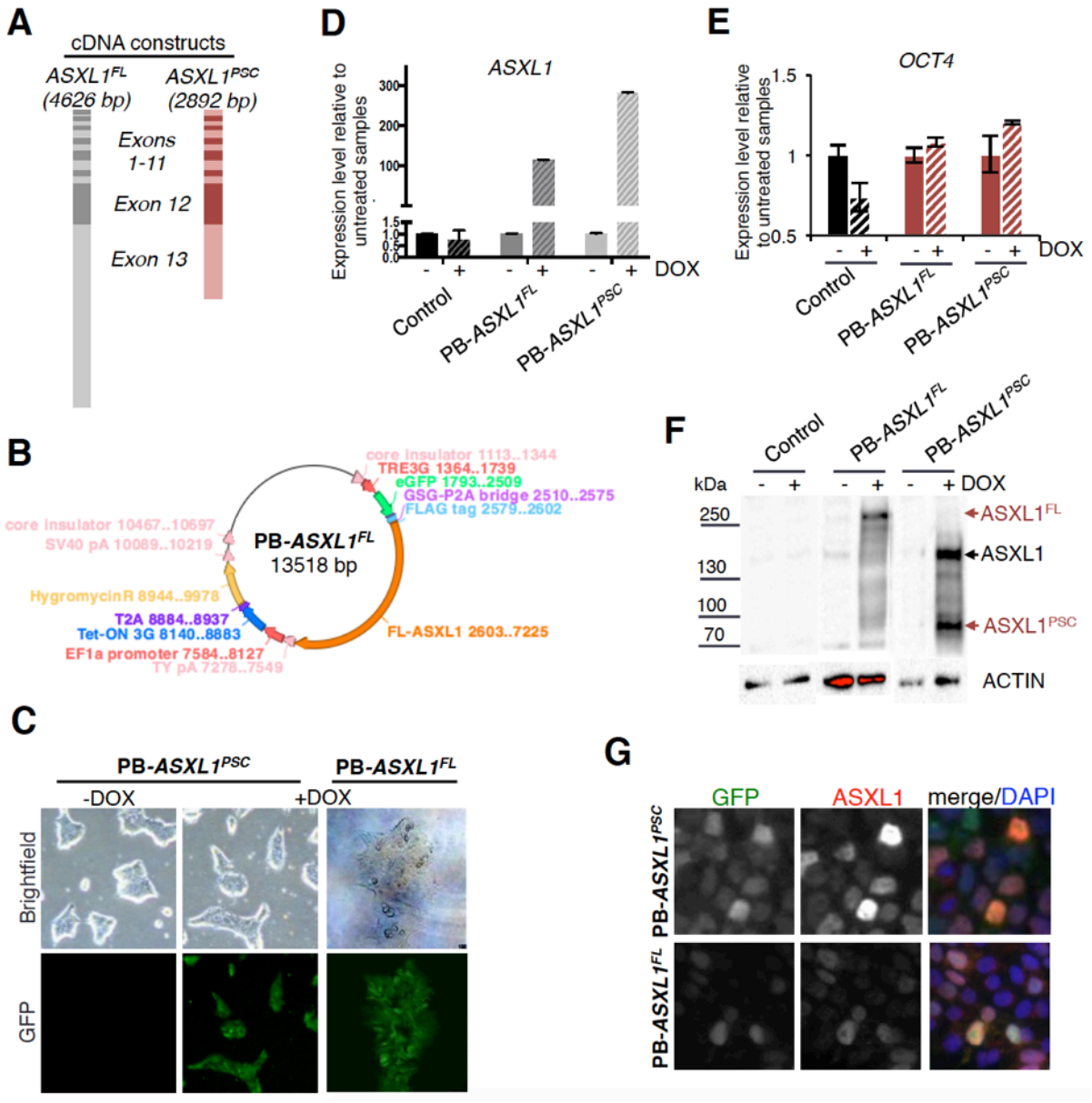

Figure 12. Generation of *ASXL1* overexpression lines and detection of ASXL1 variants by a novel monoclonal antibody.
(A, B) Scheme of full-length and truncated *ASXL1* transcripts (*ASXL1*^{FL} and *ASXL1*^{PSC}, **A**) that were cloned into DOX-inducible PiggyBac overexpression plasmids harboring an *eGFP* coding sequence (**B**). These constructs were stably introduced into control hESC to generate PB-*ASXL1*^{FL} and PB-*ASXL1*^{PSC} cell lines analyzed in (**C-G**). **(C)** Confirmation of PiggBac gene cassette via detection of live eGFP expression in PB-*ASXL1*^{PSC} and PB-*ASXL1*^{FL} hESC lines after 24 h of DOX treatment. (**D**) Detection of *ASXL1* expression in PB-*ASXL1*^{FL} and PB-*ASXL1*^{PSC} lines after 48 h of DOX induction via qPCR (*n*=2). **(E)** *OCT4* expression analyzed via qPCR in control, PB-*ASXL1*^{FL} and PB-*ASXL1*^{PSC} hESC with or without DOX treatment for 48 h (*n*=2). (**F, G**) Detection of *ASXL1* expression in PB-*ASXL1*^{FL} and PB-*ASXL1*^{PSC} lines after 48 h of DOX induction using novel monoclonal antibody clone 12F6 on Western Blots from whole cell extracts (**F**), and in immunocytochemistry using clone 12F9 (**G**).

The sequences were cloned into a PiggyBac plasmid, in an open reading frame downstream of the coding sequence for the *enhanced green fluorescent protein (eGFP)* and the viral *P2A* sequence that mediates cleavage of eGFP from the downstream peptide (plasmid backbone provided by Dr. Shaposhnikov, Helmholz Center Munich; **Fig. 12B)**. Assembled PB-*ASXL1*^{FL} and PB-*ASXL1*^{PSC} vectors were stably introduced into the cell lines mentioned above, namely H9 and the iCas9 line (**Table 3**). Integration of the plasmids was confirmed by induction of eGFP upon administration of DOX (**Fig. 12C**). Importantly, PB-*ASXL1*^{FL} and to a higher degree the PB-*ASXL1*^{PSC} cells exhibited strong induction of *ASXL1* expression within 24 h of DOX treatment (**Fig. 12D**). This did not cause an overt effect on the pluripotency factor *OCT4*, which exhibited slight reduction upon DOX-treatment of control cells, and minor increase upon induction of either the full-length or the truncated constructs PB-*ASXL1*^{PSC} and PB-*ASXL1*^{FL} (**Fig. 12E**).

I used these cell lines to test the specificity of two novel monoclonal antibodies directed against the N-terminal part of ASXL1, which were produced in rat hybridoma cultures in collaboration with Dr. Kremmer and Dr. Geerlof (Helmholtz Center Munich). Western Blot analysis of DOX treated PB-*ASXL1*^{FL} and PB-*ASXL1*^{PSC} lines validated antibody clones 4F6 and 12F9 by detection of the truncated ASXL1^{PSC} variant at approximately 80-90 kDa alongside the full length protein at around 170 kDa (predicted 165 kDa; **Fig. 12F**). The ASXL1^{FL} construct produced a 250 kDa signal (**Fig. 12F**), and the increased size could be explained by post-translational modifications of the ectopic protein, or alternatively by inefficient cleavage of the P2A peptide; however, I did not test these possibilities in detail. DOX-treated GFP-positive cells from the PB-*ASXL1*^{PSC} and PB-*ASXL1*^{FL} clones exhibited ASXL1 signal in immunocytochemistry using antibody clone 12F9, which produced better results than clone 4F6 (not shown), confirming antibody recognition of the overexpressed protein isoforms (**Fig. 12G**). Notably, overlapping DAPI and ASXL1 signals indicate the correct nuclear localization of the full-length and truncated ASXL1 variants. Since the iCas9 line carries a FLAG-tagged Cas9 enzyme, I could not use the overexpression plasmid-based N-terminal FLAG-tag **(Fig. 12B)** to detect the truncated ASXL1 construct. However, according to the successful detection of a truncated, BOS-like ASXL1 variant using the novel monoclonal antibodies, I applied clones 4F6 and 12F9 in further Western Blots and immunocytochemistry, respectively.

Table 3. Human pluripotent stem cell lines generate and/or analyzed in this study.
BOS, Bohring-Opitz syndrome; aa, amino acids

Name	**Line**	**Generation** (see **Methods** for details)	**genomic *ASXL1* background**	**ASXL1 variants expressed**
BOS-iPSC #1-0 #1-1 #2-0 #2-1	iPSC (#1=f, #2=m)	Reprogramming of BOS patient fibroblasts via mmRNA(-0) and 4-in-1-mini-intronic plasmids(-1)	heterozygous mutation in *ASXL1* (#1: c.2407_2411del5, #2: c.2893C>T)	putative truncated ASXL1 (818 aa in #1, 964 aa in #2) and wildtype ASXL1 (1542 aa)
Control iPSC	iPSC	reprogramming of control fibroblasts (2 year old donor) via mmRNA and control B-lymphocytes (12 year old donor) via 4-in-1-mini-intronic plasmids[17]	wildtype: *ASXL1*$^{+/+}$	wildtype ASXL1
Control hESC	iCas9 hESC (HUES9)	HUES9 harbouring integration of a tetracycline-inducible Caspase9[190]	wildtype: *ASXL1*$^{+/+}$	wildtype ASXL1
ASXL1$^{PSC/PSC}$	iCas9 hESC	CRISPR/Cas mediated deletion and inversion of 475-476 bp in *ASXL1*, leading to premature STOP codons (PSC)	clones A, B, C: c.2419_2894del476 clone D: c.2419_2893inv// c.2419_2893del475	putative truncated ASXL1 (809 aa/824 aa)
PB-*ASXL1*^{FL} PB-*ASXL1*^{PSC}	H9 hESC/ iCas9 hESC	Stable integration of a tet-inducible Piggybac construct bearing *GFP* and full length (4626 bp) or truncated (N-terminal 2892 bp) *ASXL1* transcript into H9 hESC (^{FL}) or iCas9 (^{PSC})	*ASXL1*$^{+/+}$; random integration of PB-*ASXL1*^{FL} or PB-*ASXL1*^{PSC}	Overexpression of full-length (1541 aa) or truncated ASXL1 construct (964 aa) and endogenous expression of wildtype ASXL1
GFP-Control *GFP*-*ASXL1*$^{PSC/PSC}$	iCas9 hESC	stable integration of a constitutively expressed Piggybac-*GFP* cassette in control hESC and *ASXL1*$^{PSC/PSC}$ clones A and D	see clones A or D or control hESC	wildtype ASXL1/putative truncated ASXL1 (809 aa/824 aa)
PB-*ZIC1*-Control PB-*ZIC1*-*ASXL1*$^{PSC/PSC}$	iCas9 hESC	stable integration of a tet-inducible Piggybac construct bearing *GFP* and *ZIC1* in control hESC or *ASXL1*$^{PSC/PSC}$ clone A	see clone A or control hESC	wildtype ASXL1/putative truncated ASXL1 (809 aa)

3.3. Characterization of BOS models in the undifferentiated state

Having established a comprehensive toolset for analyzing the pathological mechanisms of BOS, I initially investigated the impact of BOS-associated *ASXL1* mutations on expression of the protein itself, on auto- and paralog regulation and on expression of developmental genes in pluripotent cells.

3.3.1 Pluripotent stem cell models for BOS express truncated ASXL1

Based on the locations of the PSCs in *ASXL1* loci of BOS patients #1/#2 and *ASXL*$^{PSC/PSC}$ hESC, I predicted that these transcripts should escape nonsense-mediated decay (NMD) and could produce truncated protein variants of 818 and 964 amino acids, respectively, which lack the NR interaction domain and the PHD finger (**Fig. 13A**). Sanger sequencing of reverse transcribed mRNA isolated from BOS-iPSC lines revealed that mutant *ASXL1* transcripts bearing the patient-specific mutations were expressed (**Fig. 13B**). Furthermore, blocking NMD by cycloheximide treatment did not elevate *ASXL1* levels in BOS-iPSCs compared to control hiPSCs, implying that mutant transcripts are not depleted by NMD (**Fig. 13C**). In accordance, the novel antibody clone 4F6 confirmed the expression of truncated ASXL1 protein isoforms in undifferentiated BOS-iPSC and *ASXL*$^{PSC/PSC}$ hESC, but not in respective control lines, identified by weak bands at ~90-100 kDa (**Fig. 13D, E**). The 170 kDa band, supposedly representing the full-length ASXL1 protein, was still detected in *ASXL1*$^{PSC/PSC}$ cell extracts. This indicated that the monoclonal antibody (clones 4F6 and 12F9) recognized ASXL1 and ASXL2 proteins, which are of similar size (165 kDa and 153 kDa), owing to their high homology[81]. Although I could not prove or reject the cross specificity, as it proved difficult to knock down or knockout *ASXL2* on a homozygous *ASXL*$^{PSC/PSC}$ background, my working hypothesis remains that the ~170 kDa band represents endogenous ASXL1 protein. Intriguingly, both the BOS-iPSC line #1-0 and the *ASXL1*$^{PSC/PSC}$ cell clones, which express similar mutant ASXL1 forms, displayed also an additional band at around 130 kDa, which was barely detectable in control hESCs/hiPSCs (**Fig. 13D, E**). I furthermore noticed two additional bands in Western Blots of all analyzed lines, one at around 70 kDa and one clearly above 250 kDa (**Supplementary Fig. S1**). Finally, ASXL1 protein localization was not altered in BOS-iPSC in comparison to control iPSC, as shown in immunocytochemistry (**Fig. 13F**). I also observed exclusion of ASXL1 staining from mitotic nuclei (**Fig. 13F**, red arrows).

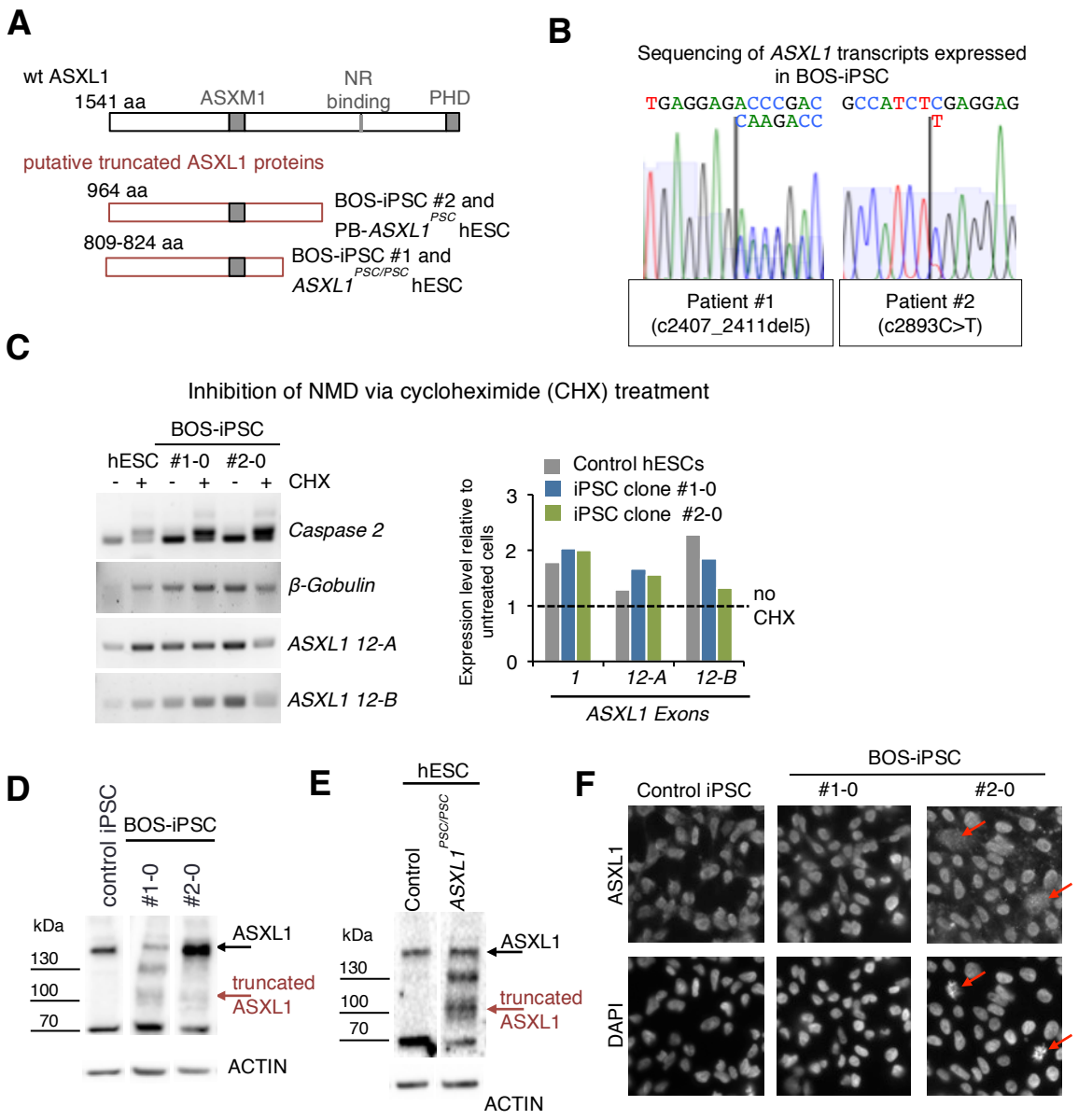

Figure 13. Human pluripotent stem cell models for BOS express truncated ASXL1.
(A) Schematics of wildtype (wt) and putative truncated ASXL1 proteins expressed in BOS-iPSC, *ASXL1*$^{PSC/PSC}$ hESC and PB-*ASXL1*^{PSC}. **(B)** Sequencing of reverse transcribed *ASXL1* transcripts isolated from BOS patient-derived iPSC lines #1-0 and #2-0. **(C)** Cycloheximide (CHX) treatment does not enhance *ASXL1* mRNA expression in BOS-iPSC lines compared to control iPSC as detected by RT-PCR (left) and qPCR (right), using primers directed against Exon 1 (1) or Exon 12 (12-A and 12-B) of *ASXL1*. Detection of Caspase 2 splice isoforms confirmed inhibition of nonsense-mediated decay (NMD) by CHX treatment, β-Gobulin served as negative control. **(D-E)** Detection of truncated ASXL1 variants in patient-derived BOS-iPSC (**D**) and *ASXL1*$^{PSC/PSC}$ hESC (**E**), but not in respective control lines in Western Blot using monoclonal antibody clone 4F6. **(F)** BOS-iPSC show nuclear localization of ASXL1, comparable to control iPSC, as detected with the monoclonal antibody clone 12F9 and DAPI in immunocytologial stainings. Note exclusion of ASXL1 staining from mitotic nuclei (red arrows).

3.3.2 Transcriptome analysis of BOS-iPSCs

As described above, BOS-iPSC lines did not exhibit overt dysregulation of the pluripotent state. However, according to the assumption that mutations in *ASXL1* might still lead to perturbations that could alter commitment towards specific lineages, I performed microarray-based transriptome profiling of undifferentiated H9 hESCs, a control hiPSC line and the #1-0 and #2-0 BOS-iPSC lines, as well as the original patient fibroblasts.
Principal component analysis revealed clustering of transcriptional profiles, and expectedly, the largest difference noted was between fibroblasts and pluripotent stem cell samples (**Fig. 14A**). Furthermore, BOS-iPSC #1-0 clustered loosely with the control hESC and iPSC lines, while BOS-iPSC #2-0 exhibited a notable distance from controls lines or the BOS-iPSC #1-0 cells (**Fig. 14A**). Despite transcriptional differences observed between the BOS-iPSC lines, I intended to determine whether they exhibit misregulation of common signaling pathways. Comparing BOS-iPSC transcriptomes to control samples, I found that 163 and 200 genes were significantly and more than twofold up- or downregulated, respectively (**Fig. 14B**). Among the most upregulated genes in the BOS-iPSC lines were several uncharacterized loci and long non-coding RNAs, the neuronal lineage inducing factor *Neuronatin 1*[215] (*NNAT 1*), and three genes involved in TGFβ signaling, *NODAL, CER1* and *GDF3*[216-218] (**Fig. 14B**). These factors and additional upregulated genes were classified with the tissue category 'germ layer' by the Genomatix Pathway System, indicating a transcriptional profile in BOS-iPSC that is concordant with pluripotency, stem cell differentiation and enhanced TGFβ signaling (**Fig. 14C, Table 4**). I was able to confirm increased levels of *GDF3* and *CER1* in BOS-iPSC via qPCR analysis (**Fig. 14D, E**). Further upregulated gene sets in BOS-iPSCs were linked to transcription-related processes, teratoma and liver cancer (**Table 4**). Gene sets with decreased expression in BOS-iPSC compared to control cells were associated with muscular processes and protein stability, neuronal and heart tissues, seizures, fetal growth retardation, and hematological disorders (**Table 4**). Expression of the pluripotency markers *OCT4, SOX2* and *REX1* did not differ between BOS-iPSC and control hiPSC/hESC, corroborating my earlier qPCR results, however I noted a slight increase in expression of *NANOG* in BOS-iPSC (**Fig. 14F**).
I also sought to identify possible effects of truncating *ASXL1* mutations on the activation of anterior *HOXA* and *HOXB* genes according to the known involvement of *ASXL* genes in *Hox* gene regulation *in vivo* and *in vitro*[99,116]. The *Hox* gene cluster is activated in response to RA treatment in murine ESC *in vitro*, mimicking the induction of *Hox* genes via RA-bound RAR during embryogenesis[219-221]. I therefore examined the response of anterior *HOXA* and *HOXB* loci to increasing doses of RA (0.5-5 μM) in control and BOS-iPSCs (**Fig. 15A**). I noted morphological responses in the treated cell cultures even at the lowest RA concentration, as shown by a representative image in **Fig. 15B**. While selected *HOX* genes displayed distinct dose-response trends and activation levels, I could not detect significant differences between induction in BOS-iPSC and control iPSC lines for genes *HOXA1, HOXA3, HOXA5, HOXB2, HOXB5*. However, I noted a negative effect on *HOXA2* and *HOXB1* induction in the BOS-iPSC lines, suggesting a link to *ASXL1* mutations (**Fig. 15A**). Furthermore, a pattern emerged, where BOS-iPSC #2 consistently expressed the highest *HOX* levels in all doses (shown for *HOXA4* or *HOXB4;* **Fig. 15A**).

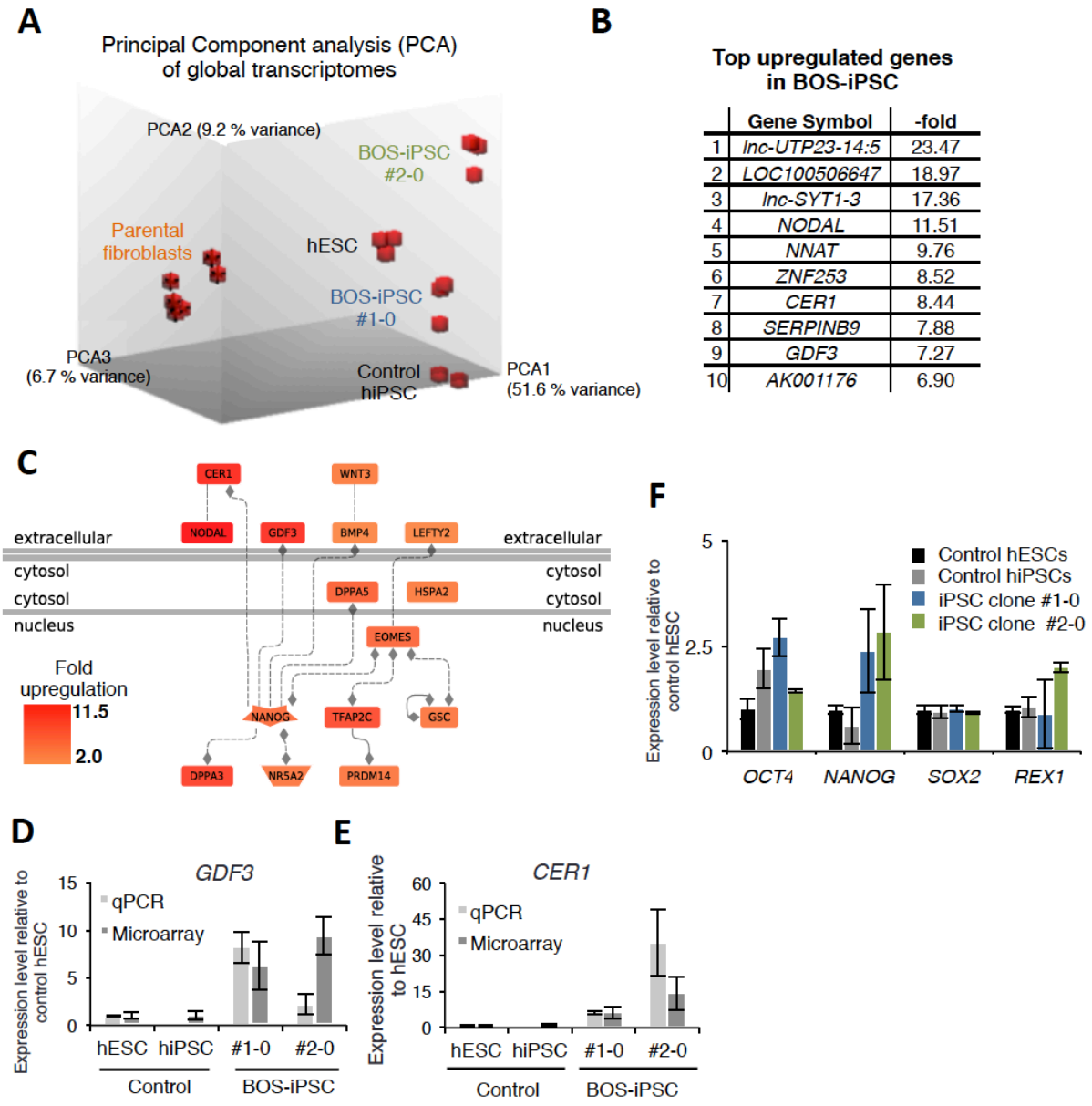

Figure 14. Global transcriptome analysis and validation of candidate genes in undifferentiated BOS-iPSC.

(A-F) Analysis of global transcriptome data obtained from microarray analysis of samples from undifferentiated BOS-iPSC#1-0 and #2-0 (3 clones per line) and parental fibroblasts (3 passages per patient), undifferentiated control hESC (3 passages) and control hiPSC (2 passages, mRNA-derived).

(A) PCA plot of global transcriptomes. **(B)** Most upregulated genes in BOS-iPSC compared to control hiPSC/hESC (Benjamini & Hochberg adjusted *p*-values BH < 0.1). **(C)** Upregulated genes in BOS-iPSC compared to control hiPSC/hESC (BH<0.1, linear change >2) are associated with germ layers (*p*-value 1.57E-12) by the Genomatix Pathway System. Dotted lines indicated co-citations, solid lines represent curated interactions. **(D, E)** Transcriptional analysis of candidate genes from microarray analyses. Expression of *GDF3* **(D)** and *CER1* **(E)** in hiPSC lines quantified via microarray analysis or SybrGreen qPCR (*n*=2, not determined in hiPSC). **(F)** Main pluripotency genes are expressed at comparable levels in BOS-iPSC and control hiPSC/hESC.

Table 4. Association of misregulated gene sets in BOS-iPSC lines with molecular functions and diseases.
Analysis of global transcriptome data in control and BOS-iPSC (related to **Figure 14**); differentially regulated genes (Benjamini & Hochberg adjusted *p*-values BH < 0.1; linear change > 2) were subjected to GeneRanker analysis with the Genomatix Software. The maximum five most significant results of every category with *p*-values calculated by the Genomatix Software are given.

	Upregulated in BOS-iPSC	***p*-value**	**Downregulated in BOS-iPSC**	***p*-value**
GO-term/ Biological Process	Regulation Of Transcription, DNA-dependent	1.44e-08	Regulation Of Muscle System Process	2.94e-04
	Regulation Of RNA Biosynthetic Process	1.77e-08	Regulation Of Protein Stability	6.46e-04
	Regulation Of RNA Metabolic Process	3.46e-08	Striated Muscle Contraction	6.99e-04
	Transcription, DNA-dependent	3.69e-08	Protein Stabilization	9.38e-04
	Regulation Of Macromolecule Metabolic Process	4.16e-08	Regulation Of Muscle Contraction	1.13e-03
Pathway	TGF β	1.85e-08	Cystic Fibrosis Transmembrane Conductance Regulator (Atp Binding Cassette Sub Family C, Member 7)	4.87e-03
	Nodal	1.56e-06	Protein Tyrosine Phosphatase, Receptor Type	9.03e-03
	Activin A Receptor, Type Ib	7.72e-06	Gonadotropin Releasing Hormone	9.88e-03
	Differentiation	3.09e-04		
	Hedgehog	1.69e-03		
Tissue	Germ Layers	1.57e-12	Oligodendroglia	2.85e-05
	Pluripotent Stem Cells	6.87e-10	Olfactory Nerve	1.94e-04
	Primitive Streak	7.79e-10	Heart	2.47e-04
	Endoderm	4.16e-09	Secretory Vesicles	3.54e-04
	Embryonic Stem Cells	1.46e-08	Mesencephalon	1.30e-03
Diseases	Fracture Adverse Event	4.58e-06	Seizures	3.26e-05
	Seminoma	1.65e-05	Fetal Growth Retardation	6.02e-05
	Teratoma	2.13e-05	Sinus Rhythm	1.24e-04
	Carcinoma, Embryonal	3.15e-05	Hyperlipoproteinemia Type Ii	3.19e-04
	Non-small Cell Carcinoma	1.19e-04	Acute Erythroid Leukemia	3.74e-04
Associated Cancer Tissues	Liver	1.25e-03	Haematopoietic and lymphoid tissue	6.84e-03
	Endometrium	4.01e-03		

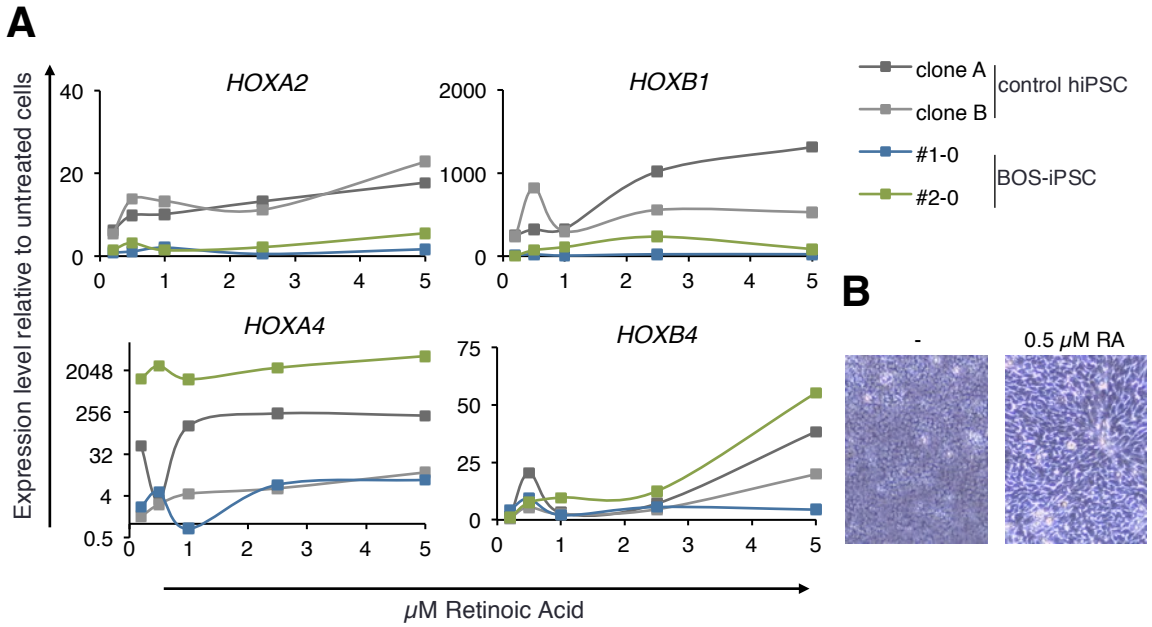

Figure 15. Undifferentiated BOS-iPSC show reduced induction of *HOXA2* and *HOXB1* upon treatment with retinoic acid (RA).
(A) Two clones of control hiPSC (mRNA-derived) and BOS-iPSC lines #1-0 and #2-0 were treated with increasing doses of RA in pluripotent conditions for 24 h, and expression of anterior *HOXA* and *HOXB* genes was determined via qPCR. **(B)** 24 h of 0.5 µM RA treatment in pluripotent conditions induces morphological changes in hESC.

Taken together, I noted subtle changes in BOS-iPSC transcriptomes, which could affect differentiation pathways and future lineage commitment, although the robustness of the pluripotent state was generally not affected.

3.3.3 Regulation of early lineage-specific genes in BOS hESC models

As noted above, similar to the BOS-iPSC lines, the molecular characteristics of BOS hESC models did not indicate overt perturbation of the pluripotency circuitry. Nonetheless, to exclude gross developmental perturbation, I analyzed a small panel of genes that govern gastrulation and are used as markers for early differentiation. Representing different germ layers, I tested *Nestin* and *PAX6* (ectoderm), *MESP1* and *T/Brachyury* (mesoderm), and *FOXA2* and *SOX17* (endoderm). Except for a 4-fold increase in *SOX17* expression, I could not detect misregulation of lineage specifiers in *ASXL1*$^{PSC/PSC}$ and PB-*ASXL1*^{PSC} lines compared to control hESC (**Fig. 16A**).
The PB-*ASXL1*^{PSC} line represents a putative aggravated form of BOS due to unphysiological induction of truncated ASXL1 protein upon DOX treatment. This led to a broader, but at maximum 4-fold increased expression of germ layer specifiers, including *Nestin, PAX6, MESP1* and T, but not *SOX17* (**Fig. 16B**). Interestingly, when subjected to short-term, undirected differentiation via bFGF removal for 24 h, overexpression of truncated ASXL1 led to twofold upregulation of *SOX17* and *FOXA2,* which was not observed in the DOX-treated control line (**Fig. 16C**).
Together, this suggested that truncated ASXL1 correlates with modest induction of endoderm-related genes in a context-dependent manner

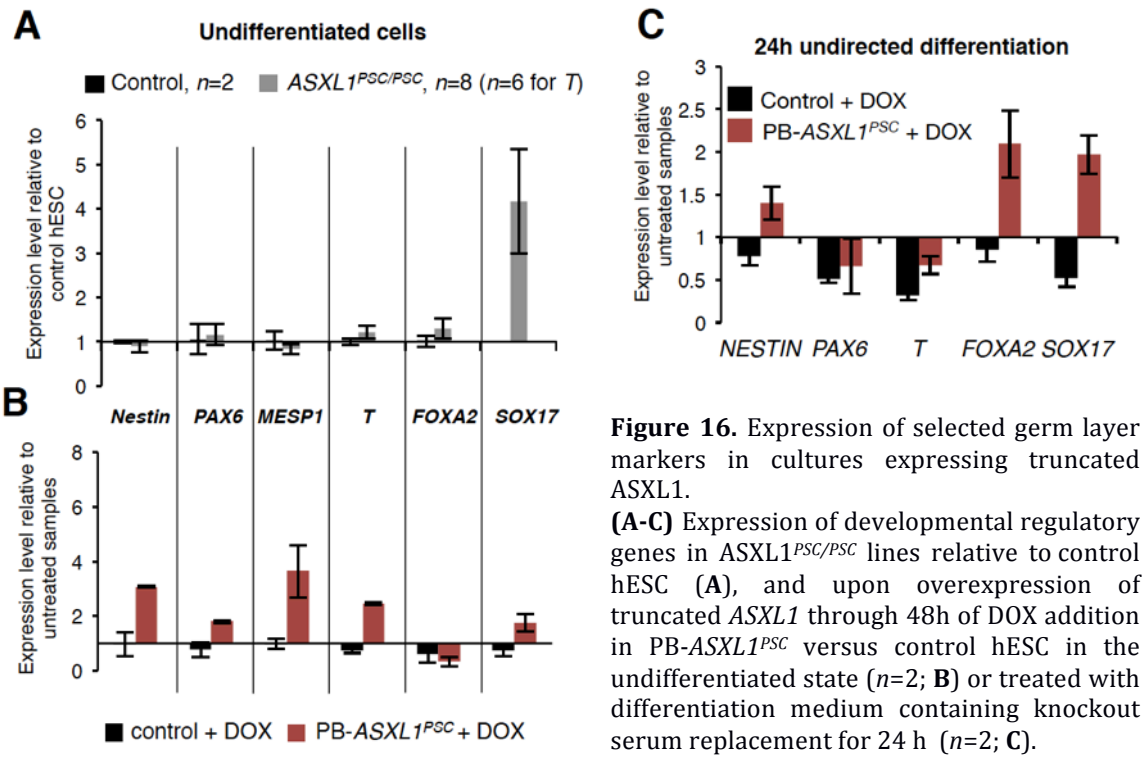

Figure 16. Expression of selected germ layer markers in cultures expressing truncated ASXL1.
(A-C) Expression of developmental regulatory genes in ASXL1$^{PSC/PSC}$ lines relative to control hESC (**A**), and upon overexpression of truncated *ASXL1* through 48h of DOX addition in PB-*ASXL1*^{PSC} versus control hESC in the undifferentiated state (n=2; **B**) or treated with differentiation medium containing knockout serum replacement for 24 h (n=2; **C**).

3.3.4 Regulation of ASXL transcript levels

Because cross-regulation of ASXL paralogs has been previously reported[111], I decided to test this possibility in the pluripotent stem cell models described herein to assess the effect of mutant *ASXL1* alleles. By analyzing levels of *ASXL1-3* in undifferentiated BOS-iPSC and *ASXL*$^{PSC/PSC}$ hESCs, I found that the BOS-iPSC clones from different donors or reprogrammed by different methods varied slightly in expression of *ASXL* genes (**Fig. 17A**), but a specific trend of misregulation was not consistently detected in both iPSC lines (**Fig. 17B**). Isogenic *ASXL1*$^{PSC/PSC}$ hESC lines did not show significant clone-to-clone variability (**Fig. 17C**), and comparable transcript levels between mutant clones and the control line suggested that no regulation of *ASXL* genes by truncated ASXL1 took place in the undifferentiated cells. To confirm this finding, I used the PB-*ASXL1*^{PSC} hESC line, which expresses exceptionally high levels of truncated ASXl1 upon treatment by DOX. Indeed, I noted similar results with only slight increase of *ASXL2* and *ASXL3* upon overexpression (**Fig. 17D**).
However, induction of differentiation programs for 5 days seemed to allow or promote autoregulatory mechanisms: treatment of hESC lines with SMAD inhibitors SB431542 and Noggin to induce neuroectoderm[182], or WNT activation via treatment with the glycogen synthase kinase 3 (GSK-3) inhibitor CHIR99021 to induce mesoderm[222], led to upregulation of *ASXL3* in PB-*ASXL1*^{PSC} cells overexpressing truncated *ASXL1* (**Fig. 17E**). This effect was not observed in Activin A-treated cultures induced towards endoderm, although *ASXL1* overexpression levels were comparable in all differentiation conditions, hence, transcriptional variability was not likely to account for differential *ASXL3* regulation (**Fig. 17E**).
I observed that PB-*ASXL1*^{PSC} exhibited higher induction of *ASXL1* than PB-*ASXL1*^{FL} hESC (**Fig. 12D**). To test whether this was a clone specific effect or due to activation

of the endogenous *ASXL1* locus by truncated ASXL1, I designed primers to detect the 3' end of the *ASXL1* transcript in RT-PCR of samples isolated from control, PB-*ASXL1*^{PSC} and PB-*ASXL1*^{FL} hESC line. This experiment did not reveal upregulation of the endogenous *ASXL1* transcript upon overexpression of truncated *ASXL1* **(Fig. 17F)**.

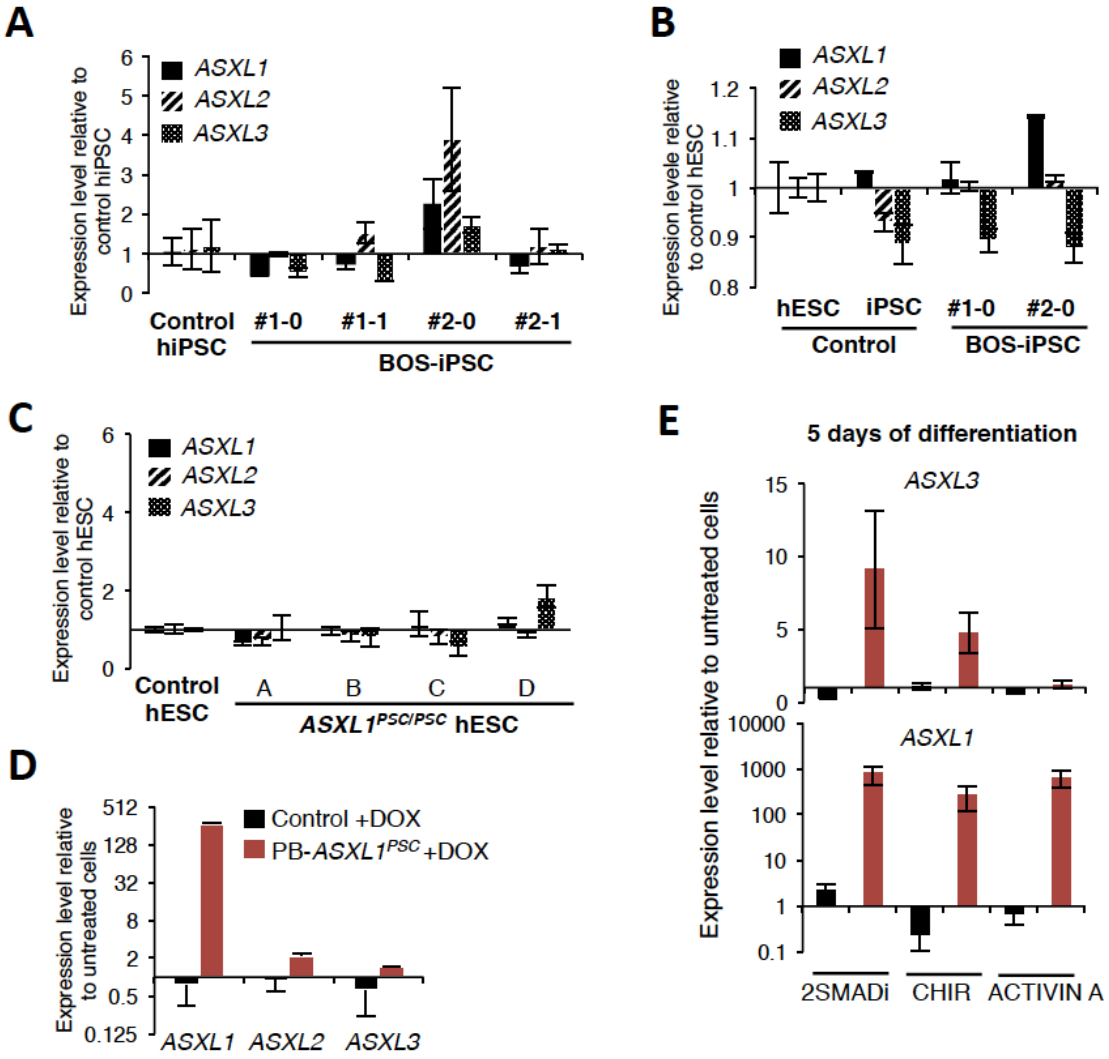

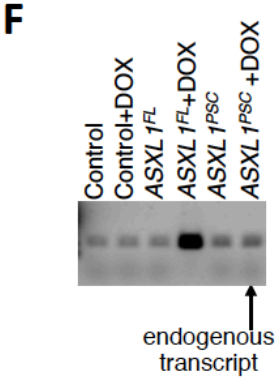

Figure 17. Transcriptional regulation of *ASXL* genes in BOS models. **(A-D)** Expression analysis of *ASXL* genes in BOS-iPSC via qPCR **(A; *n*=2)** and microarray (**B**; *n*=3), and via qPCR in mutant hESC lines (**C;** control: *n*=4; *ASXL1*$^{PSC/PSC}$ clones A, B, D: *n*=4, clone C: *n*=2) and in PB-*ASXL1*^{PSC} hESC upon DOX treatment to induce overexpression of truncated ASXL1 **(D**; *n*=2**)**; all relative to the respective control lines and treatments. **(E)** Quantification of *ASXL3* and *ASXL1* transcript levels via qPCR in 5-day differentiation cultures of DOX-treated control- and PB-*ASXL1*^{PSC} cells relative to untreated samples. Differentiation conditions were dual SMAD inhibiton (SB431542 and Dorsomorphin; 2SMADi), 1 % B27 and 5 µM CHIR (CHIR) and 1.5% FBS and 100 ng/ml Activin A; ACTIVIN A); *n*=2. (**F**) RT-PCR results for the detection of the 3' region in *ASXL1* transcripts isolated from control, PB-*ASXL1*^{FL} and PB-*ASXL1*^{PSC} hESC, untreated or after DOX addition for 24 h.

3.3.5 Regulation of ASXL protein levels

Despite the fact that *ASXL1* transcript levels were generally unaffected by truncated *ASXL1*, I noted elevated levels of wildtype ASXL1 protein in BOS-iPSC line #2-0 (**Fig. 13D**). This was not a clone/reprogramming method-specific effect, as I detected full-length ASXL1 protein in both male BOS-iPSC lines #2-0 and #2-1 that were reprogrammed by different methods, using exposure where ASXL1 in control hiPSC and female BOS-iPSC lines was too low to be detected (**Fig. 18A**).

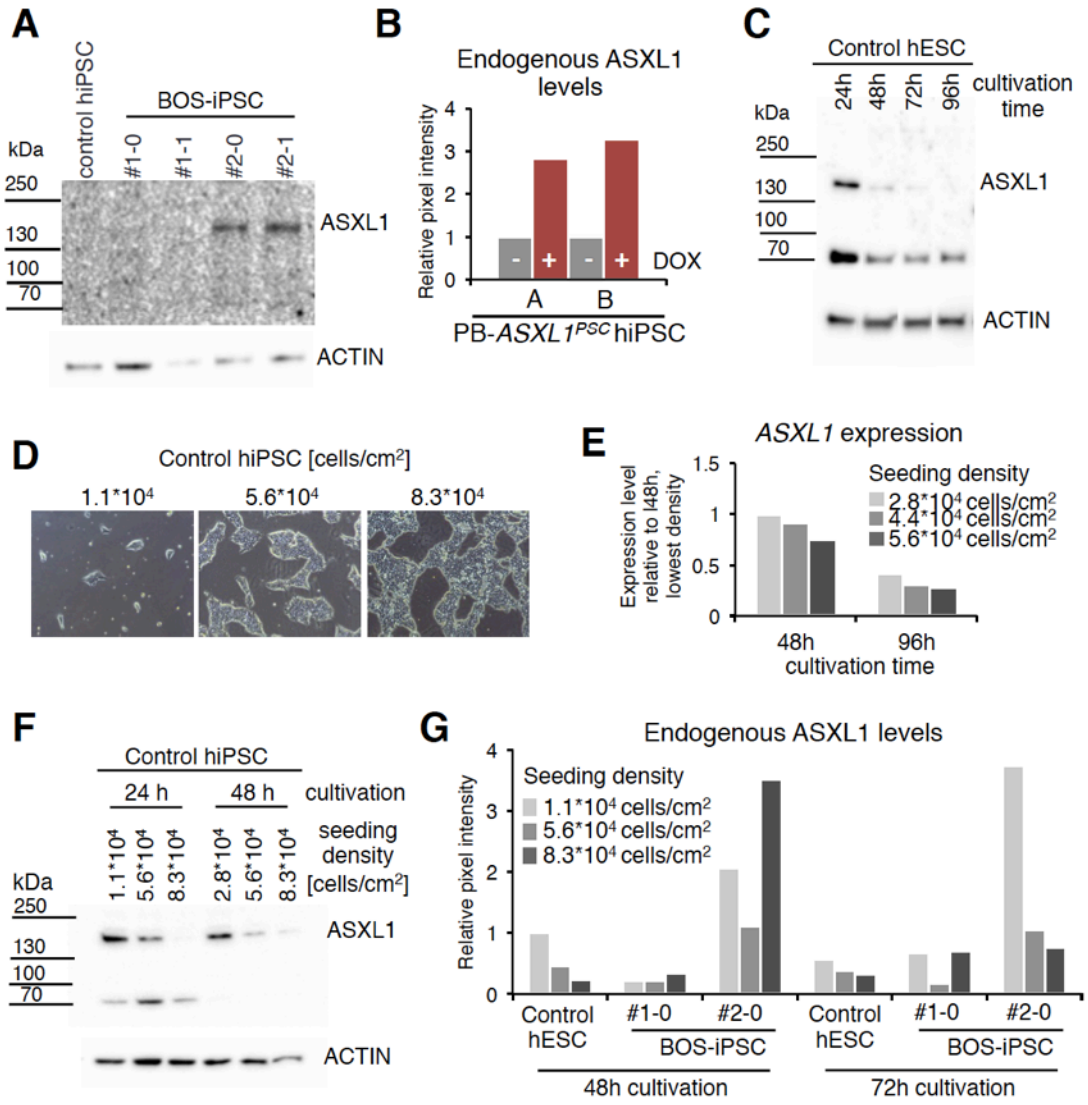

Figure 18. ASXL1 expression is dynamically regulated in pluripotent stem cells.
(A) Detection of ASXL1 protein in cell extracts of control hiPSC and BOS-iPSC. **(B)** Quantification of endogenous ASXL1 levels in two clones A and B of PB-*ASXL1*^{PSC}-hiPSC that ectopically express truncated ASXL1 after 48h of DOX treatment (+DOX), relative to untreated cells (-DOX). (**C**) Detection of ASXL1 in extracts isolated from H9 hESC at different timepoints after seeding. (**D**) Brightfield images of control hiPSC 48h after seeding at indicated cell densities. (**E**) Analysis of *ASXL1* expression via qPCR in uninduced PB-*ASXL1*^{PSC} hESC, harvested at two timepoints after seeding at different cell densities as indicated. (**F**) Detection of ASXL1 protein in extracts isolated from control hiPSC at different timepoints after seeding of different cell densities, as indicated. **(G)** Analysis of full-length ASXL1 levels in control hESC and BOS-iPSC that were collected 48h or 72h after seeding at different densities. Intensity of full-length ASXL1 bands was determined relative to that of the control hESC samples (48h and lowest seeding density).

An increase in endogenous ASXL1 protein was also observed upon overexpression of truncated ASXL1 in hESCs (**Fig. 12E**) or in hiPSCs (**Fig. 18B**). As I did not notice this effect in *ASXL1*$^{PSC/PSC}$ hESCs (**Fig. 13E**) or upon overexpression of full-length *ASXL1* (**Fig. 12E**), I propose that truncated ASXL1 variants differentially affect the stability of the wildtype copy of ASXL1.
Dynamic regulation of ASXL1 was further indicated by the observation that prolonged cultivation leads to reduction of ASXL1 levels in H9 hESCs (**Fig. 18C**). To examine whether this was due to increasing confluency, I seeded control hESC and hiPSC at varying densities (**Fig. 18D**), and collected the cultures at different time points, which revealed that both *ASXL1* mRNA and protein were downregulated in a time- and density-dependent manner (**Fig. 18E, F**). Notably, the uncharacterized band at 70 kDa exhibited a cultivation time-dependent decline as well (**Fig. 18B, F**). The inverse correlation between density and ASXL1 protein levels was perturbed in the BOS-iPSC lines in comparison to control hESC (**Fig. 18G**).
I surmise that depending on the type of mutation or construct, cells expressing truncated ASXL1 display misregulation of the wildtype ASXL1 protein.

3.3.6 Global histone modifications in pluripotent BOS models

Truncated ASXL1 was proposed to enhance the de-ubiquitinating activity of BAP1 in tumor cells, which results in decreased H2AK119 levels and consequently in reduction of H3K27me3, presumably via diminished recruitment of PRC2[69]. On the other hand, ASXL1 is able to directly bind the PRC2 proteins EZH2 and SUZ12 and promote H3K27me3 placement[99]. Thus, I sought to assess whether expression of truncated ASXL1 variants alters the global chromatin landscape in the undifferentiated state with regard to the associated histone modifications. However, quantification of global H3K27me3 and H2AK119Ub levels in *ASXL1*$^{PSC/PSC}$ hESC, induced PB-*ASXL1*^{PSC} and PB-*ASXL1*^{FL} hESC, BOS-iPSC and their parental fibroblasts in comparison to respective control cells did not reveal consistent or strong de-regulation of these chromatin modifications, except for a slight increase in global H3K27me3 levels in BOS-iPSC lines (**Fig. 19**). This was not unexpected in light of the merely mild transcriptional alterations I observed.
Hence, I concluded that expression of truncated ASXL1 did not impact viability, maintenance, transcriptional stability or histone modification landscapes of pluripotent stem cells in my analyses.

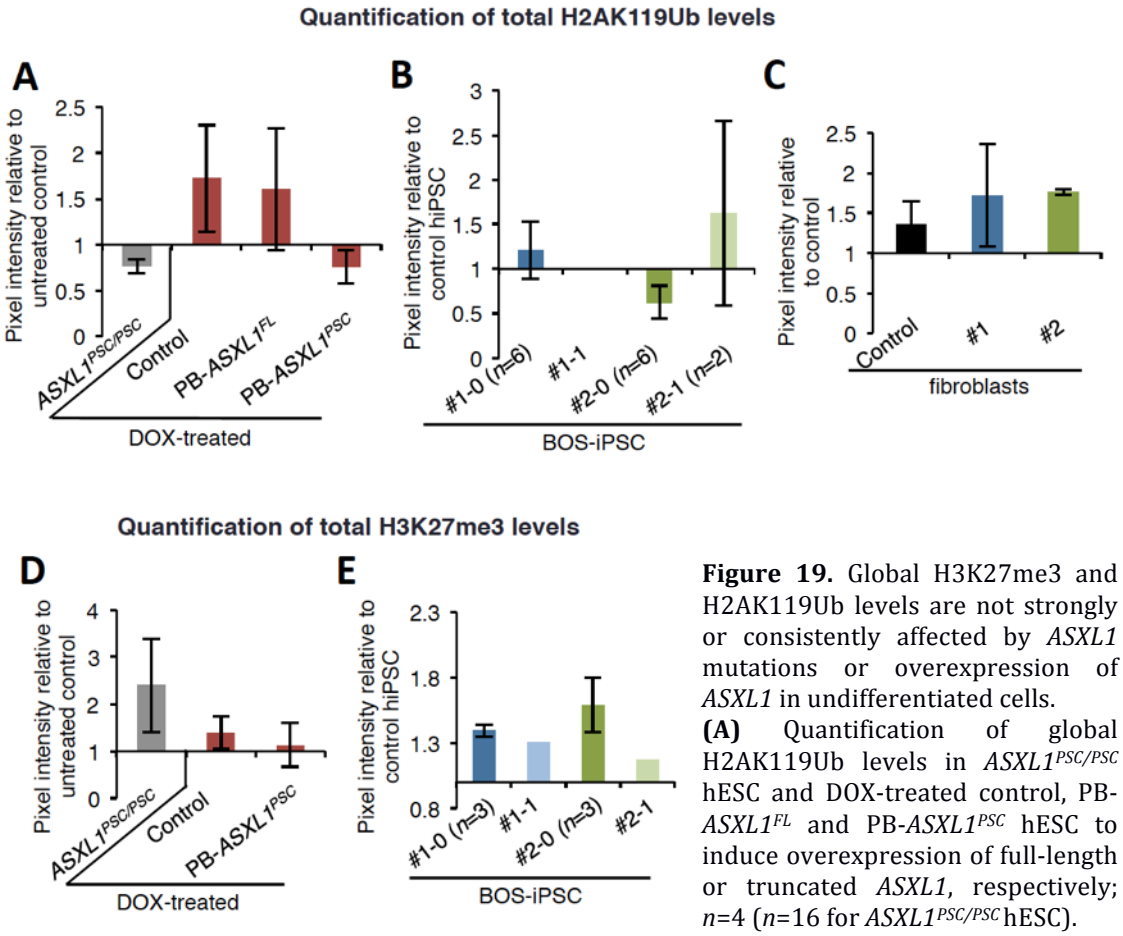

Figure 19. Global H3K27me3 and H2AK119Ub levels are not strongly or consistently affected by *ASXL1* mutations or overexpression of *ASXL1* in undifferentiated cells. **(A)** Quantification of global H2AK119Ub levels in *ASXL1*$^{PSC/PSC}$ hESC and DOX-treated control, PB-*ASXL1*^{FL} and PB-*ASXL1*^{PSC} hESC to induce overexpression of full-length or truncated *ASXL1*, respectively; n=4 (n=16 for *ASXL1*$^{PSC/PSC}$ hESC). (**B, C**) Total H2AK119Ub levels determined in control hiPSC and BOS-iPSC **(B)** and parental fibroblasts; n=2 **(C)**. (**D, E**) Quantification of global H3K27me3 levels in *ASXL1*$^{PSC/PSC}$ hESC, and DOX treated control hESC or PB-*ASXL1*^{PSC} hESC to induce overexpression of truncated *ASXL1* (n=11-12; **D),** and in control hiPSC and BOS-iPSC **(E)**. **(A-E)** H2AK119Ub/H3K27me3 band intensities were normalized to ACTIN band intensities.

3.4. Modeling neural crest development in BOS

Based on the expression of truncated ASXL1 protein in BOS-iPSC and corresponding homozygous hESC models, which however did not affect self-renewal and maintenance of pluripotency, I postulated that lineage-specific effects of mutant ASXL1 variants cause developmental defects in BOS. All patients affected by BOS display craniofacial dysmorphisms to a varying degree, including abnormal palate, small, rotated ears and protruding eyes[131]. Formation of the head and face region strongly relies on the correct emergence, migration and function of the neural crest[162] (NC), and I concluded that BOS-causing *ASXL1* mutations might affect development of the NC lineage, resulting in described facial symptoms. To confirm this hypothesis, I sought to examine involvement of ASXL proteins in NC progenitor commitment, delineate possible perturbations upon expression of the truncated ASXL1 variant, and to uncover potential molecular mechanisms underlying cellular phenotypes.

3.4.1 Implementation of a protocol for human neural crest differentiation

In order to analyze potential disruptive effects of truncated ASXL1 on human NC development, I implemented a NC differentiation method that relies on aggregation of human pluripotent stem cells to floating neuroepithelial structures, termed neurospheres, in the presence of EGF, bFGF and insulin[33] (**Fig. 20A**).

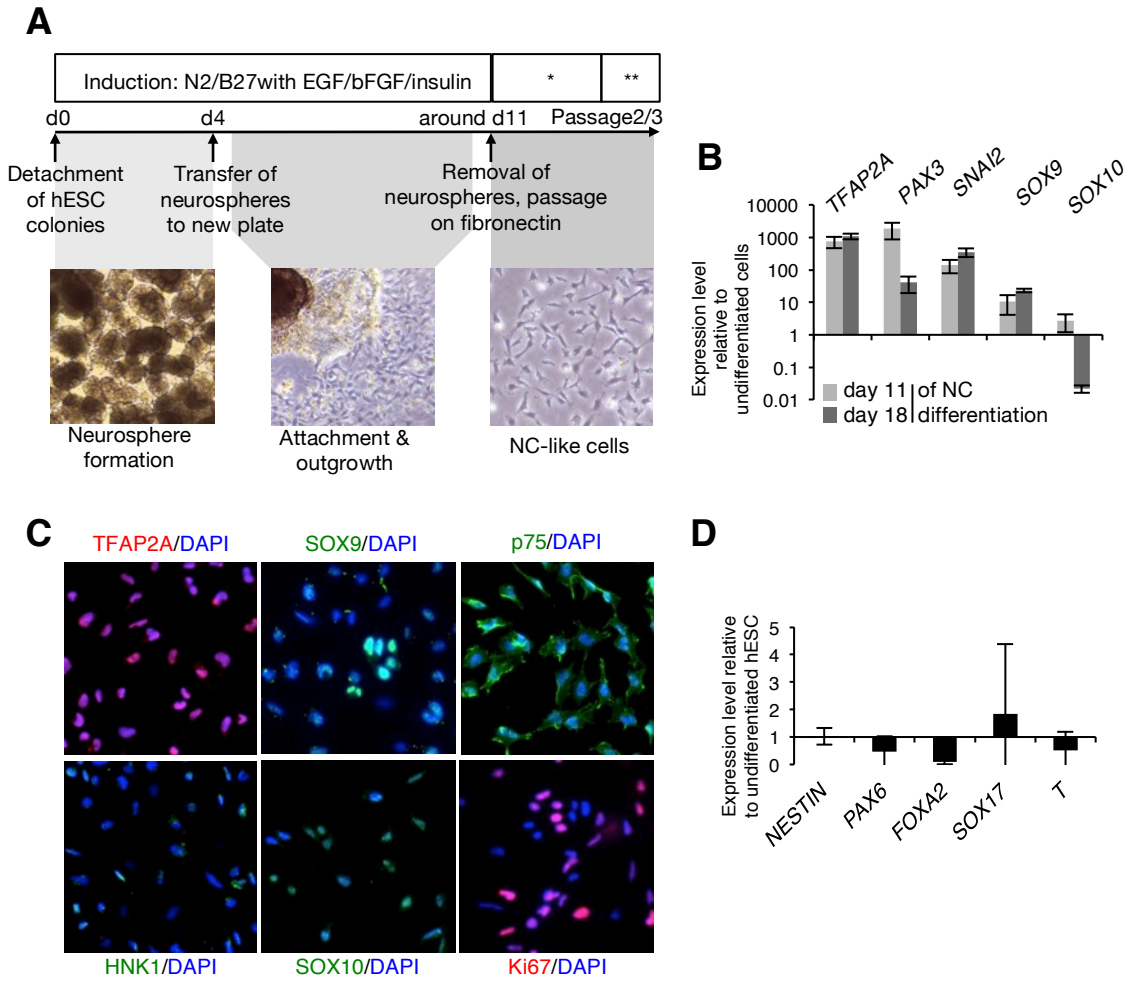

Figure 20. Differentiation of hESC to NC-like cells.
(A) Timeline of NC differentiation protocol and bright-field images of intermediate steps and final NC-like cells during *in vitro* differentiation from control hESC. Neurospheres were kept on uncoated plates in induction medium (N2/B27 + bFGF, EGF and insulin). After sufficient outgrowth of NC-like cells, neurospheres were removed and NC cells were transferred to fibronectin-coated plates in maintenance medium (*; like induction medium, replacement of insulin with bovine serum albumin). After 2-3 passages, NC cells were kept in maintenance medium supplemented with BMP2 and CHIR (**). Protocol modified from[33]. **(B, C)** Expression of NC specifying genes in control hESC-derived NC cells as determined by qPCR **(B)** and immunocytochemical staining (including Ki67; day 18 or later**; C). (D)** Expression of early primitive streak markers was undetectable or very low in hESC-derived NC cells at passage 3 (*n*=5).

The neurospheres, which mimic neurogenesis within the neural tube, are subsequently plated in uncoated tissue culture plates and give rise to delaminating and migrating neural crest-like cells. I observed this behavior in NC differentiation

cultures from control hESC as shown in representative brightfield images in **Fig. 20A**, and was able to expand and cultivate emigrated, presumptive NC cells after the removal of attached neurospheres. Expected NC specifying genes *TFAP2A, PAX3, SNAI2 (SLUG)* and *SOX9* were upregulated in the cultures at day 11 and day 18, confirming their NC identity (**Fig. 20B**). *SOX10*, which labels early NC cells at all axial levels but becomes downregulated in cranial NC cells at later developmental stages *in vivo*[223], followed a similar trend of early induction and later decline, but its levels were generally low (**Fig. 20B**). Nevertheless, expression of SOX10 was noted on the protein level, as well as of SOX9 and HNK1, albeit at low levels (**Fig. 20C**). Virtually all derived NC cells expressed TFAP2A and p75/NGFR and proliferated readily as shown by positive staining of KI-67 (**Fig. 20C**). At passage 3, transcript levels of neuronal, endoderm and mesoderm-associated genes *NESTIN, PAX6, FOXA2, SOX17* and *T* were barely detectable (**Fig. 20D**). After passage 3, NC cells were passaged roughly at 1:5 ratio every 4 days in a medium containing BSA, BMP2 and CHIR99021, until around passage 15, when cultures showed signs of senescence.
To furthermore corroborate their lineage, I tested whether the putative NC cells could give rise to mesenchymal stem cells (MSCs; **Fig. 21**), which are among the expected progeny of NC cells[162].

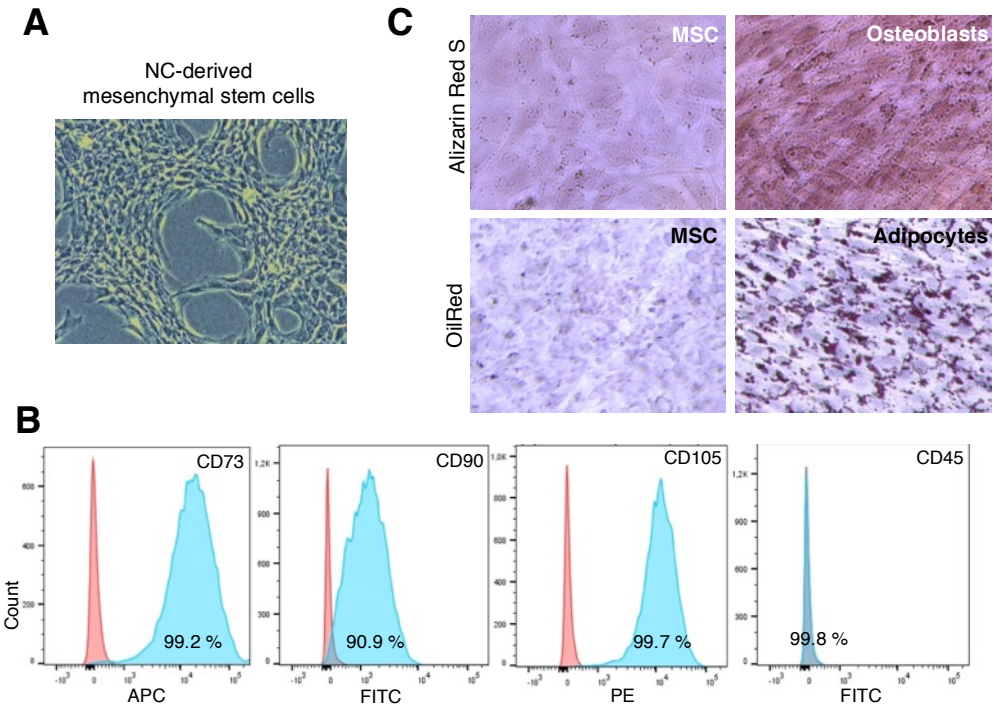

Figure 21. *In vitro* generated NC cells differentiate to mesenchymal stem cells (MSCs) and terminal lineages.
(A-C) MSCs derived from NC cells show mesenchymal morphology in brightfield microscopy **(A)**, express MSC-surface markers but not hematopoietic marker CD45 as determined by flow cytometry (red, isotype control; **B),** and can be terminally differentiated to osteoblasts and adipocytes as confirmed by positive Alizarin Red and Oil Red O staining, respectively, after 26 days of differentiation **(C)**.

Indeed, exposure of NC cultures to MSC maintenance medium as performed in published protocols[224] resulted in the manifestation of a spindle-shaped morphology characteristic of MSCs; furthermore, putative NC-derived MSCs expressed consensus MSC surface markers CD73, CD90 and CD105 but not the hematopoietic marker CD45[225], and terminally differentiated into osteoblasts and adipocytes, which I confirmed by increased levels of mineralization as shown by Alizarin Red staining, or intracellular lipid accumulation via Oil Red O staining, respectively[226] (**Fig. 21**). This concludes that *in vitro* generated NC cells were capable of generating mesenchymal derivatives, which is one of the developmental functions of embryonic NC populations *in vivo*.
The NC cells exhibited upregulation of both *ASXL1* and *ASXL3* transcripts (**Fig. 22A**), which I confirmed by co-localization of ASXL1 with TFAP2A protein via immunocytochemistry (**Fig. 22B**). This supported my hypothesis that *ASXL1* is specifically involved in NC development, as opposed to *ASXL2*, which is ubiquitously expressed but not induced in this population (**Fig. 22A**). Furthermore, I detected full-length and truncated ASXL1 protein in *ASXL1*$^{PSC/PSC}$ -derived NC cultures at day 3 and day 5, together with the band at 130 kDa that was yet unaccounted for (**Fig. 22C**). At day 7 of differentiation, full-length ASXL1 in *ASXL1*$^{PSC/PSC}$ cultures amounted to roughly 70 % of ASXL1 protein levels in control cultures (**Fig. 22C**), indicating a potential downregulation of wildtype transcripts in mutant cells during NC differentiation.

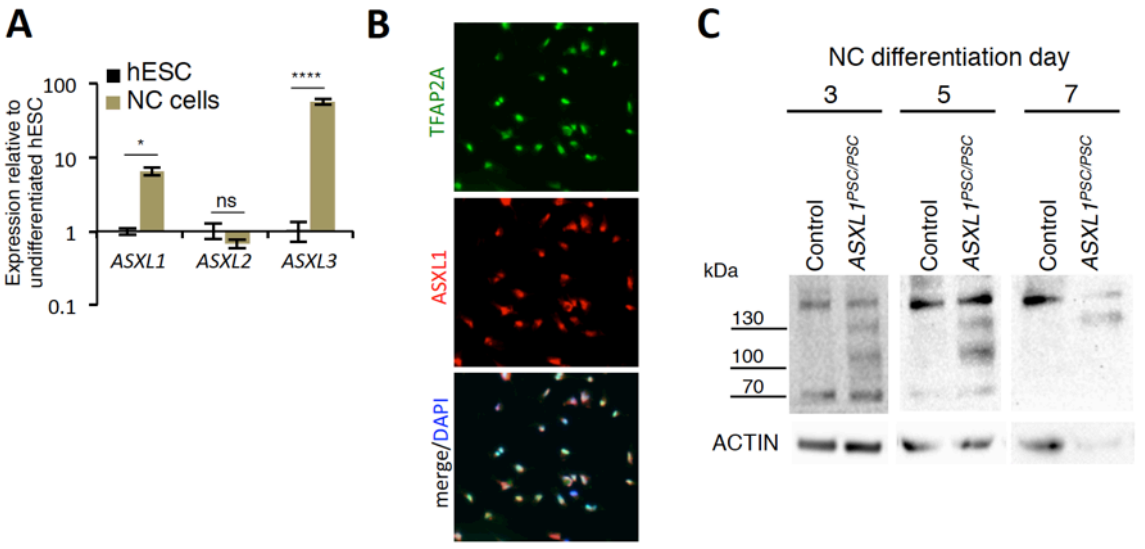

Figure 22. Expression of *ASXL* genes in NC cultures.
(A) Relative expression level of *ASXL1-3* in control hESC-derived NC cells (Passage 2); n=3-5; *p<0.05, ****p<0.0001; Wilcoxon test (*ASXL1*)/Welch's t-test (*ASXL2/3*). **(B)** Immunocytochemical stainings show co-localization of NC specifier TFAP2A and ASXL1 in control hESC-derived NC cultures at day 18. **(C)** Detection of ASXL1 protein variants by Western blot in NC cultures derived from *ASXL1*$^{PSC/PSC}$ and control hESC at day 3, 5 and 7 of differentiation.

Importantly, validation of the NC differentiation protocol together with the confirmed presence of the putative disease-causing ASXL1 variant during NC induction enabled me to assess a potential dominant perturbation of NC development in BOS model lines.

3.4.2 Truncated ASXL1 impairs differentiation to migrating neural crest cells

I noticed that *ASXL1*$^{PSC/PSC}$ mutations drastically reduced the attachment of neurospheres derived from these clones and diminished the emigration of NC-like cells (**Fig. 23A**). A similar effect was observed also, albeit to a lesser extent, in neurospheres derived from BOS-iPSCs with heterozygous *ASXL1* mutations (**Fig. 23B**). Co-variations in patient clones correlated with the method used for reprogramming and/or number of passages, as mRNA-reprogrammed clones (#1-0, #2-0) were cultivated for around 15 more passages than the episomally-reprogrammed lines (#1-1, #2-1) and showed stronger reduction in neurosphere attachment (**Fig. 23B**).

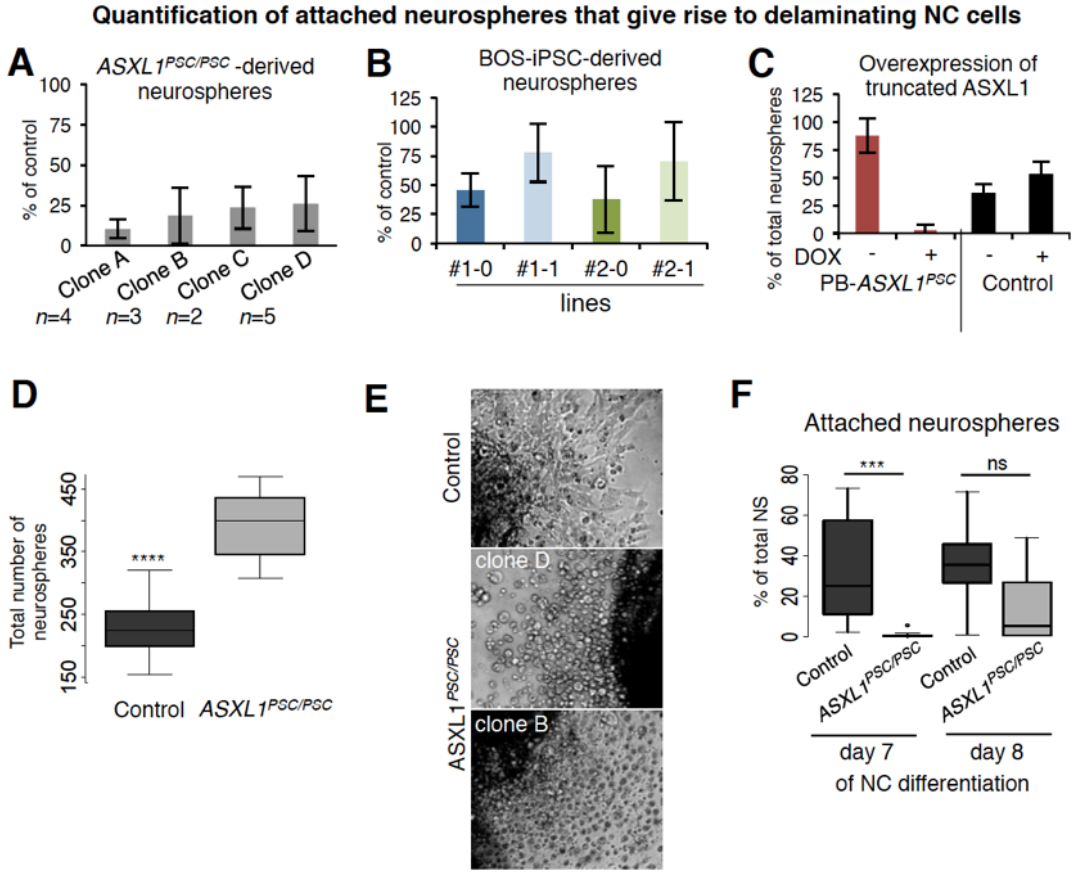

Figure 23. Differentiation to migrating NC cells is impaired by expression of truncated ASXL1.
(A,B) Percentage of attached neurospheres with emigrating cells at day 7 of NC differentiation, from ASXL1$^{PSC/PSC}$ hESC clones related to control hESC (6 independent experiments; **A**) and from BOS-iPSC related to control iPSC (*n*=3 independent experiments; **B**). **(C)** Percentage of attached neurospheres derived from control hESC and PB-*ASXL1*^{PSC} hESC without (-DOX) and with (+DOX) induced overexpression of truncated ASXL1, in relation to the total number of neurospheres that were generated; *n*=3. **(D)** Total number of neurospheres (floating and attached) derived from ASXL1$^{PSC/PSC}$ hESC and control hESC; *n*=10, ****p<0.0001; Welch's t-test. **(E)** Brightfield images of neurospheres with peripheral outgrowth (derived from control hESC) or apoptotic cells (derived from ASXL1$^{PSC/PSC}$ hESC) at day 7 of NC differentiation. **(F)** Percentage of attached, outgrowing neurospheres related to the total number of generated neurospheres at day 7 and day 8 of NC differentiation from *ASXL1*$^{PSC/PSC}$ hESC and control hESC; *n*=6-12; ***p<0.001; ns, not significant; Welch's t-test.

Dramatic impairment of NC differentiation was observed upon overexpression of truncated ASXL1, which led to a nearly complete failure of neurosphere to attach and produce migratory NC-like cells (**Fig. 23C**), emphasizing the dominant effect of the truncating mutations. Importantly, lower numbers of attached neurospheres in *ASXL1*$^{PSC/PSC}$ compared to control cultures were not due to a change in the total number of neurospheres derived from *ASXL1*$^{PSC/PSC}$ clones, which were in fact significantly higher (**Fig. 23D**). However, the appearance of floating, round cells in the periphery of weakly adherent neurospheres from *ASXL1*$^{PSC/PSC}$ lines suggested that if cells were unable to differentiate and migrate, they underwent apoptosis (**Fig. 23E**). The occurrence of weakly attached *ASXL1*$^{PSC/PSC}$ neurospheres prompted me to maintain NC cultures further in an undisturbed 'adhesion stage', which indeed seemed to allow some of the mutant cells to produce delaminating NC cells, evident at day 8 (**Fig. 23F**). This implied that NC development was delayed in cultures bearing truncated ASXL1. In this context it should be noted that successfully attaching neurospheres in *ASXL1*$^{PSC/PSC}$ and BOS-iPSC gave rise to NC cells that were indistinguishable from control cells as based on morphology (**Fig. 24A**) and expression of NC specifying genes on the mRNA (**Fig. 24B, C**) and protein level (**Fig. 24D**). I however noted reduced expression levels of *p75* and *SOX10* in the mutant cultures at passage 3 (**Fig. 24C**).

Taken together, these findings supported the notion that NC symptoms in BOS are caused by a dominant negative effect of the truncated ASXL1 protein on NC induction, which might impair and/or delay their emigration.

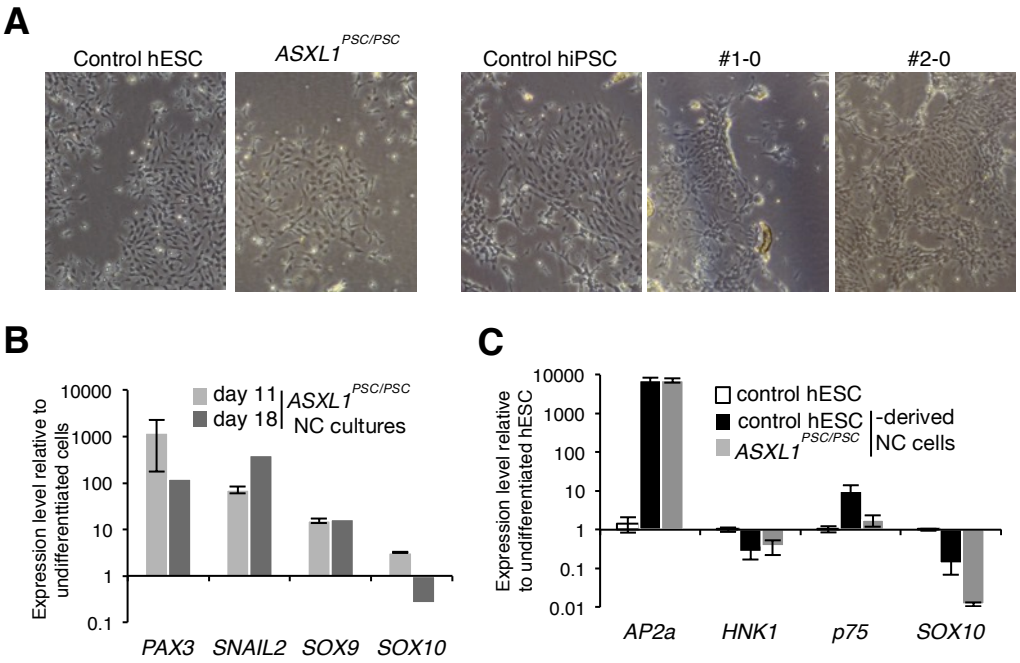

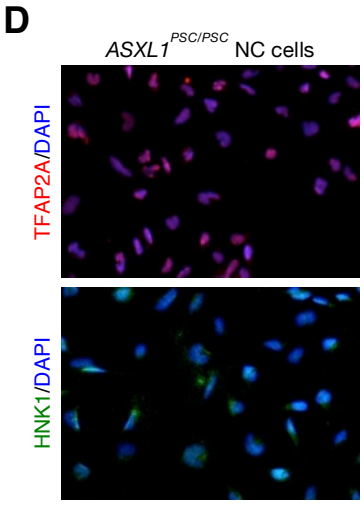

Figure 24. NC cells derived from BOS lines are comparable to control-derived NC cells.
(A) Brightfield images of NC cells of Passage 1, derived from control hESC/hiPSC, BOS-iPSC and *ASXL1*$^{PSC/PSC}$ hESC. **(B,C)** Expression levels of NC specifying genes in day 11 (*n*=2) and day 18 *ASXL1*$^{PSC/PSC}$ NC cultures related to undifferentiated *ASXL1*$^{PSC/PSC}$ hESC **(B),** and in control and *ASXL1*$^{PSC/PSC}$ NC cultures (Passage 3) related to undifferentiated control hESC **(***n*=2-5; **C)**, as determined by qPCR. **(D)** Immunocytochemical staining of NC markers TFAP2A and HNK1 in day 18 NC cells derived from *ASXL1*$^{PSC/PSC}$ hESC.

3.4.3 Truncated ASXL1 impairs NC migration *in vivo*

To corroborate these findings and rule out potential artifacts due to attachment of neurospheres on plastic dishes, I conducted functional *in vivo* assays for NC development in collaboration with Dr. Rehimi and Dr. Rada-Iglesias (CMMC Cologne, Germany). I integrated constitutive *GFP*-expression plasmids into control and *ASXL1*$^{PSC/PSC}$ hESCs (clones A and D, **Table 3**), and subjected the cultures to NC differentiation for 5 days. Resulting GFP-labeled neurospheres were transplanted into the developing hindbrain of stage HH9-10[201] chicken embryos, and migratory NC progeny delaminating from the neurospheres were analyzed 48 hours later (**Fig. 25A, B**). GFP-*ASXL1*$^{PSC/PSC}$ neurospheres showed a significant reduction in the number of emigrating cells compared to isogenic control neurospheres (**Fig. 25B, C**), despite being of similar size (**Fig. 25D**). For the cells that did emigrate, a modest

reduction in migration distance was observed in *ASXL1* mutant neurospheres (**Fig. 25E**).

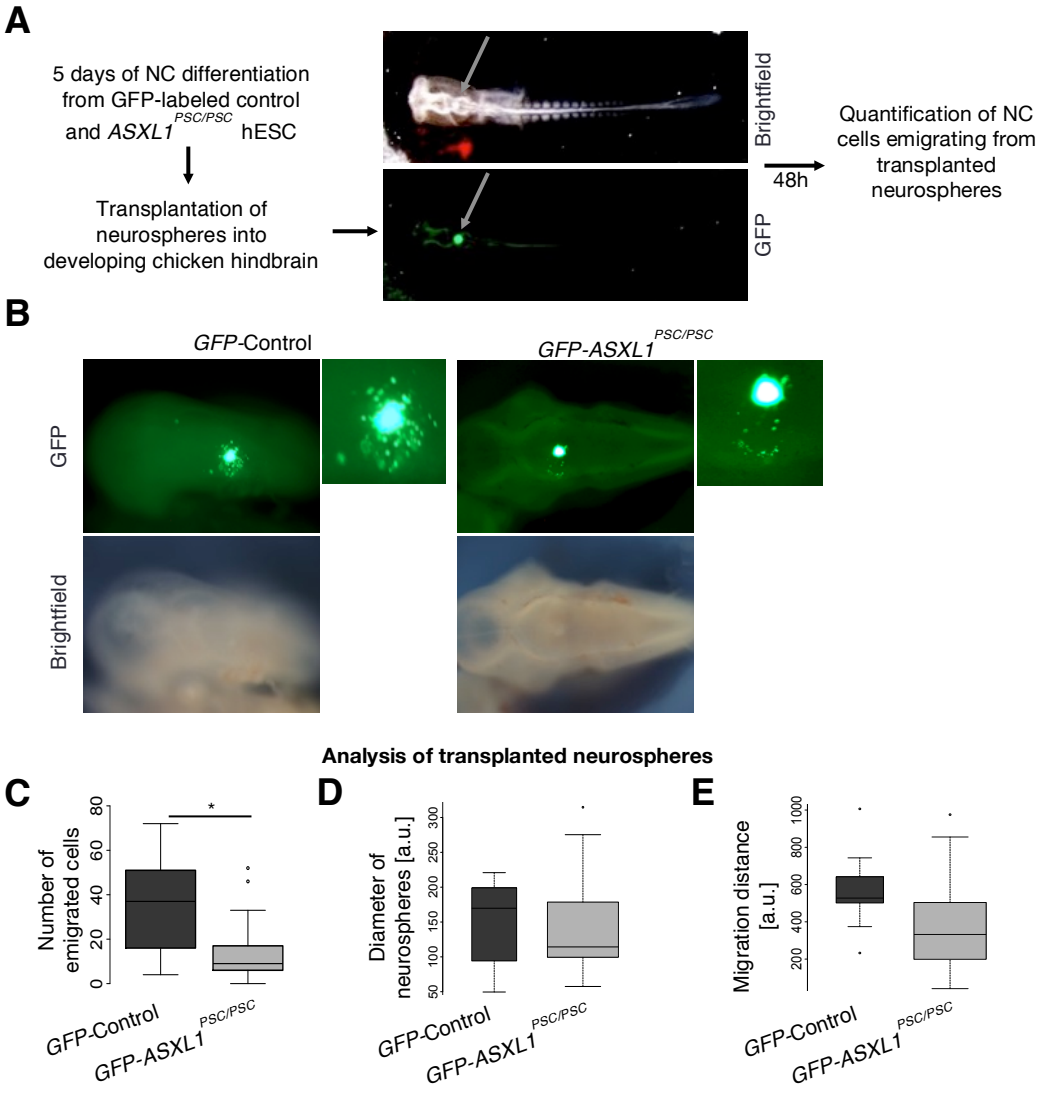

Figure 25. Transplantation of neurospheres *in ovo* confirms developmental defects of *ASXL1*$^{PSC/PSC}$ NC cells.
(A) Workflow of neurosphere transplantation experiments and representative brightfield and GFP image of a chicken embryo (dorsal view) that was engrafted with day 5 neurospheres derived from *GFP*-control and *GFP-ASXL1*$^{PSC/PSC}$ hESCs (arrows indicate transplanted neurosphere); images taken directly after transplantation. **(B)** Exemplary brightfield and GFP images of chicken embryos (dorsal view, anterior to the left) 48 h after transplantation of *GFP*-Control and *GFP-ASXL1*$^{PSC/PSC}$ hESC-derived neurospheres as outlined in **(A)**. **(C-E)** Analysis of n=9 and n=21 embryos transplanted with *GFP*-Control or *GFP-ASXL1*$^{PSC/PSC}$ neurospheres, respectively, as outlined in **(A)**: quantification of emigrating cells (p=0.037, Wilcoxon test; **C)**, diameter of transplanted neurospheres **(D)**, and distance between NS and furthest migrated cell **(**p=0.05, Welch's t-test; **E)**; a.u., arbitrary unit.

I furthermore set out to confirm the dominant effect of truncated ASXL1 on the delamination of embryonic NC cells. The chicken homolog of ASXL1 is highly similar to human ASXL1 in size and domain architecture as determined from the annotated sequence in the UniProt database[209] (**Fig. 26A**), and I constructed overexpression

plasmids harbouring *GFP* (control) or *GFP* coupled to a BOS patient-like, truncated variant of the chicken *ASXL1* transcript (chicken *ASXL1*^{PSC}, **Fig. 26A**). These plasmids were transfected into the NC progenitor zone of chicken embryos at stage HH9-10. Analysis of electroporated embryos at stages HH19 and HH24 revealed strongly inhibited delamination and reduced migration of the GFP-chicken *ASXL1*^{PSC}-transfected cells relative to cells expressing the control GFP plasmid (**Fig. 26B**). Interestingly, also cells electroporated with a plasmid encoding for the human truncated *ASXL1*^{PSC} transcript showed defective emigration (**Fig. 26B**). Collectively, this indicates that the truncated form of ASXL1 induces NC-related symptoms in BOS by diminishing the formation and migration of NC progenitors, and that this is a dominant and evolutionary conserved effect.

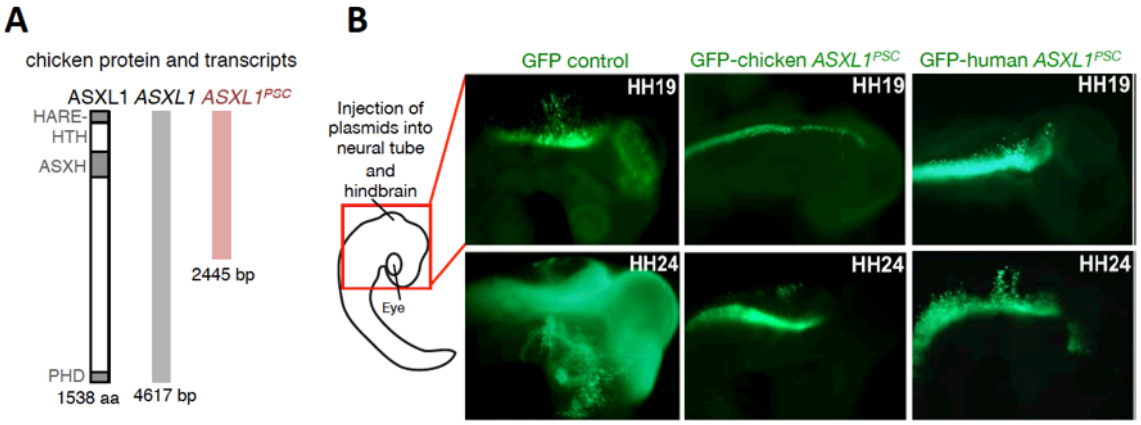

Figure 26. Overexpression of truncated chicken *ASXL1* impairs NC migration *in vivo*.
(A) Predicted chicken (*Gallus gallus*) ASXL1 protein with annotated domains (UniProt F1P445), and chicken wildtype *ASXL1* transcript and truncated *ASXL1*^{PSC} construct. **(B)** Representative fluorescence images of chicken embryos electroporated at stage HH9-10 with plasmids expressing *GFP* or *GFP* coupled to truncated chicken or human *ASXL1*^{PSC}; images taken at HH19 and HH24 (n=10 embryos). The red rectangle indicates orientation and region of the embryos (head/hindbrain) that are shown.

3.4.4 The neural crest regulatory network is misregulated in ASXL1 mutant cells

To delineate a molecular basis for the paucity of *ASXL1*$^{PSC/PSC}$ -NC cells and their migration impairment, I analyzed the transcriptomes of cultures at day 7 of NC differentiation by total RNA sequencing. Examination of global transcript cohorts revealed mutually exclusive clustering of samples harboring *ASXL1*$^{PSC/PSC}$ and wildtype alleles (**Fig. 27A**), with 1202 genes being down-, and 1448 being upregulated (p_{adj}<0.05), indicating extensive changes in expression programs (**Fig. 27B**). This was to be expected since at day 7, *ASXL1*$^{PSC/PSC}$ cultures consisted mainly of floating neurospheres, whereas control hESC-derived cultures displayed a mixture of floating and attached neurospheres together with delaminating NC-like cells. Strikingly, the neural plate border specifier *ZIC1* was most significantly and highly reduced in *ASXL1*$^{PSC/PSC}$ cultures (**Fig. 27B**).

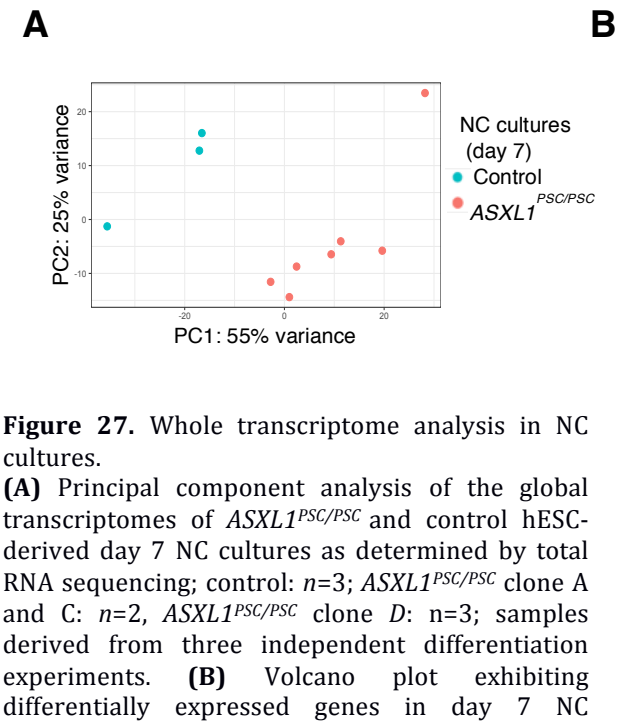

Figure 27. Whole transcriptome analysis in NC cultures.
(A) Principal component analysis of the global transcriptomes of *ASXL1*$^{PSC/PSC}$ and control hESC-derived day 7 NC cultures as determined by total RNA sequencing; control: *n*=3; *ASXL1*$^{PSC/PSC}$ clone A and C: *n*=2, *ASXL1*$^{PSC/PSC}$ clone *D*: n=3; samples derived from three independent differentiation experiments. **(B)** Volcano plot exhibiting differentially expressed genes in day 7 NC progenitor cultures, based on **(A)**.

To assess how the observed strong downregulation of the *ZIC1* locus affected the general NC identity of *ASXL1*$^{PSC/PSC}$ cultures, I evaluated the expression of published human NC markers in the datasets (**Fig. 28A**). In control cultures, early NC genes[34] (*NGFR, B3GAT1, ITGA4*), as well as human neural plate border and NC specifiers in pre-migratory and migratory stages[150,152,153] (*GBX2, PAX3/7, MSX1/2, TFAP2A, ZIC1, FOXD3, SNAI1/2, SOX9, SOX10, TWIST1*) and the nuclear receptors *NR2F1/2* that promote human NC gene expression[150] were expressed (**Fig. 28A**). NOTCH signaling pathway members *HES1/5, NOTCH1* and *JAG1*, which are important regulators of human NC differentiation[153], were also present at high transcript levels in the NC cultures (**Fig. 28A**). I furthermore noted expression of *ETS-1*, a factor that confers cranial identity in NC cells[227], whereas transcript levels of placodal genes *EYA2, SIX1* and *DLX3* were almost undetectable, excluding the assumption of cranial sensory placode identity in the cultures[152,228] (**Fig. 28A**). Most importantly, several of the human NC regulatory genes exhibited mild to strong downregulation in *ASXL1*$^{PSC/PSC}$ cultures (**Fig. 28A**). This was in line with the dramatic, 50-fold reduction in *ZIC1*, which represents one of the key regulators in the mutually supportive NC regulatory network[151]. Accordingly, many of the genes assigned to this network were negatively regulated in *ASXL1*$^{PSC/PSC}$ cultures, and I grouped the downregulated factors into different stages of NC development in **Fig. 28B**, reflective of their functional characterization in model systems[150,158,229]. The deregulated cohort included early neural plate border marker specifiers (*GBX2*), NC inducers and specifiers (*PAX3*, *ZIC1*, *MSX1*, *NRF2F1/2* and *HES5*), genes activating the delamination and migratory program (*ZEB2*, *TWIST1* and *SOX5*) and several Ephrins and their cognate receptors, which serve as guidance cues during NC migration (**Fig. 28B**). Factors governing the differentiation to NC derivatives (*COL2A1, DCT, BRN3A, MASH1*) were similarly diminished in *ASXL1*$^{PSC/PSC}$ cultures (**Fig. 28B**).

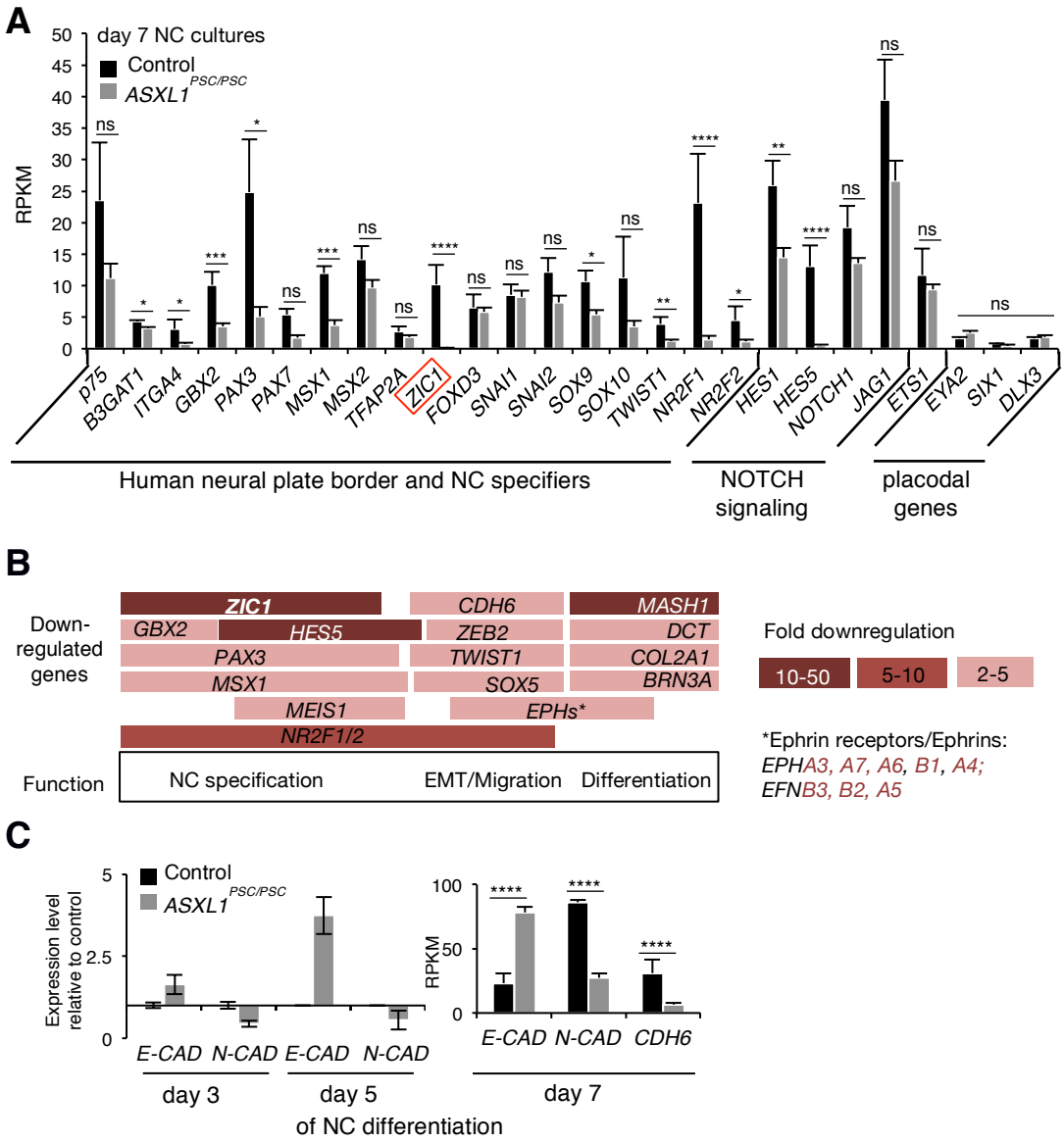

Figure 28. Expression of truncated *ASXL1* leads to misregulation of gene networks associated with NC development and EMT.
(A-C) Analysis of total RNA sequencing data derived at day 7 of three independent NC differentiation experiments. **(A)** Confirmation of NC identity in day 7 progenitor cultures based on expression of published human NC markers and NOTCH signaling pathway members, and low transcript levels of placode-associated genes. *ETS1* is a cranial NC cell transcription factor[230]. *ASXL1*$^{PSC/PSC}$-derived cultures showed reduced expression levels of several NC specifiers and NOTCH factors, *ZIC1* was the most significantly downregulated gene. RPKM, reads per kilobase per million mapped reads; ****p_{adj}<0.0001, ***p_{adj}<0.001, **p_{adj}<0.01, *p_{adj}<0.05; ns, not significant. **(B)** Diagram of functionally characterized genes important for different steps of NC development, as determined in *Xenopus*, fish, human and chicken experiments[150,151,153], and their level of misregulation (p_{adj}<0.05) in *ASXL1*$^{PSC/PSC}$ compared to control day 7 NC progenitors. **(C)** Quantification *of E-Cadherin* (*E-CAD*) and *N-Cadherin* (*N-CAD*) expression at day 3 and 5 (qPCR, *n*=2), and of *E-CAD, N-CAD* and *Cadherin-6 (CDH6)* expression at day 7 (RNA-seq) of NC differentiation from *ASXL1*$^{PSC/PSC}$ compared to control cells.

In accordance with the perturbation of NC delamination and emigration, I furthermore observed significant misregulation of *Cadherin* genes in *ASXL1*$^{PSC/PSC}$ cultures. This encompassed higher levels of the epithelial Cadherin *CDH1* and lower levels of *N-Cadherin/CDH1* and *Cadherin 6/CDH6* in comparison to control, the latter of which are expressed in NC cells during delamination[149] (**Fig. 28B, C**). The inverse expression of *E-Cadherin* and *N-Cadherin* in *ASXL1*$^{PSC/PSC}$ compared to control cells was already observed during neurosphere formation, indicating an early deregulation of signaling cascades in the neuroepithelial structures (**Fig. 28C**).

3.4.5 Ectopic expression of *ZIC1* rescues the NC differentiation defect *in vitro*

In line with a potential perturbation of the NC regulatory network already at the NPB stage, I postulated that insufficiently induced *ZIC1* levels might be critically limiting the differentiation of *ASXL1*$^{PSC/PSC}$ cells by misregulation of downstream effectors in NC differentiation and specification. To verify this hypothesis, I constructed tet-inducible *ZIC1* overexpression vectors and integrated them into control and *ASXL1*$^{PSC/PSC}$ hESCs (**Fig. 29A, Table 3**), which I then subjected to NC differentiation with or without DOX treatment from day 3 or day 4 of the protocol. Strikingly, overexpression of *ZIC1* in PB-*ZIC-ASXL1*$^{PSC/PSC}$ neurospheres led to full reversion of the attachment and outgrowth phenotype (**Fig. 29B**). While *ZIC1* expression was over 100-fold reduced in uninduced PB-*ZIC-ASXL1*$^{PSC/PSC}$ cultures (also confirming the RNA-seq results), DOX treatment equalized the levels of *ZIC1* target gene *SNAI2* and of NPB co-factor *GBX2*[151] (**Fig. 29C**). This indicated that diminished *ZIC1* levels are (at least partly) responsible for NC differentiation defects in mutant *ASXL1* cultures *in vitro*.

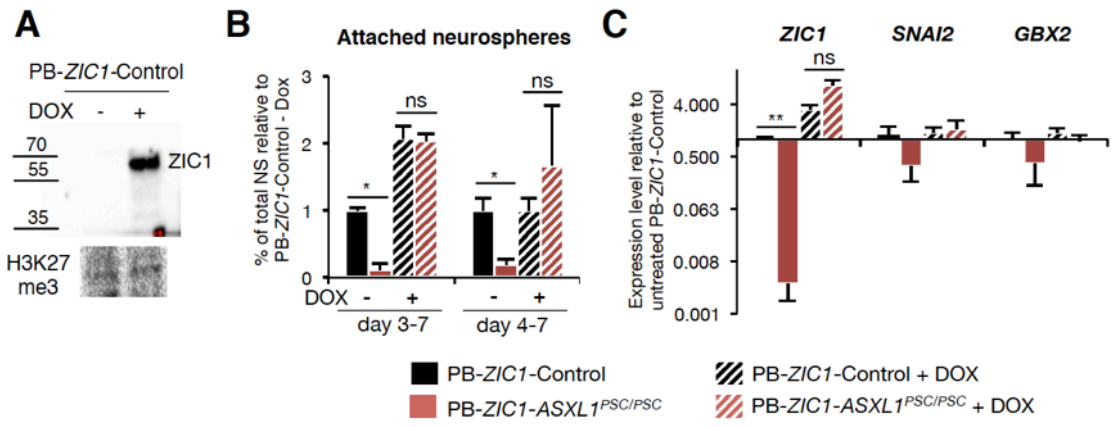

Figure 29. Rescue of the *in vitro* NC differentiation defect by *ZIC1* overexpression.
(A) Western Blot showing the detection of ZIC1 protein expression in undifferentiated control hESC that carry stable integration of a DOX-inducible PB-*ZIC1* overexpression plasmid; H3K27me3 detection served as loading control. **(B)** Analysis of attached neurospheres with emigrating cells in PB-*ZIC1*-Control and PB-*ZIC1-ASXL1*$^{PSC/PSC}$ lines at day 7, left untreated or treated with DOX to overexpress *ZIC1* from day 3 (n=2-3) or day 4 (n=3, independent experiments); *p_{adj}<0.05; ns, not significant; Welch's t-test. **(C)** Quantification of *ZIC1, SLUG* and *GBX2* expression in lines from **(B)**, with or without DOX treatment from day 4 to day 7 of differentiation; n=3, **p_{adj}<0.01; Welch's t-test.

3.4.6 The transcriptional signature of BOS NC models relates to perturbed signalling cascades and BOS symptoms

NC specification relies on WNT and BMP signals that activate neural plate border genes; furthermore, reiterated WNT signaling acts in concert with *Pax3* and *Zic1* during NC induction[151]. Corresponding to the strong reduction in *ZIC1* and other NC specifiers, I noticed that several canonical and non-canonical *WNT* ligands and frizzled receptors (*FZD*) were expressed at significantly lower levels in *ASXL1*$^{PSC/PSC}$ compared to control cultures at day 7 of NC differentiation (**Fig. 30A**). These included factors with described functions during NC development in *Xenopus*, chicken and mice[231-233] (*FZD3, WNT3A* and *WNT8B*) but also additional receptors and ligands that are less well or not characterized in NC development (*FZD7, FZD2, FZD1, FZD10, WNT7A/B, WNT2B, WNT4, WNT5B*). With regard to the equally important function of BMP signaling levels during NC induction[234], I also examined the transcript levels of *CER1, GDF3 NODAL* and *NANOG*, for which I had noted upregulation in undifferentiated BOS-iPSCs (**Fig. 14**). Interestingly, the BMP/TGFβ factors were slightly, but with the exception of *NANOG* (p_{adj}=0.04) not significantly increased in *ASXL1*$^{PSC/PSC}$ NC cultures (**Fig. 30B**).

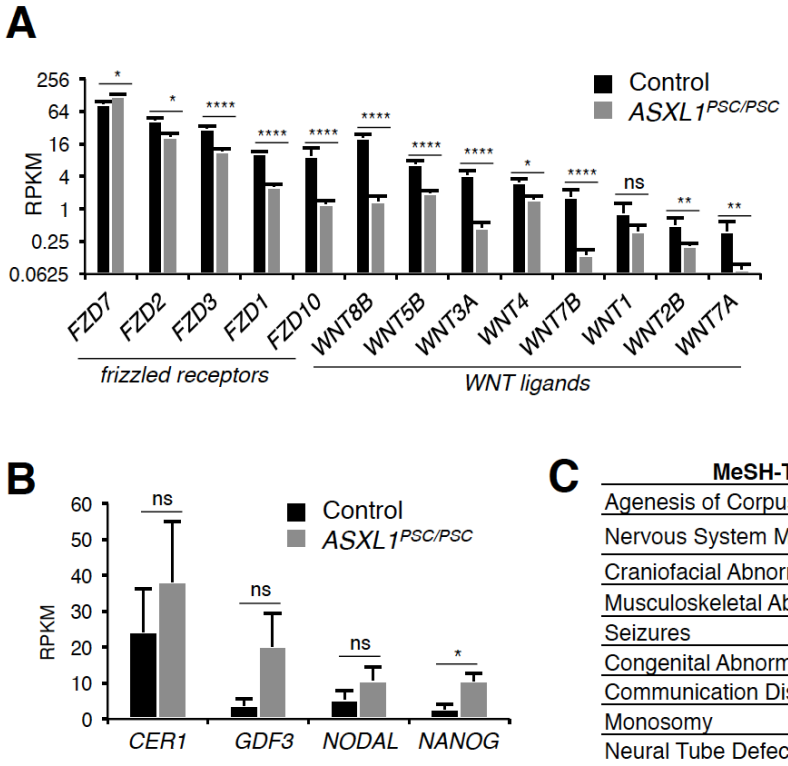

C

MeSH-Term	p-value
Agenesis of Corpus Callosum	3.62E-25
Nervous System Malformations	1.48E-24
Craniofacial Abnormalities	6.34E-21
Musculoskeletal Abnormalities	1.13E-20
Seizures	4.80E-20
Congenital Abnormalities	1.15E-19
Communication Disorders	1.32E-19
Monosomy	1.05E-18
Neural Tube Defects	2.83E-18

Figure 30. Downregulated genes in *ASXL1*$^{PSC/PSC}$ NC cultures are associated with WNT signaling, disturbed differentiation and BOS-related symptoms.
(A-C) Analysis of total RNA sequencing data at day 7 of three independent NC differentiation experiments. Shown are transcript levels of most highly expressed frizzled receptors and WNT ligands **(A)** and of BMP/TGFβ pathway regulators *CER1, GDF3* and *NODAL* and pluripotency factor *NANOG*. **(B)** in NC cultures; *p_{adj}<0.05, **p_{adj}<0.01, ****p_{adj}<0.0001; ns, not significant. **(C)** Most significant Medical Subject Headings- (MeSH-) Terms associated with downregulated genes (p_{adj}<0.05) in *ASXL1*$^{PSC/PSC}$ compared to control NC cultures.

Taken together, my transcriptome analyses indicate that truncating *ASXL1* mutations result in misregulation of crucial signaling pathways and regulatory NC transcription factors, thereby impairing NC development. Intriguingly, transcripts that were downregulated in *ASXL1*$^{PSC/PSC}$ cultures (p_{adj}<0.05) were highly and significantly associated with the Medical Subject Headings (MeSH)-Term 'craniofacial abnormalities', which is a main characteristic of BOS patients[132] (**Fig. 30C**). Additional conditions that are commonly diagnosed in BOS were also linked to gene cohorts with reduced transcripts in *ASXL1*$^{PSC/PSC}$ cultures, including 'agenesis of corpus callosum', 'nervous system malformations', 'musculoskeletal abnormalities', 'seizures' and 'communication disorders' (**Fig. 30C**). Several of these terms hint towards a general affection of neural tube development in *ASXL1* mutant cells, which was supported by the strong association of downregulated gene sets, in particular the highly downregulated *FOXP2,* with the GO-Term 'nervous system development' (**Fig. 27B, Table 5**). Providing a further link between transcriptional misregulations in NC cultures and BOS symptoms, I noticed the concordant strong downregulation of *ZIC1* and *ZIC4* **(Fig. 27B)**, which are an immediately adjacent gene pair. Deletion of the *ZIC1/ZIC4* locus is associated with Dandy-Walker malformation, a condition found in some BOS patients[137] (**Fig. 30C**). In general, the strong correlation between BOS phenotypes and gene ontology of misregulated transcripts in *ASXL1*$^{PSC/PSC}$ NC cultures supported my hypothesis that truncating *ASXL1* mutations are underlying a molecular mechanism that affects the developing NC population in BOS.

Table 5. Downregulated genes in *ASXL1*$^{PSC/PSC}$ NC cultures are associated with the GO-term 'Nervous system development'.
Genomatix pathway analysis of significantly (p_{adj}<0.05) downregulated genes in *ASXL1*$^{PSC/PSC}$- versus control hESC-derived NC cultures (RNA-seq at day 7 of differentiation, *n*=3-7). GO-term 'nervous system development' (GO:0007399) ranked highest with a *p*-value of 1,12E-60.

ABAT	*DLX1*	*GJB1*	*NCOA6*	*PHOX2A*	*SRR*
ADGRB3	*DMRT3*	*GLI3*	*NDNF*	*PLXNA4*	*ST8SIA2*
ADGRG1	*DMRTA2*	*GLRA2*	*NEFM*	*PLXNC1*	*ST8SIA4*
ADGRL3	*DNER*	*GLRB*	*NEGR1*	*POTEE*	*STMN2*
APCDD1	*DN4F6*	*GPM6A*	*NELL1*	*POU3F2/Brn2*	*STMN4*
APLP1	*DPYSL4*	*GRIK1*	*NEUROD1*	*POU3F3*	*SULF1*
ARNT2	*DPYSL5*	*GRIN3A*	*NEUROD4*	*POU4F1/Brn3a*	*TAGLN3*
ARX	*DRGX*	*GST4F6*	*NEUROG1*	*POU4F2*	*TAL2*
ASCL1	*DRP2*	*HEYL*	*NEUROG2*	*PRDM16*	*TCF12*
ASTN1	*DSCAML1*	*HIPK2*	*NF1*	*PRELP*	*TH*
ATOH8	*EFNA5*	*HOXB1*	*NFASC*	*PRRX1*	*TLX3*
BCHE	*EFNB2*	*HPCAL4*	*NHLH1*	*PTN*	*TNIK*
BCL2	*EFNB3*	*INSC*	*NKD1*	*PTPRO*	*TPBG*
BMP5	*EGR3*	*ISLR2*	*NKX6-1*	*RELN*	*TWIST1*
BMP6	*ELAVL3*	*ITGA8*	*NKX6-2*	*RFX4*	*UNC5C*
BMPR1B	*EMX1*	*KCNC1*	*NLGN1*	*RGS9*	*UNCX*
BOC	*EMX2*	*KDM6B*	*NLGN3*	*RNF165*	*VAX1*
CBLN2	*EN1*	*KIAA2022*	*NME5*	*ROBO2*	*VAX2*
CDH2	*EN2*	*KIF26B*	*NNAT*	*RORB*	*VIM*
CDKN2C	*EPHA3*	*L1CAM*	*NOVA1*	*RTN4RL1*	*WLS*
CDON	*EPHA4*	*LEF1*	*NR2E1*	*S100B*	*WNT2B*
CHD7	*EPHA7*	*LHX2*	*NR2F2*	*S1PR1*	*WNT3A*
CHL1	*EPHB1*	*LHX9*	*NR4A2*	*SARM1*	*WNT5B*
CLDN11	*F2*	*LRP2*	*NRCAM*	*SCN3A*	*WNT7A*
CNTF	*FABP7*	*LRRK2*	*NRGN*	*SCRG1*	*WNT8B*
CNTFR	*FAIM2*	*LRRTM2*	*NRN1*	*SDK2*	*XK*
CNTN2	*FAM212A*	*LSAMP*	*OLIG1*	*SEMA3A*	*ZBTB16*
CNTN3	*FAT4*	*LY6H*	*OLIG2*	*SEMA3C*	*ZEB1*
CNTN6	*FEZF2*	*MAB21L2*	*OLIG3*	*SEZ6L*	*ZEB2*
COL25A1	*FGF17*	*MAP1B*	*ONECUT2*	*SHANK1*	*ZFHX3*
COL2A1	*FGF8*	*MAP2*	*OTX1*	*SHC3*	*ZIC1*
COLQ	*FGF9*	*MAP6*	*PARK2*	*SIM2*	*ZNF521*
CRB1	*FIGF*	*MBD5*	*PAX3*	*SLC8A3*	*ZNF536*
CRB2	*FLRT1*	*MDGA1*	*PAX5*	*SLIT2*	*ZSWIM6*
CTNNA2	*FOXG1*	*MDGA2*	*PAX6*	*SLITRK1*	
CXCR4	*FOXJ1*	*MEF2C*	*PAX8*	*SLITRK5*	
CYP46A1	*FOXP2*	*MEIS1*	*PCDH12*	*SNAP25*	
DCC	*FZD1*	*METRN*	*PCDH19*	*SOX1*	
DCHS1	*FZD10*	*MSX1*	*PCDH9*	*SOX3*	
DCLK2	*FZD3*	*MYO16*	*PCDHB11*	*SOX5*	
DCT	*GBX2*	*MYT1L*	*PCSK2*	*SOX6*	
DCX	*GDF7*	*NAV1*	*PDGFC*	*SPEF2*	
DKK1	*GFRA1*	*NCAM1*	*PGAP1*	*SPHK1*	

3.4.7 Regulation of *ASXL* expression in ASXL1 mutant NC cultures

With regard to potential cross-regulatory mechanisms between ASXL paralogs (**Figs. 17, 18** and **22A,C**), I examined transcriptional regulation of *ASXL* genes in mutant NC cultures. The dominant negative *ASXL1* alleles were associated with reduced expression of both *ASXL1* and *ASXL3*, but unaltered, or even slightly increased *ASXL2* transcript levels during day 3-10 of NC differentiation (**Fig. 31A-C**). Interestingly, this was in line with co-induction of *ASXL1* and *ASXL3* in control NC cultures (**Fig. 22A**). The reduction in *ASXL1* levels persisted in passaged NC cells, while the downregulation of *ASXL3* seemed to be reversed in passaged cultures (**Fig. 31D**). *ASXL1* was also reduced in passaged NC cells derived from BOS-iPSC, suggesting that this was in fact a disease-relevant finding (**Fig. 31E**).

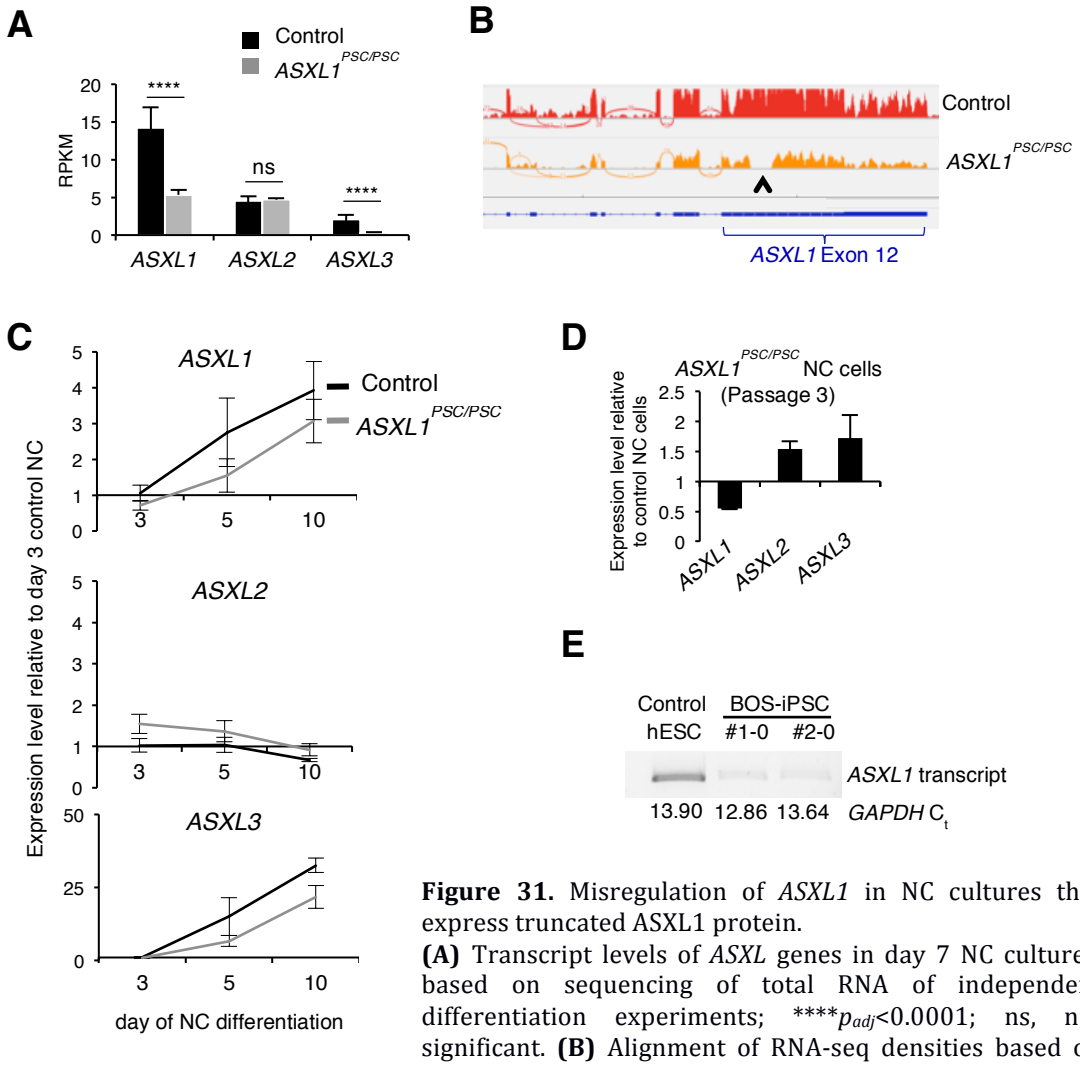

Figure 31. Misregulation of *ASXL1* in NC cultures that express truncated ASXL1 protein.
(A) Transcript levels of *ASXL* genes in day 7 NC cultures, based on sequencing of total RNA of independent differentiation experiments; ****p_{adj}<0.0001; ns, not significant. **(B)** Alignment of RNA-seq densities based on experiment outlined in **(A)** within the last exons of *ASXL1*. Arrowhead indicates CRISPR-mediated deletion.
(C,D) Quantification of *ASXL1-3* expression levels at different time points during NC differentiation (qPCR, *n*=3-5; **C)** and in Passage 3 NC cultures **(***n*=2; **D)** from *ASXL1*$^{PSC/PSC}$ hESC compared to control hESC. **(E)** RT-PCR-based detection of full-length *ASXL1* transcript in control hESC- and BOS-iPSC-derived NC cultures (Passage 2). *GAPDH* C_t values are given as normalization control.

3.4.8 Global and local chromatin modifications in BOS NC models

Transcriptional misregulations in *ASXL1*$^{PSC/PSC}$ NC cultures raised the question of whether they arise from altered chromatin modifications that are mediated by truncated ASXL1 variants. Indeed, I observed a decrease in the global levels of both H2AK119Ub and H3K27me3 in NC cultures that were derived from *ASXL1*$^{PSC/PSC}$ clones, indicating that overactivation of the PR-DUB complex and subsequent reduced PRC2 recruitment might take place in the mutant cultures[69] (**Fig. 32A-C**). Downregulation of NC specifying genes, however, suggested aberrant repressive mechanisms, and since full-length ASXL1 was shown to promote the recruitment of the PRC2 complex to chromatin[99], I hypothesized that enhanced local recruitment of PRC2 by the truncated ASXL1 protein could take place. To investigate this possibility, I performed chromatin immunoprecipitation of H3K27me3 in day 7 NC cultures, followed by qPCR using target-specific primers (ChIP-qPCR). This revealed increased H3K27me3 levels at *ZIC1* and *ZIC4* in *ASXL1*$^{PSC/PSC}$ clones compared to control cells, which was also observed in other negatively regulated loci, including of *ASXL1*, *ASXL3* and *FOXP2* **(Fig. 32D, E)**. *ACTIN* and *HOXB2* were used as positive and negative controls, respectively, and indeed these loci did not show significant differences in H3K27me3 levels between control and *ASXL1*$^{PSC/PSC}$ cultures (**Fig. 32D**). Arguing in favor of increased EZH2 recruitment via truncated ASXL1, analysis of public epigenome datasets revealed binding of EZH2 to the *ZIC1/ZIC4* locus in H1 hESC (ENCODE; **Fig. 32E**), and it was reported that truncated ASXL1 interacts with EZH2 *in vitro*[101]. In order to confirm this interaction in NC cultures, I performed initial co-immunoprecipitation experiments, which however require further optimization and did not yield conclusive results (**Supplementary Fig. S3**).
In conclusion, I found that BOS-associated mutations give rise to truncated ASXL1 variants that dominantly impair NC induction, which is accompanied by misregulation of genes associated with NC and nervous system development, BOS symptoms and reduction in *ASXL1/3* levels. Increased H3K27me3 levels at downregulated genes suggest enhanced PRC2 recruitment, presumably via the mutant ASXL protein. Moreover, I propose that these mechanisms underlie NC-related BOS symptoms and that ASXL1 (and ASXL3) are critical regulators of NC development, as elaborated in the Discussion.

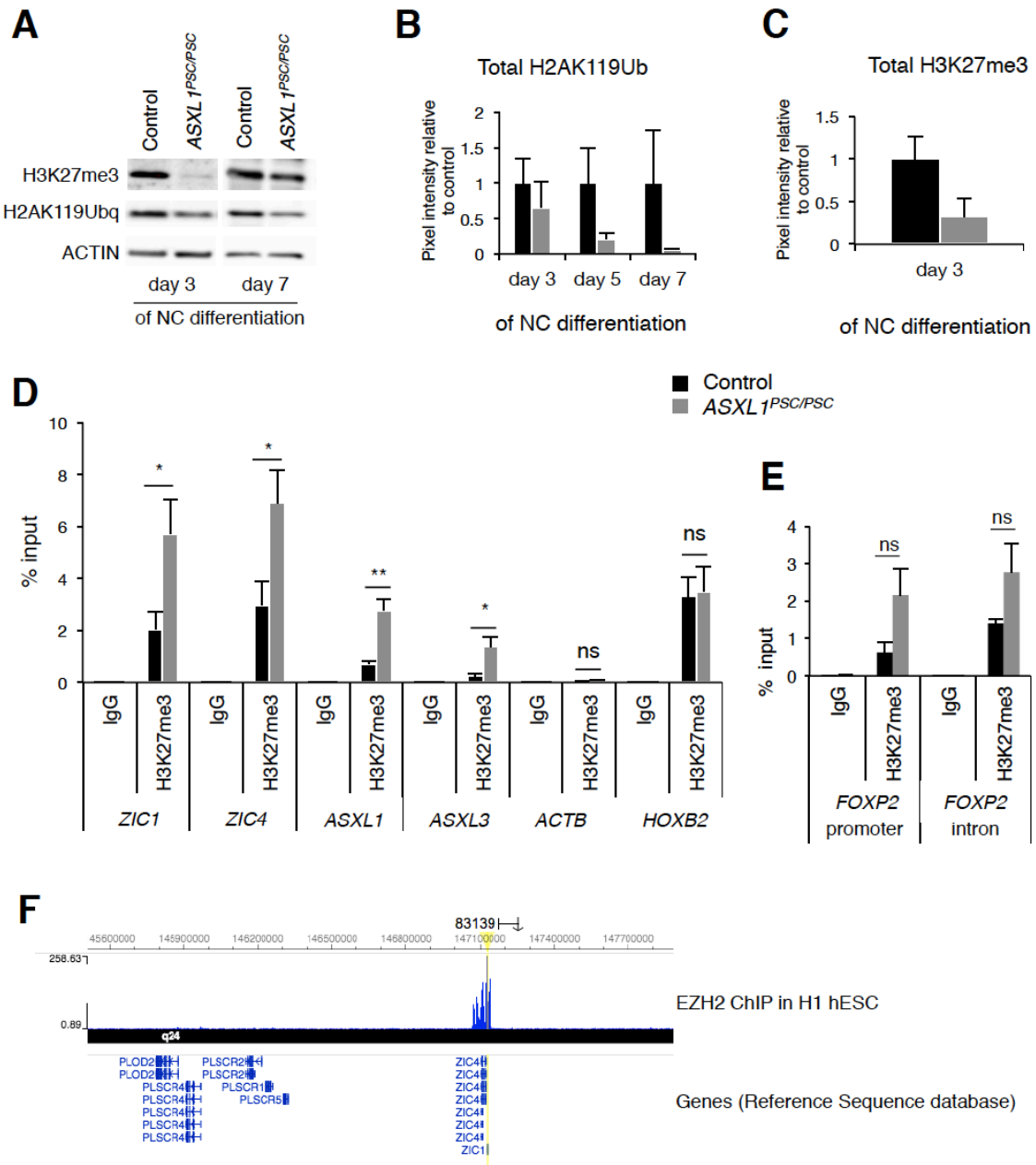

Figure 32. Expression of truncated ASXL1 is associated with global reduction of H2AK119Ub and H3K27me3 but local increase of H3K27me3 at repressed NC genes.
(A) Representative Western Blot of cell lysates from day 3, 5 and 7 NC cultures derived from *ASXL1*$^{PSC/PSC}$ (clones A and B) relative to control hESC-derived cultures. **(B-C)** Quantification of global H2AK119Ub **(B)** and H3K27me3 **(C)** levels relative to ACTIN during NC differentiation from *ASXL1*$^{PSC/PSC}$ clones and control cells (n=3). **(D)** Chromatin Immunoprecipitation for H3K27me3 followed by quantitative PCR (ChIP-qPCR) in NC progenitors derived at day 7 from *ASXL1*$^{PSC/PSC}$ and control lines. The *ACTB* and *HOXB2* loci were used as positive and negative controls for H3K27me3, respectively (n=3-7 from independent experiments; *p<0.05, **p<0.01; ns, not significant; Welch's t-test/Wilcoxon test). **(E)** ChIP-qPCR occupancy analysis of H3K27me3 at the *FOXP2* gene in day 7 NC progenitors of *ASXL1*$^{PSC/PSC}$ and control HESCs (n=3-7 from independent experiments, Welch's t-test). **(F)** ChIP-seq data from the ENCODE project[200], showing binding of EZH2 to the *ZIC1/ZIC4* locus in H1 hESC.

3.5 Characterization of *Asxl* genes in two animal models

In addition to characterization of pathological *ASXL1* variants in human differentiation systems, I set out to investigate whether these findings have relevance for tissue formation *in vivo.* To this end, I established and analyzed mouse and zebrafish models for (truncated) Asxl function in embryogenesis and fetal development.

3.5.1 Asxl1 is involved in mouse neuroectoderm development

My transcriptional analyses in human developmental progenitors implicated *ASXL1* in the formation of embryonic lineages, in particular the neural crest and neuronal lineages. To corroborate these findings, I made use of the *Asxl1*$^{tm1a(EUCOMM)Wtsi}$ mouse strain bearing a LacZ-Neomycin reporter cassette in the *Asxl1* locus, which results in functional loss of one gene copy in heterozygous animals, but enables tracing of Asxl1 expression[235]. This mouse line has been studied by McGinley and colleagues on a C57BL/6NTac background[107]. In my case, the line was generated by injection of mouse ESC line EPD0080_1_B11 (obtained from the EuMMCR at the Helmholtz Center Munich) into Balb/c embryos (T.-W. Qiao and Dr. Pertek, Helmholtz Center Munich), followed by breeding of F1 chimeras to C57BL/6NCrl wt mice. Further backbreeding of heterozygous carrier mice, as determined by PCR genotyping for each generation, to C57BL/6NCrl wt mice was performed for ten generations to ensure generation of congenic animals[203].
Initially in backcrossing generation N5 and in further generations, I noticed phenotypic changes at variable, but generally low penetrance in *Asxl1*$^{+/-}$ pups, which occasionally presented reduced birth weight and size (**Fig. 33A**), as well as unilateral or bilateral cataracts, microphthalmia or anaphthalmia (**Fig. 33B**). Reduced or missing eyes and growth defects have been described in the present and other *Asxl1* knockout lines of different backgrounds, but commonly only in homozygous animals[100,107,116]. Otherwise, behavior of affected *Asxl1*$^{+/-}$ pups was normal, they were thriving well and around postnatal day P20, heterozygous mice born at half of their littermates' size became indistinguishable from their wildtype siblings.
I analyzed *Asxl1*$^{+/-}$ embryos at embryonic days E11.5 and E14.5 after X-gal staining to determine expression of the β-Galactosidase gene within the *Asxl1* locus. This reaffirmed *Asxl1* expression in neuroectodermal tissues including brain, eyes and the closing neural tube, as well as in the heart, limbs, hair follicles, ears and pharyngeal arches as reported before[115,116] (**Fig. 33C**). Staining of the closing neural tube and pharyngeal arches indicated expression of *Asxl1* in the NC and NC-derived tissues, which corresponded to the craniofacial features reported in homozygous *Asxl1* null mice[100] (**Fig. 33C**).
Overall, the *Asxl1-LacZ* Knock-in mouse proved useful to delineate presumptive functions for *Asxl1* in NC and neuroectoderm development, which I inferred here from embryonic expression patterns. With regard to the craniofacial and ophthalmic features that are reported in BOS patients[137], this should provide critical clues to the clarification of BOS pathogenesis.

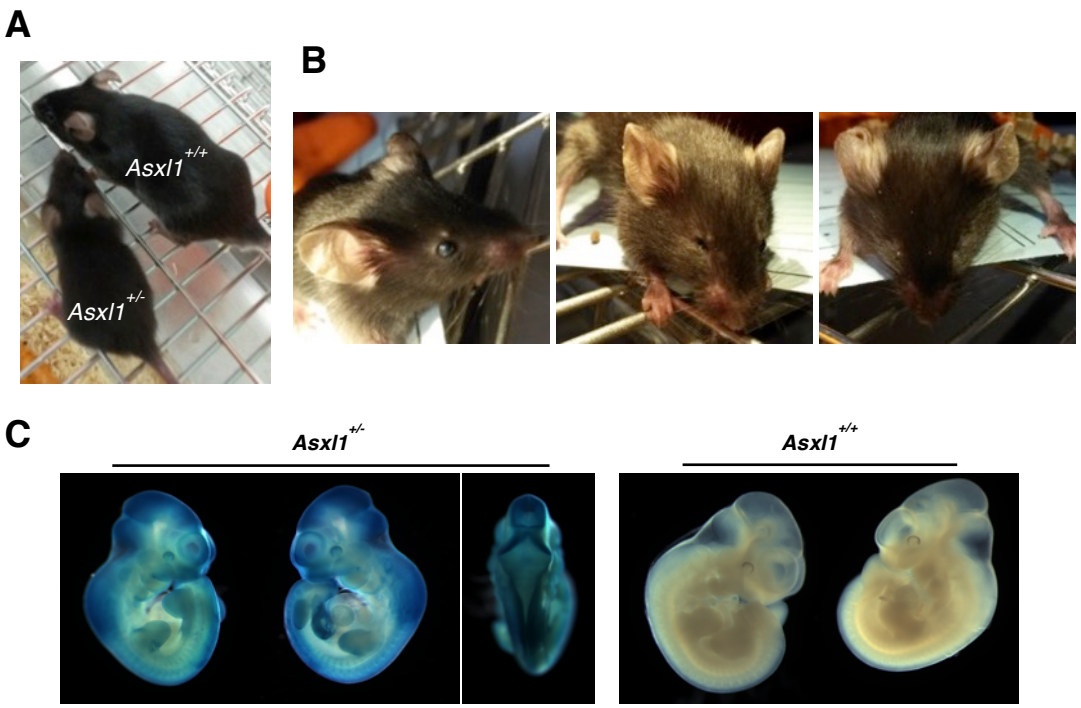

Figure 33. Murine *Asxl1* is expressed in neuro-ectodermal lineages and involved in eye formation in mice.
(A-C) Analysis of the *Asxl1*$^{tm1a(EUCOMM)Wtsi}$ mouse strain that carries a lacZ reporter knocked into the *Asxl1* locus. **(A)** *Asxl1*$^{+/-}$ and *Asxl1*$^{+/+}$ (wt) littermates (P15). **(B)** *Asxl1*$^{+/-}$ mice display cataracts (left) and unilateral and bilateral microphthalmia (middle and right). **(C)** LacZ staining in whole-mount *Asxl1*$^{+/-}$ and wt embryos of embryonic day E11.5. *Asxl1* is highly expressed in the closing neural tube and brain and also detected in limb buds and pharyngeal arches.

3.5.2 Identification and analysis of zebrafish *asxl1* and *asxl2* genes

Owing to the ease of manipulation and analysis of transparent embryos, the zebrafish (*Danio rerio*) belongs to the preferred biomedical model organisms, and is widely used to investigate mechanisms of embryonic morphogenesis, including NC formation and migration[236]. Hence, in collaboration with Dr. López-Schier and Dr. Viader Llargues (Helmholtz Center Munich), I sought to identify hitherto uncharacterized *Asxl* homologs in the zebrafish and establish a disease-relevant system to analyze the potentially conserved function of truncated ASXL variants.

3.5.2.1 asxl1 and asxl2 are expressed during zebrafish larvae development

Analysis of public databases revealed homology-based prediction of two ASX orthologs in the zebrafish genome, *asxl1* and *asxl2* (**Fig. 34A**). Interestingly, the evolutionary history of *ASX* genes suggests that the teleost fish, including the zebrafish, lost the *Asxl3* paralog that presumably resulted from speciation of a theoretical Asxl1/Asxl3 precursor gene and is still found in the spotted gar, a ray-finned fish that split off from the teleost fish branch[237] (**Fig. 34A**).

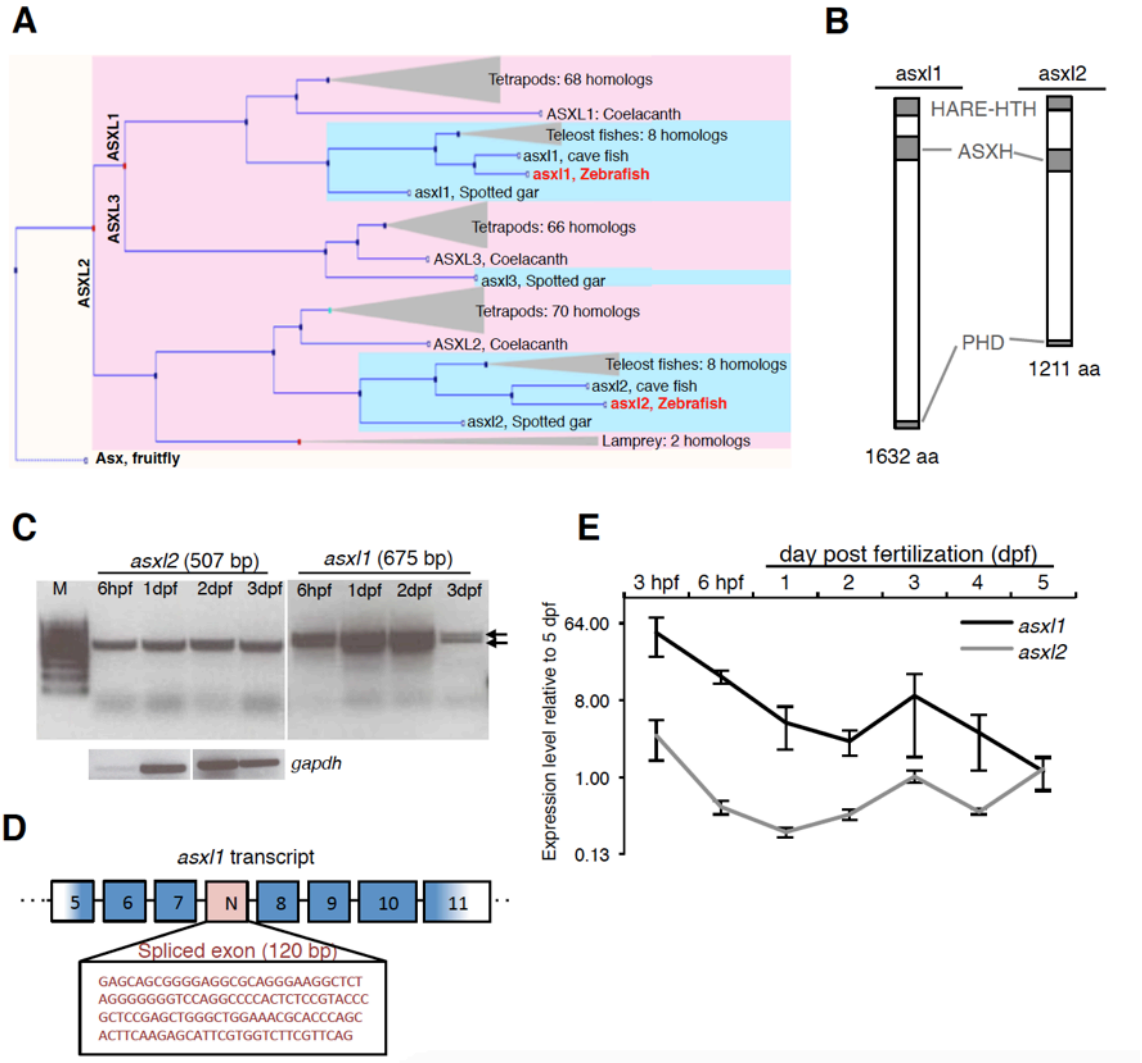

Figure 34. Zebrafish ASX homologs *asxl1* and *asxl2* are expressed in embryos and larvae.
(A) Gene/protein tree representing the evolutionary history of *Asx* and orthologous genes. Predicted zebrafish *asxl1* and *asxl2* genes are shown in red. Red nodes indicate duplication events; blue nodes represent speciation towards paralogs and orthologs. From[238]. **(B)** Predicted zebrafish asxl1 and asxl2 proteins (UniProt Q6P6X8 and E7FG88) show conservation of domains HARE-HTH, ASXH and PHD. **(C)** Expression of *asxl1* and *asxl2* in wildtype zebrafish embryos 6 hours post fertilization (hpf) and 1-3 days post fertilization (dpf) as determined by RT-PCR. Predicted transcript sizes are given; two transcripts were detected for *asxl1* (arrows). *Gapdh*, normalization control; M, molecular marker. **(D)** Identification of a novel, alternatively spliced exon between annotated exons 7 and 8 of zebrafish *asxl1* confirmed by sequencing of *asxl1* transcripts from (**C**). **(E)** qPCR analysis of zebrafish *asxl1* and *asxl2* during embryo and larvae development; normalization using *elongation factor 1 alpha* (*elfa*); *n*=3.

I conducted BLAST search of the *asxl1/2* sequences, which indicated that despite the genome duplication event in teleost fish[239], the *asxl1* and *asxl2* loci are not present in duplicated form. Predicted protein sequences harbor the conserved HARE-HTH, ASXH and PHD sequences (UniProt ID F1Q5H5 and E7FG88), and the total protein identity between human and zebrafish orthologs is 39% and 52% for asxl1 and asxl2, respectively (**Fig. 34B**). I furthermore identified putative NR-binding motifs (LVTQLL) in translations of both sequences, indicating that the ASXM2 domain is retained in the zebrafish homologs as well.

To identify whether the genes are transcribed, I performed RT-PCR in samples isolated at different stages of embryonic zebrafish, which confirmed expression of *asxl1* and *asxl2* from 6 hours post fertilization (hpf) to 3 days post fertilization (dpf; **Fig. 34C**). I detected two *asxl1* transcripts at all analyzed stages, and sequencing confirmed an alternatively spliced, novel exon of 120 bp between annotated exons 7 and 8 (*asxl1* transcript XM_001341206.5, NCBI Reference sequence; **Fig. 34C, D**). *Asxl1* and *asxl2* transcripts showed a highly similar, dynamic expression pattern in zebrafish embryos, with strong decline from 3 hpf to 1-2 dpf, followed by a steady increase in *asxl2* levels while *asxl1* transcript levels remained constant (**Fig. 34D**).
To analyze the expression pattern in embryonic tissues, I performed whole-mount *in situ* hybridization using sense and antisense mRNA probes constructed from *asxl2* and *asxl1* transcripts. *Asxl1* mRNA was detected in 6 hpf embryos, in brain structures and pectoral fin buds of 36 hpf embryos, and eyes and otic capsules at 48 hpf (**Fig. 35A**). Similarly, I detected *Asxl2* expression in the otic capsule and the eye, albeit at low levels, in 48 hpf embryos (**Fig. 35B**). Notably, similar expression patterns were detected using two different probes of each *asxl1* (one including the novel exon) and *asxl2*.

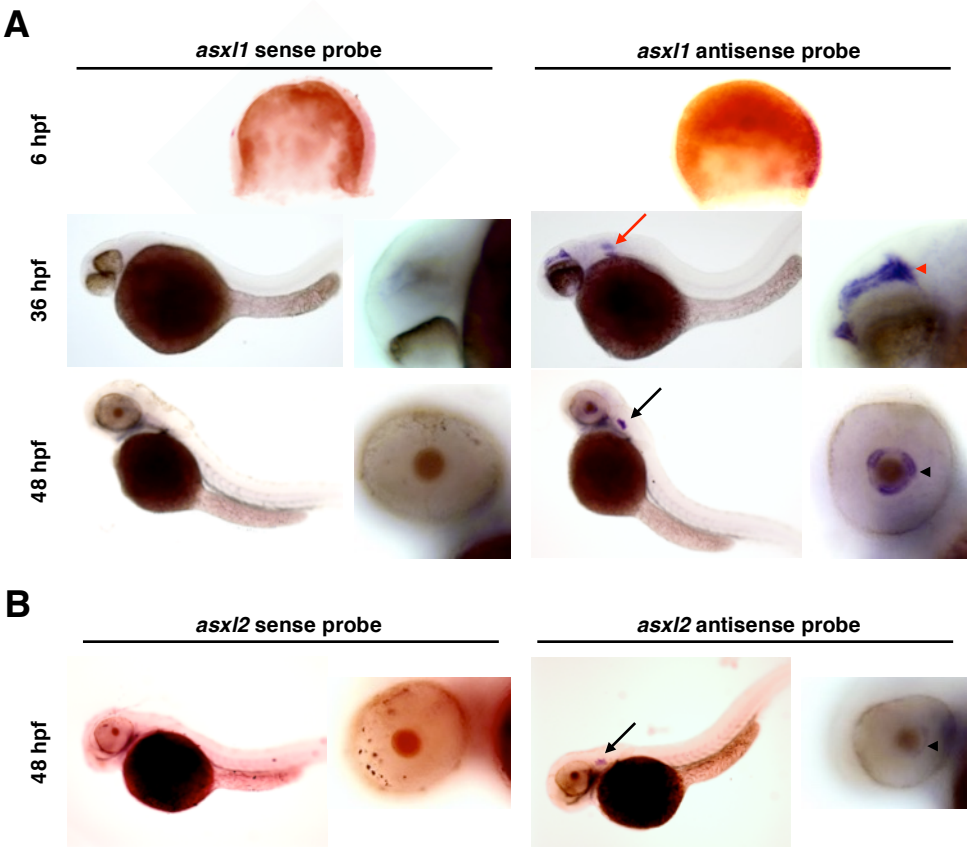

Figure 35. Expression patterns of *asxl1* and *asxl2* in zebrafish embryos.
(A, B) RNA *in situ* hybridization of whole-mount zebrafish embryos at different developmental stages with *asxl1* (**A**) and *asxl2* (**B**) sense (negative control) and antisense probes shows labeling of the pectoral fin buds (red arrow), brain structures (red arrowhead), the otic capsules, i.e. the developing inner ear (black arrows) and the retina (black arrowhead).

3.5.2.2 Manipulation of zebrafish asxl1

In an attempt to generate a BOS-relevant *in vivo* disease model, I employed the CRISPR/Cas technique to induce mutations within the central region of the zebrafish *asxl1* locus, corresponding to the mutated alleles in BOS patients. Genome editing in zebrafish requires injection of the *Cas9* mRNA and the targeting gRNAs into embryos at the 1-cell stage (**Fig. 36A**). To optimize editing efficiency, I validated two injection protocols[207,208] by targeting the albino gene *slc34a2*, and one injection method gave rise to embryos and larvae with disrupted pigmentation (**Fig. 36B**). I followed this method for injection of a gRNA against the *asxl1* locus, targeting the region around bp 2120 of the 4980 bp transcript. Analysis of F1 and F2 progeny revealed at least 9 different types of mutations that had been produced, including deletions, insertions and base conversions (**Fig. 36A,C**). All of the mutations furthermore resulted in PSCs that predicted expression of truncated protein in mutated fish. Offspring of heterozygous F1 crossings showed variable phenotypes, and mainly comprised pericardial and yolk sac edemas and caudal truncations to varying degrees, from slightly shortened or bend fish to runts (**Fig. 36D**). These malformations were also observed in around 50% of 'wildtype' fish not bearing targeted mutations in *asxl1*, indicating that these might be unspecific developmental defects (**Fig. 36E**); however, I did not exclude off-target effects in the phenotypic putative wt fish. Moreover, all of the larvae bearing mutations were associated with phenotypes at 80 % to 100 % penetrance, and the combined presence of edema and truncated tail was only found in confirmed mutant fish (**Fig. 36E**).
Taken together, I verified expression of *asxl1* and *asxl2* homologs in the zebrafish, and the establishment of mutant *asxl1* lines can serve as a tool fur future studies on the conservation of functional roles for BOS-relevant mutations in embryogenesis.

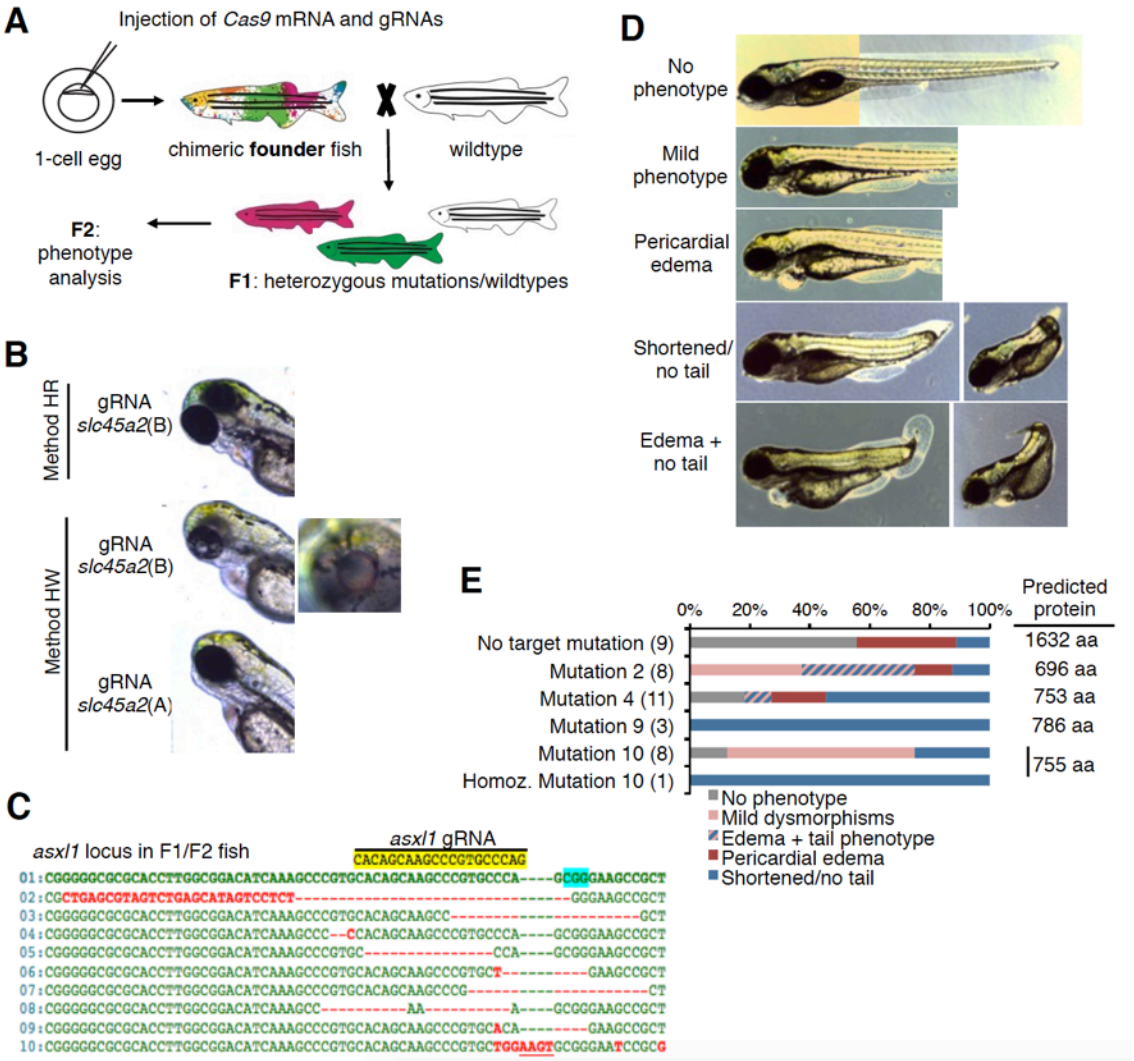

Figure 36. Generation of zebrafish *asxl1* mutants via CRISPR/Cas genome editing.
(**A**) Scheme of CRISPR/Cas editing and breeding procedure. Injection of *Cas9* mRNA and *asxl1*-targeting gRNA into 1-cell stage embryos leads to the development of chimeric founder fish. These are crossed to wt fish to generate heterozygous F1 progeny, which after genotyping can be inbred to generate heterozygous and homozygous F2 fish for phenotypic analysis. **(B)** Validation of CRISPR editing protocols via generation of albino mutants; shown are founder fish (larval stage). Two different protocols (HW and HR) were followed to inject two different gRNAs (A or B), targeted against tthe *slc45a2 (albino)* gene[240]. Note reduced pigmentation in the eye (magnified image), indicating successful targeting of the *slc45a2* gene. **(C)** CRISPR-mediated target mutations as determined by sequencing of the *asxl1* locus in F1/F2 fish. 1 represents the wildtype sequence, numbers 2-10 label different mutations including conversion of bases (red bases), deletions (red dashes) and insertions (underscored). The targeting site of the *asxl1* gRNA (yellow) used to create these mutations is indicated, as well as the Protospacer Adjacent Motif (PAM, blue). **(D, E)** Exemplary images of phenotypes observed in F2 *asxl1* mutants **(D)** and their quantification according to the associated mutation **(E)**. Mutation numbers refer to **(C)**; numbers in parentheses indicate the number of analyzed fish. 'No target mutation' indicates that no mutations were found in the analyzed region of the *asxl1* locus. Predicted asxl1 protein sizes were calculated from the location and type of mutation that was identified in the respective fishes.

4. Discussion

4.1. Human ASXL paralogs are differentially expressed during hESC differentiation

The ASXL family is a versatile group of homologous proteins that appear to serve as epigenetic platforms: owing to a multi-domain structure, they associate with transcription factors and chromatin modifiers at target gene sites, presumably conferring specificity to Polycomb-associated regulatory mechanisms[77,241]. Developmental roles of *ASXL* genes in spatiotemporal gene control, best documented for the *Hox* loci, were reported in animal models and in studies employing cell lines and tissue progenitors[81,96,99,100,103,106,107,116,242,243]. This work is to my knowledge the first study to investigate and discuss roles of the *ASXL* genes during differentiation of human pluripotent stem cells, in particular for a pathological variant of *ASXL1* that is connected to congenital birth defects.

I initially found that human *ASXL1-3* genes exhibit distinct expression patterns in hESC differentiation. *ASXL1/2* are expressed in undifferentiated cells and are rapidly upregulated in response to differentiation cues (**Fig. 9C**), mirroring the induction pattern of *Asxl1* during *in vitro* differentiation from mouse ESC[244] and the expression of murine *Asxl1/2* during early stages of embryogenesis[115], which suggests similar early roles in human development. Also corresponding to mouse development[115], *ASXL3* is not significantly expressed in undifferentiated cells and becomes (slightly) activated only at late stages of neuronal differentiation (**Fig. 9E)**. The presence of an alternatively spliced exon in *ASXL3*, which harbors STOP codons in all reading frames and is degraded via NMD, was reported recently[1]. I also detected the presence of the 'NMD-exon' in *ASXL3* transcripts isolated from hESCs (**Supplementary Fig. S2**), indicating that this posttranscriptional mechanism is involved in regulating *ASXL3* expression[1].

The presence of both repressive and activating chromatin marks on *ASXL1/ASXL3* TSSs suggests a bivalent condition in the pluripotent state, however this should be interpreted with caution because *ASXL1* is detected at significant levels in undifferentiated cells (**Fig. 9A,B**). Therefore, rather than bivalency, heterogeneity in the culture might explain the co-localization of H3K4me3 and H3K27me3 marks in the *ASXL1* locus better. This is supported by the fact that in undifferentiated cells, *ASXL1* is expressed at different levels also depending on confluency and cultivation time (**Figs. 17, 18**). With regard to *ASXL3*, the hypothesis of this gene being poised is more likely, as it is not expressed in undifferentiated cells and becomes activated in specific developmental lineages (NC and neuronal differentiation). Silencing in other developmental states, including hematopoietic cells[120] (H3K27 trimethylation of the TSS in a lymphoblast cell line[200]) also supports this notion. *ASXL2* however appears to be a 'epigenetic housekeeping factor' based on its constant expression and H3K4 trimethylated state in the analyzed lines. Indeed it has been postulated that *Asxl2* might be more important for the maintenance of histone marks than for their initial placement[106].

The diverged functions of *ASXL1/ASXL3* and *ASXL2* is also supported by their distinct expression patterns; while *ASXL1/3* is upregulated during fetal brain development and neuronal differentiation *in vitro*, *ASXL2* is constantly expressed at low to moderate levels in the CNS or in neuronal progenitors (**Fig. 9E, F**). Moreover, *de novo* mutations in *ASXL1/3* or *ASXL2* lead to distinct brain abnormalities including macrocephaly or

microcephaly, respectively[137]. Finally, the proposed evolutionary history of *ASX* genes involves early separation of putative ASXL2 and ASXL1/ASXL3 precursor proteins (**Fig. 34A**). This is reflected for instance in the shared HP1 binding motif in ASXL1/3, which is absent in ASXL2, and the corresponding repressive roles of the former proteins in chromatin regulation[95,97]. Taken together, this brings me to conclude specific versus redundant roles of the *ASXL* paralogs in maintenance of human pluripotent stem cells and differentiation.

4.2 Generation of human developmental models for BOS

The concurrence of phenotypically overlapping congenital defects, caused by mutations that are all located in the penultimate or last exon of paralogous genes, raises the question of common pathogenic mechanisms and developmental pathways in *ASXL*-associated disorders. The elucidation of molecular mechanisms underlying BOS is of particular interest: firstly, truncating mutations in *ASXL1* are very common in myeloid transformations as well (for instance, in 50% of myelomonocytic leukemia cases[245]), and secondly, ASXL1 is involved in the function of important epigenetic complexes, including PR-DUB and PRC2[79], and their roles in human embryonic development are not clear yet.
To address this question, I generated a toolset that enabled me to examine the role of BOS mutations in pluripotent stem cells and progenitor commitment. Importantly, I relied on using iPSCs derived by two different integration-free reprogramming methods per line to obtain BOS-iPSC clones, allowing for the subtraction of potential method-related effects. Moreover, this provided a measure to reduce artifacts that are derived from cell line variability, which was indeed observed in transcriptional analysis of undifferentiated BOS-iPSCs (**Figs. 10C, 15, 17A**) and their sphere attachment properties (**Fig. 23B**). I postulate that several factors might contribute to these inconsistencies, including i) donor-specific genetic polymorphisms that are unrelated to the disease-causing mutations, ii) genetic/epigenetic aberrations that can be introduced in reprogramming, and iii) unknown functions of *ASXL1* during somatic reprogramming, a process relying on alteration of the chromatin landscapes[246]. Nevertheless, phenotypes including ASXL1 protein regulation and the general defect in NC differentiation were consistent across the clones, showing that my approach provided me a way to subtract line-specific artifacts.
Due to these issues, I have generated a system of isogenic cell lines, a concept that was shown to lower clone-specific confounding effects in studying disease-related phenotypes in iPSC and hESCs[247,248]. In accordance, isogenic *ASXL1*$^{PSC/PSC}$ hESC lines exhibited little clonal variability (**Fig. 17C, Fig. 23A**), arguing for their application to study the molecular pathogenesis of BOS. Although I did not analyze the CRISPR/Cas targeted hESC clones for potential off-target effects, careful selection of gRNAs and most importantly the inclusion of several clones in the majority of my experiments should decrease the influence of potential off-target effects to a minimum[249,250]. I had initially attempted to generate *ASXL1*$^{PSC/+}$ lines to faithfully model the situation in BOS patients; the unambiguous identification of heterozyous clones was however not feasible, and I therefore concentrated my analyses on homozygous *ASXL1*$^{PSC/PSC}$ clones. The phenotypes uniformly seen in all of these clones should thus exclusively be connected to the function of putative truncated ASXL1 protein. Moreover, the possibility of interactions between truncated and full-length ASXL1 is eliminated in *ASXL1*$^{PSC/PSC}$ lines, meaning they cannot fully recapitulate mechanisms in BOS-iPSC. However, I conducted additional analyses in

PB-*ASXL1*^{PSC} hESC, which constitute an aggravated 'heterozygous' BOS model due to strong overexpression of a truncated ASXL1 variant on a wildtype background.
The overexpression line furthermore allowed to validate monoclonal antibodies that detect the N-terminus of ASXL1. Despite that the novel antibody clones 4F6 and 12F9 were selected in binding assays also based on negative reaction towards N-terminal ASXL2 peptides, detection of additional bands and most importantly the constant band detected at ~170 kDa (also in the *ASXL1*$^{PSC/PSC}$ cell lines) suggests that the antibodies recognized ASXL isoforms or paralogs. I attempted to examine the possibility of ASXL2 recognition by generating a double *ASXL1*$^{PSC/PSC}$/*ASXL2*$^{PSC/PSC}$ line or alternatively via knocking down *ASXL2* in *ASXL1*$^{PSC/PSC}$, but these attempts were not yet unsuccessful. I presume that I was unable to derive compound clones because of crucial functional redundancy, as both ASXL1 and ASXL2 are required to maintain the PR-DUB complex[111] and also indicated by the number of shared target genes in pre-adipocyte cells[95]. In line with this rational, *ASXL1* and *ASXL2* mutations never coincide in human cancers, whereas *ASXL1* and *ASXL3* mutations are found in combination[251]. Hence, this suggests that hESCs might not be able to cope with concomitant loss of *ASXL1* and *ASXL2*.
The novel antibody detected additional bands of 70 kDa, 130 kDa and above 300 kDa at different levels in wildtype and mutant cells (**Fig. 13D, E** and **Supplementary Fig. S1**). Notably, Inoue *et al* mentioned similar backgrounds when using antibodies targeting the N-terminus of ASXL1 in heterozygous ASXL1 mutant lines[101,126], which implies that sequence homology to other proteins can impede the specific detection of N-terminal ASXL1 variants. It is unlikely for ASXL3 with its predicted molecular weight of 240 kDa to have produced bands at 300 kDa, considering that it was nearly undetected in undifferentiated hESCs. Nevertheless, I propose that the 70 kDa and 130 kDa bands represent ASXL isoforms based on the dynamic regulation of these genes that is dependent on the presence of specific ASXL1 mutations and cell density, and reports of alternative splicing and usage of different polyadenylation sites in *ASXL* transcripts[80,81]. Furthermore, when I performed initial immunoprecipitation experiments to identify interactions of overexpressed ASXL1 constructs and EZH2 in PB-*ASXL1*^{PSC} cells, targeting of EZH2 led to enrichment of a 70 kDa protein, indicating an interaction with a short isoform of ASXL1 in these preliminary experiments (**Supplementary Fig. S3**). Proteomic analysis of candidate isoforms could clarify this issue and provide new insights into the complex regulation of ASXL proteins in human pluripotent stem cell differentiation and disease. Interestingly, a recent study predicted the generation of conserved ASXL1 and ASXL2 variants of 77 kDa and 89 kDa, respectively, that result from ribosomal frameshifting events, connecting the N-terminal ASXN and ASXH domains to transframe products[252]. However, ribosomal frameshifting is though to occur only in 1-2 % of transcripts[252], which renders detection via Western Blot highly unlikely, unless these proteins are highly stabile.
ASXL1 proteins contain motifs allowing for nuclear transportation, and immunocytochemical analyses in this and other studies suggest mainly nuclear localization of ASXL1[101,111,253], but also faint cytoplasmatic detection (**Figs. 12G and 22B**), which is in line with suggested functions of Asxl1 in the cytoplasma[254] and presence of Drosphila Asx in both nuclei and cytoplasm[78].
In all, I have generated a novel monoclonal antibody targeting the N-terminus of human ASXL1, and a set of BOS pluripotent stem cell models. These include disease-relevant lines with presumed physiological expression of mutant ASXL1 proteins (BOS-iPSC), an 'enhanced' model for analyzing the dominant function of truncated ASXL1 (PB-*ASXL1*^{PSC})

and an isogenic model system that focuses on the isolated function of BOS-associated mutations (*ASXL1*$^{PSC/PSC}$ hESC).

4.3 BOS-associated mutations in *ASXL1* lead to expression of truncated protein

The implementation of BOS model lines in combination with a monoclonal antibody confirmed the stable expression of truncated ASXL1 variants in undifferentiated *ASXL1*$^{PSC/PSC}$ hESC and importantly also in BOS-iPSCs (**Fig. 13**). This was already hinted by the detection of mutant *ASXL1* transcripts, which escaped NMD as I predicted according to the location of the mutation within the large terminal exon[255]. Similar mechanisms have been proposed for *ASXL1*-associated mutations in leukemias[101,126-128], and for *ASXL2* mutations causing a novel neurodevelopmental syndrome[139]. Decreased *ASXL3* transcript and protein levels were observed in one BRS patient; however, degradation via NMD was not assessed in the corresponding study[112].
Evolutionary conserved features that characterize ASXL proteins are the N-terminal HARE-HTH motif and ASX-H domain and the C-terminal PHD finger. Comparison between homologs indicates lower conservation of the central part of the protein and high conservation of the N- and C-terminus, illustrating the functional importance of the domains[115]. Since the ASX-H domain mediates binding to BAP1/calypso and is also present in Asx, it appears that activity in the PR-DUB complex is one of the most fundamental tasks of ASX orthologs besides PcG/TrxG mediated gene regulation[75,79]. Concerning the PHD finger, exact mechanisms are less well understood. It encompasses one part of the bipartite SET-domain binding motif in Drosophila Asx[75], and it would be of interest to determine whether these dual binding motifs, enabling interaction with both PcG and TrxG proteins, are also found in the human protein. However arguing against this possibility, one study showed that truncated ASXL1 can still bind to EZH2[101]. PHD domains confer the ability to bind modified histones[83], thus serving as 'readers' of epigenetic states, and mutations within PHD fingers are involved in various human diseases[256]. Structural properties of ASXL PHD fingers theoretically allow binding of internally methylated histone tails such as H3K27me3[83], which offers an attractive model concerning how ASXLs could be involved in fine-tuning H3K27me3 deposition. Pathogenic truncations within the ASXL1 protein thus uncouple the modules responsible for hypothetical DNA targeting (the HARE-HTH domain) and chromatin modification (via co-factors) from the chromatin reading module. Accordingly, it would be of particular interest to compare the binding capacities of wildtype and truncated ASXL1 protein, for instance in mononucleosome binding assays[257,258], to determine how loss of the PHD domain affects ASXL1 function.
Interestingly, *Asx* frameshift mutants in the fruit fly also lead to expression of truncated Asx protein (aa 1-432) at levels comparable to the wildtype protein (1669 aa)[105]. In general, truncated Asx mutants had a stronger phenotype in de-repression of target genes than deletion of the entire *Asx* locus[73]. This indicates a gain-of-function of the truncated protein, and supports the notion of a comparable dominant ASXL1^{PSC} function in mammalian developmental contexts.
Truncated ASXL1 proteins retain PEST sequences and the ubiqutination site at K351, all of which promote proteolytic degradation. I generally observed lower levels of truncated ASXL1 compared to wildtype protein, and the difficulties I and others encountered while attempting to detect the truncated variants[101] might stem from

enhanced degradation of the mutant variant, which could furthermore explain why truncated ASXL1 variants were not found in other studies[99,125].
Taken together, with increasing evidence leading to the general consensus on a gain-of-function of truncated ASXL1 variants in human myeloid disorders[69,101,126,128,259], I showed here for the first time that a truncated ASXL1 protein is likewise expressed in BOS patient-derived iPSC and related hESC models, and might thus contribute to BOS pathogenesis.

4.4 Cross-regulation of ASXL transcript and protein levels

My studies did not reveal deregulation of endogenous *ASXL1, ASXL2* or *ASXL3* transcripts upon expression of truncated ASXL1 in undifferentiated cells (**Fig. 17A-D**). However, concomitant reduction of *ASXL1* and *ASXL3,* but not of *ASXL2* was evident in NC cultures derived from *ASXL1*$^{PSC/PSC}$ clones (**Fig. 31**). Moreover, *ASXL3* expression was induced by strong overexpression of truncated ASXL1 after short-term differentiation (**Fig. 17E**) but not in pluripotent conditions, which promotes the concept of (truncated) ASXL1 regulating gene expression in developmental contexts rather than in undifferentiated pluripotent stem cells. Reduced ASXL1 transcript and protein levels in established *ASXL1*$^{PSC/PSC}$ NC cultures (**Figs. 22C and 31**) agree with studies in Drosophila and in the mouse, which have suggested that the Asx(l) protein binds and autoregulates the genetic locus[78,100]. This observation furthermore reinforces the hypothesis that transcriptional regulation by mutant ASXL1 proteins occurs in developmental progenitors but not in pluripotent stem cells.
Notwithstanding these findings, I noted variable band intensities of ASXL1 in Western blotting of undifferentiated BOS models (**Figs 13D,E and 18A,B,G**). DOX-induced PB-*ASXL1*^{PSC} and BOS-iPSC lines #2-0 and #2-1, which all express the ASXL1 variant of 964 aa, exhibited increased levels of the putative ASXL1/2 band at 170 kDa, but very low levels of a 130 kDa band. In contrast, *ASXL1*$^{PSC/PSC}$ hESC clones and BOS-iPSC lines #1-0 and #1-1, which express ASXL1 variants of 809-824 aa, showed lower or equal levels of the 170 kDa band and pronounced 130 kDa bands in comparison to control cells. Of note, these results were obtained in cell cultures collected at similar densities. The truncated ASXL1 protein did not alter the general ASXL1 localization as detected by immunocytochemical staining in BOS-iPSC and PB-*ASXL1*^{PSC} (**Figs. 12G and 13F**), which is in line with other studies where extopically expressed truncated ASXL1 variants were nuclear[69,101]. I concluded that truncated ASXL1 influences the stability of ASXL1 (isoforms) and/or paralogs in a mutation-dependent manner, which might be relevant for BOS pathogenesis. Future studies should thus attempt to identify observed bands at 130 and 170 kDa, and examine how amino acids 824-964 of mutant ASXL1 proteins might function in regulating the respective proteins. I propose that analysis of posttranscriptional mechanisms[141,252] or ubiquitination pathways[88] could give valuable insights in this matter.
On another note, I noted inverse correlation between ASXL1/2 levels (170 kDa band) and cellular density of analyzed control cultures (**Fig. 18C-G**). Both ASXL1 and ASXL2 are involved in the regulation of proliferation[111,113,260], and correspondingly, transcript and protein levels might be dynamically adjusted according to the cell cycle stage.
Taken together, my analyses identified *ASXL* regulation on the transcript level in developmental progenitors, potentially including regulation via chromatin modifications in NC cultures (**Fig. 32D**), and on the protein level in accordance to cell density and the

presence of truncated ASXL1 variants (**Fig. 37A**). These regulatory mechanisms seem to be perturbed in BOS models, and might contribute to different pathogenic outcomes. This adds to the knowledge of the complex regulation of ASXLs by splicing[80,141], NMD[1] and auto-/cross-regulatory mechanisms[100,111,253].

4.5 Expression of truncated ASXL1 does not impair maintenance of the pluripotent state

In line with a proposed role of ASXL1 in progenitor specification, but not during induction or maintenance of pluripotency, I neither observed obvious defects in reprogramming of BOS patient fibroblasts, nor did I note significant deviations in rates of spontaneous differentiation in BOS-iPSC in comparison to control lines. Accordingly, *ASXL1* mutations did not dramatically affect expression of selected pluripotency-relevant genes (**Figs. 10C, 14F**). Analysis of germ layer-associated genes, *HOX* genes and iPSC transcriptomes gave indications for subtle to modest changes in the transcriptional landscapes of cells expressing truncated *ASXL1*, which is consistent with a minor role of *ASXL1* mutations in pluripotency (**Figs. 14, 15** and **Table 4**).
Interestingly, while transcriptomes of patient fibroblasts clustered together in principal component analysis, those of the derived BOS-iPSC lines did not (**Fig. 14A)**. BOS-iPSC showed deviations of the genomewide transcriptional landscape, with 606 and 798 genes being up- and downregulated, respectively, in #2-0 versus control lines, while only 172 and 273 genes were up- and downregulated, respectively, in line #1-0 compared to control lines. I also noted slightly enhanced cell size, and persistently enhanced *HOX* and *ASXL* transcription in the #2-0 iPSCs. These findings were not consistent in line #2-1, which expressed *ASXL* genes similar to control levels and showed normal morphology, suggesting clone-specific effects.
In an attempt to subtract clone-dependent variations, I conducted paired analysis of the two BOS-iPSC lines relative to control iPSC and hESC lines. This crude approach masked subtle transcriptional changes due to combination of different cell lines in each group, but certainly resulted in a list of robust and relevant transcriptional changes with regard to *ASXL1* truncations. I initially focused on developmental regulators and found upregulation of three factors that participate in TGF-β signaling, namely the TGFβ-ligand *Nodal*, and the BMP antagonists *Cerberus 1* (*CER1*) and *Growth and differentiation factor 3* (*GDF3*)[217,261,262]. Interestingly, Nodal/Activin signaling is required to maintain the undifferentiated state of hESCs via activation of *NANOG*, whereas BMP signaling antagonizes it[263,264]. This was in line with slightly enhanced transcript levels of *NANOG* in BOS-iPSCs and *ASXL1*$^{PSC/PSC}$ hESCs (**Figs. 11F and 14F**). Furthermore, Activin/Nodal signaling and CER1, GDF3 and Nodal are implicated in induction and specification of the definitive endoderm[265,266]. This is noteworthy, as levels of endoderm-related genes *SOX17* or both *SOX17* and *FOXA2*[267,268] increased in *ASXL1*$^{PSC/PSC}$ hESCs, and in short-term differentiation cultures overexpressing truncated ASXL1, respectively. Endoderm-related pathways were classified among a list of tissues associated with upregulated genes in BOS-iPSCs (**Table 4**). Hence, integration of results obtained with different BOS models indicates that expression of truncated ASXL1 enhances TGFβ signaling, and in aggravated models such as homozygous *ASXL1*$^{PSC/PSC}$ hESC and the PB-*ASXL1*^{PSC} overexpression line, this promoted modest induction of endoderm-related genes (**Fig. 37A**). Analysis of phosphorylated SMAD2/3 and SMAD1/5/8 levels should conclusively prove this proposition[269]. While these findings might have implications for progenitor

commitment, as I indeed also saw minor increase in *NODAL*, *GDF3*, *CER1* and *NANOG* levels in *ASXL1*$^{PSC/PSC}$ NC cultures compared to control cultures (**Fig. 30B**), I propose that they had a negligible, or potentially enhancing impact on the stability of pluripotency in BOS lines.
Another candidate from the list of upregulated genes in BOS-iPSC is *Neuronatin 1 (NNAT1)*, an inducer of neuronal differentiation that is believed to participate in brain development[215,270]. Neuronal features are present in all BOS patients, and analyses of neuroepithelial *ASXL1*$^{PSC/PSC}$ cultures pointed out misregulation of several genes implied in neuronal differentiation, as discussed further below. Intriguingly, gene sets with decreased expression in BOS-iPSC compared to control cells were also associated with seizures, a common finding in BOS. Further disease-relevant associations included muscular processes and protein stability, heart tissue and fetal growth retardation (**Table 4**). As both in the microarray datasets derived from undifferentiated BOS-iPSCs, and in RNA-seq analysis of *ASXL1*$^{PSC/PSC}$ NC cultures, downregulated gene sets were consistently associated with BOS-relevant tissues and BOS symptoms, this conclusively hints towards a dominant, repressive function of truncated ASXL1 as one of the major causes of BOS pathogenesis.
The *HOX* loci are known targets of Asxl1[116], and my initial analyses of undifferentiated cells hinted an impaired induction of *HOXA2* and *HOXB1* in BOS-iPSCs (**Fig. 15**). Although *HOX* genes were not expressed or detected only at low levels in NC cultures, I also noted negative regulation of *HOXB1* in RNA-seq analyses of *ASXL1*$^{PSC/PSC}$ NC progenitors, thus overall supporting these findings. Strong repression of *HOX* genes was also reported in heterozygous *ASXL3* mutant fibroblasts isolated from a BRS patient[112], and although the pathogenesis of BRS is also not entirely understood yet, there is a possibility of negative *HOX* regulation being implicated in the developmental defects of both BOS and BRS.
Considering that *ASXL1*$^{PSC/PSC}$ did not alter the pluripotency characteristics of the cells or promote differentiation, I conclude that *ASXL1* mutations contribute to the molecular etiology of BOS after the dissolution of pluripotency.

4.6 BOS-associated mutations in *ASXL1* impair NC development and perturb *ZIC1* expression and the NC regulatory network

The spectrum of BOS symptoms comprises many tissues and organs that contain NC derivatives, including the craniofacial region, the heart and the gastrointestinal system[35,137]. For the first time, my study linked BOS-associated mutations in *ASXL1* with perturbations in NC specification and emigration, and provided initial molecular mechanisms that are underlying these developmental phenotypes.

4.6.1 Generation of migrating and differentiating NC cells *in vitro*

For my analyses, I applied an *in vitro* NC differentiation protocol that in a previous study served the identification of CHD7 as an important regulator of NC development[33]. This approach does not rely on tightly controlled conditions via administration of BMP or WNT signaling modulators[152,234], but on self-organizing neuroepithelial spheres, which represent neural rosette structures. It has been shown that early neural rosette cultures derived from hPSCs are not homogenous but rather consist of neural stem cells, different subtypes of neurons and NC cells[271]. NC cells generated within neurospheres in

the presence of bFGF and EGF are of pre-migratory, dorsal neural fold identity but lose their stemness character upon detachment from the neurospheres, when they migrate and differentiate[272]. Correspondingly, NC-like cells obtained in this study proliferated for 10-15 passages at most, expressed p75, a marker of migrating human NC cells *in vivo*[184], and occasionally stained positive for HNK1, which labels a subset of migratory NC cells in human embryos[184]. The loss of the pre-migratory properties and presentation of advanced fates in the isolated NC cultures is furthermore in line with the downregulation of the *bona fide* NC specifier *SOX10*. I detected *SOX10* in RNA-seq data at day 7, and in established cultures at day 10, however the transcripts and protein was lost in passaged cultures (**Figs. 28A and 20B**). It was shown that SOX10 is downregulated in late migratory trunk NC cells[223], and taken together with the low expression or absence of *HOX* genes and detection of *ETS1* in NC cultures at day 7, I conclude that my differentiation approach generated cultures of mostly cranial identity[273]. Importantly, established NC-like cells were validated based on their developmental capacity to differentiate into MSCs and two of their derivatives, adipocytes and osteocytes. While thorough examination of NC identity would have required the additional evidence of differentiation into neurons, glia and melanocytes[224], I focused on a potential craniofacial contribution of generated NC cells, and NC-derived MSCs are crucial for the organization of head morphogenesis[162]. Moreover supporting acquisition of a NC fate, the cultures exhibited robust expression of the NC specifying factor TFAP2A, which is found in migrating human NC cells[150,152,184,224]. Since TFAP2A also marks non-neural ectoderm and is involved in sensory placode commitment[152,274], I affirmed absence of early placodal markers[228] in day 7 NC cultures, and furthermore confirmed expression of a whole panel of factors involved in human NC differentiation *in vitro*[150,152,153] (**Figure 28A**).

4.6.2 *ASXL1* is expressed during NC development, and truncated ASXL1 dominantly impairs emigration of NC cells

By means of a neurosphere-based NC differentiation strategy, I was able to detect induction of *ASXL1* and *ASXL3* in human NC cells and the presence of truncated ASXL1 variants in *ASXL1*$^{PSC/PSC}$ NC cultures (**Fig. 22C**), and identified NC delamination and emigration phenotypes resulting from expression of truncated ASXL1 (**Figs. 23, 25, 26**). The developmental defect was dramatic in homozygous *ASXL1*$^{PSC/PSC}$ cultures, where a very low percentage of neurospheres attached to the plate. In contrast, heterozygous BOS-iPSC adhered at rates 25%-50% lower than control iPSC. As discussed before, the homozygous hESC model does not truly reflect the pathophysiological situation in BOS patients and I hypothesized that homozygous truncating mutations would evoke severe phenotypes not compatible with sufficient formation of NC cells *in vivo*. Interestingly, a recent mouse model bearing a truncating mutation in the endogenous *Asxl1* locus showed embryonic lethality in homozygous mice, whereas heterozygous mice were viable[127]. Unfortunately, these mice were not analyzed further on potential NC-related defects. The presence of a modest attachment and outgrowth phenotype in BOS-iPSC-derived neurospheres suggests that *ASXL1*$^{PSC/PSC}$ hESC lines indeed presented disease-relevant phenotypes, albeit in an enhanced manner that might be dependent on the dose of truncating ASXL1 protein. Supportive of this idea, overexpression of the ASXL1^{PSC} on a wildtype background nearly abolished neurosphere attachment and delamination of NC cells. I conducted further analyses in NC cells derived from isogenic hESC lines to avoid

donor-dependent variability as seen in BOS-iPSC lines (**Fig. 23B**), and to examine the isolated effects of truncated ASXL1 expression.
Diminished attachment of the NSs indicated that cells within the neurospheres harbor immature cytoskeletal structures that do not support adhesion to untreated plastic dishes, a phenotype that is similar to the properties of undifferentiated hESCs. Moreover, the significantly increased number of (smaller) neurospheres in *ASXL1*$^{PSC/PSC}$ cultures (**Fig. 23D**) indicated that the integrity of large spheres could not be properly maintained. Neural rosette structures typically express N-Cadherin[271], and interestingly, I noted a delay in the expected *E*- and *N-Cadherin* switch in the mutant versus control cultures as early as day 3, which showed that cells residing with mutant neurospheres retained epithelial identity. The developmental defect seen in BOS model cultures was however not merely an *in vitro* artifact of reduced attachment of neurospheres to plastic dishes, but was functionally validated in orthotopic xenotransplantation experiments in chicken embryos (**Fig. 25**). Progeny of transplanted control neurospheres emigrated as single cells or in streams into the developing chicken embryo, while this behavior was significantly diminished in *ASXL1*$^{PSC/PSC}$ neurospheres, similarly to what has been observed after transplantation of iPSCs derived from CHARGE patients, a designated neurocristopathy[34]. Mutant and control neurospheres of similar size were transplanted to ensure equal number of starting populations. Importantly, ectopic expression of truncated chicken or human ASXL1 impaired embryonic NC cells in the developing chicken (**Fig. 26**), confirming a dominant, evolutionary conserved effect. It will be interesting for futures studies to examine chicken embryos that have been electroporated with truncated ASXL1 variants at later developmental stages, to assess the resulting effects on craniofacial morphogenesis.
Taken together, expression of truncated ASXL1 delays or impairs, but does not completely diminish the induction and/or proliferation of migratory NC cells *in vitro* and *in vivo* (**Fig. 37B**). This is based on the finding that *ASXL1*$^{PSC/PSC}$ neurospheres required longer incubation times for adhesion and NC cell delamination to occur (**Fig. 23F**); however, from those mutant cells that did migrate, expression profiles and developmental potency seemed comparable to control cells (**Fig. 24**). Comparison of different BOS-related models indicates that the associated developmental defects are dependent on the dose of truncated ASXL1 that is expressed in developing NC cells, which is interesting with regard to the symptomatic range that BOS patients display. 'Reverse' experiments, in which wildtype ASXL1 is introduced into *ASXL1*$^{PSC/PSC}$ cells, should further investigate this hypothesis.

4.6.3 Expression of truncated ASXL1 negatively regulates expression of *ZIC1* and NC specifiers

Transcriptional analysis of neurospheres at the attachment stage further supported the concept of perturbed NC induction and specification in *ASXL1*$^{PSC/PSC}$ cultures, as it revealed deregulation of the central set of NC specifiers that have been characterized in *Xenopus*, zebrafish or chicken *in vivo*, including most significantly *ZIC1* (**Fig. 28**). The list also included strongly downregulated factors that are crucial for human NC differentiation *in vitro*, namely *HES1*, *HES5* and *NR2F1*[150,153]. This conclusively shows that expression of truncated ASXL1 can perturb human NC regulatory networks (**Fig. 37B**).

Zic genes are primary specifiers of the neural plate border, and together with *Pax3/7* and *Msx1*, they are crucial factors for the acquisition of NC identity[151,275]. *Xenopus* models have suggested a minimum circuit of NC induction, encompassing Wnt signaling, *Pax3* and *Zic1*, which cooperatively activate downstream effectors that control NC specification, proliferation, migration and differentiation[276]. Interestingly, all of these regulatory modules were represented by the downregulated gene cohort in the *ASXL1$^{PSC/PSC}$* NC cultures. This indicates that *ZIC1* has a central role in NC specification, a notion that is supported also by the presence of *ZIC1* binding motifs at a subset of human NC enhancer elements[150]. According to its instructive role in NC development, I could show that re-establishment of *ZIC1* expression in *ASXL1$^{PSC/PSC}$* NC cultures rescued the attachment and delamination defect (**Fig. 29**). This implies that insufficient *ZIC1* induction represents a critical bottleneck for NC cultures that express truncated ASXL1, which is the first direct evidence for the significance of *ZIC1* in human NC differentiation, and is in line with animal studies highlighting the importance of *Zic* gene dosage during development[277].

I suggest that the strong repression of *ZIC1* is however is not the sole factor that hampers proper emigration of NC cells in the model. This is based on the (unquantified) observation that while *ASXL1$^{PSC/PSC}$* neurospheres overexpressing *ZIC1* attached to an extent that was comparable to control neurospheres, less prospective NC cells were emigrating from these neurospheres, indicating that proliferation or efficient induction was still impaired to some extent. Furthermore, the *Foxd3* gene is a known target of Zic1 during NC development[151], but I did not find downregulation of *FOXD3* in the mutant NC cultures. This might owe to species-specific differences, but it could also imply that not the entire 'ZIC1-axis' of the interconnected NC regulatory network was concurrently downregulated.

Pathways that should be considered in acting upstream or concomitantly to inefficient *ZIC1* activation are BMP and WNT signaling, both of which are involved in different stages of NC development. Induction of the NC at the NPB critically relies on intermediate levels of BMP signaling[151], and the importance of specific BMP concentrations for human NC differentiation has been confirmed *in vitro*[234]. Slightly increased expression levels of *Nodal*, *GDF3*, *CER1,* and more pronouncedly *NANOG,* in mutant NC cultures suggested enhanced Activin/NODAL signaling, which I had noted already in undifferentiated BOS-iPSC lines. It would be of interest to determine whether perturbations in these pathways contribute to the developmental phenotype in cultures expressing truncated ASXL1. Particularly regarding increased *NANOG* levels, they might furthermore be an indicator for delayed differentiation in *ASXL1$^{PSC/PSC}$* cells. Of note, *OCT4* transcripts could neither be detected in control, nor in mutant NC cultures.

WNT signaling is indispensable for human NC induction and specification *in vitro*[152], and animal models revealed that the Wnt pathway and *Zic1* are in a mutual regulatory relationship during NC development, with Wnt activating *Zic*, but also *Gbx2*, and *vice versa*[275,278,279]. The striking downregulation of a whole panel of frizzled receptors and WNT ligands in *ASXL1$^{PSC/PSC}$* NC cultures very likely contributes to defective NC specification (**Fig. 30A**). Future studies should investigate whether canonical WNT pathway activation can, similarly to *ZIC1,* rescue the attachment and delamination phenotypes, for instance via application of the GSK3 inhibitor CHIR during NC differentiation from control and *ASXL1$^{PSC/PSC}$* lines.

Apart from identification of negatively regulated genes pertaining to the induction, specification and differentiation modules, my transcriptional analysis also indicated the

delamination phenotype on a molecular level. This includes the deregulated switch from *E-Cadherin* to *N-Cadherin*, which presumably contributed to the impaired adhesion of neurospheres as discussed earlier, and negatively regulated *Cadherin 6*, which is activated during delamination of NC cells *in vivo*[151] (**Fig. 28C**).
I concluded from transcriptional analyses and cellular phenotypes that the molecular network controlling NC induction, delamination and differentiation is impaired in NC cultures expressing ASXL1^{PSC}, and this is critically dependent on negative regulation of *ZIC1* (**Fig. 37B**). To conclusively prove the translational relevance of the uncovered mechanisms, it would be important to show downregulation of *ZIC1* and NC specifiers, and respective rescue experiments, in patient-derived iPSCs.

4.6.4 Proposed roles for ASXL1 in neuroectoderm and neuronal development

The transcriptome analysis of day 7 *ASXL1$^{PSC/PSC}$* NC cultures revealed downregulation of a set of genes that are implicated in NC development, and also more exclusively in neuronal differentiation and nervous system development (**Table 5**). Detection of neuronal specifiers is expected owing to the aforementioned heterogeneity of cultures, which were comprised of neural rosette-like structures and delaminating NC cells. Notably, initiation of NC and neural induction are not only occurring side-by-side during development, but also rely on the same signals and are closely linked[151]. This is evident for instance in the formation of the birthplace of nascent NC cells, the NPB, which is defined by inhibitory actions between neural and non-neural TFs[151].
ZIC1, the most significantly and highly repressed gene in *ASXL1$^{PSC/PSC}$* cultures, is expressed in the neural plate and dorsal neural folds *in vivo*[275], and besides being involved the NC regulatory program, *Zic* genes promote the proliferation of precursors in the neural tube[275,280-282]. Interestingly, it was shown that Zic1 is important for RA-induced neuronal differentiation of mouse embryoid bodies via induction of neurogenic genes such as *Pax3/7* and *Zic4* in cooperation with Brn2/Pou3f2[283]. Correspondingly, *POU3F2, PAX3* and *ZIC4*, but also ZIC1 target gene *Engrailed 2*[275,284](*EN2*) were among the repressed genes in *ASXL1$^{PSC/PSC}$* NC cultures. I suggest that negative regulation of these neuronal factors evokes some of the nervous system-related symptoms in BOS. For instance, repression of the *ZIC1/ZIC4* locus in *ASXL1$^{PSC/PSC}$* lines can be linked to reports of BOS patients exhibiting Dandy-Walker malformation[131,137], a brain defect that is associated with the loss of the genomic *ZIC1/ZIC4* locus[282,285]. Analysis of neural progenitor/stem cells from the neurospheres could give indications on whether the reduction of *ZIC1* (and *ZIC4*) in the mutant cultures is involved in the specification of neurons.
Another possibility is that overactivation of Activin/Nodal, which requires validation on the protein level, might inhibit neuroectoderm formation in *ASXL1$^{PSC/PSC}$* cultures upstream of NC differentiation[286]. Further interesting candidates among the list of downregulated genes in *ASXL1$^{PSC/PSC}$* NC cultures are the *Hes* genes, which are effectors of Notch signalling and important for the maintenance of neural stem cells[287]. Similarly, *ASCL1/Mash1* and, highly significantly, the forkhead TF *FOXP2* were downregulated (**Figs. 27B** and **28B, Table 5**). *Mash1* is a neural-specific gene expressed in the developing neural tube, and interestingly also later in NC-derived enteric neurons[288]. Similarly, FOXP2 induces neuronal differentiation via neural target genes[289,290], and functional loss leads to neural tube defects[291]. Interestingly, *FOXP2* is associated with language disorders and autism in humans[292], and it is tempting to speculate that the

speech disorders in BOS patients are partially derived from strong repression of *FOXP2* during development. *FOXP2* expression patterns would have to be investigated in a more thorough manner in CNS progenitor populations derived from *ASXL1* mutant hESC and BOS-iPSC to delineate a potential contribution of *FOXP2* to specific BOS symptoms.
It would furthermore be instructive to test by ChIP experiments whether *ZIC1, FOXP2* and other highly downregulated gene in *ASXL1*$^{PSC/PSC}$ cultures, which exhibit increased H3K27me3, are direct targets of truncated and wildtype ASXL1 (**Fig. 37A**). Examination of expression patterns in mouse embryos (**Fig. 33C**) and during human brain development (**Fig. 9F**) suggests that ASXL1 is directly involved in neurodevelopment, and that this function might be conserved, since *Drosophila* Asx shows ubiquitous expression patterns during embryogenesis, but highly increased levels in the neuroectoderm and later in the CNS[78]. During *in vitro* differentiation to neural stem cells, the upregulation of *ASXL1* precedes that of *PAX6* (**Fig. 9E**), an important neuronal TF that is required for neuroectoderm formation[293]. This could imply that ASXL1 contributes to the re-arrangement of chromatin states required for neural commitment. To verify this, ASXL1 protein levels and recruitment of ASXL1 at early neuroectoderm specifiers would have to be tested. Furthermore, application of more defined differentiation protocols in futures studies might clarify distinct effects of ASXL1 mutations on neuroectoderm and separately on the neural crest.

4. 7 Truncated ASXL1 in the global and local regulation of histone marks

As my results indicate negative regulation of neural and NC specifiers in *ASXL1*$^{PSC/PSC}$ NC cultures in correlation to enhanced H3K27me3 in affected genes (**Fig. 32D,E**), the next step should be the attempt to discover a mechanistic link between expression of truncated ASXL1 and Polycomb-mediated transcriptional repression. To assess the possibility of direct regulation, the binding of truncated ASXL1 to EZH2 (**Supplementary Fig. S3**) and recruitment of both proteins to downregulated genes should be tested.
Several observations are nonetheless already compliant with the notion of enhanced EZH2 targeting by truncated ASXL1. It is has been shown that normal ASXL1 is important for the recruitment of PRC2 to several targets including the *HOX* loci[88,99,100], and that truncated ASXL1 variants can also bind EZH2[101]. Furthermore, *Ezh2* regulates *Zic1* during NC induction in *Xenopus*[160], and EZH2 and SUZ12 associate to the bivalent *ZIC1/ZIC4* locus in undifferentiated hESCs[200] (**Fig. 32F**). Bivalent or poised states are set up by Polycomb PRC1/PRC2 and TrxG SET1A/B/MLL complexes[68], and previous studies suggested that H3K27me3 is important for the repression of bivalent lineage-regulatory genes in pluripotent stem cells[294]. The prevailing model states that developmental signals tip the equilibrium of bivalent states by the recruitment of lineage TFs together with histone demethylases to enhancers and promoters, and thereby counteract PcG-mediated repression[68]. In light of this mechanism, I hypothesize that mutant ASXL1 might retain PRC2 at regulatory genes such as *ZIC1* during NC induction, thus contributing to delayed activation of NC fate determinants. This is in line with my observations on the transcriptional and cellular level that suggested delayed differentiation. It is noteworthy in this context that I noted decreased expression of *CBX8*, but increased levels of *CBX7* in RNA-seq analysis of *ASXL1*$^{PSC/PSC}$ NC cultures (not shown). Presence of different CBX proteins discriminates PRC1 complexes in developmental contexts, and in progenitors, CBX8/2/4 take over the role that CBX7

plays in pluripotent stem cells[57,72,295]. Thus, the interplay of the PRC1 subunits is another mechanistic possibility here.
Strikingly, my targeted analysis of histone modifications, which showed local increase in H3K27me3 levels, did not reflect genome-wide chromatin landscapes in *ASXL1*$^{PSC/PSC}$ NC cultures, as I noted reduced global levels of both H3K27me3 and H2AK119Ub (**Fig. 32**). The latter are in line with reports on somatic mutations of ASXL1, which enhance the activity of the BAP1-containing PR-DUB complex, resulting in reduced H2AK119Ub levels[69]. It was hypothesized that the global decrease of H3K27me3 in these settings might be a consequence of impaired PRC2 targeting[69] according to the 'alternative' model of PRC2 recruitment, which relies on H2AK119 ubiquitination by non-canonical PRC1 complexes (**Fig. 3A, Fig. 6C**). I cannot conclusively confirm this possibility on the basis of my Western Blot results, but time course analyses of these histone modifications in *ASXL1*$^{PSC/PSC}$ NC cultures might reveal whether the decline of H2AK119 ubiquitination precedes that of H3K27me3. Notably, my results are the first to be obtained in a human developmental model expressing physiological levels of truncated ASXL1 protein, as opposed to the ectopic overexpression of mutant ASXL1 protein in the former study, which used somatic cells[69]. Interestingly, in line with the proposed developmental role of ASXL1, no consistent global changes in H3K27me3 or H2AK119 levels were observed in undifferentiated BOS lines (**Fig. 19**).
Despite the reduction in total H3K27me3 and H2AK119Ub in *ASXL1*$^{PSC/PSC}$ NC cultures, I did not detect global upregulation of genes, or de-repression of PRC2 targets such as the *HOX* genes, which has been reported in a study on truncated ASXL1 function in the hematopoietic system[101]. However, Balasubramani *et al* noted that the de-ubiquitination activity of overactive PR-DUB seemed to target specific bivalent genes in hematopoieitic precursor cells, and even massive de-ubiquitination did not lead to de-repression of silenced genes *per se*[69]. In line with this finding, it has been shown that the PRC1 complex can repress *Hox* genes independently of the ubiquitination activity of Ring1B[296]. The implications of truncated ASXL1 to histone modifications are likely broader than H3K27me3 and H2AK119Ub, judging from the protein structure of this 'epigenetic platform'. Indeed, a recent study showed that ectopically expressed truncated ASXL1 binds to the bromodomain-factor BRD4, which is associated with an increase in H3K27 and H3K122 acetylation and a relaxed chromatin status[128]. The underlying *in vivo* analyses relied on transgene knock-in with unphysiological expression of truncated ASXL1, and it remains to be seen why full-length ASXL1 did not bind BRD4; nevertheless, the study identified an interesting gain-of-function of pathological ASXL1 variants that could potentially be relevant for BOS pathogenesis as well. Nevertheless, the highly context-dependent and possibly gene-specific functionality of ASXL1 can impede inference from studies employing orthogonal cell systems, and reports on truncated proteins versus knockout. For instance, not all studies in *Asxl1* truncation or knockout models reported alteration of H3K27me3 levels[128,259,260]. In *Asxl1*$^{-/-}$ mouse embryonic fibroblasts, H3K27me3 levels were unchanged but H3K9me3 levels were reduced by a half[260], indicating that in this particular cell type, the recruitment of HP1 constitutes a main function of Asxl1[95]. In contrast, *Asxl1* knockout decreased both H3K4me3 and H3K27me3 levels, but not H2AK19Ub levels, in murine erythroblasts [104].
Taken together, the multivalent, context-dependent properties of ASXL1 might complicate the elucidation of molecular mechanisms of BOS. Nevertheless, I have made very important contributions by discovering indications that truncated ASXL1 leads to H3K27me3 and H2AK119Ub reduction, therefore indicating for functional PR-DUB

enhancement, and also identified discordance between local and global patterns of histone modifications in cells expressing truncated ASXL1 (**Fig. 37A**). These findings could be relevant to myloid disorders caused by truncating ASXL1 mutations, and potentially also for truncating mutations of ASXL2/3. The target-specific mechanisms most importantly still have to be uncovered, and I speculate that they might involve increased recruitment of EZH2 via truncated ASXL1, providing a basis for developing therapeutic approaches. Further studies should also investigate other chromatin modifications, including H3K9me3, H3K4me3 and H3 acetylation, and interaction of truncated ASXL1 with the corresponding histone modifiers. These endeavors should enhance understanding of ASXL/Polycomb-mediated regulation of embryonic transcription programs, and thus should strongly support the delineation of BOS pathogenesis. On a fundamental level, my studies are the first to investigate Polycomb-mediated regulation of human NC development, and can be a point of departure to elucidate the still poorly understood epigenetic mechanisms controlling NC induction and specification, in particular in the setting of genetic diseases[157,159].

4.8 Animal models of the developmental role of truncated and wildtype ASXL1

To complement my *in vitro* findings, I analyzed the expression of *Asxl1* in a reporter mouse model, and furthermore developed chicken and zebrafish models that allow for the investigation of truncated Asxl1 during embryogenesis.

While I suggest that *Asxl1* null mice are not suitable to model BOS as they lack the characteristic truncating *Asxl1* mutations, several interesting aspects arose from the analysis of reporter/knockout mouse mutants. In accordance to my *in vitro* NC differentiation experiments, I detected expression of *Asxl1* along the closing neural tube and in several neuroectodermal and NC-derived tissues during embryogenesis in *vivo* (**Fig. 33C**). Transcription patterns and eye defects observed here and in other studies[100,115,116,254] (**Fig. 33B,C**) hint towards a direct involvement of *Asxl1* in neuroectoderm formation. Expression of murine *Asxl2* in the nuclear layer of the retina and in cells of the ganglion layer has been reported[119], indicating that both *Asxl1* and *Asxl2* could be implicated in eye development. Interestingly, unilateral eye defects in *Asxl1*$^{+/-}$ mice demonstrated a clear bias towards the right eye, an effect that has been noted in other mouse mutants[297], including *Bmp2/Bmp4* compound heterozygous mice[298]. My initial observations can serve as a cornerstone to decipher a general neuroectodermal role of *Asxl1*, which might be relevant for the human situation regarding ophthalmic features and intellectual defects reported in BOS patients. Nevertheless, critical aspects to consider in the analysis of *Asxl1* mouse mutants are strain-specific effects, which can have an impact on phenotypes[102,107,116]. This might explain why I saw phenotypes in heterozygous mice on a pure background (10 generations of backcrossing) that where not observed on mixed backgrounds in other studies[100,107].

Contrary to the mouse, *Asxl* functions in the chicken or zebrafish are hitherto unknown. Analysis of predicted chicken and zebrafish ASXL1 protein sequences indicated the presence of the N-and C-terminal domains HARE-HTH, ASXH and PHD, as well as the more centrally located NR-binding motifs LVKQLL (chicken) and LVTQLL (zebrafish), respectively. This could imply functional similarities between the human and animal orthologs in their wildtype and potentially also their truncated form, which I confirmed

in electroporation experiments, where both human and chicken truncated ASXL1 variants impaired chicken NC development. Many insights into NC development were gained from the analysis of chicken embryos[151], and I suggest that the proposed role of Asxl1 in neuroectoderm and NC specification could be further delineated in this model. Transplantation of neurospheres has, to my knowledge, only been performed in one neurocristopathy-related study thus far[34], and largely contributed to the elucidation of *ASXL1* mutation-related NC defects in this work.

Initial analyses of the putative BOS zebrafish model bearing truncating *asxl1* mutations however did not reveal a NC-specific phenotype, which warrants further, more detailed investigation. Comparable to chicken, quail and frog, zebrafish are widely employed to decipher NC regulatory circuits[236,299], which together with the ease of genetic manipulation and examination of embryos incited me to establish *asxl1* mutants. According to the particular situation in teleost fish, where a majority of the genes exists in duplicated form[239], redundancy can be an impeding factor in genetic analysis. However, BLAST search suggested that zebrafish not only lost duplicated copies of *asxl1* and *asxl2*, but also the *asxl3* paralog, which apparently took place only in the teleost fish (**Fig. 34A**), and might indicate the adoption of novel functions for *Asxl3* in tetrapods. The identification of an unannotated, alternatively spliced exon in this study is not unexpected given the detection of multiple *Asxl* transcript variants in other species[81]. Closely resembling Drosophila *Asx* expression kinetics[78], *asxl1* and *asxl2* transcript levels were relatively high 3 hours post fertilization, then dropped sharply, rose again slightly, and remained constant during larvae development. This expression pattern is suggestive of maternal loading of *asxl1/2* mRNA, which was reported to be crucial for early function of *Asx* in fly embryos[73,78], and might underlie the strong phenotype of caudal truncations observed in *asxl1* mutants, which closely resembles zebrafish *no tail* (*ntl*) mutants[300,301]. *Ntl* is the zebrafish homolog of the human/mouse *T*/*Brachyury*, which is crucial for the formation of dorsal mesoderm[300]. This suggests a possible role of *asxl1* in mesoderm development in the zebrafish, but since *in situ* hybridization experiments did not support mesodermal expression of *asxl1* thus far, these intriguing observations clearly warrant further investigation to assess the specificity of the observed phenotypes[302]. Clear signals of *asxl1* mRNA was detected in a very specific and restricted pattern in the otic vesicles, brain (potentially mid/hindbrain vesicles) and the retina of the eye, which correlated with neuroectoderm expression seen in the fly[78] and the mouse. The lack of specific antibodies detecting wildtype and putative truncated fish *asxl1* variants hampered further analyses, and future experiments should in addition validate the *in situ* hybridization results with more probes, including those that detect the mutant mRNA variant.

In all, I propose that the confirmation of *asxl1/2* gene expression in zebrafish embryos and the establishment of *asxl1* mutants provides a base for the identification of novel and conserved roles of ASXL orthologs in developmental contexts. As in the case of *zic1*, loss of which does not affect neural crest development in the zebrafish[303], *asxl1* might have gained or lost functions in comparison to its mammalian counterparts. Nevertheless, initial results indicate that a neuroectodermal role might is be conserved, and future studies should validate the specificity of the phenotypes I observed in zebrafish mutants, and investigate molecular mechanisms.

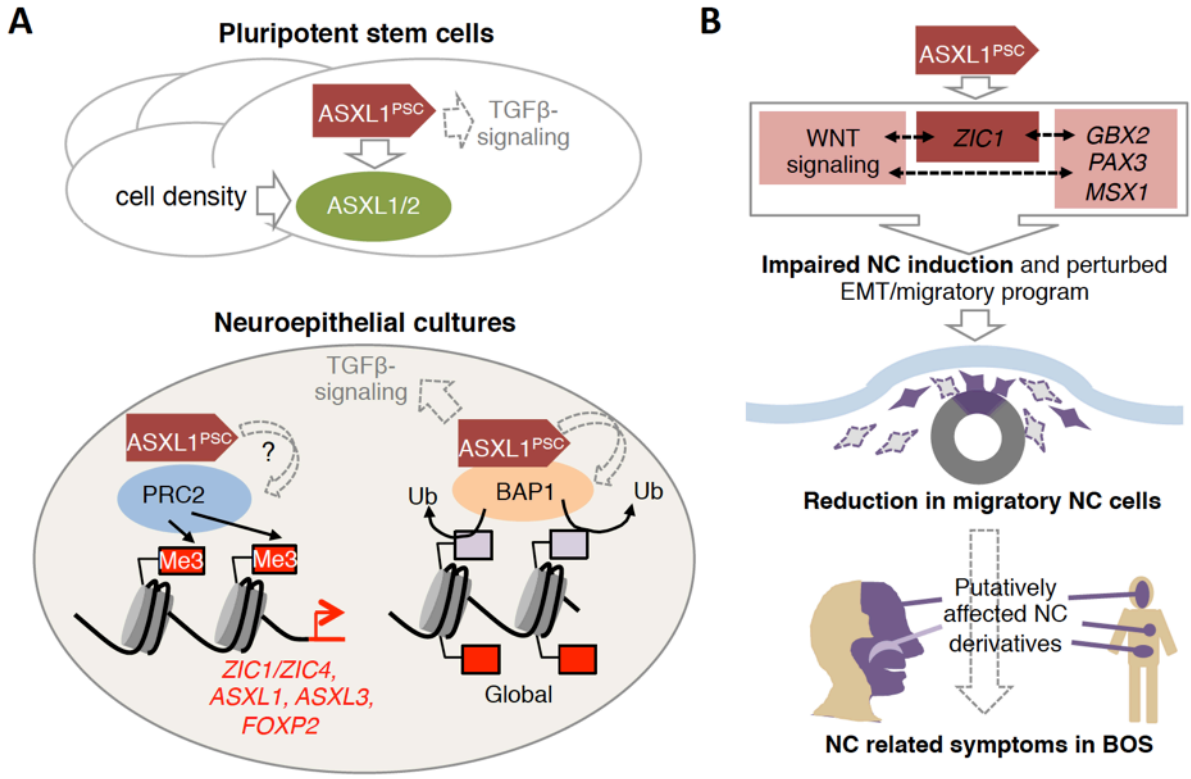

Figure 37. Proposed models for the regulation and role of (truncated) ASXL1 in pluripotent stem cells, neuroepithelial progenitor cultures and in putative NC-related defects in BOS.
(A) Expression of truncated ASXL1 does not impair maintenance of pluripotency in hESC/BOS-iPSC, but appears to slightly enhance TGFβ-signaling. *ASXL1* mutations furthermore affect protein levels of wildtype ASXL1/2 and putative isoforms, which are also regulated according to cell density (upper panel). In NC progenitor cultures expressing truncated ASXL1 (lower panel), global H3K27me3 and H2AK119 levels are reduced, presumably via overactivation of the PR-DUB complex followed by reduced recruitment of PRC2. In contrast, increased local H3K37me3 deposition at the *ZIC1/ZIC4*, *ASXL1*, *ASXL3* and *FOXP2* loci might arise from increased targeting of PRC2 by truncated ASXL1, which still needs to be confirmed experimentally. (**B**) In NC cultures, expression of truncated ASXL1 leads to dramatic reduction in *ZIC1* levels concomitantly with impaired or delayed activation of gene regulatory networks that are crucial for NC induction and EMT. This is proposed to be the cause of reduced emigration of NC progenitors derived from BOS-iPSC and homozygous *ASXL1*$^{PSC/PSC}$ hESC, and to evoke the NC-related phenotypes observed in BOS, including the characteristic craniofacial features.

4.9 Implications of *ASXL1* mutant models for BOS and related disorders

My analyses strongly indicate that truncated ASXL1 proteins contribute to BOS pathogenesis, presumably via altered histone modifications and subsequent transcriptional misregulation, and that at least a subset of BOS symptoms arises as a consequence of compromised neuroectoderm and NC development (**Fig. 37A, B**).
Multiple evidences connect the defects in the *ASXL1*$^{PSC/PSC}$ NC progenitor model to BOS and additional syndromes. First, loss of the *ZIC1/ZIC4* locus is associated with Dandy-Walker malformation[282,285,304], a brain development defect observed in some BOS patients[131]. Evaluation of *ZIC1/ZIC4* induction in BOS-iPSC-derived neuroepithelial cultures is required to conclusively confirm this link. Furthermore, heterozygous mutations in *ZIC1* correlate with premature fusion of the skull sutures[284], a process that might lead to trigonocephaly and associated hypertelorism[305] in BOS patients[137]. GO

terms analysis pointed out that not sufficiently induced gene cohorts in *ASXL1*$^{PSC/PSC}$ NC cultures were significantly associated with additional CNS-related conditions diagnosed in BOS, including 'agenesis of corpus callosum', 'nervous system malformations', 'seizures' and 'communication disorders'. This shows that expression of truncated ASXL1 in developmental models indeed provokes misregulations that are relevant to BOS disease phenotypes. Delineation of presumptive functions of (truncated) ASXL1 in neuroectoderm development might shed light on the molecular etiology of these conditions, and should furthermore elucidate a potential relationship between *ASXL1* and *FOXP2*, which could be relevant for neuropathological features in BOS patients.

Defects in neural tube development furthermore present a plausible link between potential neuronal and NC-related features of BOS. Timely migration of NC cells is crucial for their correct integration and function in designated fetal tissues, for instance during head development[162]. Delayed or reduced generation of migratory NC cells, as suggested by my observations in BOS models *in vitro*, might thus evoke, among others, craniofacial features in BOS. In line with this notion, *ASXL1*$^{PSC/PSC}$ NC cultures showed significant, 8-fold downregulation of *DLX1*, a gene that is identified with anterior dorsal NC cells, which will give rise to the ectomesenchyme that forms the head[150,306-308]. Cephalic NC cells furthermore have the capacity to differentiate into pericytes and smooth muscle cells of all blood vessels irrigating the forebrain and facial structures[309]. The majority of BOS patients display port-wine stains (nevus flammeus) on their forehead, which are capillary vascular malformations, and plausibly, delayed or reduced contribution of cranial NC cells to facial structures might be the underlying cause.

Based on the assumption that not only cranial, but also trunk NC cells are affected by *ASXL1* mutations, frequent reports of bowel malrotation or obstruction in BOS could be a consequence of insufficient innervation of the enteric system due to reduced colonization by NC cells and neuronal derivatives[166]. Disruption of peripheral neuron development might furthermore underlie feeding difficulties emerging from esophagal reflux, and the absence of tears in BOS patients[310] (*https://bohring-opitz.org/bosasxl1/list-of-symptoms/*). Finally, malformations like palpebral fissures anomalies, hand and limb anomalies, all of which are also observed in BOS, are common to neurocristopathies[150,311]. Taken together, accumulating evidence based on similarities of BOS to NC-related disorders such as CHARGE syndrome or X-linked Opitz syndrome[146,312,313] strongly supports my *in vitro* and *in vivo* results on the impairment of NC development by truncated ASXL1, and suggests that BOS should be considered a neurocristopathy. With respect to the diversity of NC derivatives and the cooperation of NC cells with other lineages during morphogenesis, abnormal development of the NC results in organ and tissue defects with highly diverse features[146], which might explain the seemingly unspecific and variable features reported in BOS case studies[137]. Another interesting aspect in this context is the transcriptional regulation of *ASXL1* transcripts. While I noted that mutant transcripts escape NMD in BOS-iPSC, it is known that the degradation process is cell- and tissue-specific, and can largely modulate disease outcome[255]. Generally, when a transcript escapes NMD, it produces truncated proteins that exert dominant effects, which lead to phenotypes that are more severe than those caused by the loss of one allele[255]. These mechanisms could account for the variability between BOS patients, and are especially noteworthy in light of my findings on dissimilar ASXL1 levels in BOS-iPSC lines that were derived from different patients.

Interestingly, mouse knockout phenotypes partly reflect clinical features of BOS. For example, both *Asxl1* Knockout mice and BOS patients display severely reduced birth

weight and size, which is usually re-gained during postnatal development[100,107,118,132,136]. Eye defects that I and others noted in heterozygous *Asxl1*$^{+/-}$ mice furthermore correlate with opththalmic features that are frequently reported in BOS[137]. Most importantly, the craniofacial malformations observed in homozygous *Asxl1* Null mice[100] hint towards perturbation of the murine NC lineage in response to loss of *Asxl1*. As I noted decreased *ASXL1* levels in my homozygous BOS model upon NC differentiation, this might argue towards a shared pathogenic mechanism involving reduction of *ASXL1* levels. While the following hypothesis clearly warrants further examination, one plausible explanation that reconciles *ASXL1* loss-of-function- and truncation studies involves retention of H3K27me3 (and potentially EZH2) at specific targets, including the *ASXL1/ASXL3* loci, during early differentiation. As a consequence, expression of developmental regulators and *ASXL1/ASXL3* are insufficient in the progress of induction and specification of affected lineages. Transcriptional perturbations should thus overlap in models for *ASXL1* loss/reduction and dominant mutations, and lead to similar outcomes on the cellular level. Several lines of evidence would be required to affirm this hypothesis, including genome-wide detection of ASXL1, EZH2 and H3K27me3 during differentiation from *ASXL1* mutant cultures, to show ASXL1^{PSC}-mediated recruitment of the repressive complex to target genes, and importantly the *ASXL1* locus. In a more straightforward experiment, re-introduction of wildtype *ASXL1* into *ASXL1*$^{PSC/PSC}$ NC cultures should reveal whether increased *ASXL1* levels can rescue the differentiation phenotype, or whether additional dominant effects of the truncated ASXL1 protein would prevent this.
My results obtained in *ASXL1*$^{PSC/PSC}$ NC cultures may also explain the close resemblance but milder severity of *ASXL3*-associated BRS compared to BOS, as truncated ASXL1 negatively regulates *ASXL3* in tandem with *ASXL1*, implying a mechanistic correspondence. Despite significant phenotypic overlap, specific differences between the three *ASXL*-related disorders lie in the manifestation of microcephaly (BOS, BRS) versus macrocephaly (NDS), reduced (BOS, BRS) versus normal (NDS) height and weight, severe (BOS, BRS) versus variable intellectual disabilities (NDS), presence (BOS, NDS) versus absence (BRS) of a facial nevus flammeus and normal (NDS, BRS) versus specific (BOS) posture (**Table 2***)*. These specifications indicate different neurodevelopmental and growth-related roles of *ASXL1/ASXL3* and *ASXL2*, supported by expression patterns *in vitro* and *in vivo (***Figs. 9F, 22A, 31A,C***)*. It would be of interest to determine whether truncated variants of ASXL2 and ASXL3 can also enhance PR-DUB activity, associating a unifying molecular mechanism to all ASXL-related disorders.
Taken together, my study has thus uncovered initial mechanisms of BOS pathogenesis that involve NC defects, and taking into account the similarity between additional syndromes and the large homology between paralogs, my results may (partially) be applicable to other NC and ASXL-associated disorders. The latter conditions, as I suggest, join a group of neuronal disorders and intellectual disabilities arising from transcriptional deregulations, caused by heterozygous mutations in epigenetic modifiers, including other members of the Polycomb family[144,256,314-316]. Future studies will certainly uncover important functions of ASXL proteins in regulating chromatin processes during neuroectoderm development.

5. Literature

1 Lowe, C. B., Bejerano, G., Salama, S. R. & Haussler, D. Endangered species hold clues to human evolution. *The Journal of heredity* **101**, 437-447, doi:10.1093/jhered/esq016 (2010).

2 Hochedlinger, K. & Plath, K. Epigenetic reprogramming and induced pluripotency. *Development* **136**, 509-523, doi:10.1242/dev.020867 (2009).

3 Kalinka, A. T. & Tomancak, P. The evolution of early animal embryos: conservation or divergence? *Trends in ecology & evolution* **27**, 385-393, doi:10.1016/j.tree.2012.03.007 (2012).

4 Madissoon, E. *et al.* Differences in gene expression between mouse and human for dynamically regulated genes in early embryo. *PloS one* **9**, e102949, doi:10.1371/journal.pone.0102949 (2014).

5 Prescott, S. L. *et al.* Enhancer divergence and cis-regulatory evolution in the human and chimp neural crest. *Cell* **163**, 68-83, doi:10.1016/j.cell.2015.08.036 (2015).

6 Shen-Orr, S. S., Pilpel, Y. & Hunter, C. P. Composition and regulation of maternal and zygotic transcriptomes reflects species-specific reproductive mode. *Genome biology* **11**, R58, doi:10.1186/gb-2010-11-6-r58 (2010).

7 Thomson, J. A. *et al.* Embryonic stem cell lines derived from human blastocysts. *Science* **282**, 1145-1147 (1998).

8 Takahashi, K. & Yamanaka, S. Induction of pluripotent stem cells from mouse embryonic and adult fibroblast cultures by defined factors. *Cell* **126**, 663-676, doi:10.1016/j.cell.2006.07.024 (2006).

9 Keller, G. Embryonic stem cell differentiation: emergence of a new era in biology and medicine. *Genes & development* **19**, 1129-1155, doi:10.1101/gad.1303605 (2005).

10 Zhu, Z. & Huangfu, D. Human pluripotent stem cells: an emerging model in developmental biology. *Development* **140**, 705-717, doi:10.1242/dev.086165 (2013).

11 Gauthier, M., Maury, Y., Peschanski, M. & Martinat, C. Human pluripotent stem cells for genetic disease modeling and drug screening. *Regenerative medicine* **6**, 607-622, doi:10.2217/rme.11.46 (2011).

12 Siller, R., Greenhough, S., Park, I. H. & Sullivan, G. J. Modelling human disease with pluripotent stem cells. *Current gene therapy* **13**, 99-110 (2013).

13 Schwartz, S. D. *et al.* Human embryonic stem cell-derived retinal pigment epithelium in patients with age-related macular degeneration and Stargardt's macular dystrophy: follow-up of two open-label phase 1/2 studies. *Lancet* **385**, 509-516, doi:10.1016/S0140-6736(14)61376-3 (2015).

14 Mandai, M., Kurimoto, Y. & Takahashi, M. Autologous Induced Stem-Cell-Derived Retinal Cells for Macular Degeneration. *The New England journal of medicine* **377**, 792-793, doi:10.1056/NEJMc1706274 (2017).

15 Smith, A. G. Embryo-derived stem cells: of mice and men. *Annual review of cell and developmental biology* **17**, 435-462, doi:10.1146/annurev.cellbio.17.1.435 (2001).

16 Warren, L. *et al.* Highly efficient reprogramming to pluripotency and directed differentiation of human cells with synthetic modified mRNA. *Cell stem cell* **7**, 618-630, doi:10.1016/j.stem.2010.08.012 (2010).

17 Diecke, S. *et al.* Novel codon-optimized mini-intronic plasmid for efficient, inexpensive, and xeno-free induction of pluripotency. *Scientific reports* **5**, 8081, doi:10.1038/srep08081 (2015).

18 Kim, D. *et al.* Generation of human induced pluripotent stem cells by direct delivery of reprogramming proteins. *Cell stem cell* **4**, 472-476, doi:10.1016/j.stem.2009.05.005 (2009).

19 Tsankov, A. M. *et al.* A qPCR ScoreCard quantifies the differentiation potential of human pluripotent stem cells. *Nature biotechnology* **33**, 1182-1192, doi:10.1038/nbt.3387 (2015).

20 Fontes, A. & Lakshmipathy, U. Advances in genetic modification of pluripotent stem cells. *Biotechnology advances* **31**, 994-1001, doi:10.1016/j.biotechadv.2013.07.003 (2013).

21 Garneau, J. E. *et al.* The CRISPR/Cas bacterial immune system cleaves bacteriophage and plasmid DNA. *Nature* **468**, 67-71, doi:10.1038/nature09523 (2010).

22 Cong, L. *et al.* Multiplex genome engineering using CRISPR/Cas systems. *Science* **339**, 819-823, doi:10.1126/science.1231143 (2013).

23 Cho, S. W. *et al.* Analysis of off-target effects of CRISPR/Cas-derived RNA-guided endonucleases and nickases. *Genome Res* **24**, 132-141, doi:10.1101/gr.162339.113 (2014).

24 Simara, P., Motl, J. A. & Kaufman, D. S. Pluripotent stem cells and gene therapy. *Translational research : the journal of laboratory and clinical medicine* **161**, 284-292, doi:10.1016/j.trsl.2013.01.001 (2013).

25 Ebert, A. D., Liang, P. & Wu, J. C. Induced pluripotent stem cells as a disease modeling and drug screening platform. *Journal of cardiovascular pharmacology* **60**, 408-416, doi:10.1097/FJC.0b013e318247f642 (2012).

26 Perrimon, N., Pitsouli, C. & Shilo, B. Z. Signaling mechanisms controlling cell fate and embryonic patterning. *Cold Spring Harbor perspectives in biology* **4**, a005975, doi:10.1101/cshperspect.a005975 (2012).

27 Murry, C. E. & Keller, G. Differentiation of embryonic stem cells to clinically relevant populations: lessons from embryonic development. *Cell* **132**, 661-680, doi:10.1016/j.cell.2008.02.008 (2008).

28 Ferrer-Vaquer, A. & Hadjantonakis, A. K. Birth defects associated with perturbations in preimplantation, gastrulation, and axis extension: from conjoined twinning to caudal dysgenesis. *Wiley interdisciplinary reviews. Developmental biology* **2**, 427-442, doi:10.1002/wdev.97 (2013).

29 Negoro, T., Okura, H. & Matsuyama, A. Induced Pluripotent Stem Cells: Global Research Trends. *BioResearch open access* **6**, 63-73, doi:10.1089/biores.2017.0013 (2017).

30 Doyle, M. J. *et al.* Human Induced Pluripotent Stem Cell-Derived Cardiomyocytes as a Model for Heart Development and Congenital Heart Disease. *Stem cell reviews* **11**, 710-727, doi:10.1007/s12015-015-9596-6 (2015).

31 Liu, J. A. & Cheung, M. Neural crest stem cells and their potential therapeutic applications. *Developmental biology* **419**, 199-216, doi:10.1016/j.ydbio.2016.09.006 (2016).

32 Trainor, P. A. Craniofacial birth defects: The role of neural crest cells in the etiology and pathogenesis of Treacher Collins syndrome and the potential for prevention. *American journal of medical genetics. Part A* **152A**, 2984-2994, doi:10.1002/ajmg.a.33454 (2010).

33 Bajpai, R. *et al.* CHD7 cooperates with PBAF to control multipotent neural crest formation. *Nature* **463**, 958-962, doi:10.1038/nature08733 (2010).

34 Okuno, H. *et al.* CHARGE syndrome modeling using patient-iPSCs reveals defective migration of neural crest cells harboring CHD7 mutations. *eLife* **6**, doi:10.7554/eLife.21114 (2017).

35 Mayor, R. & Theveneau, E. The neural crest. *Development* **140**, 2247-2251, doi:10.1242/dev.091751 (2013).

36 Dulac, C. Brain function and chromatin plasticity. *Nature* **465**, 728-735, doi:10.1038/nature09231 (2010).

37 Spivakov, M. & Fisher, A. G. Epigenetic signatures of stem-cell identity. *Nature reviews. Genetics* **8**, 263-271, doi:10.1038/nrg2046 (2007).

38 Egger, G., Liang, G., Aparicio, A. & Jones, P. A. Epigenetics in human disease and prospects for epigenetic therapy. *Nature* **429**, 457-463, doi:10.1038/nature02625 (2004).

39 Dambacher, S., Hahn, M. & Schotta, G. Epigenetic regulation of development by histone lysine methylation. *Heredity* **105**, 24-37, doi:10.1038/hdy.2010.49 (2010).

40 Ang, Y. S., Gaspar-Maia, A., Lemischka, I. R. & Bernstein, E. Stem cells and reprogramming: breaking the epigenetic barrier? *Trends in pharmacological sciences* **32**, 394-401, doi:10.1016/j.tips.2011.03.002 (2011).

41 Vissers, L. E. *et al.* Mutations in a new member of the chromodomain gene family cause CHARGE syndrome. *Nature genetics* **36**, 955-957, doi:10.1038/ng1407 (2004).

42 Petrij, F. *et al.* Rubinstein-Taybi syndrome caused by mutations in the transcriptional co-activator CBP. *Nature* **376**, 348-351, doi:10.1038/376348a0 (1995).

43 Lee, T. I. & Young, R. A. Transcriptional regulation and its misregulation in disease. *Cell* **152**, 1237-1251, doi:10.1016/j.cell.2013.02.014 (2013).

44 Abdel-Wahab, O., Patel, J. & Levine, R. L. Clinical implications of novel mutations in epigenetic modifiers in AML. *Hematology/oncology clinics of North America* **25**, 1119-1133, doi:10.1016/j.hoc.2011.09.013 (2011).

45 Ernst, T. *et al.* Inactivating mutations of the histone methyltransferase gene EZH2 in myeloid disorders. *Nature genetics* **42**, 722-726, doi:10.1038/ng.621 (2010).

46 Morey, L. & Helin, K. Polycomb group protein-mediated repression of transcription. *Trends in biochemical sciences* **35**, 323-332, doi:10.1016/j.tibs.2010.02.009 (2010).

47 Berdasco, M. & Esteller, M. Genetic syndromes caused by mutations in epigenetic genes. *Human genetics* **132**, 359-383, doi:10.1007/s00439-013-1271-x (2013).

48 Feinberg, A. P., Koldobskiy, M. A. & Gondor, A. Epigenetic modulators, modifiers and mediators in cancer aetiology and progression. *Nature reviews. Genetics* **17**, 284-299, doi:10.1038/nrg.2016.13 (2016).

49 Lewis, E. B. A gene complex controlling segmentation in Drosophila. *Nature* **276**, 565-570 (1978).

50 Schuettengruber, B., Bourbon, H. M., Di Croce, L. & Cavalli, G. Genome Regulation by Polycomb and Trithorax: 70 Years and Counting. *Cell* **171**, 34-57, doi:10.1016/j.cell.2017.08.002 (2017).

51 Ringrose, L. & Paro, R. Epigenetic regulation of cellular memory by the Polycomb and Trithorax group proteins. *Annual review of genetics* **38**, 413-443, doi:10.1146/annurev.genet.38.072902.091907 (2004).

52 Schwartz, Y. B. & Pirrotta, V. Polycomb complexes and epigenetic states. *Current opinion in cell biology* **20**, 266-273, doi:10.1016/j.ceb.2008.03.002 (2008).

53 Schwartz, Y. B. & Pirrotta, V. Polycomb silencing mechanisms and the management of genomic programmes. *Nature reviews. Genetics* **8**, 9-22, doi:10.1038/nrg1981 (2007).

54 Whitcomb, S. J., Basu, A., Allis, C. D. & Bernstein, E. Polycomb Group proteins: an evolutionary perspective. *Trends in genetics : TIG* **23**, 494-502, doi:10.1016/j.tig.2007.08.006 (2007).

55 Gao, Z. *et al.* PCGF homologs, CBX proteins, and RYBP define functionally distinct PRC1 family complexes. *Molecular cell* **45**, 344-356, doi:10.1016/j.molcel.2012.01.002 (2012).

56 Turner, S. A. & Bracken, A. P. A "complex" issue: deciphering the role of variant PRC1 in ESCs. *Cell stem cell* **12**, 145-146, doi:10.1016/j.stem.2013.01.014 (2013).

57 Morey, L. *et al.* Nonoverlapping functions of the Polycomb group Cbx family of proteins in embryonic stem cells. *Cell stem cell* **10**, 47-62, doi:10.1016/j.stem.2011.12.006 (2012).

58 Leeb, M. & Wutz, A. Ring1B is crucial for the regulation of developmental control genes and PRC1 proteins but not X inactivation in embryonic cells. *The Journal of cell biology* **178**, 219-229, doi:10.1083/jcb.200612127 (2007).

59 Blackledge, N. P. *et al.* Variant PRC1 complex-dependent H2A ubiquitylation drives PRC2 recruitment and polycomb domain formation. *Cell* **157**, 1445-1459, doi:10.1016/j.cell.2014.05.004 (2014).

60 Pengelly, A. R., Kalb, R., Finkl, K. & Muller, J. Transcriptional repression by PRC1 in the absence of H2A monoubiquitylation. *Genes & development* **29**, 1487-1492, doi:10.1101/gad.265439.115 (2015).

61 Kadoch, C. & Crabtree, G. R. Mammalian SWI/SNF chromatin remodeling complexes and cancer: Mechanistic insights gained from human genomics. *Science advances* **1**, e1500447, doi:10.1126/sciadv.1500447 (2015).

62 Piunti, A. & Shilatifard, A. Epigenetic balance of gene expression by Polycomb and COMPASS families. *Science* **352**, aad9780, doi:10.1126/science.aad9780 (2016).

63 Tie, F. *et al.* CBP-mediated acetylation of histone H3 lysine 27 antagonizes Drosophila Polycomb silencing. *Development* **136**, 3131-3141, doi:10.1242/dev.037127 (2009).

64 Schmitges, F. W. *et al.* Histone methylation by PRC2 is inhibited by active chromatin marks. *Molecular cell* **42**, 330-341, doi:10.1016/j.molcel.2011.03.025 (2011).

65 Shao, Z. *et al.* Stabilization of chromatin structure by PRC1, a Polycomb complex. *Cell* **98**, 37-46, doi:10.1016/S0092-8674(00)80604-2 (1999).

66 Boyer, L. A. *et al.* Polycomb complexes repress developmental regulators in murine embryonic stem cells. *Nature* **441**, 349-353, doi:10.1038/nature04733 (2006).

67 Cantone, I. & Fisher, A. G. Epigenetic programming and reprogramming during development. *Nature structural & molecular biology* **20**, 282-289, doi:10.1038/nsmb.2489 (2013).

68 Voigt, P., Tee, W. W. & Reinberg, D. A double take on bivalent promoters. *Genes & development* **27**, 1318-1338, doi:10.1101/gad.219626.113 (2013).

69 Balasubramani, A. *et al.* Cancer-associated ASXL1 mutations may act as gain-of-function mutations of the ASXL1-BAP1 complex. *Nature communications* **6**, 7307, doi:10.1038/ncomms8307 (2015).

70 Steffen, P. A. & Ringrose, L. What are memories made of? How Polycomb and Trithorax proteins mediate epigenetic memory. *Nature reviews. Molecular cell biology* **15**, 340-356, doi:10.1038/nrm3789 (2014).

71 Morey, L., Aloia, L., Cozzuto, L., Benitah, S. A. & Di Croce, L. RYBP and Cbx7 define specific biological functions of polycomb complexes in mouse embryonic stem cells. *Cell reports* **3**, 60-69, doi:10.1016/j.celrep.2012.11.026 (2013).

72 O'Loghlen, A. *et al.* MicroRNA regulation of Cbx7 mediates a switch of Polycomb orthologs during ESC differentiation. *Cell stem cell* **10**, 33-46, doi:10.1016/j.stem.2011.12.004 (2012).

73 Jürgens, G. A group of genes controlling the spatial expression of the bithorax complex in Drosophila. *Nature* **316**, 153, doi:10.1038/316153a0 (1985).

74 Milne, T. A., Sinclair, D. A. & Brock, H. W. The Additional sex combs gene of Drosophila is required for activation and repression of homeotic loci, and interacts specifically with Polycomb and super sex combs. *Molecular & general genetics : MGG* **261**, 753-761 (1999).

75 Li, T., Hodgson, J. W., Petruk, S., Mazo, A. & Brock, H. W. Additional sex combs interacts with enhancer of zeste and trithorax and modulates levels of trimethylation on histone H3K4 and H3K27 during transcription of hsp70. *Epigenetics & chromatin* **10**, 43, doi:10.1186/s13072-017-0151-3 (2017).

76 Petruk, S., Smith, S. T., Sedkov, Y. & Mazo, A. Association of trxG and PcG proteins with the bxd maintenance element depends on transcriptional activity. *Development* **135**, 2383-2390, doi:10.1242/dev.023275 (2008).

77 Soto, M. C., Chou, T. B. & Bender, W. Comparison of germline mosaics of genes in the Polycomb group of Drosophila melanogaster. *Genetics* **140**, 231-243 (1995).

78 Sinclair, D. A. *et al.* The Additional sex combs gene of Drosophila encodes a chromatin protein that binds to shared and unique Polycomb group sites on polytene chromosomes. *Development* **125**, 1207-1216 (1998).

79 Katoh, M. Functional and cancer genomics of ASXL family members. *British journal of cancer* **109**, 299-306, doi:10.1038/bjc.2013.281 (2013).

80 Koh, W. *et al.* Dynamic ASXL1 Exon Skipping and Alternative Circular Splicing in Single Human Cells. *PloS one* **11**, e0164085, doi:10.1371/journal.pone.0164085 (2016).

81 Fisher, C. A human homolog of Additional sex combs, ADDITIONAL SEX COMBS-LIKE 1, maps to chromosome 20q11. *Gene* **306**, 115-126, doi:10.1016/s0378-1119(03)00430-x (2003).

82 Sanchez-Pulido, L., Kong, L. & Ponting, C. P. A common ancestry for BAP1 and Uch37 regulators. *Bioinformatics* **28**, 1953-1956, doi:10.1093/bioinformatics/bts319 (2012).

83 Aravind, L. & Iyer, L. M. The HARE-HTH and associated domains: novel modules in the coordination of epigenetic DNA and protein modifications. *Cell cycle* **11**, 119-131, doi:10.4161/cc.11.1.18475 (2012).

84 Cho, Y. S., Kim, E. J., Park, U. H., Sin, H. S. & Um, S. J. Additional sex comb-like 1 (ASXL1), in cooperation with SRC-1, acts as a ligand-dependent coactivator for retinoic acid receptor. *The Journal of biological chemistry* **281**, 17588-17598, doi:10.1074/jbc.M512616200 (2006).

85 Sahtoe, D. D., van Dijk, W. J., Ekkebus, R., Ovaa, H. & Sixma, T. K. BAP1/ASXL1 recruitment and activation for H2A deubiquitination. *Nature communications* **7**, 10292, doi:10.1038/ncomms10292 (2016).

86 Brock, H. W. & Fisher, C. L. Maintenance of gene expression patterns. *Developmental dynamics : an official publication of the American Association of Anatomists* **232**, 633-655, doi:10.1002/dvdy.20298 (2005).

87 Rechsteiner, M. & Rogers, S. W. PEST sequences and regulation by proteolysis. *Trends in biochemical sciences* **21**, 267-271 (1996).

88 Inoue, D., Nishimura, K., Kozuka-Hata, H., Oyama, M. & Kitamura, T. The stability of epigenetic factor ASXL1 is regulated through ubiquitination and USP7-mediated deubiquitination. *Leukemia* **29**, 2257-2260, doi:10.1038/leu.2015.90 (2015).

89 Russell, B. & Graham, J. M., Jr. Expanding our knowledge of conditions associated with the ASXL gene family. *Genome medicine* **5**, 16, doi:10.1186/gm420 (2013).

90 Li, Z. *et al.* ASXL1 interacts with the cohesin complex to maintain chromatid separation and gene expression for normal hematopoiesis. *Science advances* **3**, e1601602, doi:10.1126/sciadv.1601602 (2017).

91 Gkikas, D., Tsampoula, M. & Politis, P. K. Nuclear receptors in neural stem/progenitor cell homeostasis. *Cellular and molecular life sciences : CMLS* **74**, 4097-4120, doi:10.1007/s00018-017-2571-4 (2017).

92 Huang, P., Chandra, V. & Rastinejad, F. Retinoic acid actions through mammalian nuclear receptors. *Chemical reviews* **114**, 233-254, doi:10.1021/cr400161b (2014).

93 Dhiman, V. K., Bolt, M. J. & White, K. P. Nuclear receptors in cancer - uncovering new and evolving roles through genomic analysis. *Nature reviews. Genetics*, doi:10.1038/nrg.2017.102 (2017).

94 Canzio, D. *et al.* Chromodomain-mediated oligomerization of HP1 suggests a nucleosome-bridging mechanism for heterochromatin assembly. *Molecular cell* **41**, 67-81, doi:10.1016/j.molcel.2010.12.016 (2011).

95 Park, U. H., Yoon, S. K., Park, T., Kim, E. J. & Um, S. J. Additional sex comb-like (ASXL) proteins 1 and 2 play opposite roles in adipogenesis via reciprocal regulation of peroxisome proliferator-activated receptor {gamma}. *The Journal of biological chemistry* **286**, 1354-1363, doi:10.1074/jbc.M110.177816 (2011).

96 Izawa, T. *et al.* ASXL2 Regulates Glucose, Lipid, and Skeletal Homeostasis. *Cell reports* **11**, 1625-1637, doi:10.1016/j.celrep.2015.05.019 (2015).

97 Shin, N., Lee, Y. K., Park, U. H., Jeong, J. C. & Um, S. J. Repression of LXRalpha by a novel member of additional sex comb-like family, ASXL3. *Biochemical and biophysical research communications* **454**, 479-485, doi:10.1016/j.bbrc.2014.10.074 (2014).

98 Nasmyth, K., Peters, J. M. & Uhlmann, F. Splitting the chromosome: cutting the ties that bind sister chromatids. *Science* **288**, 1379-1385 (2000).

99 Abdel-Wahab, O. *et al.* ASXL1 mutations promote myeloid transformation through loss of PRC2-mediated gene repression. *Cancer cell* **22**, 180-193, doi:10.1016/j.ccr.2012.06.032 (2012).

100 Abdel-Wahab, O. *et al.* Deletion of Asxl1 results in myelodysplasia and severe developmental defects in vivo. *The Journal of experimental medicine* **210**, 2641-2659, doi:10.1084/jem.20131141 (2013).

101 Inoue, D. *et al.* Myelodysplastic syndromes are induced by histone methylation-altering ASXL1 mutations. *The Journal of clinical investigation* **123**, 4627-4640, doi:10.1172/JCI70739 (2013).

102 Lai, H. L. *et al.* Maintenance of adult cardiac function requires the chromatin factor Asxl2. *Journal of molecular and cellular cardiology* **53**, 734-741, doi:10.1016/j.yjmcc.2012.08.014 (2012).

103 Micol, J. B. *et al.* ASXL2 is essential for haematopoiesis and acts as a haploinsufficient tumour suppressor in leukemia. *Nature communications* **8**, 15429, doi:10.1038/ncomms15429 (2017).

104 Shi, H. *et al.* ASXL1 plays an important role in erythropoiesis. *Scientific reports* **6**, 28789, doi:10.1038/srep28789 (2016).

105 Scheuermann, J. C. *et al.* Histone H2A deubiquitinase activity of the Polycomb repressive complex PR-DUB. *Nature* **465**, 243-247, doi:10.1038/nature08966 (2010).

106 Lai, H. L. & Wang, Q. T. Additional sex combs-like 2 is required for polycomb repressive complex 2 binding at select targets. *PloS one* **8**, e73983, doi:10.1371/journal.pone.0073983 (2013).

107 McGinley, A. L., Li, Y., Deliu, Z. & Wang, Q. T. Additional sex combs-like family genes are required for normal cardiovascular development. *Genesis* **52**, 671-686, doi:10.1002/dvg.22793 (2014).

108 Reyes-Turcu, F. E., Ventii, K. H. & Wilkinson, K. D. Regulation and cellular roles of ubiquitin-specific deubiquitinating enzymes. *Annual review of biochemistry* **78**, 363-397, doi:10.1146/annurev.biochem.78.082307.091526 (2009).

109 Dey, A. *et al.* Loss of the tumor suppressor BAP1 causes myeloid transformation. *Science* **337**, 1541-1546, doi:10.1126/science.1221711 (2012).

110 Gutierrez, L. *et al.* The role of the histone H2A ubiquitinase Sce in Polycomb repression. *Development* **139**, 117-127, doi:10.1242/dev.074450 (2012).

111 Daou, S. *et al.* The BAP1/ASXL2 Histone H2A Deubiquitinase Complex Regulates Cell Proliferation and Is Disrupted in Cancer. *The Journal of biological chemistry* **290**, 28643-28663, doi:10.1074/jbc.M115.661553 (2015).

112 Srivastava, A. *et al.* De novo dominant ASXL3 mutations alter H2A deubiquitination and transcription in Bainbridge-Ropers syndrome. *Human molecular genetics* **25**, 597-608, doi:10.1093/hmg/ddv499 (2016).

113 Wu, X. *et al.* Tumor suppressor ASXL1 is essential for the activation of INK4B expression in response to oncogene activity and anti-proliferative signals. *Cell research* **25**, 1205-1218, doi:10.1038/cr.2015.121 (2015).

114 Machida, Y. J., Machida, Y., Vashisht, A. A., Wohlschlegel, J. A. & Dutta, A. The deubiquitinating enzyme BAP1 regulates cell growth via interaction with HCF-1. *The Journal of biological chemistry* **284**, 34179-34188, doi:10.1074/jbc.M109.046755 (2009).

115 Fisher, C. L., Randazzo, F., Humphries, R. K. & Brock, H. W. Characterization of Asxl1, a murine homolog of Additional sex combs, and analysis of the Asx-like gene family. *Gene* **369**, 109-118, doi:10.1016/j.gene.2005.10.033 (2006).

116 Fisher, C. L. *et al.* Additional sex combs-like 1 belongs to the enhancer of trithorax and polycomb group and genetically interacts with Cbx2 in mice. *Developmental biology* **337**, 9-15, doi:10.1016/j.ydbio.2009.10.004 (2010).

117 Moon, S., Um, S. J. & Kim, E. J. Role of Asxl1 in kidney podocyte development via its interaction with Wtip. *Biochemical and biophysical research communications* **466**, 560-566, doi:10.1016/j.bbrc.2015.09.077 (2015).

118 Zhang, P. *et al.* Loss of Asxl1 Alters Self-Renewal and Cell Fate of Bone Marrow Stromal Cell, Leading to Bohring-Opitz-like Syndrome in Mice. *Stem cell reports* **6**, 914-925, doi:10.1016/j.stemcr.2016.04.013 (2016).

119 Baskind, H. A. *et al.* Functional conservation of Asxl2, a murine homolog for the Drosophila enhancer of trithorax and polycomb group gene Asx. *PloS one* **4**, e4750, doi:10.1371/journal.pone.0004750 (2009).

120 LaFave, L. M. *et al.* Loss of BAP1 function leads to EZH2-dependent transformation. *Nature medicine* **21**, 1344-1349, doi:10.1038/nm.3947 (2015).

121 Farber, C. R. *et al.* Mouse genome-wide association and systems genetics identify Asxl2 as a regulator of bone mineral density and osteoclastogenesis. *PLoS genetics* **7**, e1002038, doi:10.1371/journal.pgen.1002038 (2011).

122 Yavropoulou, M. P. & Yovos, J. G. Osteoclastogenesis--current knowledge and future perspectives. *Journal of musculoskeletal & neuronal interactions* **8**, 204-216 (2008).

123 Abdel-Wahab, O. & Dey, A. The ASXL-BAP1 axis: new factors in myelopoiesis, cancer and epigenetics. *Leukemia* **27**, 10-15, doi:10.1038/leu.2012.288 (2013).

124 Gelsi-Boyer, V. *et al.* Mutations in ASXL1 are associated with poor prognosis across the spectrum of malignant myeloid diseases. *Journal of hematology & oncology* **5**, 12, doi:10.1186/1756-8722-5-12 (2012).

125 Valletta, S. *et al.* ASXL1 mutation correction by CRISPR/Cas9 restores gene function in leukemia cells and increases survival in mouse xenografts. *Oncotarget* **6**, 44061-44071, doi:10.18632/oncotarget.6392 (2015).

126 Inoue, D. *et al.* Truncation mutants of ASXL1 observed in myeloid malignancies are expressed at detectable protein levels. *Experimental hematology* **44**, 172-176 e171, doi:10.1016/j.exphem.2015.11.011 (2016).

127 Hsu, Y. C. *et al.* The distinct biological implications of Asxl1 mutation and its roles in leukemogenesis revealed by a knock-in mouse model. *Journal of hematology & oncology* **10**, 139, doi:10.1186/s13045-017-0508-x (2017).

128 Yang, H. *et al.* Gain of function of ASXL1 truncating protein in the pathogenesis of myeloid malignancies. *Blood* **131**, 328-341, doi:10.1182/blood-2017-06-789669 (2018).

129 Oak, J. S. & Ohgami, R. S. Focusing on frequent ASXL1 mutations in myeloid neoplasms, and considering rarer ASXL2 and ASXL3 mutations. *Current medical research and opinion* **33**, 781-782, doi:10.1080/03007995.2017.1284049 (2017).

130 Duployez, N. *et al.* Unlike ASXL1 and ASXL2 mutations, ASXL3 mutations are rare events in acute myeloid leukemia with t(8;21). *Leukemia & lymphoma* **57**, 199-200, doi:10.3109/10428194.2015.1037754 (2016).

131 Bohring, A., Oudesluijs, G. G., Grange, D. K., Zampino, G. & Thierry, P. New cases of Bohring-Opitz syndrome, update, and critical review of the literature. *American journal of medical genetics. Part A* **140**, 1257-1263, doi:10.1002/ajmg.a.31265 (2006).

132 Hastings, R. *et al.* Bohring-Opitz (Oberklaid-Danks) syndrome: clinical study, review of the literature, and discussion of possible pathogenesis. *European journal of human genetics : EJHG* **19**, 513-519, doi:10.1038/ejhg.2010.234 (2011).

133 Hoischen, A. *et al.* De novo nonsense mutations in ASXL1 cause Bohring-Opitz syndrome. *Nature genetics* **43**, 729-731, doi:10.1038/ng.868 (2011).

134 Magini, P. *et al.* Two novel patients with Bohring-Opitz syndrome caused by de novo ASXL1 mutations. *American journal of medical genetics. Part A* **158A**, 917-921, doi:10.1002/ajmg.a.35265 (2012).

135 Bohring, A. *et al.* Severe end of Opitz trigonocephaly (C) syndrome or new syndrome? *Am J Med Genet* **85**, 438-446, doi:Doi 10.1002/(Sici)1096-8628(19990827)85:5<438::Aid-Ajmg2>3.0.Co;2-A (1999).

136 Pierron, S. *et al.* Evolution of a patient with Bohring-Opitz syndrome. *American journal of medical genetics. Part A* **149A**, 1754-1757, doi:10.1002/ajmg.a.32910 (2009).

137 Russell, B. *et al.* Clinical management of patients with ASXL1 mutations and Bohring-Opitz syndrome, emphasizing the need for Wilms tumor surveillance. *American journal of medical genetics. Part A* **167A**, 2122-2131, doi:10.1002/ajmg.a.37131 (2015).

138 Balasubramanian, M. *et al.* Delineating the phenotypic spectrum of Bainbridge-Ropers syndrome: 12 new patients with de novo, heterozygous, loss-of-function mutations in ASXL3 and review of published literature. *Journal of medical genetics* **54**, 537-543, doi:10.1136/jmedgenet-2016-104360 (2017).

139 Shashi, V. *et al.* De Novo Truncating Variants in ASXL2 Are Associated with a Unique and Recognizable Clinical Phenotype. *American journal of human genetics* **99**, 991-999, doi:10.1016/j.ajhg.2016.08.017 (2016).

140 Bainbridge, M. N. *et al.* De novo truncating mutations in ASXL3 are associated with a novel clinical phenotype with similarities to Bohring-Opitz syndrome. *Genome medicine* **5**, 11, doi:10.1186/gm415 (2013).

141 Hori, I. *et al.* Novel splicing mutation in the ASXL3 gene causing Bainbridge-Ropers syndrome. *American journal of medical genetics. Part A* **170**, 1863-1867, doi:10.1002/ajmg.a.37653 (2016).

142 Koboldt, D. C. *et al.* A de novo nonsense mutation in ASXL3 shared by siblings with Bainbridge-Ropers syndrome. *Cold Spring Harbor molecular case studies*, doi:10.1101/mcs.a002410 (2018).

143 Kuechler, A. *et al.* Bainbridge-Ropers syndrome caused by loss-of-function variants in ASXL3: a recognizable condition. *European journal of human genetics : EJHG* **25**, 183-191, doi:10.1038/ejhg.2016.165 (2017).

144 De Rubeis, S. *et al.* Synaptic, transcriptional and chromatin genes disrupted in autism. *Nature* **515**, 209-215, doi:10.1038/nature13772 (2014).

145 Gans, C. & Northcutt, R. G. Neural crest and the origin of vertebrates: a new head. *Science* **220**, 268-273, doi:10.1126/science.220.4594.268 (1983).

146 Etchevers, H. C., Amiel, J. & Lyonnet, S. Molecular bases of human neurocristopathies. *Advances in experimental medicine and biology* **589**, 213-234, doi:10.1007/978-0-387-46954-6_14 (2006).

147 Groves, A. K. & Bronner-Fraser, M. Neural crest diversification. *Current topics in developmental biology* **43**, 221-258 (1999).

148 Milet, C. & Monsoro-Burq, A. H. Neural crest induction at the neural plate border in vertebrates. *Developmental biology* **366**, 22-33, doi:10.1016/j.ydbio.2012.01.013 (2012).

149 Sauka-Spengler, T. & Bronner-Fraser, M. A gene regulatory network orchestrates neural crest formation. *Nature reviews. Molecular cell biology* **9**, 557-568, doi:10.1038/nrm2428 (2008).

150 Rada-Iglesias, A. *et al.* Epigenomic annotation of enhancers predicts transcriptional regulators of human neural crest. *Cell stem cell* **11**, 633-648, doi:10.1016/j.stem.2012.07.006 (2012).

151 Simoes-Costa, M. & Bronner, M. E. Establishing neural crest identity: a gene regulatory recipe. *Development* **142**, 242-257, doi:10.1242/dev.105445 (2015).

152 Leung, A. W. *et al.* WNT/beta-catenin signaling mediates human neural crest induction via a pre-neural border intermediate. *Development* **143**, 398-410, doi:10.1242/dev.130849 (2016).

153 Noisa, P. *et al.* Notch signaling regulates the differentiation of neural crest from human pluripotent stem cells. *Journal of cell science* **127**, 2083-2094, doi:10.1242/jcs.145755 (2014).

154 Dady, A., Blavet, C. & Duband, J. L. Timing and kinetics of E- to N-cadherin switch during neurulation in the avian embryo. *Developmental dynamics : an official publication of the American Association of Anatomists* **241**, 1333-1349, doi:10.1002/dvdy.23813 (2012).

155 Liu, J. A. *et al.* Phosphorylation of Sox9 is required for neural crest delamination and is regulated downstream of BMP and canonical Wnt signaling. *Proceedings of the National Academy of Sciences of the United States of America* **110**, 2882-2887, doi:10.1073/pnas.1211747110 (2013).

156 Taneyhill, L. A. & Schiffmacher, A. T. Should I stay or should I go? Cadherin function and regulation in the neural crest. *Genesis* **55**, doi:10.1002/dvg.23028 (2017).

157 Prasad, M. S., Sauka-Spengler, T. & LaBonne, C. Induction of the neural crest state: control of stem cell attributes by gene regulatory, post-transcriptional and epigenetic interactions. *Developmental biology* **366**, 10-21, doi:10.1016/j.ydbio.2012.03.014 (2012).

158 Simoes-Costa, M. & Bronner, M. E. Establishing neural crest identity: a gene regulatory recipe. *Development* **142**, 242-257, doi:10.1242/dev.105445 (2015).

159 Strobl-Mazzulla, P. H., Marini, M. & Buzzi, A. Epigenetic landscape and miRNA involvement during neural crest development. *Developmental dynamics : an official publication of the American Association of Anatomists* **241**, 1849-1856, doi:10.1002/dvdy.23868 (2012).

160 Tien, C. L. *et al.* Snail2/Slug cooperates with Polycomb repressive complex 2 (PRC2) to regulate neural crest development. *Development* **142**, 722-731, doi:10.1242/dev.111997 (2015).

161 Theveneau, E. & Mayor, R. Collective cell migration of the cephalic neural crest: the art of integrating information. *Genesis* **49**, 164-176, doi:10.1002/dvg.20700 (2011).

162 Adameyko, I. & Fried, K. The Nervous System Orchestrates and Integrates Craniofacial Development: A Review. *Frontiers in physiology* **7**, 49, doi:10.3389/fphys.2016.00049 (2016).

163 Baggiolini, A. *et al.* Premigratory and migratory neural crest cells are multipotent in vivo. *Cell stem cell* **16**, 314-322, doi:10.1016/j.stem.2015.02.017 (2015).

164 Bronner, M. E. & LeDouarin, N. M. Development and evolution of the neural crest: an overview. *Developmental biology* **366**, 2-9, doi:10.1016/j.ydbio.2011.12.042 (2012).

165 Kelsh, R. N. Sorting out Sox10 functions in neural crest development. *BioEssays : news and reviews in molecular, cellular and developmental biology* **28**, 788-798, doi:10.1002/bies.20445 (2006).

166 Vega-Lopez, G. A., Cerrizuela, S. & Aybar, M. J. Trunk neural crest cells: formation, migration and beyond. *The International journal of developmental biology* **61**, 5-15, doi:10.1387/ijdb.160408gv (2017).

167 Le Douarin, N. M. & Smith, J. Development of the peripheral nervous system from the neural crest. *Annual review of cell biology* **4**, 375-404, doi:10.1146/annurev.cb.04.110188.002111 (1988).

168 Cordero, D. R. *et al.* Cranial neural crest cells on the move: their roles in craniofacial development. *American journal of medical genetics. Part A* **155A**, 270-279, doi:10.1002/ajmg.a.33702 (2011).

169 Gong, S. G. Cranial neural crest: migratory cell behavior and regulatory networks. *Experimental cell research* **325**, 90-95, doi:10.1016/j.yexcr.2014.03.015 (2014).

170 Betancur, P., Bronner-Fraser, M. & Sauka-Spengler, T. Assembling neural crest regulatory circuits into a gene regulatory network. *Annual review of cell and developmental biology* **26**, 581-603, doi:10.1146/annurev.cellbio.042308.113245 (2010).

171 Roybal, P. G. *et al.* Inactivation of Msx1 and Msx2 in neural crest reveals an unexpected role in suppressing heterotopic bone formation in the head. *Developmental biology* **343**, 28-39, doi:10.1016/j.ydbio.2010.04.007 (2010).

172 Wu, T., Chen, G., Tian, F. & Liu, H. X. Contribution of cranial neural crest cells to mouse skull development. *The International journal of developmental biology* **61**, 495-503, doi:10.1387/ijdb.170051gc (2017).

173 Everson, J. L. *et al.* Sonic hedgehog regulation of Foxf2 promotes cranial neural crest mesenchyme proliferation and is disrupted in cleft lip morphogenesis. *Development* **144**, 2082-2091, doi:10.1242/dev.149930 (2017).

174 Blake, K. D. & Prasad, C. CHARGE syndrome. *Orphanet journal of rare diseases* **1**, 34, doi:10.1186/1750-1172-1-34 (2006).

175 Martin, D. M. Chromatin remodeling in development and disease: focus on CHD7. *PLoS genetics* **6**, e1001010, doi:10.1371/journal.pgen.1001010 (2010).

176 Wilson, M. D. & Odom, D. T. Evolution of transcriptional control in mammals. *Current opinion in genetics & development* **19**, 579-585, doi:10.1016/j.gde.2009.10.003 (2009).

177 Lee, G., Chambers, S. M., Tomishima, M. J. & Studer, L. Derivation of neural crest cells from human pluripotent stem cells. *Nature protocols* **5**, 688-701, doi:10.1038/nprot.2010.35 (2010).

178 Menendez, L. *et al.* Directed differentiation of human pluripotent cells to neural crest stem cells. *Nature protocols* **8**, 203-212, doi:10.1038/nprot.2012.156 (2013).

179 Jiang, X. *et al.* Isolation and characterization of neural crest stem cells derived from in vitro-differentiated human embryonic stem cells. *Stem cells and development* **18**, 1059-1070, doi:10.1089/scd.2008.0362 (2009).

180 Pomp, O., Brokhman, I., Ben-Dor, I., Reubinoff, B. & Goldstein, R. S. Generation of peripheral sensory and sympathetic neurons and neural crest cells from human embryonic stem cells. *Stem cells* **23**, 923-930, doi:10.1634/stemcells.2005-0038 (2005).

181 Avery, J. & Dalton, S. Methods for Derivation of Multipotent Neural Crest Cells Derived from Human Pluripotent Stem Cells. *Methods in molecular biology* **1341**, 197-208, doi:10.1007/7651_2015_234 (2016).

182 Chambers, S. M. *et al.* Highly efficient neural conversion of human ES and iPS cells by dual inhibition of SMAD signaling. *Nature biotechnology* **27**, 275-280, doi:10.1038/nbt.1529 (2009).

183 Cimadamore, F. *et al.* Human ESC-derived neural crest model reveals a key role for SOX2 in sensory neurogenesis. *Cell stem cell* **8**, 538-551, doi:10.1016/j.stem.2011.03.011 (2011).

184 Betters, E., Liu, Y., Kjaeldgaard, A., Sundstrom, E. & Garcia-Castro, M. I. Analysis of early human neural crest development. *Developmental biology* **344**, 578-592, doi:10.1016/j.ydbio.2010.05.012 (2010).

185 Chimge, N. O. & Bayarsaihan, D. Generation of neural crest progenitors from human embryonic stem cells. *Journal of experimental zoology. Part B, Molecular and developmental evolution* **314**, 95-103, doi:10.1002/jez.b.21321 (2010).

186 Cooper, J. E. *et al.* In Vivo Transplantation of Enteric Neural Crest Cells into Mouse Gut; Engraftment, Functional Integration and Long-Term Safety. *PloS one* **11**, e0147989, doi:10.1371/journal.pone.0147989 (2016).

187 Liu, J. A. & Cheung, M. Neural crest stem cells and their potential therapeutic applications. *Developmental biology* **419**, 199-216, doi:10.1016/j.ydbio.2016.09.006 (2016).

188 Schlieve, C. R. *et al.* Neural Crest Cell Implantation Restores Enteric Nervous System Function and Alters the Gastrointestinal Transcriptome in Human Tissue-Engineered Small Intestine. *Stem cell reports* **9**, 883-896, doi:10.1016/j.stemcr.2017.07.017 (2017).

189 Aloia, L., Di Stefano, B. & Di Croce, L. Polycomb complexes in stem cells and embryonic development. *Development* **140**, 2525-2534, doi:10.1242/dev.091553 (2013).

190 Gonzalez, F. *et al.* An iCRISPR platform for rapid, multiplexable, and inducible genome editing in human pluripotent stem cells. *Cell stem cell* **15**, 215-226, doi:10.1016/j.stem.2014.05.018 (2014).

191 Kunze, C. *et al.* Synthetic AAV/CRISPR vectors for blocking HIV-1 expression in persistently infected astrocytes. *Glia* **66**, 413-427, doi:10.1002/glia.23254 (2018).

192 Koressaar, T. & Remm, M. Enhancements and modifications of primer design program Primer3. *Bioinformatics* **23**, 1289-1291, doi:10.1093/bioinformatics/btm091 (2007).

193 Ludwig, T. E. *et al.* Feeder-independent culture of human embryonic stem cells. *Nat Methods* **3**, 637-646, doi:10.1038/nmeth902 (2006).

194 Ran, F. A. *et al.* Genome engineering using the CRISPR-Cas9 system. *Nature protocols* **8**, 2281-2308, doi:10.1038/nprot.2013.143 (2013).

195 Afgan, E. *et al.* The Galaxy platform for accessible, reproducible and collaborative biomedical analyses: 2016 update. *Nucleic acids research* **44**, W3-W10, doi:10.1093/nar/gkw343 (2016).

196 Liao, Y., Smyth, G. K. & Shi, W. featureCounts: an efficient general purpose program for assigning sequence reads to genomic features. *Bioinformatics* **30**, 923-930, doi:10.1093/bioinformatics/btt656 (2014).

197 Love, M. I., Huber, W. & Anders, S. Moderated estimation of fold change and dispersion for RNA-seq data with DESeq2. *Genome biology* **15**, 550, doi:10.1186/s13059-014-0550-8 (2014).

198 Feederle, R. *et al.* Generation of Pax1/PAX1-Specific Monoclonal Antibodies. *Monoclonal antibodies in immunodiagnosis and immunotherapy*, doi:10.1089/mab.2016.0029 (2016).

199 Krendl, C. *et al.* GATA2/3-TFAP2A/C transcription factor network couples human pluripotent stem cell differentiation to trophectoderm with repression of pluripotency. *Proceedings of the National Academy of Sciences of the United States of America* **114**, E9579-E9588, doi:10.1073/pnas.1708341114 (2017).

200 Consortium, E. P. An integrated encyclopedia of DNA elements in the human genome. *Nature* **489**, 57-74, doi:10.1038/nature11247 (2012).

201 Hamburger, V. & Hamilton, H. L. A series of normal stages in the development of the chick embryo. 1951. *Developmental dynamics : an official publication of the American Association of Anatomists* **195**, 231-272, doi:10.1002/aja.1001950404 (1992).

202 Schindelin, J. *et al.* Fiji: an open-source platform for biological-image analysis. *Nat Methods* **9**, 676-682, doi:10.1038/nmeth.2019 (2012).

203 Markel, P. *et al.* Theoretical and empirical issues for marker-assisted breeding of congenic mouse strains. *Nature genetics* **17**, 280-284, doi:10.1038/ng1197-280 (1997).

204 Kimmel, C. B., Ballard, W. W., Kimmel, S. R., Ullmann, B. & Schilling, T. F. Stages of embryonic development of the zebrafish. *Developmental dynamics : an official publication of the American Association of Anatomists* **203**, 253-310, doi:10.1002/aja.1002030302 (1995).

205 McCurley, A. T. & Callard, G. V. Characterization of housekeeping genes in zebrafish: male-female differences and effects of tissue type, developmental stage and chemical treatment. *BMC molecular biology* **9**, 102, doi:10.1186/1471-2199-9-102 (2008).

206 Thisse, B. & Thisse, C. In situ hybridization on whole-mount zebrafish embryos and young larvae. *Methods in molecular biology* **1211**, 53-67, doi:10.1007/978-1-4939-1459-3_5 (2014).

207 Hruscha, A. *et al.* Efficient CRISPR/Cas9 genome editing with low off-target effects in zebrafish. *Development* **140**, 4982-4987, doi:10.1242/dev.099085 (2013).

208 Hwang, W. Y. *et al.* Efficient genome editing in zebrafish using a CRISPR-Cas system. *Nature biotechnology* **31**, 227-229, doi:10.1038/nbt.2501 (2013).

209 The UniProt, C. UniProt: the universal protein knowledgebase. *Nucleic acids research* **45**, D158-D169, doi:10.1093/nar/gkw1099 (2017).

210 Zhang, P. B. *et al.* Short-term BMP-4 treatment initiates mesoderm induction in human embryonic stem cells. *Blood* **111**, 1933-1941, doi:10.1182/blood-2007-02-074120 (2008).

211 Janesick, A., Wu, S. C. & Blumberg, B. Retinoic acid signaling and neuronal differentiation. *Cellular and molecular life sciences : CMLS* **72**, 1559-1576, doi:10.1007/s00018-014-1815-9 (2015).

212 D'Amour, K. A. *et al.* Efficient differentiation of human embryonic stem cells to definitive endoderm. *Nature biotechnology* **23**, 1534-1541, doi:10.1038/nbt1163 (2005).

213 Wu, J. Q. *et al.* Dynamic transcriptomes during neural differentiation of human embryonic stem cells revealed by short, long, and paired-end sequencing. *Proceedings of the National Academy of Sciences of the United States of America* **107**, 5254-5259, doi:10.1073/pnas.0914114107 (2010).

214 Francis, F. *et al.* Doublecortin is a developmentally regulated, microtubule-associated protein expressed in migrating and differentiating neurons. *Neuron* **23**, 247-256 (1999).

215 Lin, H. H. *et al.* Neuronatin promotes neural lineage in ESCs via Ca(2+) signaling. *Stem cells* **28**, 1950-1960, doi:10.1002/stem.530 (2010).

216 Belo, J. A. *et al.* Cerberus-like is a secreted BMP and nodal antagonist not essential for mouse development. *Genesis* **26**, 265-270 (2000).

217 Levine, A. J., Levine, Z. J. & Brivanlou, A. H. GDF3 is a BMP inhibitor that can activate Nodal signaling only at very high doses. *Developmental biology* **325**, 43-48, doi:10.1016/j.ydbio.2008.09.006 (2009).

218 Pauklin, S. & Vallier, L. Activin/Nodal signalling in stem cells. *Development* **142**, 607-619, doi:10.1242/dev.091769 (2015).

219 Boncinelli, E., Simeone, A., Acampora, D. & Mavilio, F. HOX gene activation by retinoic acid. *Trends in genetics : TIG* **7**, 329-334 (1991).

220 Kashyap, V. *et al.* Epigenomic reorganization of the clustered Hox genes in embryonic stem cells induced by retinoic acid. *The Journal of biological chemistry* **286**, 3250-3260, doi:10.1074/jbc.M110.157545 (2011).

221 Langston, A. W. & Gudas, L. J. Retinoic acid and homeobox gene regulation. *Current opinion in genetics & development* **4**, 550-555 (1994).

222 Kempf, H. *et al.* Bulk cell density and Wnt/TGFbeta signalling regulate mesendodermal patterning of human pluripotent stem cells. *Nature communications* **7**, 13602, doi:10.1038/ncomms13602 (2016).

223 Aoki, Y. *et al.* Sox10 regulates the development of neural crest-derived melanocytes in Xenopus. *Developmental biology* **259**, 19-33, doi:10.1016/S0012-1606(03)00161-1 (2003).

224 Lee, G. *et al.* Isolation and directed differentiation of neural crest stem cells derived from human embryonic stem cells. *Nature biotechnology* **25**, 1468-1475, doi:10.1038/nbt1365 (2007).

225 Ramos, T. L. *et al.* MSC surface markers (CD44, CD73, and CD90) can identify human MSC-derived extracellular vesicles by conventional flow cytometry. *Cell Commun Signal* **14**, doi:10.1186/s12964-015-0124-8 (2016).

226 Kraus, N. A. *et al.* Quantitative assessment of adipocyte differentiation in cell culture. *Adipocyte* **5**, 351-358, doi:10.1080/21623945.2016.1240137 (2016).

227 Theveneau, E., Duband, J. L. & Altabef, M. Ets-1 Confers Cranial Features on Neural Crest Delamination. *PloS one* **2**, doi:ARTN e1142 10.1371/journal.pone.0001142 (2007).

228 Streit, A., Christophorou, N. & Lleras, L. Molecular networks controlling the specification of sensory organ progenitors. *Developmental biology* **319**, 535-535, doi:10.1016/j.ydbio.2008.05.248 (2008).

229 Fedtsova, N. G. & Turner, E. E. Brn-3.0 expression identifies early post-mitotic CNS neurons and sensory neural precursors. *Mechanisms of development* **53**, 291-304 (1995).

230 Tahtakran, S. A. & Selleck, M. A. J. Ets-1 expression is associated with cranial neural crest migration and vasculogenesis in the chick embryo. *Gene Expr Patterns* **3**, 455-458, doi:10.1016/S1567-133X(03)00065-6 (2003).

231 Deardorff, M. A., Tan, C., Saint-Jeannet, J. P. & Klein, P. S. A role for frizzled 3 in neural crest development. *Development* **128**, 3655-3663 (2001).

232 Dorsky, R. I., Moon, R. T. & Raible, D. W. Control of neural crest cell fate by the Wnt signalling pathway. *Nature* **396**, 370-373, doi:Doi 10.1038/24620 (1998).

233 Lewis, J. L. *et al.* Reiterated Wnt signaling during zebrafish neural crest development. *Development* **131**, 1299-1308, doi:10.1242/dev.01007 (2004).

234 Hackland, J. O. S. *et al.* Top-Down Inhibition of BMP Signaling Enables Robust Induction of hPSCs Into Neural Crest in Fully Defined, Xeno-free Conditions. *Stem cell reports* **9**, 1043-1052, doi:10.1016/j.stemcr.2017.08.008 (2017).

235 Skarnes, W. C. *et al.* A conditional knockout resource for the genome-wide study of mouse gene function. *Nature* **474**, 337-U361, doi:10.1038/nature10163 (2011).

236 Eisen, J. S. & Weston, J. A. Development of the neural crest in the zebrafish. *Developmental biology* **159**, 50-59, doi:10.1006/dbio.1993.1220 (1993).

237 Braasch, I. *et al.* The spotted gar genome illuminates vertebrate evolution and facilitates human-teleost comparisons. *Nature genetics* **48**, 427-437, doi:10.1038/ng.3526 (2016).

238 Zerbino, D. R. *et al.* Ensembl 2018. *Nucleic acids research* **46**, D754-D761, doi:10.1093/nar/gkx1098 (2018).

239 Glasauer, S. M. & Neuhauss, S. C. Whole-genome duplication in teleost fishes and its evolutionary consequences. *Molecular genetics and genomics : MGG* **289**, 1045-1060, doi:10.1007/s00438-014-0889-2 (2014).

240 Tsetskhladze, Z. R. *et al.* Functional assessment of human coding mutations affecting skin pigmentation using zebrafish. *PloS one* **7**, e47398, doi:10.1371/journal.pone.0047398 (2012).

241 Ruthenburg, A. J., Li, H., Patel, D. J. & Allis, C. D. Multivalent engagement of chromatin modifications by linked binding modules. *Nat Rev Mol Cell Bio* **8**, 983-994, doi:10.1038/nrm2298 (2007).

242 Lee, S. W. *et al.* ASXL1 represses retinoic acid receptor-mediated transcription through associating with HP1 and LSD1. *The Journal of biological chemistry* **285**, 18-29, doi:10.1074/jbc.M109.065862 (2010).

243 Park, U. H. *et al.* Reciprocal regulation of LXRalpha activity by ASXL1 and ASXL2 in lipogenesis. *Biochemical and biophysical research communications* **443**, 489-494, doi:10.1016/j.bbrc.2013.11.124 (2014).

244 Chen, Y. T., Liu, P. & Bradley, A. Inducible gene trapping with drug-selectable markers and Cre/loxP to identify developmentally regulated genes. *Molecular and cellular biology* **24**, 9930-9941, doi:10.1128/MCB.24.22.9930-9941.2004 (2004).

245 Pratcorona, M. *et al.* Acquired mutations in ASXL1 in acute myeloid leukemia: prevalence and prognostic value. *Haematologica* **97**, 388-392, doi:10.3324/haematol.2011.051532 (2012).

246 Wang, Y. X., Bi, Y. & Gao, S. R. Epigenetic regulation of somatic cell reprogramming. *Current opinion in genetics & development* **46**, 156-163, doi:10.1016/j.gde.2017.07.002 (2017).

247 Woodard, C. M. *et al.* iPSC-Derived Dopamine Neurons Reveal Differences between Monozygotic Twins Discordant for Parkinson's Disease. *Cell reports* **9**, 1173-1182, doi:10.1016/j.celrep.2014.10.023 (2014).

248 Martinez, R. A. *et al.* Genome engineering of isogenic human ES cells to model autism disorders. *Nucleic acids research* **43**, doi:Artn E65 10.1093/Nar/Gkv164 (2015).

249 Suzuki, K. *et al.* Targeted Gene Correction Minimally Impacts Whole-Genome Mutational Load in Human-Disease-Specific Induced Pluripotent Stem Cell Clones. *Cell stem cell* **15**, 31-36, doi:10.1016/j.stem.2014.06.016 (2014).

250 Veres, A. *et al.* Low Incidence of Off-Target Mutations in Individual CRISPR-Cas9 and TALEN Targeted Human Stem Cell Clones Detected by Whole-Genome Sequencing (vol 15, pg 27, 2014). *Cell stem cell* **15**, 254-254, doi:10.1016/j.stem.2014.07.009 (2014).

251 Micol, J. B. *et al.* Frequent ASXL2 mutations in acute myeloid leukemia patients with t(8;21)/RUNX1-RUNX1T1 chromosomal translocations. *Blood* **124**, 1445-1449, doi:10.1182/blood-2014-04-571018 (2014).

252 Dinan, A. M., Atkins, J. F. & Firth, A. E. ASXL gain-of-function truncation mutants: defective and dysregulated forms of a natural ribosomal frameshifting product? *Biol Direct* **12**, doi:Artn 24 10.1186/S13062-017-0195-0 (2017).

253 Cho, Y. S., Kim, E. J., Park, U. H., Sin, H. S. & Um, S. J. Additional sex comb-like 1 (ASXL1), in cooperation with SRC-1, acts as a ligand-dependent coactivator for retinoic acid receptor. *Journal of Biological Chemistry* **281**, 17588-17598, doi:10.1074/jbc.M512616200 (2006).

254 Youn, H. S. *et al.* Asxl1 deficiency in embryonic fibroblasts leads to cellular senescence via impairment of the AKT-E2F pathway and Ezh2 inactivation. *Scientific reports* **7**, doi:Artn 5198 10.1038/S41598-017-05564-X (2017).

255 Miller, J. N. & Pearce, D. A. Nonsense-mediated decay in genetic disease: Friend or foe? *Mutat Res-Rev Mutat* **762**, 52-64, doi:10.1016/j.mrrev.2014.05.001 (2014).

256 Baker, L. A., Allis, C. D. & Wang, G. G. PHD fingers in human diseases: Disorders arising from misinterpreting epigenetic marks. *Mutat Res-Fund Mol M* **647**, 3-12, doi:10.1016/j.mrfmmm.2008.07.004 (2008).

257 Ragvin, A. *et al.* Nucleosome binding by the bromodomain and PHD finger of the transcriptional cofactor p300. *Journal of molecular biology* **337**, 773-788, doi:10.1016/j.jmb.2004.01.051 (2004).

258 Mansfield, R. E. *et al.* Plant Homeodomain (PHD) Fingers of CHD4 Are Histone H3-binding Modules with Preference for Unmodified H3K4 and Methylated H3K9. *Journal of Biological Chemistry* **286**, 11779-11791, doi:10.1074/jbc.M110.208207 (2011).

259 Hsu, Y. C. *et al.* The distinct biological implications of Asxl1 mutation and its roles in leukemogenesis revealed by a knock-in mouse model. *Journal of hematology & oncology* **10**, doi:Artn 139 10.1186/S13045-017-0508-X (2017).

260 Youn, H. S. *et al.* Asxl1 deficiency in embryonic fibroblasts leads to cellular senescence via impairment of the AKT-E2F pathway and Ezh2 inactivation. *Scientific reports* **7**, 5198, doi:10.1038/s41598-017-05564-x (2017).

261 Levine, A. J. & Brivanlou, A. H. GDF3, a BMP inhibitor, regulates cell fate in stem cells and early embryos. *Development* **133**, 209-216, doi:10.1242/dev.02192 (2006).

262 Aykul, S. & Martinez-Hackert, E. New Ligand Binding Function of Human Cerberus and Role of Proteolytic Processing in Regulating Ligand-Receptor Interactions and Antagonist Activity. *Journal of molecular biology* **428**, 590-602, doi:10.1016/j.jmb.2016.01.011 (2016).

263 Vallier, L., Alexander, M. & Pedersen, R. A. Activin/Nodal and FGF pathways cooperate to maintain pluripotency of human embryonic stem cells. *Journal of cell science* **118**, 4495-4509, doi:10.1242/jcs.02553 (2005).

264 Xu, R. H. *et al.* NANOG is a direct target of TGFbeta/activin-mediated SMAD signaling in human ESCs. *Cell stem cell* **3**, 196-206, doi:10.1016/j.stem.2008.07.001 (2008).

265 Iwashita, H. *et al.* Secreted Cerberus1 as a Marker for Quantification of Definitive Endoderm Differentiation of the Pluripotent Stem Cells. *PloS one* **8**, doi:ARTN e64291 10.1371/journal.pone.0064291 (2013).

266 Brennan, J. *et al.* Nodal signalling in the epiblast patterns the early mouse embryo. *Nature* **411**, 965-969, doi:Doi 10.1038/35082103 (2001).

267 Teo, A. K. K. *et al.* Pluripotency factors regulate definitive endoderm specification through eomesodermin. *Genes & development* **25**, 238-250, doi:10.1101/gad.607311 (2011).

268 Wang, P., Rodriguez, R. T., Wang, J., Ghodasara, A. & Kim, S. K. Targeting SOX17 in human embryonic stem cells creates unique strategies for isolating and analyzing developing endoderm. *Cell stem cell* **8**, 335-346, doi:10.1016/j.stem.2011.01.017 (2011).

269 Wrighton, K. H., Lin, X. & Feng, X. H. Phospho-control of TGF-beta superfamily signaling. *Cell research* **19**, 8-20, doi:10.1038/cr.2008.327 (2009).

270 Joseph, R. M. Neuronatin gene: Imprinted and misfolded Studies in Lafora disease, diabetes and cancer may implicate NNAT-aggregates as a common downstream participant in neuronal loss. *Genomics* **103**, 183-188, doi:10.1016/j.ygeno.2013.12.001 (2014).

271 Elkabetz, Y. *et al.* Human ES cell-derived neural rosettes reveal a functionally distinct early neural stem cell stage (vol 22, pg 152, 2008). *Genes & development* **22**, 1257-1257 (2008).

272 Kerosuo, L., Nie, S. Y., Bajpai, R. & Bronner, M. E. Crestospheres: Long-Term Maintenance of Multipotent, Premigratory Neural Crest Stem Cells. *Stem cell reports* **5**, 499-507, doi:10.1016/j.stemcr.2015.08.017 (2015).

273 Huang, M. *et al.* Generating trunk neural crest from human pluripotent stem cells. *Scientific reports* **6**, 19727, doi:10.1038/srep19727 (2016).

274 Dincer, Z. *et al.* Specification of Functional Cranial Placode Derivatives from Human Pluripotent Stem Cells. *Cell reports* **5**, 1387-1402, doi:10.1016/j.celrep.2013.10.048 (2013).

275 Merzdorf, C. S. Emerging roles for zic genes in early development. *Developmental dynamics : an official publication of the American Association of Anatomists* **236**, 922-940, doi:10.1002/dvdy.21098 (2007).

276 Sato, T., Sasai, N. & Sasai, Y. Neural crest determination by co-activation of Pax3 and Zic1 genes in Xenopus ectoderm. *Development* **132**, 2355-2363, doi:10.1242/dev.01823 (2005).

277 Grinberg, I. & Millen, K. J. The ZIC gene family in development and disease. *Clinical genetics* **67**, 290-296, doi:10.1111/j.1399-0004.2005.00418.x (2005).

278 Merzdorf, C. S. & Sive, H. L. The zic1 gene is an activator of Wnt signaling. *International Journal of Developmental Biology* **50**, 611-617, doi:10.1387/ijdb.052110cm (2006).

279 Li, B., Kuriyama, S., Moreno, M. & Mayor, R. The posteriorizing gene Gbx2 is a direct target of Wnt signalling and the earliest factor in neural crest induction. *Development* **136**, 3267-3278, doi:10.1242/dev.036954 (2009).

280 Aruga, J. The role of Zic genes in neural development. *Molecular and Cellular Neuroscience* **26**, 205-221, doi:10.1016/j.mcn.2004.01.004 (2004).

281 Marchal, L., Luxardi, G., Thome, V. & Kodjabachian, L. BMP inhibition initiates neural induction via FGF signaling and Zic genes. *Proceedings of the National Academy of Sciences of the United States of America* **106**, 17437-17442, doi:10.1073/pnas.0906352106 (2009).

282 Blank, M. C. *et al.* Multiple developmental programs are altered by loss of Zic1 and Zic4 to cause Dandy-Walker malformation cerebellar pathogenesis. *Development* **138**, 1207-1216, doi:10.1242/dev.054114 (2011).

283 Urban, S. *et al.* A Brn2-Zic1 axis specifies the neuronal fate of retinoic-acid-treated embryonic stem cells. *Journal of cell science* **128**, 2303-2318, doi:10.1242/jcs.168849 (2015).

284 Twigg, S. R. F. *et al.* Gain-of-Function Mutations in ZIC1 Are Associated with Coronal Craniosynostosis and Learning Disability. *American journal of human genetics* **97**, 378-388, doi:10.1016/j.ajhg.2015.07.007 (2015).

285 Grinberg, I. *et al.* Heterozygous deletion of the linked genes ZIC1 and ZIC4 is involved in Dandy-Walker malformation. *Nature genetics* **36**, 1053-1055, doi:10.1038/ng1420 (2004).

286 Smith, J. R. *et al.* Inhibition of Activin/Nodal signaling promotes specification of human embryonic stem cells into neuroectoderm. *Developmental biology* **313**, 107-117, doi:10.1016/j.ydbio.2007.10.003 (2008).

287 Hatakeyama, J. *et al.* Hes genes regulate size, shape and histogenesis of the nervous system by control of the timing of neural stem cell differentiation. *Development* **131**, 5539-5550, doi:10.1242/dev.01436 (2004).

288 Memic, F. *et al.* Ascl1 Is Required for the Development of Specific Neuronal Subtypes in the Enteric Nervous System. *The Journal of neuroscience : the official journal of the Society for Neuroscience* **36**, 4339-4350, doi:10.1523/JNEUROSCI.0202-16.2016 (2016).

289 Vernes, S. C. *et al.* High-throughput analysis of promoter occupancy reveals direct neural targets of FOXP2, a gene mutated in speech and language disorders. *American journal of human genetics* **81**, 1232-1250, doi:10.1086/522238 (2007).

290 Devanna, P., Middelbeek, J. & Vernes, S. C. FOXP2 drives neuronal differentiation by interacting with retinoic acid signaling pathways. *Frontiers in cellular neuroscience* **8**, 305, doi:10.3389/fncel.2014.00305 (2014).

291 Rousso, D. L. *et al.* Foxp-mediated suppression of N-cadherin regulates neuroepithelial character and progenitor maintenance in the CNS. *Neuron* **74**, 314-330, doi:10.1016/j.neuron.2012.02.024 (2012).

292 Enard, W. *et al.* Molecular evolution of FOXP2, a gene involved in speech and language. *Nature* **418**, 869-872, doi:10.1038/nature01025 (2002).

293 Zhang, X. Q. *et al.* Pax6 Is a Human Neuroectoderm Cell Fate Determinant. *Cell stem cell* **7**, 90-100, doi:10.1016/j.stem.2010.04.017 (2010).

294 Vastenhouw, N. L. & Schier, A. F. Bivalent histone modifications in early embryogenesis. *Current opinion in cell biology* **24**, 374-386, doi:10.1016/j.ceb.2012.03.009 (2012).

295 Creppe, C., Palau, A., Malinverni, R., Valero, V. & Buschbeck, M. A Cbx8-containing polycomb complex facilitates the transition to gene activation during ES cell differentiation. *PLoS genetics* **10**, e1004851, doi:10.1371/journal.pgen.1004851 (2014).

296 Eskeland, R. *et al.* Ring1B compacts chromatin structure and represses gene expression independent of histone ubiquitination. *Molecular cell* **38**, 452-464, doi:10.1016/j.molcel.2010.02.032 (2010).

297 Nordstrand, L. M. *et al.* Mice lacking Alkbh1 display sex-ratio distortion and unilateral eye defects. *PloS one* **5**, e13827, doi:10.1371/journal.pone.0013827 (2010).

298 Uchimura, T., Komatsu, Y., Tanaka, M., McCann, K. L. & Mishina, Y. Bmp2 and Bmp4 genetically interact to support multiple aspects of mouse development including functional heart development. *Genesis* **47**, 374-384, doi:10.1002/dvg.20511 (2009).

299 Klymkowsky, M. W., Rossi, C. C. & Artinger, K. B. Mechanisms driving neural crest induction and migration in the zebrafish and Xenopus laevis. *Cell Adhes Migr* **4**, 595-608, doi:10.4161/cam.4.4.12962 (2010).

300 Schulte-Merker, S., van Eeden, F. J., Halpern, M. E., Kimmel, C. B. & Nusslein-Volhard, C. no tail (ntl) is the zebrafish homologue of the mouse T (Brachyury) gene. *Development* **120**, 1009-1015 (1994).

301 Xie, Y., Chen, X. & Wagner, T. E. A ribozyme-mediated, gene "knockdown" strategy for the identification of gene function in zebrafish. *Proceedings of the National Academy of Sciences of the United States of America* **94**, 13777-13781 (1997).

302 Place, E. S. & Smith, J. C. Zebrafish atoh8 mutants do not recapitulate morpholino phenotypes (vol 12, e0171143, 2017). *PloS one* **12**, doi:ARTN e0175608 10.1371/journal.pone.0175608 (2017).

303 Maurus, D. & Harris, W. A. Zic-associated holoprosencephaly: Zebrafish Zic1 controls midline formation and forebrain patterning by regulating Nodal, Hedgehog and retinoic acid signalling. *Mechanisms of development* **126**, S201-S201, doi:10.1016/j.mod.2009.06.495 (2009).

304 Tohyama, J. *et al.* Dandy-Walker Malformation Associated With Heterozygous ZIC1 and ZIC4 Deletion: Report of a New Patient. *American Journal of Medical Genetics Part A* **155A**, 130-133, doi:10.1002/ajmg.a.33652 (2011).

305 Fearon, J. A., Kolar, J. C. & Munro, I. R. Trigonocephaly-associated hypotelorism: is treatment necessary? *Plastic and reconstructive surgery* **97**, 503-509; discussion 510-511 (1996).

306 Minoux, M. & Rijli, F. M. Molecular mechanisms of cranial neural crest cell migration and patterning in craniofacial development. *Development* **137**, 2605-2621, doi:10.1242/dev.040048 (2010).

307 Zhang, H. *et al.* Heterodimerization of Msx and Dlx homeoproteins results in functional antagonism. *Molecular and cellular biology* **17**, 2920-2932 (1997).

308 Qiu, M. *et al.* Role of the Dlx homeobox genes in proximodistal patterning of the branchial arches: mutations of Dlx-1, Dlx-2, and Dlx-1 and -2 alter morphogenesis of proximal skeletal and soft tissue structures derived from the first and second arches. *Developmental biology* **185**, 165-184, doi:10.1006/dbio.1997.8556 (1997).

309 Etchevers, H. C., Vincent, C., Le Douarin, N. M. & Couly, G. F. The cephalic neural crest provides pericytes and smooth muscle cells to all blood vessels of the face and forebrain. *Development* **128**, 1059-1068 (2001).

310 Vallet, A. E. *et al.* Neurological features in adult Triple-A (Allgrove) syndrome. *Journal of neurology* **259**, 39-46, doi:10.1007/s00415-011-6115-9 (2012).

311 Tucker, A. S. *et al.* Conserved regulation of mesenchymal gene expression by Fgf-8 in face and limb development. *Development* **126**, 221-228 (1999).

312 Latta, E. J. & Golding, J. P. Regulation of PP2A activity by Mid1 controls cranial neural crest speed and gangliogenesis. *Mechanisms of development* **128**, 560-576, doi:10.1016/j.mod.2012.01.002 (2012).

313 Keyte, A. & Hutson, M. R. The neural crest in cardiac congenital anomalies. *Differentiation; research in biological diversity* **84**, 25-40, doi:10.1016/j.diff.2012.04.005 (2012).

314 Kim, J. H., Lee, J. H., Lee, I. S., Lee, S. B. & Cho, K. S. Histone Lysine Methylation and Neurodevelopmental Disorders. *International journal of molecular sciences* **18**, doi:10.3390/ijms18071404 (2017).

315 Greene, N. D., Stanier, P. & Moore, G. E. The emerging role of epigenetic mechanisms in the etiology of neural tube defects. *Epigenetics* **6**, 875-883 (2011).

316 Beunders, G. *et al.* Exonic deletions in AUTS2 cause a syndromic form of intellectual disability and suggest a critical role for the C terminus. *American journal of human genetics* **92**, 210-220, doi:10.1016/j.ajhg.2012.12.011 (2013).

6. Appendix

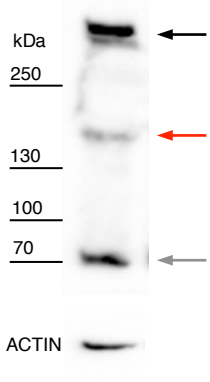

Supplementary Figure S1. Detection of ASXL1 in control hESC via Western Blot using monoclonal antibody clone 4F6. Note putative ASXL1/2 band at approximately 170 kDa (red arrow), and additional bands above 300 kDa (black arrow) and at 70 kDa (grey arrow).

A

ACCCCGGCATGGCTTGGAGACAGCGTTGGtGT
GTATGAAGGATCTTCCTCCAATGAAGGATTTGG
GACAACTTTCCATGATGATTATATTAGAGCCTC
AGCTGCTTTCGTGTTGGTCATGAGGTGATG
CTGAACCGAATGCTTGAACTAGCAGGAGTG
GCTGGGATTGCATTGGAGTGGTTCCGTTCA
TTCCTTCCGG**AAA**

B

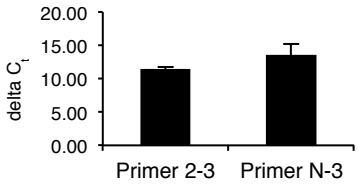

Supplementary Figure S2. Detection of the alternatively spliced 'NMD'-exon[1] between annotated exons 2 and 3 of human *ASXL3*.
(A) Sequence of 'NMD' exon based on sanger sequencing of the *ASXL3* transcript isolated from hESC treated with 10 µM RA. Red underlined base triplets indicate premature STOP codons, **bold letters** denote additional base pairs within the transcript that were presumably spliced from within the subsequent intron. **(B)** Detection of 'NMD-exon' by specific primer pair 'Primer N-3', in comparison to 'Primer 2-3' pair, which spans all transcripts, including and excluding the additional exon. Samples from hESC treated with 10 µM RA (*n*=2).

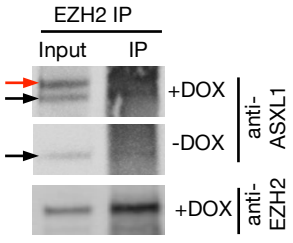

Supplementary Figure S3. Preliminary ASXL1^{PSC}-EZH2 co-immunoprecipitation results.
Western Blot of immunoprecipitated (IP) EZH2 in nuclear extract samples from PB-*ASXL1*^{PSC} neurospheres (day 3) that were left untreated (-DOX) or treated (+DOX) to express truncated ASXL1 (red arrow). Antibodies towards ASXL1 and EZH2, respectively, were used for blotting as indicated on the side; FT, flow-through supernatant after IP. Black arrows denote a putative ASXL isoform at approximately 70 kDa.

List of abbreviations

a.a.	amino acids
ac	acetylation
ASX(L)	Additional sex combs (-like)
BAP1	BRCA1-associated protein-1
BMP	Bone Morphogenic Protein
BOS	Bohring-Opitz syndrome
bp	base pair
BRS	Bainbridge-Ropers syndrome
Cas9	Caspase 9
cat. #	catalog number
cDNA	Complementary DNA
ChIP	Chromatin Immunocprecipitation
ChIP-qPCR	Chromatin Immunocprecipitation paired with quantitative real-time PCR
COMPASS	Complex proteins Associated with Set 1
CpG	Cytosine-phosphate-Guanine
CRISPR/Cas	Clustered Regularly Interspaced Short Palindromic Repeats/CRISPR associated
Ct	Cycle threshold
DAPI	4’,6-Diamidino-2-Phenylindole
DMEM	Dulbecco's Modified Eagle's Medium
DMSO	Dimethyl Sulfoxide
Dox	Doxycycline
DTT	Dithiothreitol
EDTA	Ethylenediaminetetraacetic Acid
eGFP	enhanced Green Fluorescent Protein
EGTA	Ethylene Glycol-bis(β-aminoethyl ether)-N,N,N',N'-Tetraacetic Acid
elfa	elongation factor 1 alpha
EMT	Epithelial-to-mesenchymal transition
ENCODE	Encyclopedia of DNA Elements
FACS	Fluorescence-Activated Cell Sorting
FBS	Fetal Bovine Serum
FGF2	Fibroblast Growth Factor 2 (basic FGF, bFGF)
GAPDH	Glyceraldehyde 3-phosphate dehydrogenase
GO-term	Gene Ontology term
GRN	gene regulatory network
gRNA	Guide RNA
H2AK119	Histone 2 Lysine 119
H3K4/9/27	Histone 3 Lysine 4/9/27
HAT	Histone Acetyl Transferase
HDAC	Histone Deacethylase
hESC	human Embryonic Stem Cells
hiPSC	human induced pluripoten stem cell
HP1	Heterochromatin Protein 1 (CBX5)
HRP	horseradish peroxidase
iCas9 hESC	HUES9 hESC harboring the inducible Caspase 9 endonuclease
IgG	Immunoglobulin G
IP	Immunoprecipitation
kb	kilo bases
KSR	Knockout Serum Replacement
LSD1	Lysine-specific histone demethylase 1a (KDM1A)
me1	Mono-Methylation
me2	Di-Methylation
me3	Tri-Methylaion
MLL	Mixed Lineage Leukemia
mRNA	messenger RNA

NC	Neural crest
NCOA1	Nuclear Receptor Co-Activator 1
NDS	neurodevelopmental syndrome
NEAA	Non Essential Amino Acids
NEB	New England Biolabs
NPB	neural plate border
NR	Nuclear Receptor
PBS	Phosphate-buffered saline
PBS-T	Phosphate- buffered saline containing Tween-20
PCA	Principal Component Analysis
PcG	Polycomb group
PCGF	Polycomb group ring finger
PHD	Plant Homeodomain
PMSF	Phenylmethane Sulfonyl Fluoride
PPARγ	peroxisome proliferater-activated receptor γ
PRC1/2	Polycomb repressive complex ½
PSC	premature STOP codon
qPCR	quantitative real-time PCR
RA	Retinoic Acid
RAR/RXR	Retinoic Acid Receptor/Retinoic X Receptor
RefSeq	Reference Sequence
RING1	ring finger protein 1
RIPA buffer	radioimmunoprecipiation assay buffer
RNA-Seq	RNA Sequencing
ROCKi	Rho- associated, Coiled-Coil Containing Protein Kinase Inhibitor
rpm	Revolutions Per Minute
RT	Room Temperature
RT-PCR	Reverse Transcription PCR
SDS	Sodium Dodecyl Sulfate
SHH	Sonic hedghehog
SWI/SNF	Switch/Sucrose non-fermentable
TBS-T	Tris-Buffered Saline with Tween-20
TE buffer	Tris-EDTA Buffer
TF	Transcription Factor
TGFβ	transforming growth factor β
tRNA	Transfer RNA
TrxG	Trithorax Group
TSS	Transcription Start Side
ub	ubiquitination
wt	Wild Type
ZIC1	Zic family member 1

List of figures

List of tables

Acknowledgements

This work was carried out from November 2012 to November 2017 at the Institute for Stem Cell Research of the Helmholtz Center Munich, Neuherberg, under supervision of Dr. Micha Drukker and Prof. Dr. Magdalena Götz.

I wish to sincerely thank my supervisor and group leader, Dr. Micha Drukker, for providing so many ideas and the freedom, great support and guidance I needed to choose and pursue this project. All the members of the Drukker lab, past and present, were very supportive and helpful and created a great working atmosphere, making long hours in the lab much more fun. I wish to thank all of them, and in particular Ejona Rusha and Dr. Anna Pertek, who provided a lot of support during the project. I am furthermore thankful to Dr. Dmitri Shaposhnikov, Valenytna Rishko, Lena Molitor, Dr. Christian Krendl, Orla Deevy, Polyxeni Nteli, Jean-Christophe LaChance, Jennifer Sales and Shiavash Khoshravi for their contributions to this work, and to Karen Biniossek and Nina Fuchs for help in all organizational matters.
I would like to very much thank my TAC committee members and supervisors Prof. Dr. Magdalena Götz and Dr. Ralph Rupp for their great support and advice.
Many thanks also go to all the people who helped me in collaborations: Prof. Dr. Maria Luisa Giovannucci Uzielli, Dr. Pamela Magini, Dr. Matteo de la Monica and Dr. Gioacchino Scarano in Italy, who enabled the generation of BOS-iPSC, Dr. Rizwan Rehimi and Dr. Alvaro Rada-Iglesias at the CMMC in Cologne for their help with a fantastic developmental system, and scientists at the Helmholtz Center Munich: Dr. Elisabeth Kremmer, Dr. Regina Feederle, Andrew Flatley and Dr. Arie Geerlof for providing antibodies, the animal caretakers at the zebrafish and mouse facilities, Dr. Hernan López-Schier, Oriol Viader-Llargues, Laura Pola, Dr. Prisca Chapouton, the EuMMCR, Dr. Lukas Simon, Dr. Kamyar Hadian and Dr. Kenji Schorpp, Dr. Silvia Engert and Dr. Johannes Klaus.
My thanks also go to friends inside and outside of Munich and PhD fellows at the Center, who helped me to overcome the small and big hurdles during this work.
Most importantly, I would not have been able to carry out this at times very demanding and busy project without the constant support, motivation and positive spirit of my family and my boyfriend, Valentin. Danke, danke, danke für alles!

Eidesstattliche Versicherung

Matheus, Friederike

Ich erkläre hiermit an Eides statt, dass ich die vorliegende Dissertation mit dem Thema

The role of *Additional sex combs-like* genes in human pluripotent stem cell differentiation and congenital disorders

selbständig verfasst, mich außer der angegebenen keiner weiteren Hilfsmittel bedient und alle Erkenntnisse, die aus dem Schrifttum ganz oder annähernd übernommen sind, als solche kenntlich gemacht und nach ihrer Herkunft unter Bezeichnung der Fundstelle einzeln nachgewiesen habe.

Ich erkläre des Weiteren, dass die hier vorgelegte Dissertation nicht in gleicher oder in ähnlicher Form bei einer anderen Stelle zur Erlangung eines akademischen Grades eingereicht wurde.

München, 28.08.2018	Friederike Matheus
Ort, Datum	Unterschrift Doktorandin/Doktorand